THE ENGINEERING GEOLOGY OF FRANKTON ARM.

A thesis

submitted in partial fulfilment

of the requirements for the degree

of

Master of Science in Engineering Geology

in the

University of Canterbury

by

DEBORAH LOUISE STOSSEL

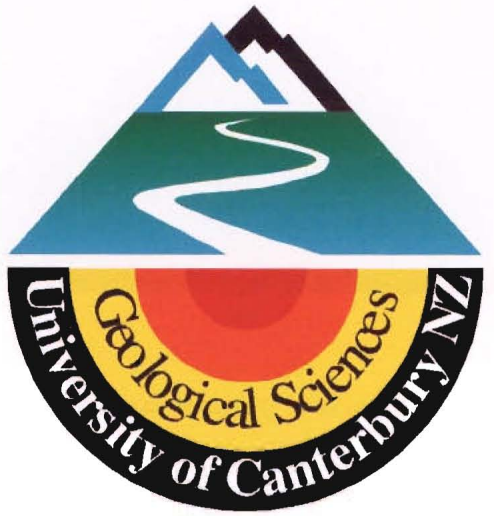

University of Canterbury,

June, 1999.

Frontispiece: Frankton Arm, Queenstown, looking south west. (Photo by L. Homer).

ABSTRACT.

Seven bedrock landslides situated within quartzofeldspathic schist exist up slope of the residential area along the Frankton Arm of Lake Wakatipu, South Island, New Zealand. Engineering geological and geotechnical failure models for these landslides have been established using engineering geological mapping at scales of 1:5000 and 1:10000, geotechnical testing, and the development of limit-equilibrium sensitivity models.

Geotechnical testing of artificially fractured schist bedrock obtained shear strength values of $\phi = 24°\text{-}36°$ and zero cohesion, and point load strength indexes of 0.6-3.83MPa for rock tested perpendicular to foliation, and 0.11-0.92 for rock tested parallel to foliation. Testing of shear zone material gave values of $\phi = 6°\text{-}11°$ and zero cohesion.

The largest failure is the Queenstown Hill Landslide, with an estimated volume of 240M m^3, which is interpreted as a retrogressive translational landslide with the toe forming a compressional bulge in the mid-slope area of Queenstown Hill. Three phases of movement have taken place, the earliest phase probably being initiated in the southeastern area of the slide mass by ice scouring and the oversteepening of slopes during the final stages of the Last Glaciation. On retreat of the glacial ice, lateral support was removed and increased pore water pressures may have acted to reduce the shear strength of the slope along critical failure or shear surfaces. Movement is inferred to have been by translational planar sliding by slow rock mass creep, not from buckling in the toe, partly along foliation shear zones and a stepped failure surface in fractured schist bedrock immediately following glacial retreat.

The second and third phases of movement were initiated as a result of the removal of support by the previous phase, with the second phase forming small translational slides and retrogressive features, and the third phase forming the toe bulging by gravitational creep down slope.

Six smaller bedrock failures (up to 2.8M m^3 each in volume) are situated further east along Frankton Arm. These landslides are interpreted as shallow retrogressive translational failures, with their slide bases orientated sub-parallel to the schist foliation. These failures may have initially occurred following glacial retreat (similar to the Queenstown Hill Landslide), with the slides situated at lower elevations activated by seismic events at a much later stage – following deposition of lake beaches as the enlarged Lake Wakatipu was lowering.

The only evidence for continual movement for within the last 100 years is on Slide No. 3 and Slide No. 4. Minor wedge failures have occurred from the head scarp, but the high frictional interlock between the displaced blocks creates minimal risk to the residential areas below and if further development was to occur in these areas, prudent engineering geological practices should be implemented.

Future sub-surface work needs to be completed to accurately locate the depth, shape and angle of the failure surfaces for each landslide. This work would also determine the parts of the failure surfaces that occur through foliation shear zones, or fractured schist.

TABLE OF CONTENTS.

LIST OF FIGURES.

LIST OF TABLES.

LIST OF FIGURES IN MAP POCKET.

Map Figure Number

CHAPTER 1

INTRODUCTION.

1.1 PROJECT BACKGROUND.

The Wakatipu Basin and Catchment lie on the northwest side of the Otago Province (figure 1.1). The Basin is defined as the low-lying area of land bounded by the Ben Lomond, Remarkables, Coronet Peak, Crown Ranges and Lake Wakatipu. The township of Queenstown is situated in a naturally formed bay on the middle 'arm' of Lake Wakatipu. Development over the last thirty years has seen the residential area expand rapidly to the east and west along the lower slopes bordering the lake and Frankton Arm, to the extent that the settlement as of 1994 covered approximately 6.3 x $10^6 m^2$ (Cunningham, 1994). This is causing increased development of marginal land for uses other than agriculture, which has traditionally been the predominant land-use. Approximately 20 subdivisions have been approved in the last 20 years, with landowners intending to develop residential property even on dormant bedrock landslides. Engineering geology has a very important role to play in land-use planning and in the assessment of limitations to residential development especially in the Queenstown area.

This thesis is an engineering geological study of Frankton Arm, Queenstown, New Zealand. Seven ancient landslides in the Otago Schist bedrock exist up slope of the residential area along the lake shore (figure 1.2 – map pocket). This project was initiated to develop failure models for these landslides and to investigate landslide stability. Sensitivity analyses using a limit equilibrium stability model were done to examine the physical conditions likely to have initiated failure. Laboratory testing was performed to determine representative material properties for the bedrock in the Frankton Arm/Queenstown area.

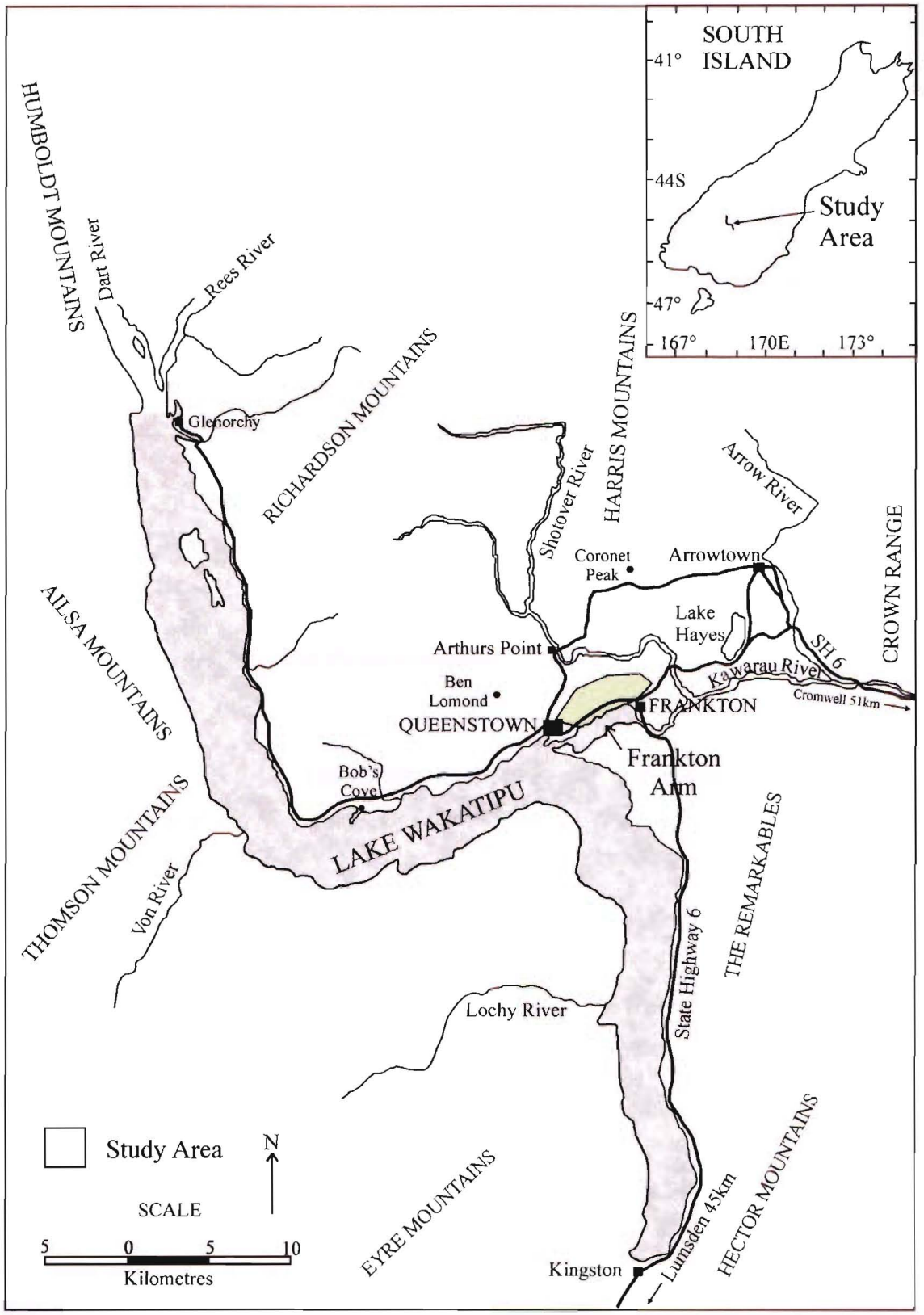

Figure 1.1: Locality Diagram. (Modified and redrawn after Watts, 1988).

1.2 THESIS OBJECTIVES.

The principal objectives of the thesis were:

1. To provide a detailed engineering geological map of Frankton Arm at a map scale of 1:5000 with particular emphasis on the northern (Queenstown Hill) side where significant residential development is presently taking place;
2. To establish engineering geological and geotechnical failure models for the seven schist bedrock landslides along the northern part of Frankton Arm;
3. To carry out sensitivity analyses to determine conditions during failure of the landslides along Frankton Arm.

1.3 DESCRIPTION OF FIELD AREA.

1.3.1 Location and Physiography.

The study area lies between Frankton and Queenstown, on the northern side of the Frankton Arm of Lake Wakatipu. The area is shown in Figure 1.1 and Figure 1.2 (Map volume).

The topographically highest point is Queenstown Hill at 910m above sea level, with the lowest point at lake level (310m above sea level). The study area has moderate slopes (20-25°) with deeply incised streams (figure 1.2 – map pocket, and figure 1.3). Frankton Arm has a depth of up to 25m and the deepest point within Lake Wakatipu is 380m.

The terrain in the Wakatipu area has been extensively glaciated, and is typically steep and mountainous, with relief of 600 to 2000m (figure 1.3). Figure 1.1 shows the setting of the field area in relation to the major physiographic features. Lake Wakatipu is a large glacial lake, formed by glacial erosion during successive glaciations over the last 2 million years. However, there is little or no evidence of the earlier events prior to 500000 years ago

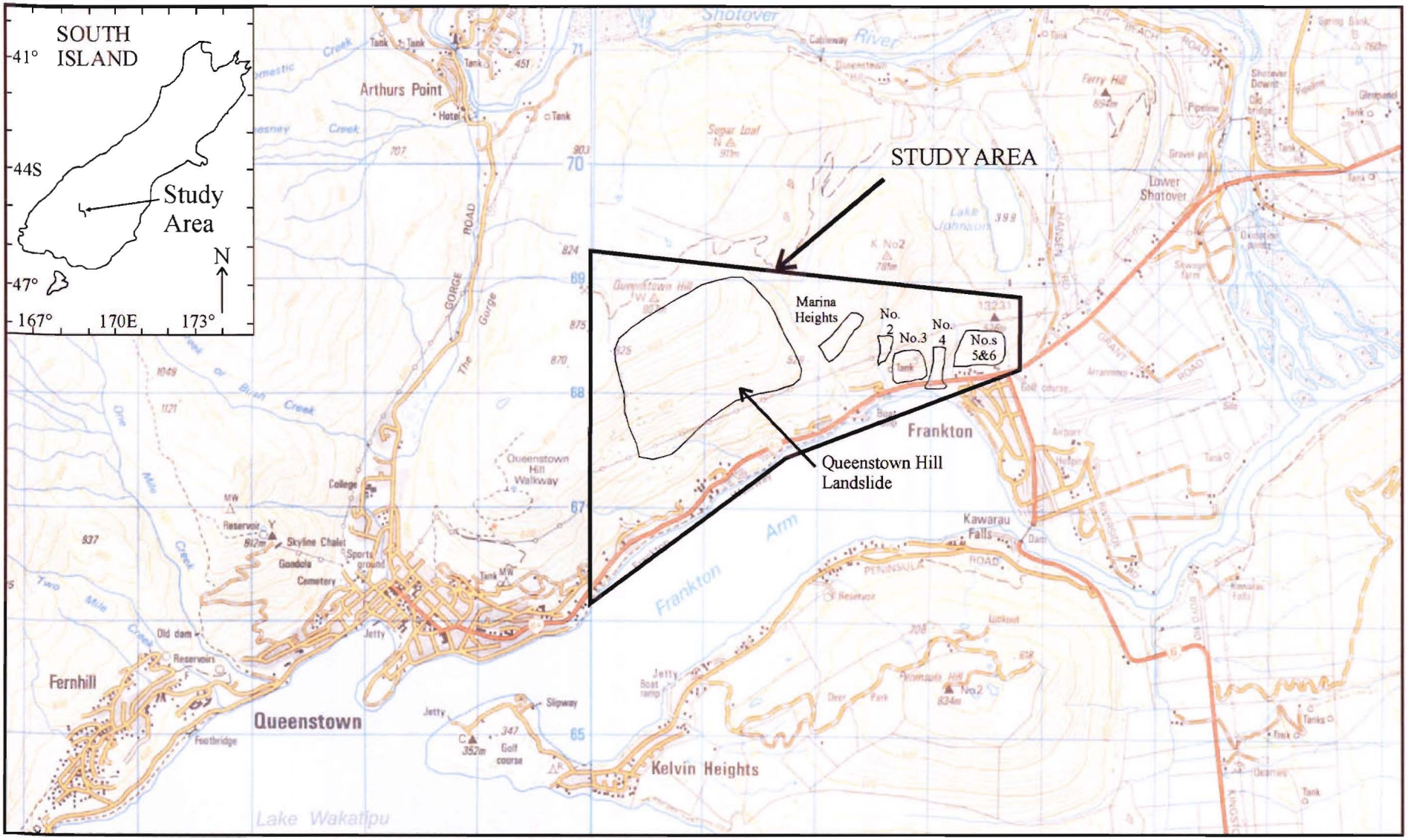

Figure 1.3: Location of study area and the Frankton Arm Landslides. Source: Department of Survey and Land Information, 1:50000 Series Topographical Map. NZMS 260 Sheet F41, Arrowtown.

(Bell, 1982). Glacial landforms such as steep U-shaped valleys, roches mountonnees and moraines are striking features of the Wakatipu area.

1.3.2 Climate.

The present day climate in the Queenstown area has average annual temperatures ranging from 3°C to 16°C. The annual temperature range between winter and summer is around 12°C. Air temperatures as low as –6°C (July) and as great as 26°C (December) have been recorded in Queenstown within the last eight years. Total annual rainfall over the last 15 years averages about 790mm, with highest rainfall usually during summer. Frosts are common in the winter months, with on average about 73 days of occurrence per year. The majority of days with snow occur between May and September. The study area receives on average close to 2000 sunshine hours per year (Source: National Institute of Water and Atmospheric Research, 1998). Tables and accompanying graphs are given in Appendix C.

1.3.3 Existing Land-Use.

The lower slopes along Frankton Arm (310m to 440m above sea level) contain residential areas that are rapidly encroaching up slope as subdividing of land continues, however development on the lower slopes does not occur on all six of the smaller Frankton Arm failures as in some cases the topography is not suitable. The Queenstown Hill landslide (located 1.75km from Frankton township) is used as pastoral land on the upper and lower slopes (sheep and cattle), with *pinus radiata* gradually colonising up slope. Many of the gullies are scrub-clad, consisting of gorse, broom and matagouri. The landslide is also used for recreational purposes, with the 4WD access track being used by motorbikes. The land-use on the Frankton wedge failures is primarily for pasture.

1.4 REGIONAL GEOLOGY AND GEOMORPHIC SETTING.

The basement rock type present in the Wakatipu Basin is Otago Schist, which is composed of quartzofeldspathic, pelitic and green schist. The schist is part of the Haast Schist Terrane, a major metamorphic belt extending across the lower part of the South Island (figure 1.4). The schist formed from an original sequence of sedimentary rock (sandstone and mudstone) and minor volcanic rock with Torlesse Terrane in the north and east, and Caples Terrane in the south and west (figure 1.5). The Otago Schist represents the deformed and metamorphosed amalgam of two greywacke terranes of different provenance whose contact lies within the schist. The metamorphism took place during the Rangitata Orogeny, a phase of mountain building that affected the New Zealand region during the Jurassic and Cretaceous Periods (Mortimer, 1993).

No Tertiary-age sediments are preserved in the Wakatipu Basin; however, small remnants have been preserved as sedimentary inliers along major faults outside the study area. This indicates active tectonism has taken place within the region. These sediments were formed during the mid-Tertiary marine transgression over parts of the Otago schist belt, and are preserved at Bobs Cove (figure 1.1). Deposits formed from freshwater lakes, streams and swamps occur at Coal Pit Saddle and near Crown Saddle (figure 2.1). Deposition of the Plio-Pleistocene Maori Bottom Gravels took place with the continuation of the Kaikoura Orogeny.

There is evidence for at least four major periods of ice advance and retreat in the Wakatipu Basin over the last 500000 years. Ice from the Wakatipu Glacier originated to the west and northwest of the present day Lake Wakatipu. As the glacier encountered The Remarkables, ice flowed northeast past Frankton Arm towards Arrowtown, forming the Wakatipu Basin ice tongue, while the main Wakatipu Valley ice tongue continued south towards Kingston (figure 2.6). During some of the glacial periods, the Wakatipu Basin ice tongue extended for some distance down the Kawarau River, and subsidiary ice tongues pushed up the Arrow and Shotover valleys, while the Wakatipu valley ice tongue at times extended south beyond Athol in the Mataura Valley (Barrell et. al., 1994).

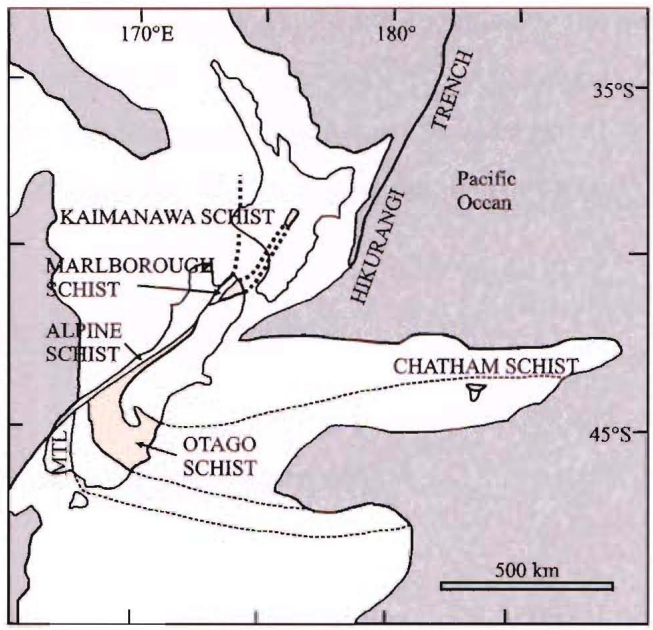

Figure 1.4: Distribution of the Otago, Alpine, Marlborough, Kaimanawa, and Chatham schists (Haast Schist Terrane) in relation to the Median Tectonic Line (MTL) and present-day plate boundary (heavy black lines). Offshore extent of New Zealand continental crust is left unshaded (Redrawn from Mortimer, 1993).

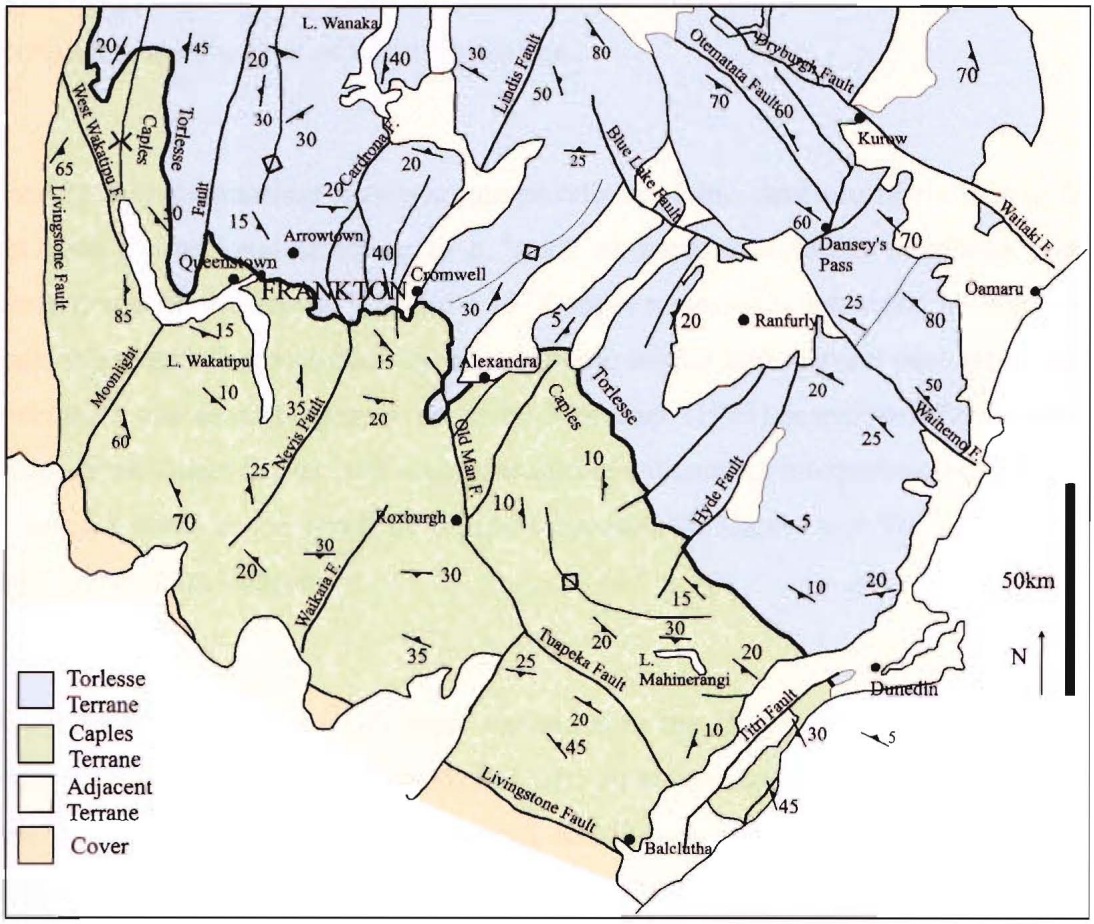

Figure 1.5: Simplified geological map of the Otago Schist and constituent terranes (Redrawn from Mortimer, 1993). Geology is from Mortimer (1992).

As the ice retreated, an enlarged Lake Wakatipu formed, producing lake beach deposits at various elevations (for example, 48, 35, 27 and 23m) above the present lake level and the lake was then possibly lowered by the downcutting of the Kawarau outlet over the last 10000 years. On retreat of the Wakatipu Glacier, sandy ablation till and silty lodgement till was deposited as a veneer up to 5m thick over irregular ice-shorn bedrock surfaces.

1.5 Previous Investigations.

1.5.1 Geological Investigations.

James Park produced one of the earlier geological investigations on the Wakatipu Basin in 1908, for the New Zealand Geological Survey. However Hector (1863) was the first to recognise the basin as being extensively glaciated and produced one of the earliest maps of the Queenstown area. Park (1906, 1908) recorded numerous schist foliation attitudes, identified green schist and metachert (quartzite) bands as well as many faults, and gave petrographic descriptions of schist lithologies.

Wood (1963) summarises previous interpretations of the structure of the Otago Schist and concludes the regional structure as a "stack of nappe-like folds "overthrust" or "facing" eastward and northeastward". Wood's 1978 paper reviews the structural interpretation of the Otago schist and discusses possible plate tectonic origins and relevant post-metamorphic plate movements and assemblages. A paper by Mortimer (1993) reanalyses the Jurassic tectonic history of the Otago Schist, and concludes (along with earlier interpretations of the schist) that the schist formed as the result of collision between the Caples and Torlesse Terranes in the Jurassic Rangitata Orogeny.

Craw (1984) described the lithologic variations in the Otago Schist of the Mount Aspiring area (to the north of the Wakatipu Basin). The author recognises psammitic schist, two types of pelitic schist (grey and porphyroblastic), and four types of green schist at outcrop scale in textural zone IV of the Otago Schist.

Bishop (1974) described textural zones, which are based on the degree of metamorphic segregation layering between quartz-feldspar and sheet silicate minerals (for example, micas). Bishop described transitions from non-schistose material (zone I) through schists lacking segregation layering (zone II) to schists with conspicuous layering (zones III and IV). Within the Frankton Arm area, Otago Schist textural zone IV outcrops. Bishop originally mapped the schist within the chlorite zone as subzones called chlorite I, II, III and IV. Norris and Bishop (1990) discussed textural zones in more detail, indicating that the causative process of textural zones is solution transfer (figure 2.2). Norris and Bishop, (1990) also found that the textural subzones crosscut mineralogical zones, and were thus called textural zones.

Bishop et. al. (1976) successfully mapped the Caples Terrane along the western margin of the Haast Schist in the Humboldt Mountains of northwest Otago. The authors concluded that the terrane grades north and east into the Haast Schist Terrane (figure 1.4), which in turn grades east into the Torlesse Terrane (figure 1.5). Caples and Torlesse rocks are petrographically and lithologically distinct; thus the Haast Schist represents a metamorphosed amalgamation of these two rock suites.

Turnbull (1979) completed work on the stratigraphy and sedimentology of the Caples Terrane of the Thomson Mountains west of Lake Wakatipu. He interpreted the terrane to be of Late Permian to early Triassic age, which formed as a submarine fan complex in a trench slope or trench floor environment. Mortimer and Roser (1992) provided geochemical evidence for the position of the Caples-Torlesse Terrane boundary in the Otago Schist. Mortimer's (1993) "Geology of the Otago Schist and adjacent rocks" is an updated version of the structure in the Geological Map of New Zealand by Wood (1962). However, Wood (1962) maps the stratigraphic units in more detail, whereas Mortimer (1993) focuses on textural zones and distinction between the Caples and Torlesse Terranes.

1.5.2 Geomorphological Investigations.

Park (1906, 1908) systematically mapped and carefully observed rock types foreign to the various catchments of the Wakatipu Basin, and provided the basis for reconstructing the geomorphic evolution of the Queenstown and surrounding districts. Park visualized a single ice sheet covering the Queenstown area in late Pleistocene times, with the higher mountain peaks projecting above its surface. However Park worked before the concept of multiple glaciations was understood. Fifty years after Park, multiple glaciation in New Zealand was demonstrated by Gage (1958) and other workers, and Suggate (1965) provided a four-glaciation framework for the interpretation and correlation of late Quaternary climatic events. McKellar (1960) established a chronology of glacial events in the upper Clutha Valley, and Wood (1962) correlated Pleistocene deposits in the various Wakatipu catchments. Bell (1976) summarised evidence for at least three glacial episodes within the Kawarau Valley, and correlations with adjacent areas were discussed in later publications (Bell, 1976, 1977).

Bell (1982) suggests a complex geomorphic evolution for the eastern Lake Wakatipu district during the late Pleistocene, because of the pattern of ice movements and the extreme drainage modification that has occurred, particularly in the Arrowtown Basin.

Turnbull and Forsyth (1988) produced a simple geological guide for the Queenstown area. The guide describes the rocks, landforms and glacial history of the district. Barrell et. al., (1994) undertook a program of reconnaissance geological mapping to define the nature and distribution of surficial geological deposits within the Wakatipu Basin. Included in his report is a 1:50000 scale map and interpretive cross-sections. Various subdivision reports by Bell (1985-1997, unpublished) with maps of several different scales (1:100 to 1:500) give brief summaries of the geomorphic development of Wakatipu Basin, including the glaciated history of the basin.

1.5.3 Engineering Geology Investigations.

A paper by Bell (1987) reviews aspects of the K9 landslide in the Kawarau Gorge. One of the main objectives was to discuss the rock slope failure mechanisms (such as toe buckling and gravitational spreading) and the geomorphological and geotechnical implications of large-scale mass movements in schist terrain.

Watts (1988) carried out an engineering geological investigation of roading aggregate with the objective of identifying potential aggregate source areas, which comply with New Zealand-wide specifications. Investigations included mapping at scales of 1:10000 and 1:1500, and the excavation of test pits. He recognised six Late Quaternary aggregate sources within the Wakatipu Basin, three of which are glacial and three are post-glacial. He found that mixed schist and greywacke aggregate produce the highest quality roading aggregate in the Wakatipu Basin.

Cunningham (1994) undertook an engineering geological investigation to determine the nature and distribution of the geological material in the Wakatipu Basin. The Basin was mapped at 1:25000 scale, with the Queenstown urban area mapped at 1:10000. The maps produced show bedrock and surficial geology, as well as geomorphology. In addition, Cunningham compiled a Development Suitability Map for the Queenstown urban area (1:10000 scale) identifying physical constraints in the area.

Bell (unpublished) has produced numerous subdivision reports between 1985 and 1998, on various sections within the Queenstown-Frankton area. Each report provides engineering geological assessment of the property concerned, including site description, development considerations, recommendations and further investigations necessary.

1.5.4 Geotechnical Investigations.

Watts (1988) conducted a geotechnical testing program for assessing the quality of aggregate from various source areas within Wakatipu Basin. Tests carried out include grain size analysis; Atterberg Limits; clay index testing and X-ray diffraction. Limited laboratory testing was undertaken by Cunningham (1994) to determine the grain size distributions of various surficial deposits. Bell's unpublished subdivision reports include engineering geology logs of investigation trenches (descriptive terminology following Bell and Pettinga, 1983) conducted at each site. A report on the Marina Heights Service Station retaining wall failure includes test reports on particle size distribution and water content.

1.6 THESIS ORGANISATION.

1.6.1 Field Investigations.

Preliminary fieldwork was done in January 1998, with detailed mapping in March 1998 for the 1:5000 and 1:10000 maps and cross-sections. Additional field mapping of the Frankton Failures was conducted in May 1998 along with defect surveying of the Commonage Subdivision, Queenstown. Sampling of materials in January 1999 was undertaken for subsequent laboratory testing of bedrock and shear zone material. Limited Schmidt Hammer testing was also performed on intact schist material in the field in order to determine joint wall compressive strength.

1.6.2 Laboratory Studies.

The following geotechnical testing program was used to determine bedrock and shear zone material properties:

(a) Point Load testing;

(b) Shear Strength testing;

(c) Ring Shear testing; and

(d) X-ray Diffraction analysis.

The geotechnical testing was performed at the University of Canterbury, Geological Sciences Rock Mechanics and Engineering Geology Laboratories.

1.6.3 Thesis Layout.

The first two chapters of this thesis are introductory. Chapter 2 reviews the geology and geomorphological evolution of the field area, and thus sets a framework from which landslide assessment along Frankton Arm can be made.

Chapter 3 presents the engineering geological investigations that were done, and details the results of the geotechnical characterisation of bedrock and shear zone materials relating to slope stability. In addition, results of defect surveys are illustrated and examined.

Chapter 4 details the Queenstown Hill Landslide and gives engineering geological and geotechnical failure models. Factor of Safety sensitivity analysis was undertaken to confirm mechanisms that initiate failure.

Chapter 5 presents a review of the Frankton failures and discusses failure mechanisms, kinematics and sensitivity. In Chapter 6 the summary and conclusions are presented.

CHAPTER 2

GEOLOGY AND GEOMORPHOLOGY.

2.1 INTRODUCTION.

In this chapter, a brief summary of the geology and geomorphology of Otago is presented, concluding with the geomorphology of Frankton Arm in section 2.5. A description of the lithotypes, structure and origin of the Otago Schist and Caples Group – the main basement rock types present in the Wakatipu Basin – is only brief, as this thesis concentrates on Frankton Arm: the materials present, geomorphic evolution and failure models for the landslides in that area.

Sections 2.2 and 2.3 discuss the geological evolution of Central Otago beginning with the Jurassic-Cretaceous Rangitata Orogeny, which was the main influence in the formation of the structure of the Otago Schist. The Kaikoura Orogeny, a major deformational event commencing in the Miocene, produced the obvious "basin and range" topography of Central Otago.

As discussed in section 2.4, Quaternary glaciations within the Wakatipu Basin played a major role in the physiographic development of the basin. Many landforms within the basin were formed during the younger ice advances even though the oldest ice advances, for example Athol, were much more extensive, but their landforms have subsequently been destroyed. Glacial till has been deposited as a thin veneer generally less than 3m deep (although locally much thicker, for example, in moraines) in some places over the schist bedrock surface. During glacial retreat at the end of the Last Glaciation, an enlarged Lake Wakatipu formed 45m above present lake level, and the prominent lake beach terrace surfaces were formed as the lake was progressively lowered to its present level.

2.2 BASEMENT GEOLOGY.

2.2.1 Otago Schist.

2.2.1.1 Distribution.

The Otago Schist is part of a major metamorphic belt in New Zealand known as the Haast Schist. The latter includes the Kaimanawa, Marlborough, Alpine, Otago and Chatham schists. The Otago Schist is the part of the Haast Schist that underlies the regional province of Otago (Norris and Bishop, 1990), having an outcrop area of just under 20000km^2. It occupies a broad belt trending northwest from the east coast of Otago, through Central Otago and then continues northeast as a narrowing strip to the schists of the Southern Alps (figure 1.4).

Within the Haast Schist Terrane textural zones occur as belts, with textural zone I situated in the southern-most area grading up to textural zone IIIB in the north (figure 2.1 and figure 2.2). Textural zone IIIB occurs as a transition between the Caples and Torlesse terranes. In the western area, the terrane boundary is marked by a short (1km) lithologic transition from structurally high, weakly segregated, psammitic Caples schist to structurally lower, thickly segregated, pelitic Torlesse schist (Mortimer, 1993). The position and geometry of the terrane boundary are less well known in the eastern area because of the presence of more pelitic lithologies, poor exposure, low relief and low dips (Mortimer, 1993).

2.2.1.2 Lithotypes.

The Otago Schist consists of two main rock types, both of which outcrop along Frankton Arm:

1. quartzofeldspathic schist, or greyschist, which represents metamorphosed sedimentary rocks. This type can be subdivided into (a) psammitic schist, composed of the metamorphic mineral assemblage quartz-albite +/- epidote-chlorite-muscovite-calcite and muscovite-chlorite +/- actinolite-epidote-biotite-titanite-quartz-albite, and (b) grey pelitic (mica-rich) schist, composed of muscovite-chlorite-albite-quartz-epidote-actinolite-calcite-titanite. Schist type becomes weaker and more ductile with increasing mica content (Rosen, 1997).

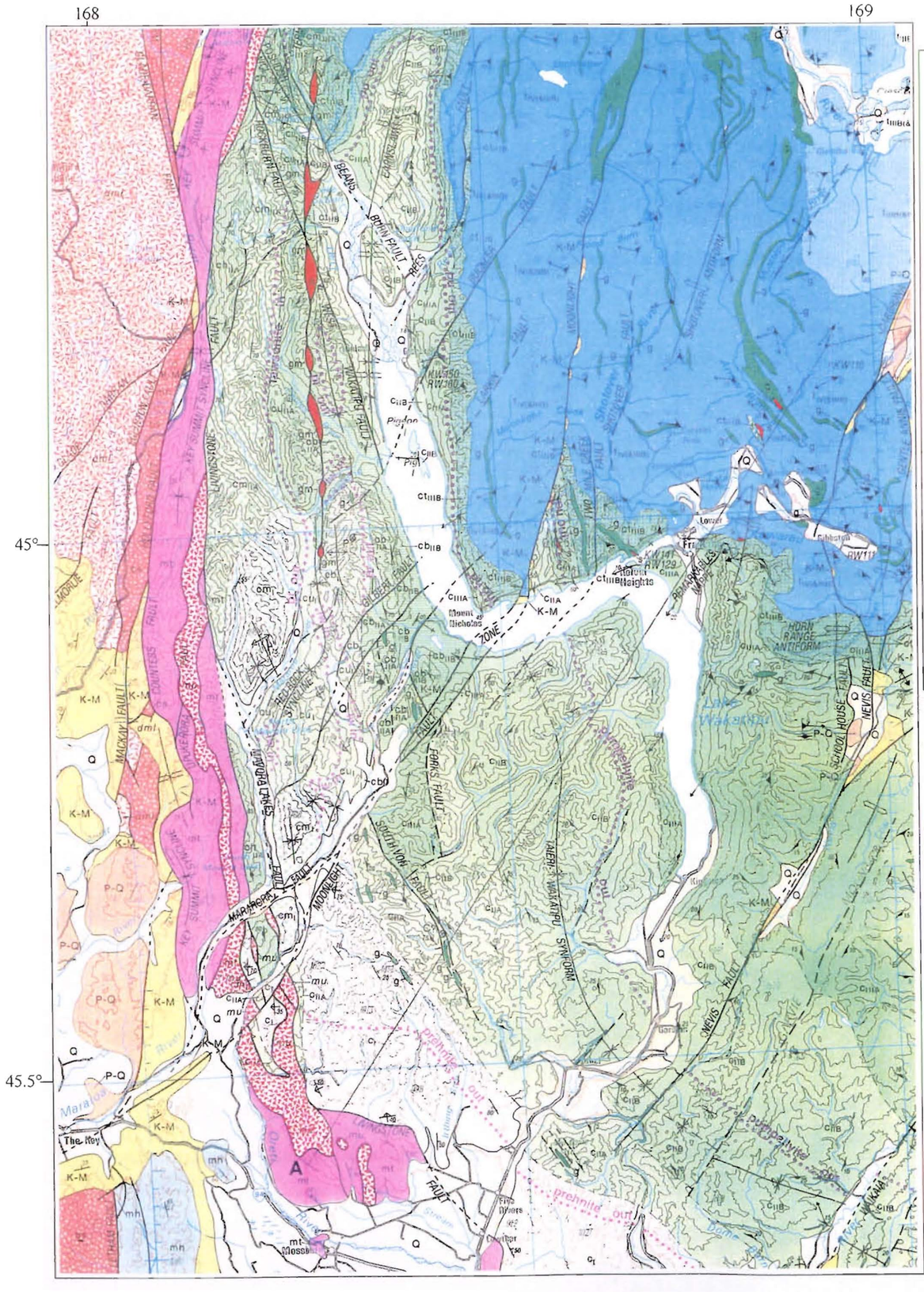

GEOLOGICAL LEGEND

Alluvial and glacial outwash deposits.

QUATERNARY (Wanganui-Hawera Series)

REGIONAL UNCONFORMITY

Weathered, slightly warped and faulted piedmont gravels (Maori Bottom & Prospect formations, Clydevale and Gore Piedmont gravels, Schoolhouse Fanglomerate, Kurow Group).

PLIOCENE-LOWER QUATERNARY (Taranaki Series)

REGIONAL UNCONFORMITY

Marine, estuarine, deltaic, and fluvial strata in west and Central Otago (Manuherikia Group, Bobs Cove Beds), Southland (Gore Lignite Measures, Annick Group, Waiau Group) and east Otago and South Canterbury (Taratu, Wangaloa, Ngarara, Greenisland, Burnside, Amuri, Concord, Weka Pass, Bluecliffs, Southburn, Blue Spur Conglomerate and Whiterock formations and their equivalents (Carter 1988)). v = intercalated mafic volcanic rocks (Dunedin Volcanic Complex, Waipata, Deborah and Waiareka volcanics).

LATE CRETACEOUS-MIOCENE (Mata-Southland Series)

REGIONAL UNCONFORMITY

Non-marine conglomerate and breccia (Shag Point Group, Kyeburn Formation, Henley Breccia).

MIDDLE CRETACEOUS (Clarence-Raukumara Series)

REGIONAL UNCONFORMITY

WESTERN PROVINCE[1] — EASTERN PROVINCE

MEDIAN TECTONIC LINE | LETHAM FAULT | HILLFOOT FAULT | LIVINGSTONE FAULT

DARRAN COMPLEX, MACKAY INTRUSIVES, LARGS TERRANE

Leucogabbro, diorite, granite, granophyre, migmatite,biotite gneiss, andesite, tuff & breccia (Darran Leucogabbro, Nurse Glade, and Hut Plutonic suites,Hollyford Gabbroic Suite, Mistake Diorite, Gunn Dolerite, Largs terrane). Sandstone of Martins Bay Formation north-west of Alpine Fault.

BROOK STREET TERRANE

Basalt, augite porphyry, andesite, diorite, minor ultramafic rocks, volcanic breccia and greywacke (Plato terrane, Eglinton Volcanics, Skippers Group, Takitimu Group).

MURIHIKU TERRANE

Sandstone, siltstone, argillite, tuff and minor conglomerate (Murihiku Supergroup).

MAITAI TERRANE

mt = gabbro, altered mafic volcanic rocks, volcanic breccia, limestone, sandstone, siltstone and argillite (Maitai Group, part of Humboldt Group, part of Dun Mountain Ophiolite Belt). *mu* = ultramafic rocks, serpentinite and serpentinite-matrix melange (part of Humboldt Group and Dun Mountain Ophiolite Belt)

OTAGO SCHIST

CAPLES TERRANE, TORLESSE TERRANE, AND OTAGO SCHIST[2]

EARLY CRETACEOUS

JURASSIC

TRIASSIC

PERMIAN

CARBONIFEROUS

CAPLES TERRANE (c). In tz I, dominantly grey-green volcaniclastic sandstone, siltstone and argillite with subordinate conglomerate, chert, volcanic rocks, and limestone. Schistose equivalents occur in tz IIA–IIIB. West of Lake Wakatipu, the Caples terrane has been subdivided into the Harris Saddle Formation and West Burn Semischist (ch); Mcinus Sandstone and Mount Campbell Formation (cm); Bold Peak Formation (cb); Upper Peak, Kays Creek, and Cosmos formations (cu); Greenstone Mélange (gm).

TORLESSE TERRANE (t). In tz I, dominantly grey quartzofeldspathic sandstone, siltstone and argillite with subordinate conglomerate, chert, volcanic rocks and limestone, mainly of Rakaia subterrane. ta = Akatarawa subterrane. Schistose equivalents occur in tz IIA–IV. Tz IV of the Torlesse terrane as shown on this map broadly coincides with the Aspiring lithologic association of Craw (1984).

UNDIFFERENTIATED CAPLES OR TORLESSE TERRANE (ct). Includes wedge-shaped area in southeasternmost Caples terrane containing schist geochemically similar to Torlesse terrane rocks; lenses of lower textural grade Caples-like schist in tz IV Torlesse schist, and zone of uncertainty of position of terrane boundary proposed by Mortimer and Roser (1992)

DIFFERENTIATED LITHOLOGIES[4]
Greenschist (g), serpentinite, talc schist,and tremolite schist (s)

TEXTURAL ZONES (tz) (Bishop 1972) Characteristics of schist derived from psammitic protoliths (original sandstone):
- I: Indurated, nonfoliated medium-grained sandstone.
- IIA: Slightly foliated metasandstone with widely spaced cleavage.
- IIB: Penetratively and well foliated semischist.
- IIIA: Strongly foliated schist with segregation lamellae 1-10mm long.
- IIIB: As for IIIA, but segregation lamellae > 10mm and < 2mm thick.
- IV: As for IIIA, but segregation lamellae > 2mm thick.

Established | Inferred | Concealed

CONTACT
Sedimentary contact, lithologic contact, and terrane boundary within schist.

FAULT
Ticks on downthrown side, teeth on upper plate of thrust where known.

ISOTECT
Approximately located.

ISOGRAD
Very approximately located, annotation on upgrade side. pr = prehnite, pu = pumpellyite, lw = lawsonite.

MESOZOIC MACROSCOPIC FOLDS[3]
FIRST GENERATION: FORM SURFACE IS BEDDING
- Axial trace of upright antiform
- Axial trace of upright synform
- Axial trace of steeply-plunging fold (symbol indicates closure).
- Axial trace of recumbent antiform
- Axial trace of recumbent synform

SECOND OR LATER GENERATION: FORM SURFACE IS FOLIATION
- Axial trace of upright antiform
- Axial trace of recumbent antiform
- Axial trace of recumbent synform

CENOZOIC MACROSCOPIC FOLDS[3]
FORM SURFACE IS BEDDING, FOLIATION AND/OR PENEPLAIN SURFACE
- Axial trace of upright antiform
- Axial trace of upright synform
- Axial trace of overturned synform

Dipping | Vertical | Overturned (where known)

BEDDING

DOMINANT FOLIATION[5]
INCLUDING ENVELOPING SURFACE
- First generation
- Second or later generation
- Axial plane foliation

LINEATION AND MESOSCOPIC FOLD AXIS[5]
- Axis of stretched conglomerate clasts or clastic grains.
- Quartz rodding lineation, quartz fibre lineation or mineral lineation.
- Axis of open-tight fold with vergence.
- Axis of open-tight fold with symmetrical vergence.
- Axis of tight-isoclinal fold with vergence.
- Axis of tight-isoclinal fold with symmetrical vergence.

MISCELLANEOUS
- Fossil locality in Caples and Torlesse terranes with probable age. C = Carboniferous P = Permian Tr = Triassic J = Jurassic ? = uncertain age determination
- Radiometric age locality in Caples and Torlesse terranes with age (Ma)[4]. *KW* = potassium-argon whole rock; *KB* = potassium-argon biotite; *RW* = rubidium-strontium whole rock isochron; *RM* = rubidium-strontium mineral isochron

Figure 2.1: 1:500000 regional geological map for the study area. (Sourced from: Mortimer, 1993)

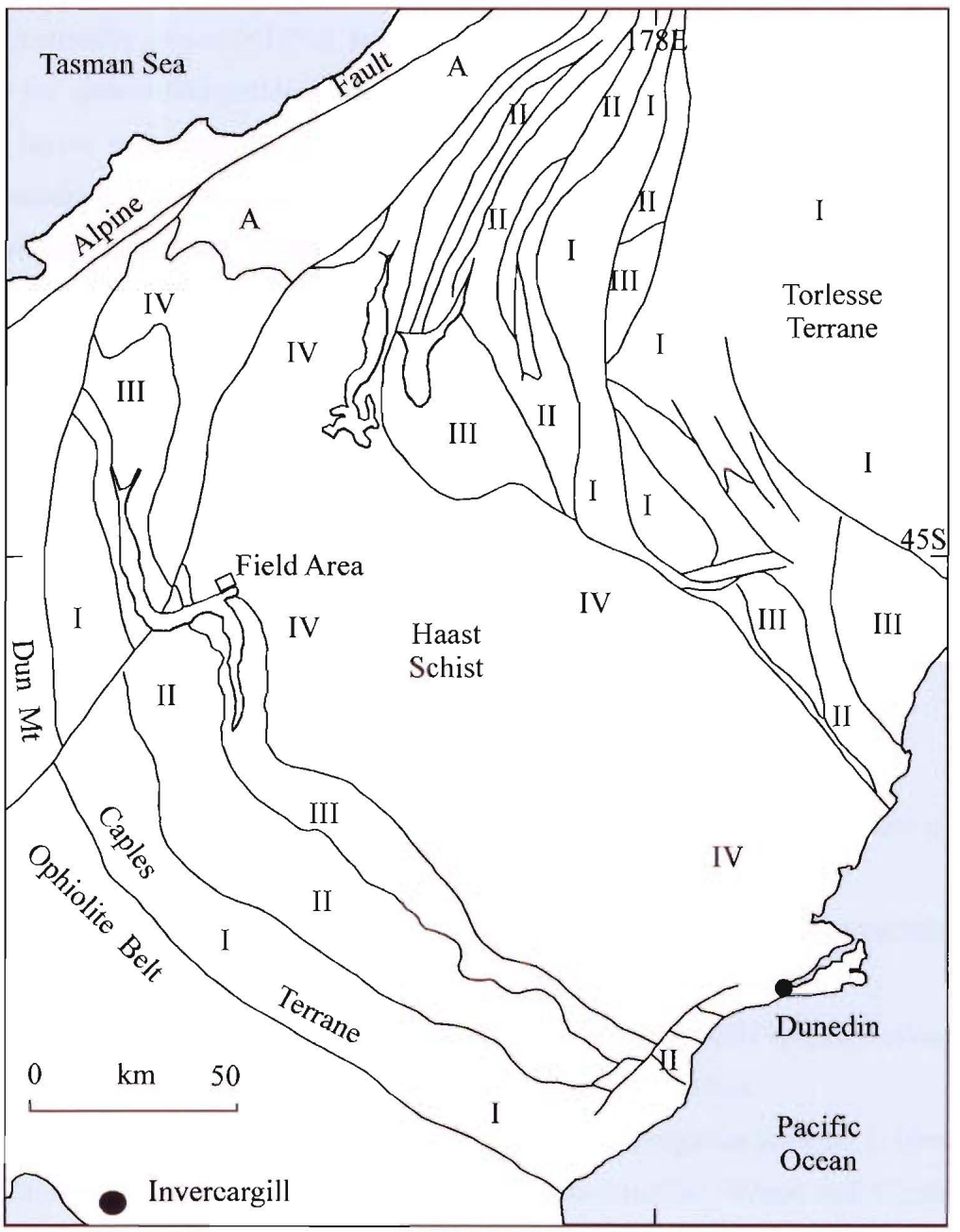

Figure 2.2: Map of southern South Island, showing textural zonation of the Otago Schists. I, II, III and IV are textural zones I-IV in prehnite-pumpellyite, pumpellyite-actinolite and greenschist facies; A is the area of amphibolite facies schist (redrawn from Norris and Bishop, 1990).

2. green schist, which is derived from the metamorphism of volcanic material, and is composed of albite-epidote-chlorite-titanite with minor magnetite (or pyrite and pyrrhotite), actinolite, stilpnomelane, biotite, quartz, muscovite, calcite and apatite in various proportions (Rosen, 1997). In the Wakatipu Basin, green schist is common but volumetrically minor (<10%), and occurs as bands (1cm to >100m thick) interlayered with the quartzofeldspathic schists. Most green schist bands are laterally extensive with thin layers persisting for many metres and thicker layers extending for tens or even thousands of metres. Green schist commonly contains much calcite, and weathered carbonate pits are also prominent in some green schist rocks (Rosen, 1997). Massive to thinly laminated metachert or quartzite units, usually associated with green schist, range in thickness from <1cm to 4m. Individual bands may extend laterally for many metres, with metachert-rich horizons covering several kilometres. The metachert consists of quartz (≥90%) ± albite, chlorite, muscovite, actinolite, epidote, piemontite, spessartine, magnetite, hematite, and calcite. Marble (calcite ± quartz-albite-chlorite-muscovite-opaques), is found as rare pods and bands up to 0.5m thick in association with green schists, which rarely extend for more than ten metres (Turnbull, 1981).

2.2.1.3 Structure.

The Otago schist is subdivided and mapped on the basis of textural parameters such as the degree of layering and some marker lithologies (see figure 2.1).

Textural zones of Bishop (1974); (the criteria are based on an original sandstone lithology):

Textural Zone I: Indurated, nonfoliated medium grained sandstone.

Textural Zone II: Slightly foliated metasandstone with widely spaced cleavage.

Textural Zone IIB: Penetratively and well foliated semischist.

Textural Zone IIIA: Strongly foliated schist with segregation lamellae 1-10mm long.

Textural Zone IIIB: As for IIIA, but segregation lamellae >10mm and <2mm thick.

Textural Zone IV: As for IIIB but segregation lamellae >2mm thick (Bishop, 1974; Mortimer, 1993; figure 2.2).

Most of the schist in the Wakatipu Basin and within the Frankton Arm landslides is textural zone IV, and is defined by thick prominent layers (up to 25mm in thickness). The metamorphic and textural subzones, along with gross foliation, define a broad, regional antiformal structure in the Otago Schist (figure 2.1 and figure 2.2), with metamorphic (and

textural) grade generally decreasing from greenschist facies near the antiform axis to prehnite-pumpellyite facies in the flanking nonschistose rocks. The contact between the Caples and Torlesse terranes has been overprinted by metamorphism and ductile deformation, and follows a sinuous course near the centre of the schist (see figure 1.5); (Mortimer, 1993).

2.2.1.4 Origin.

Torlesse terrane rocks within the Otago Schist were derived from an active continental magmatic arc, probably located along the Gondwana margin, while Caples terrane greywackes were derived mainly from an active intraoceanic magmatic arc, with some contribution from a continental source (Mortimer and Roser, 1992). The Otago Schist represents the deformed and metamorphosed amalgam of two greywacke terranes of different provenance with their contacts lying within the schist. The metamorphism took place during the Rangitata Orogeny - a phase of mountain building that affected the New Zealand region during the Jurassic and Cretaceous Periods (Mortimer, 1993).

2.2.2 Caples Group.

2.2.2.1 Lithotypes.

Caples Group sandstones are lithologically and petrographically distinct from the partly contemporaneous Torlesse Supergroup sandstones. The differences in clastic mineralogy indicate the Caples source area was quite deficient in quartz and coarse-grained micas, and was generally of a basic to intermediate volcanogenic nature compared with the metamorphic/plutonic source of the Torlesse sediments (Bishop et. al., 1976).

Caples Group clasts occur as exotics within the glacial till along Frankton Arm and the group has been subdivided into six lithostratigraphic units by Bishop et. al., (1976; see also figures 2.3 and 2.4 for unit descriptions).

Within the Caples Group the Greenstone Melange occupies a steep fault zone that cuts across formation boundaries, isograds and isotects between the Beans Burn and the upper Mararoa River (see figure 2.3). This Melange is a dike-like body of disrupted rocks, containing talc

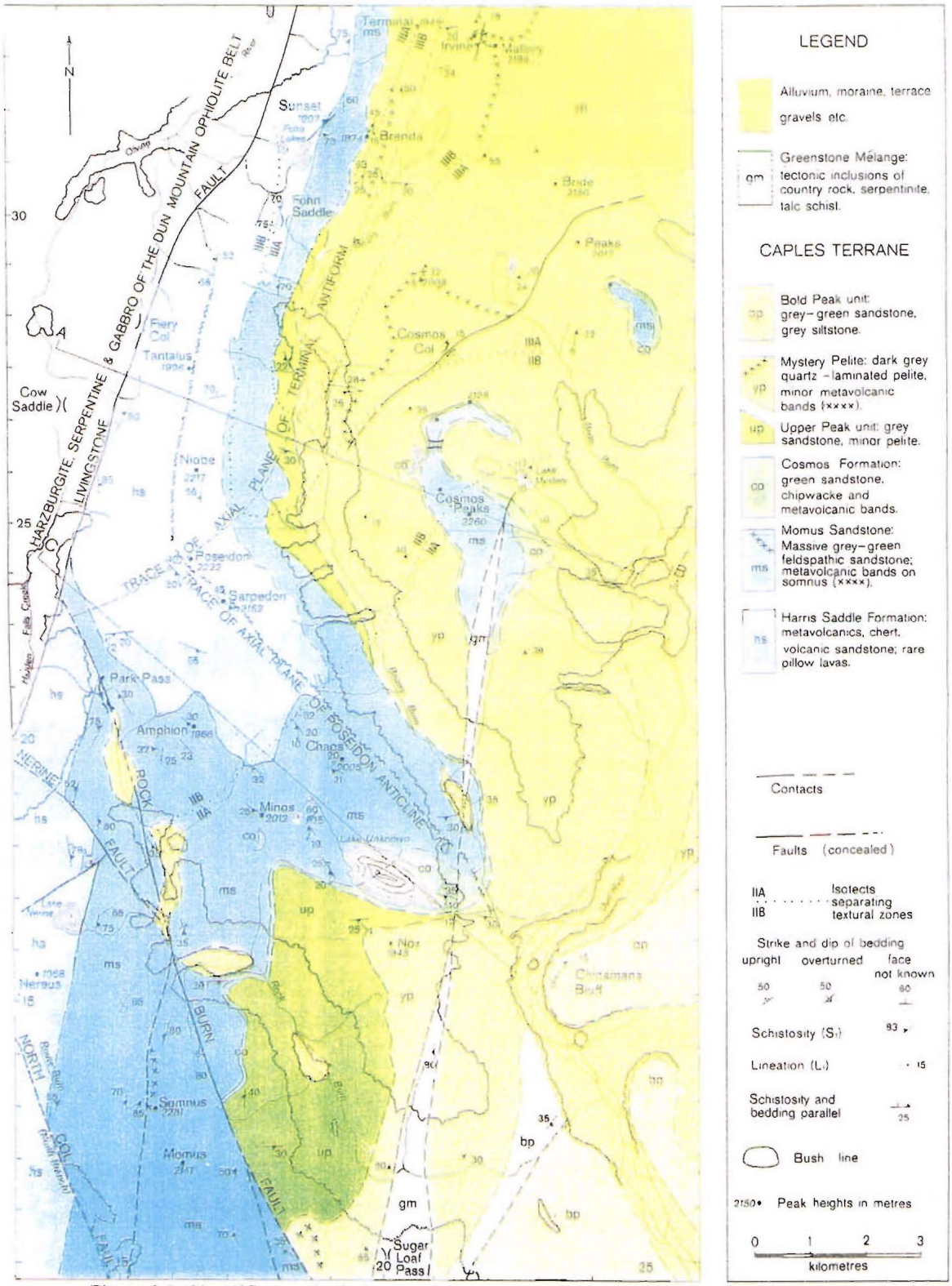

Figure 2.3: Simplified geological map of the northern Humboldt Mountains (Bishop et. al.. 1976).

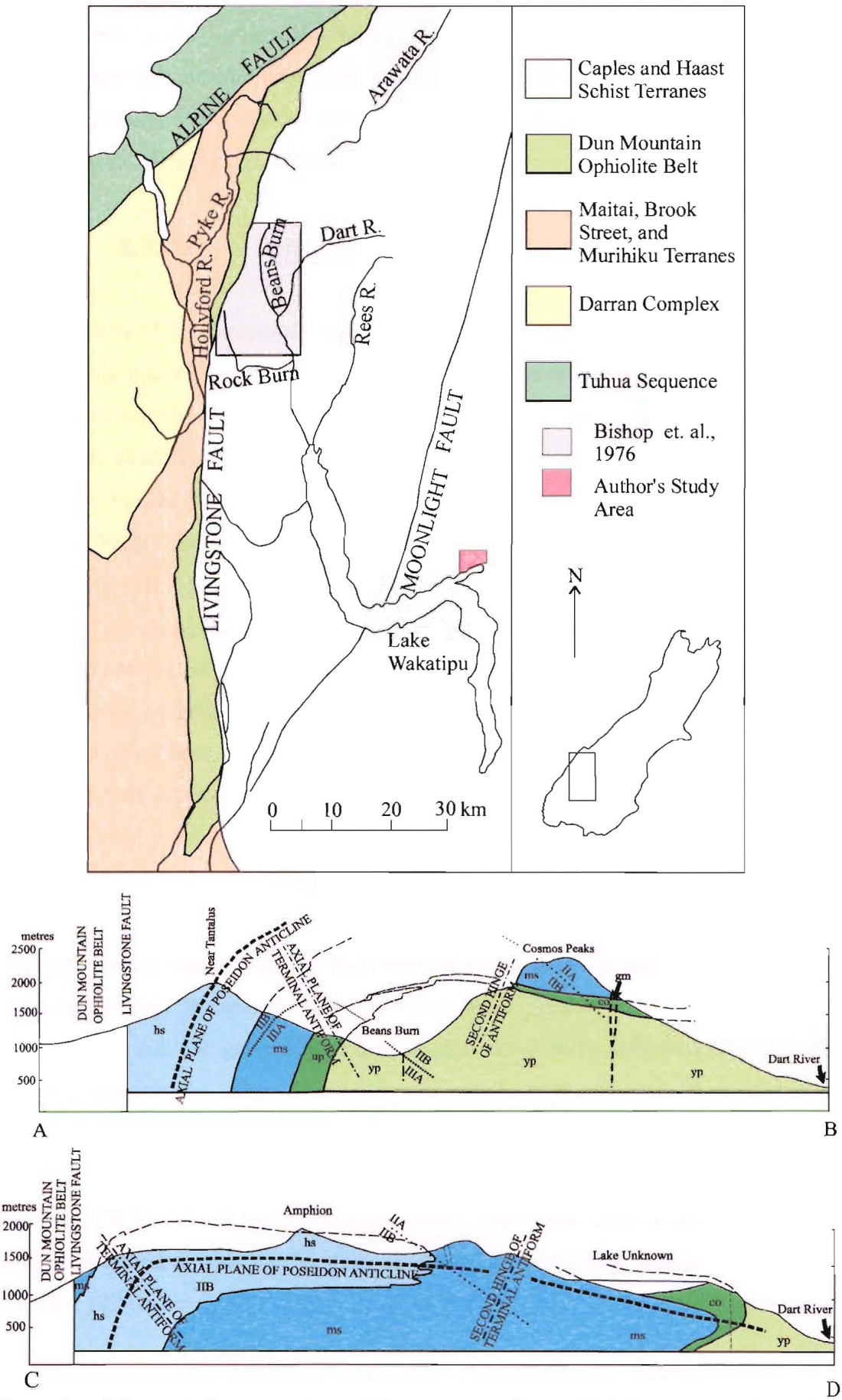

Figure 2.4: Map and Cross-sections of the northern Humboldt Mountains region of west Otago showing the area mapped in this study and by Bishop et. al. 1976. Locations of Cross-sections shown in Figure 2.3.

and serpentinite (mainly mixed lithologies of ultramafic and volcanic rocks), that was either tectonically intruded or diapirically injected (Bishop et. al., 1976). A similar steep fault zone can also be traced southeast from the Moonlight Fault into the Eyre Mountains, as shown in figure 2.1 (from Bishop et. al., 1976).

2.2.2.2 Structure.

The distribution of the formations within the Caples Group results from the superposition of two major fold phases, and the pattern of textural zones reflects the later deformation event. The Poseidon Anticline represents the earliest phase of deformation (F1). This anticline is a large, tight to isoclinal, partly recumbent fold, with the Harris Saddle Formation situated in the core (see figures 2.3 and 2.4). Further north the trace of the axial surface intersects the Livingstone Fault. The second phase of deformation was post-metamorphic folding (F2) of the schistosity (S1). This resulted in the formation of the Terminal Antiform, an open, steeply inclined fold plunging southwest at 25° (Bishop et. al., 1976). The western limb dips 75-85° west and the eastern limb has an undulating dip of 25-35° southeast. Isotects defined by the degree of development of S1 schistosity are folded by the Terminal Antiform. The trends of the Poseidon Anticline, the Terminal Antiform and the Livingstone Fault are sub-parallel, suggesting a similar tectonic history within this part of northwest Otago (Bishop et. al., 1976).

2.2.2.3 Origin.

The Caples Group source area was the Permian island-arc volcanics equivalent to the Brook Street and Eglinton terranes to the south and west. These rocks have only been slightly metamorphosed and can generally be described as dominantly greywackes and argillites that gradually grade into the Otago Schist (Coombs et. al., 1976). The sandstone-dominated units were deposited on a volcanic-pelitic sequence (Harris Saddle Formation) as submarine deposits in structurally controlled lower trench-slope basins, and on the trench floor (Mortimer, 1993). The Kays Creek Formation originated from a basaltic-andesite intra-oceanic volcanic arc, with the Momus Sandstone forming from a more continental source (Mortimer, 1993).

Park (1906; 1908) observed rock types foreign to various catchments within the Wakatipu and Clutha regions. Bell (1982) suggests the presence of rounded Caples Group exotics (distinctive green and purple volcanogenic mudstones and sandstones) at the mouth of the Kawarau Gorge above Ripponvale, provides evidence of drainage integration with the western side of Lake Wakatipu. He indicates their derivation and transport was by ice and/or fluvial reworking during earlier glacial events, and they may have been deposited as glaciofluvial sediments beyond the limit of ice advance down the Kawarau Valley. Gravel derived from Caples Group rocks also occurs in the Wakatipù Basin, and is likewise inferred to have been deposited by glacial action. The presence of "greywacke" Caples Group exotics within the surficial deposits indicates either a glacial origin, or that the deposit contains reworked glacial debris (Barrell et al 1994).

2.2.3 Basement Evolution.

The Rangitata Orogeny was a phase of continental collision, metamorphism and folding of schists, followed by uplift and mountain building, that occurred from the Late Jurassic into the Mid Cretaceous (Turnbull and Forsyth, 1988). These processes ultimately formed the Otago Schist.

The Otago Schist originated in a complex sequence of Paleozoic-Mesozoic plate interactions near the southwest Pacific margin of Gondwanaland. It included part of a volcaniclastic frontal arc basin assemblage (Murihiku and Caples Terrane) lying northeast of an older crystalline foreland, and a quartzofeldspathic assemblage of plutonic-metamorphic provenance lying further to the northeast (Torlesse Terrane). Parts of these terranes underwent greenschist facies metamorphism during Late Jurassic subduction-collision to form the Otago Schist.

The metamorphic climax in the Rangitata Orogeny was when the medial spreading zone passed into the westerly subduction zone, thus permitting the convergent zones to collide, with the Torlesse sediments caught between them (Wood, 1978). This spreading system continued to function, and soon after this collision caused Late Jurassic-Cretaceous rifting of the siliceous edge of Gondwanaland. Uplift and cooling persisted through most of the Cretaceous, and following metamorphism, the Otago Schist was exposed by mid-Cretaceous

extensional faulting and then deformed by late Cenozoic oblique compressional faulting, related to the inception of a Pacific-Australia plate boundary (the Alpine Fault) through the New Zealand continent (Mortimer, 1993). Sea-floor spreading then commenced in the Tasman Sea and later in the southwest Pacific Ocean (Wood, 1978).

Mortimer (1993) confirms the original concept of the Otago Schist resulting from the mutual collision of the Caples and Torlesse terranes in the Rangitata Orogen by stating the following points:

1. The two-sided aspect of the Otago Schist belt with high-grade rocks flanked by low-grade rocks to the northeast and southwest. High grade rocks (greenschist facies metamorphism) occur along the regional antiform axis (figure 2.1) with rocks grading into pumpellyite then to prehnite facies metamorphism further away from the fold axis. The high grade to low grade sequence occurs on both sides of the fold axis, hence the two-sided aspect.
2. The inferred thrust-dominated geometry of the Caples terrane on the Torlesse terrane.
3. Concentration of ultramafic pods close to the terrane boundary.
4. Stretching lineations at different structural levels in the schist that indicates a single, consistent kinematic picture throughout the metamorphic pile.

In addition, Mortimer (1993) proposes the Livingstone Fault and Median Tectonic Line are potential candidate structures along which Early Jurassic strike-slip motion may have been accommodated.

2.3 TERTIARY COVER DEPOSITS.

2.3.1 Tertiary Sediments.

2.3.1.1 General.

Between the end of the Rangitata Orogeny (Early Cretaceous, 125-90Ma, when sea-floor spreading began in the Tasman Sea) and the middle of the Tertiary Period, the area that is now Otago was gradually eroded, forming a peneplain. The Te Anau Basin was extended towards the west and produced a brief marine transgression, and the sea extended over what is now the Wakatipu Basin. Small remnants of Tertiary (upper Oligocene to Pliocene) sedimentary deposits of marine and lacustrine origin (limestones, sandstones, mudstones and

lignite) are found bordering the Wakatipu Basin at Bobs Cove (figure 1.1). The deposits (Oligocene marine limestones) extend now as narrow exposures for 40km in a general north-south direction along the Moonlight Fault as far as the upper Shotover River (Rosen et. al., 1997).

Evidence from the Te Anau region to the southwest implies that the sea had retreated from the Queenstown area by the mid-Miocene, so it is likely that the arm of the sea that followed the Moonlight Fault only lasted about ten million years (Turnbull and Forsyth, 1988).

2.3.1.2 Marine Sediments.

Sediments were deposited as a result of the mid Tertiary marine transgression at Bobs Cove as the sea encroached from the west. They consist of a sedimentary sequence at least 450 metres thick, with beds of breccia (angular, cemented gravel), mudstone, sandstone, limestone and interlayered conglomerate and more breccia. Nearly all contain fossils of marine origin (lower to mid-Cenozoic in age) – bivalves, gastropods, corals and algae. The beds have been folded into synclines and anticlines plunging south into Lake Wakatipu.

Turnbull et. al., (1975) divided the sediments of the Bobs Cove beds into three natural subdivisions from a depositional point of view:

1. An early phase of faulting in the Oligocene caused the sudden depression of the Bobs Cove area to shallow "shelf" depths below sea level. The topographic depression was partly fault-bounded, and from Bobs Cove, fans of schist detritus reached into the sea.
2. Following faulting was a brief period of relative stability during which shallow shelf marine sediments were deposited (suitable habitats for invertebrate assemblages).
3. Renewed subsidence of the marine basin was caused by further movement on the boundary faults. Terrigenous material and sea-floor bioclastic detritus were transported towards the Bobs Cove basin down steep submarine slopes by inertia-flow and turbidity flow.

The general environment of deposition was thus a submarine slope leading towards a flysch basin, probably in the deep marine environment out to the west (Turnbull et. al., 1975).

2.3.1.3 Fluvial and Lacustrine Sediments.

As the rate of tectonic uplift increased with the advancement of the Kaikoura Orogeny, and as drainage became better integrated, there was rapid erosion along the actively rising fault scarps bounding the major basins of Central Otago (Arrowtown, Gibbston, Victoria, Cromwell, Lower and Upper Nevis Basins, see figure 2.5). The Maori Bottom Gravels (piedmont gravels) were deposited in the Plio-Pleistocene (~2Ma), thus forming an angular unconformity over the Manuherikia Group (lacustrine sediments). Within the Cromwell Basin these gravels consist mainly of rounded, low metamorphic grade, schistose greywackes derived from the upstream reaches of an ancestral Clutha River (Bell, 1982).

Further to the east of Bobs Cove, sediments are preserved along major faults that cross the Kawarau Gorge and Crown Range (figure 2.1). The sediments are known as the Manuherikia Group (Miocene in age), and remnants occur at Coal Pit Saddle and near Crown Saddle. These deposits formed from freshwater lakes, streams and coal swamps during the marine transgression from the east, south and west on to the Tertiary peneplain surface (which had been eroded into the Otago schist). This indicates that the limit of the marine transgression has to lie between Bobs Cove and Crown Saddle.

Fluviatile erosion of both Plio-Pleistocene and Miocene strata has taken place, and localised upturning of Maori Bottom Gravels at the fault-bounded basin margins indicates the continuation of Kaikoura diastrophism (Bell, 1982).

2.4 QUATERNARY GEOLOGY.

2.4.1 Kaikoura Orogeny.

Deformation during the Plio-Pleistocene times of the Kaikoura Orogeny (which began in the Miocene) was dominated by faulting in the basement rocks with locally strong folding of the covering strata throughout Central Otago. The fault pattern indicates vertical uplift instead of lateral shortening or extension, with the reactivation of older (Cretaceous) normal faults, generally with a reversal in the sense of movement (Bishop, 1974). Bishop suggests A large proportion of the regional strain is accommodated by 10km scale antiforms and synforms in

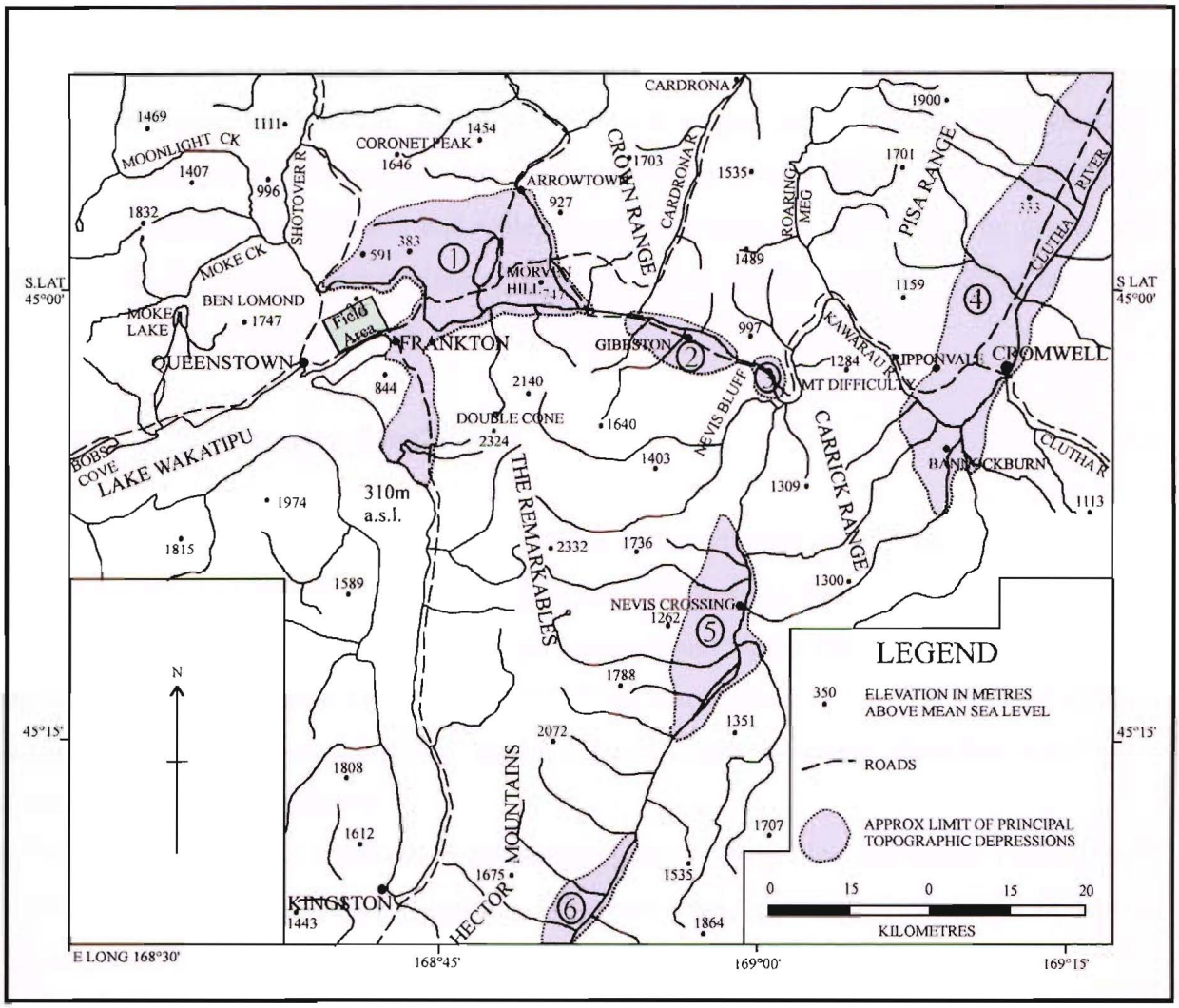

Figure 2.5: Map of the Kawarau and tributary valleys, showing the modern drainage pattern, spot heights and roads. The topographic depressions shown are: 1 - Arrowtown Basin; 2 - Gibbston Basin; 3 - Victora Basin; 4 - Cromwell Basin; 5 - Lower Nevis Basin; 6 - Upper Nevis Basin (redrawn from Bell, 1985).

foliation within the schist, however overthrust and/or horizontal offset relations can be seen at a number of faults. The fact that range-front faults and folds affect Miocene strata constrains most of the deformation to be Miocene or younger (Mortimer, 1993).

Barrell et. al., (1994) notes the possibility that the Wakatipu Basin could be a downfolded area that has been cut into and modified by glacial action, but not principally formed by erosion. Alternatively, they suggest these areas may have been uniformly uplifted during the Kaikoura Orogeny and the basin and valley areas have been entirely formed by glacial and river erosion, leaving the surrounding ranges standing as remnants of the uplifted land. It is not known which model is correct.

2.4.2 Quaternary Glaciations.

There is evidence for at least four major periods of ice advance and retreat in the Wakatipu Basin over the last 500,000 years. Bell (1977) points out the fact that reliable correlation between the glacial advances in the adjacent Kawarau and Upper Clutha valleys has yet to be made, and goes on to state Late Pleistocene glacial correlations in the South Island of New Zealand have been unsatisfactorily related. The glacial advances identified within the Kawarau Valley are as follows:

1. Pre-Waitiri Advance: Ice limits may have been the Roaring Meg and Athol. The ancestral Shotover River was flowing north of Coronet Peak, and deposited 150m of fluvial sediments in Deep Creek.
2. Waitiri Advance: Ice extended down the Oreti and Mararoa valleys, down the Kawarau Valley to Waitiri, over the Crown Terrace (600m above sea level) and up the Arrow River. The Crown Terrace may be a remnant of the valley floor during the Waitiri Advance.
3. Gibbston Advance: This is considered to be the Late Otiran Maximum of the Wakatipu Glacier system in the Kawarau Valley and was at a maximum prior to 25000 years ago. Following interglacial status (the Oturian) at greater than 45000 years before present, ice again pushed into the Von as far as the South Von area, down the Kawarau to Gibbston and south to Kingston and beyond.
4. Post Gibbston Advance: Occurred 18000 years ago (figure 2.6). Ice covered most of the Arrow Basin, but only reached as far as Kingston. The post-Gibbston glacial advance is

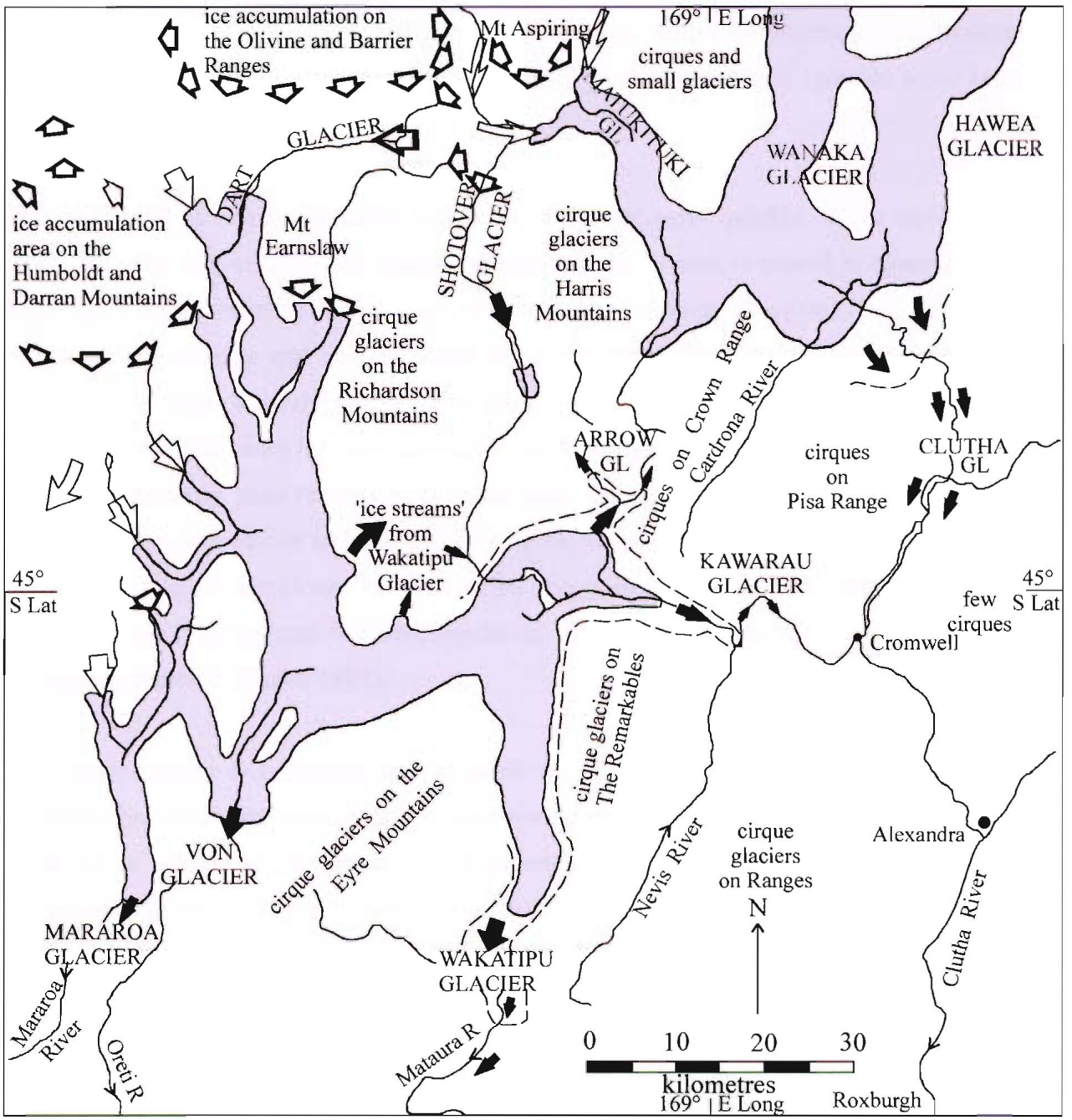

Figure 2.6: Map showing maximum ice limits for the Last (stippled) and Penultimate (dashed) Glaciations in the Wakatipu and Clutha catchments. Open arrows show the approximate directions of ice movement away from the snow accumulation areas, and the infilled arrows indicate the resultant glacier patterns (Bell, 1992).

responsible for the majority of glacial deposits within the Wakatipu Basin (Turnbull and Forsyth, 1988; Cunningham, 1994). The depression now occupied by Lake Hayes may have been excavated at a late stage in the Otiran, and there is evidence for a prominent former lake shore 45m above the present level of Lake Wakatipu (present level 310m above sea level).

The waning of the Otiran Glaciation is thought to have occurred quickly, with a rapid retreat of the ice. The beginning of the present interglacial, the Aranui, is placed at approximately 14000 years ago, when the final Otiran advance began receding (Suggate, 1990). This date marks the approximate end of the coldest phases in the South Island although very minor advances and retreats are thought to have taken place on the east side of the Southern Alps from 14000 to 8000 years BP. An extended Lake Wakatipu was dammed behind the terminal moraine at Kingston after retreat of Last Glaciation (Otiran) ice, with the lake level reaching approximately 45m above the present lake level. Creeks flowing into the enlarged lake produced fan-delta complexes, which can be recognised at the higher lake levels. Lake Wakatipu was progressively lowered, producing successively lower wave cut benches and fan-delta complexes (Watts, 1988).

The Crown Terrace is interpreted as a remnant of the Penultimate Glaciation valley floor of the Wakatipu Basin, its outer (western) part revealing ice-shorn schist bedrock on which is preserved a veneer of weathered till deposited both as ground and ablation moraine. Successive phases of glacial erosion have worked to maintain the basin floor at a similar elevation relative to sea level, however ongoing uplift of the region has resulted in the higher elevation of the Crown Terrace relative to the present day basin floor (Bell, 1982).

At the southern end of Lake Wakatipu, a drainage outlet through the Kingston Moraine (figure 2.1) was established at about 400m above sea level, and progressively became incised through the glacial deposits, eventually reaching schist bedrock at about 355m above sea level. There was a major standstill in lake level at about 45m above the present lake level, with the development of prominent beaches. The Kingston outlet was eventually abandoned as the Kawarau River outlet became incised to lower elevations (Bell, 1982).

It has been suggested that the Kawarau outlet was not in existence as a bedrock ridge existed south of Morven Hill to the foot of The Remarkables (figure 2.7). The Shotover River then became entrenched into bedrock south of Morven Hill, lowering its elevation by the amount necessary to capture the outflow from Lake Wakatipu through Frankton Arm (possibly about 5000 years ago). As the lake level lowered to its present level, several poorly defined intermediate-level beaches were cut, and many of the streams and rivers have cut flights of terraces into their fan/delta deposits as they readjusted to maintain grade to the diminishing lake. The deposits of the Shotover fan/delta complex impounded Lake Hayes as the lake levels fell (Bell, 1982; figure 2.7).

2.4.3 Glacial and Related Deposits.

Quaternary sediments such as glacial till form a veneer on the slopes of the hills and cover the floor of the Wakatipu Basin. Within the Wakatipu Basin the deposits are derived from the schist, with a significant proportion (up to 30%) of greywacke gravel from the Caples Group sediments. The glaciers that existed within the basin progressively scoured and then 'dumped' the eroded debris as moraines. This debris can be seen today in the Kawarau Gorge at Gibbston and Waitiri, southwest of Mt. Nicholas in the Oreti Catchment, and beyond Kingston and Garston south of the present Lake Wakatipu. Successive ice advances were progressively smaller, so their terminal moraines are now found upstream from the maxima of earlier advances. The oldest ice advance reached Athol or beyond and had ice up to 1000 metres above the present lake level (Turnbull and Forsyth, 1988). After the retreat of late Otiran ice from the Gibbston Basin, ice is thought to have occupied the Arrowtown Basin, but complex stadial and interstadial events may have taken place. Younger moraines have been found near Arthurs Point and at Wye Creek, and the depression occupied by Lake Hayes was almost certainly excavated by ice advancing through Frankton Arm during post-Gibbston times (Bell, 1977).

Lateral moraine remnants can be found at Brackens Gully, at 900 metres elevation, 4km east-northeast of Arrowtown. These deposits consist of unweathered to slightly weathered variable sands and gravel, interpreted to be ice-margin sediments and ablation till. Lodgement till and ablation tills can be found along Frankton Arm, with most remnants containing some silt, schist and Caples boulders. The majority of the till is composed of massive compact sandy

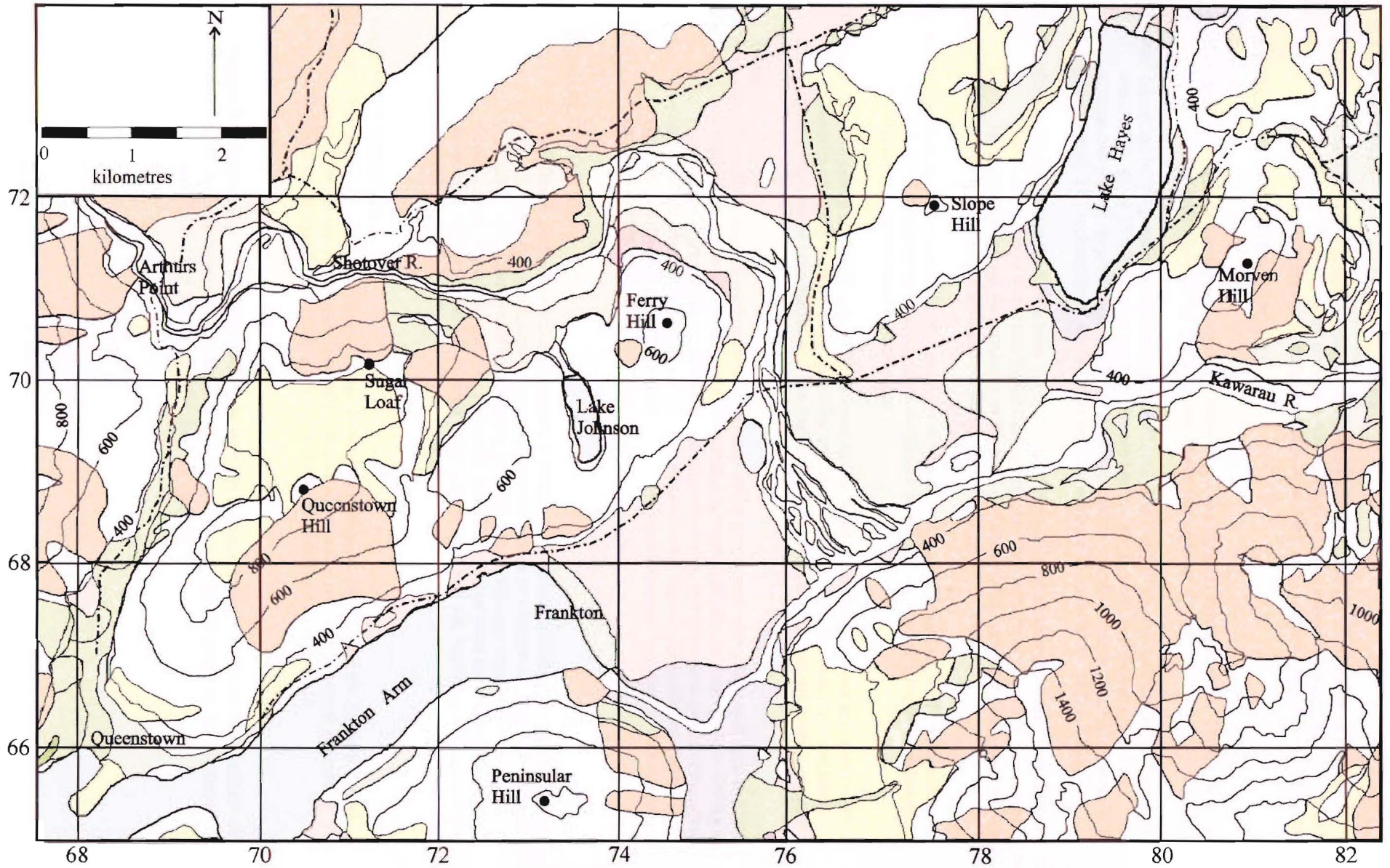

Figure 2.7: Surficial geology of the Wakatipu Basin(redrawn from Barrell et. al., 1994) . Key is on the next page.

SLOPE DEPOSITS KEY

Landslide: Gravitationally displaced materials, typically characterised by the presence of hummocky topography. Predominantly comprise schist debris and schist-derived materials. Thickness may range from a few metres to many tens of metres. May include extensive cover of colluvium.

STREAM, RIVER AND LAKE DEPOSITS.

Recent
Floodplain: Unvegetated or poorly vegetated, low-lying areas adjacent to major rivers. Comprise generally loose sands and gravels. Prone to inundation during large floods.

Fan: Identified by the presence of fan-shaped landforms. The slope of the fan surfaces range from less than 10° to about 25°. Typically, the deposits are layered sandy gravels with some silt. The coarse component ranges in size from fine gravel to boulders, and ranges in shape from angular to subrounded. The inclination of the layers is broadly subparallel to the slope of the fan surface.

Fan/Delta: Formed where fans have built out into lakes. Principally developed at a time when Lake Wakatipu was at levels up to 80 metres higher than at present. The deposits are typically dominated by well layered sandy gravel, in proximity to the head of the fan/delta, generally fining to layered sand and silt with increasing distance from the ancient shoreline.

Lake: Found extensively near Lake Hayes and to the south and east of Peninsular Hill. Predominantly consist of subhorizontally layered, thinly to thickly bedded, micaceous silt, locally containing significant amounts of calcium carbonate.

Beach: Overlie gently sloping benches cut by wave action when Lake Wakatipu was at higher levels. Deposits comprise layered sandy, gravelly, and locally silty, sediments, ranging in thickness from a few tens of centimetres to a few metres. Linear storm beach ridges are locally present.

Terrace
Alluvium: Typically consist of subhorizontally layered sandy gravel with minor layers of sand and silt. Generally underlie gently-sloping (<5°) terrace surfaces. Includes outwash gravels developed downstream from glacial moraines (aggradation deposits), and gravelly deposits underlying lower level terraces incised into outwash gravels or older deposits (degradation deposits). Aggradation deposits may be up to tens of metres thick, whereas degradation deposits may be as thin as one or two metres.

GLACIAL DEPOSITS

Undifferentiated unit which incorporates a variety of materials including till (deposited by glacier ice) and ice-margin sediments (laid down by water beside or beneath the ice). Tills are generally unstratified and comprise either compact, gravelly, sandy, silt-clay, deposited at the base of the glacier (basal till), or loose clayey and sandy gravel, deposited from melting ice (ablation till). Ice-margin sediments include layered sandy gravel, sand and silt, typically with contorted or deformed layers.

BASEMENT GEOLOGY.

Schist: The predominant underlying rock type, formed by metamorphism during the Jurassic Period (about 200 million years ago). Typically comprises laminated rock composed of alternating light-coloured (quartz and feldspar-rich) and dark-coloured (mica-rich) layers.

Figure 2.8: Geological key of Figure 2.7. Map from Science Report 94/39 of the Institute of Geological & Nuclear Sciences Limited. Geological information obtained by R. Thomson, V.J. Cunningham, B.W. and P.M. Riddolls, and D. Barrell.

gravels or gravelly sands. Along the western margin of the Crown Terrace, at elevations of between 600-700 metres, there are moraines composed of slightly weathered, compact basal till and loose ablation till. Across the Kawarau River from the southern end of the Crown Terrace, near Cowcliff Hill, till and ice-margin sediments occur at elevations of between 470-510 metres, overlain by lake sediments and terrace alluvium (Barrell et. al., 1994. For locations refer accompanying map in Barrell et. al., 1994 and Figure 2.7).

2.4.4 Fluvioglacial Deposits.

During the successive advances and retreats of the Otiran Glaciation the Wakatipu Glacier deposited lodgement till directly on to bedrock. Outwash gravels were deposited by streams flowing from terminal moraines, and the sediment carried by the glacier was also deposited in streams flowing at the sides of the glacier as kame terraces. During the waning stages of the Last Glaciation successively lower kame terraces and ablation till were deposited and alluvial fans were deposited by streams flowing down the steep glacial valley sides (Watts, 1988).

Large amounts of gravel and sand were released into melt-water rivers at the end of the Last Glaciation. The material is built up into outwash plains, such as those beyond Kingston and southwest of Mt. Nicholas. The terraces and flats of the upper Clutha Valley toward Lake Wanaka are outwash plains from the Wanaka and Hawea glaciers, as are the flat valleys of the Dart and Rees rivers at the head of Lake Wakatipu (Turnbull and Forsyth, 1988).

2.4.5 Glaciolacustrine Deposits.

Various stream, river and lake deposits are exposed in the Wakatipu Basin. Terrace alluvium, which include different combinations of gravel, sand and silt, underlie a discontinuous set of terraces which extend around the northern and eastern margin of the Arrowtown end of the Wakatipu Basin and into the Gibbston Basin. Terrace alluvium also occurs along the Shotover River in localised areas to the west of The Remarkables (Barrell et. al., 1994). Along Frankton Arm, sandy fine and medium sands and gravels laid down by lakes, rivers and glacial outwash streams and clayey to gravelly silts deposited at the bottom of the elevated Lake Wakatipu have all accumulated throughout the Quaternary.

Raised beaches are well developed along the glacial lakes in the Otago region, particularly along Frankton Arm. Discoidal pebbles and gravels have been deposited on wave-cut benches formed at elevations where the lake level has progressively lowered during the last 10000 years. Stream fans or deltas may become benched as the lake level falls, for example the Shotover River delta which was built out into Frankton Arm when Lake Wakatipu was 60 metres higher than its present level (Turnbull and Forsyth, 1988).

Alluvial fans are extensively developed on the lower slopes of the Wakatipu Basin. The character of the deposits underlying fan surfaces is variable, and is influenced by stream size and the geology of the stream catchment. Sandy and muddy gravels deposited by alluvial fans have formed in places around Frankton Arm. The Shotover River fan/delta isolated the Lake Hayes basin from Lake Wakatipu, and fan/delta deposits have left Lake Hayes impounded at 20 metres higher than the present level of Lake Wakatipu (Figure 2.7; Barrell et. al., 1994).

Lake sediments occur in exposures around Lake Hayes and also occur at a variety of elevations east of Morven Hill and in the Gibbston Basin (see Barrell et. al., 1994 - map 1). The lake sediments consist of thinly bedded (<60mm) micaceous silt, locally with interbedded thin layers of fine sand. These sediments also occur from Frankton to the south and east of Peninsula Hill and are inferred to grade laterally into fan/delta deposits towards The Remarkables. In the area east of Morven Hill there are isolated occurrences of lake sediments which are thought to pre-date the deposits of post-glacial enlarged Lake Wakatipu (Barrell et. al., 1994).

Beach sediments occur at a variety of elevations along Frankton Arm, ranging from 400 metres elevation down to below present lake level (figure 2.9). They are primarily concentrated at about 355 metres elevation, which represents a long stand of the lake at this level (Barrell et. al., 1994).

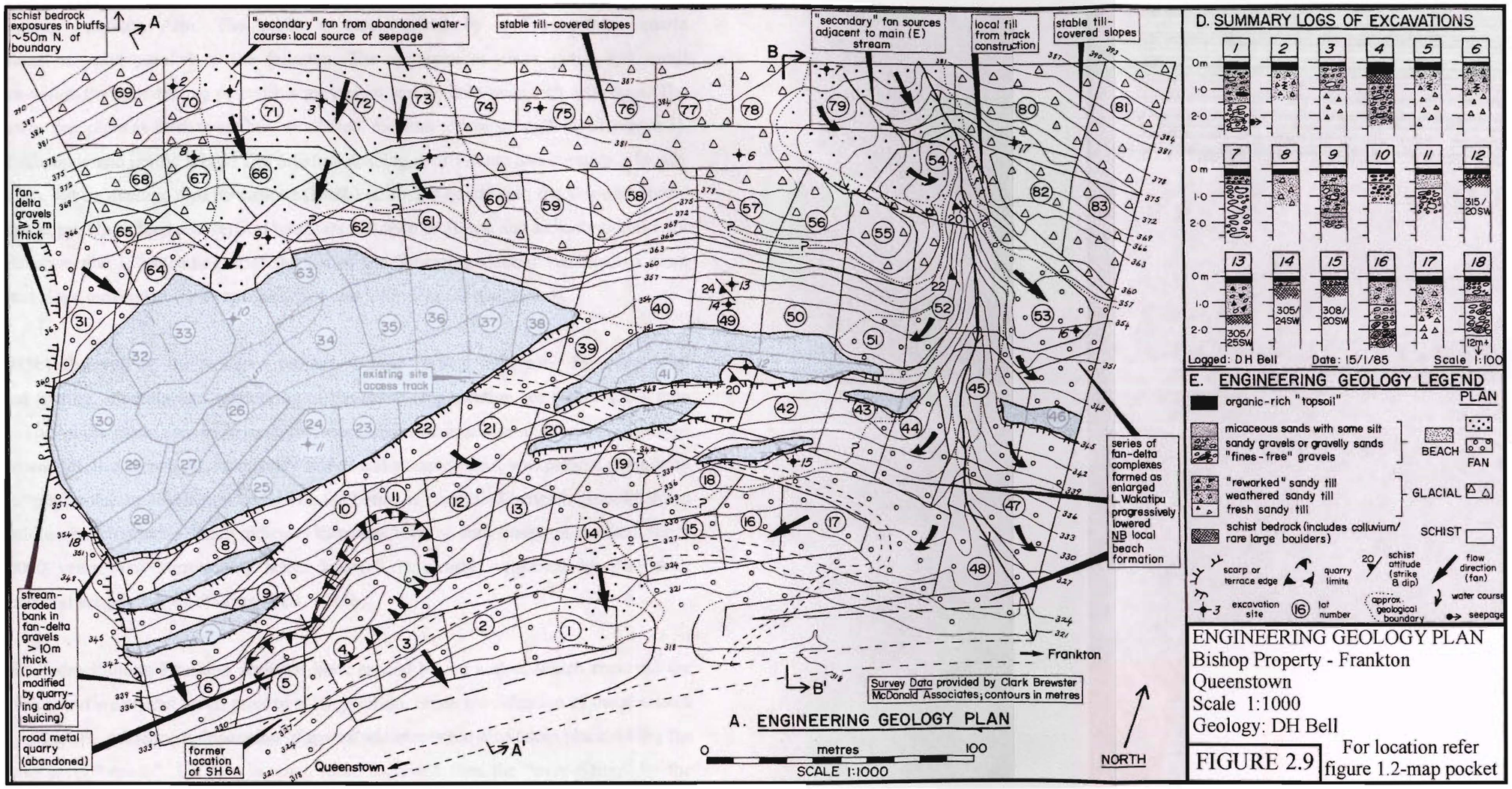

ENGINEERING GEOLOGY PLAN
Bishop Property - Frankton
Queenstown
Scale 1:1000
Geology: DH Bell

FIGURE 2.9 For location refer figure 1.2-map pocket

2.5 THE GEOLOGY OF FRANKTON ARM.

2.5.1 Bedrock Geology.

Two varieties of greyschist (psammitic and pelitic) and minor outcrops of greenschist are present along Frankton Arm. The schist is characterised by millimetre-thick quartz segregations or veins parallel to the foliation. The segregations show pinch and swell structures within the surrounding psammitic greyschist and contain mica-rich selvedges. The schist can be described as fresh to slightly weathered, medium to low strength (see Chapter 3), quartzofeldspathic and pelitic schist. The foliation spacing is of 1-5mm and contains a locally variable dip, but on average dips downslope (south) at 20-30° controlling the slope geometry and morphology. Up to four sub-vertical joint sets are open to 10mm and indicate minor rock mass relaxation due to unloading after the ice of the Wakatipu Glacier retreated or from subsequent slope movement (refer to Chapters 4 and 5 for detailed discussion).

Bell (1985b) observed on the Newman property a near vertical fault zone 3m wide, with associated folding, shearing and weathering of the schist (for location see figure 1.2 – map pocket). This fault zone can be traced for more than 1km across the lower slopes of Queenstown Hill. In a trench pit, intensively folded and sheared schist was present along with clay-rich "pug" zones up to 150mm wide. The fault zone is concealed beneath glacial till and high level lake beach gravels which indicates there has been no movement on the fault for at least 10000 years. The surrounding schist bedrock is clearly weakened by past fault movements and subsequent weathering (Bell, 1985b).

The schist bedrock along Frankton Arm has been eroded by ice action, which removed the upper weaker and weathered schist prior to till deposition. Some modification of the glaciated bedrock surface by subsequent deposition of glacial sediments has also taken place during the higher lake level "stands", but this is much more localised than the "over-riding" by the Kawarau lobe of the Wakatipu Glacier. In addition, wedge failures occurring up slope of the Marina Heights subdivision, and further east were controlled by the intersection of favourably oriented joints and foliation, and probably relate to ice retreat or perhaps episodic lake lowering in postglacial times (Bell, 1985a).

2.5.2 Surficial Deposits.

2.5.2.1 Glacial Deposits.

Glacial till discontinuously covers ice-eroded schist bedrock along Frankton Arm in map view, and in places is 1-3m thick (figure 1.2 – map pocket). The till is typically sandy gravel (ablation) or gravelly silt (lodgement) and in some areas schist and Caples boulders are present within the till.

The till often outcrops above the +45m lake beach level. Locally, the sandy gravels are loose due either to reworking or to deposition as ablation till. In some of the deeper profiles of till, lenses of water-sorted fine-medium sands are present. The effect of weathering has been to turn the fine soil fraction slightly to moderately plastic (which infers that some clay is present) (Bell, 1985a).

2.5.2.2 Post-Glacial Deposits.

Lake margin sediments overlie the glacial till in places, and occur at six or seven different elevations, respectively about 45, 35 and 15m above present lake level. All three lake levels are cut into schist bedrock and the thickness of interlayered sands and gravels is typically 1-2m on the upper two beach levels, while on the lower surface the deposits may be up to 5m thick.

Lake silts outcrop in small measures beneath lake margin gravels, and represent lake bottom sediments deposited during the highest lake level.

Alluvial fan gravels and sands have been deposited by streams as the lake progressively lowered. The fan gravels, which include highly weathered schist blocks and Caples Group boulders (0.5m maximum dimension), post-date the formation of the upper lake beach surface. 'High-angle' fan deposits have formed contemporaneously with the highest lake level (+45m). These fan gravels contain lenses of fine to medium sand between layers of sandy gravels and more open-textured 'fines-free' gravels (Bell, 1985a).

Schist colluvium outcrops along the eastern margin of Marina Heights (Slide No. 3) and the north-west corner of Hensman property (figure 1.2 – map pocket). This deposit is derived from shallow or exposed bedrock and post-dates the formation of the upper beach surfaces. The colluvium is slightly to highly weathered, massive, medium to coarse sandy gravel with interlayered medium sand.

2.5.3 Geomorphological Evolution.

The Frankton Arm of Lake Wakatipu was excavated by the Kawarau Lobe of the Wakatipu Glacier, with the ice extending through to the northern end of Lake Hayes during the late Otiran advance 18000 years ago (Bell, 1985a). In the earlier Gibbston advances the glacier overrode the sides and summit of Queenstown Hill and Deer Park Heights, leaving "freshly" glaciated topography, that is, largely unmodified by water or subsequent erosion. The effect of glaciation has been to "strip" the weaker pelitic schist from the slope to form an irregular profile controlled by the southwest dipping foliation attitude and various joint sets, thus exposing fresh bedrock to post-glacial weathering within the last 14000 years (Bell, 1985a).

Before and during the retreat of the Wakatipu Glacier in the period 15-10000 years ago, sandy ablation till and silty lodgement till was deposited as a discontinuous veneer (up to 3m thick) over the irregular ice-shorn bedrock surfaces. The lodgement till contains a finer grain size as a result of the grinding action beneath the sole of the glacier, whereas the ablation till was deposited directly from the ice as it ablated. Post-glacial weathering commenced 10-12000 years ago causing a typical brown soil profile which grades into fresh sandy till below a depth of 800-1200mm (Bell, 1985a).

Most of the ice-generated landforms preserved in the Wakatipu Basin are those formed during the Gibbston Advance (prior to 25500 years ago). Typical landforms included the bedrock troughs that form Lake Wakatipu, Lake Hayes and Lake Johnston, the faceted hills, the ice-rounded roches moutonnees (for example Ferry Hill and Peninsula Hill), and the low, mamillated ridges within the basin, the truncated spurs of the surrounding ranges, and the very prominent Crown Terrace surface and terrace scarp. Glacial depositional features include kame and outwash terraces, moraines and perched erratics (Cunningham, 1994).

In earlier ice advances the Glacier overrode the shoulders and summit of Queenstown Hill, and a shallow topographic depression or hanging valley was formed behind the summit of Queenstown Hill (figure 2.10), with a series of arcuate transverse ridges (open towards the west) leading down into the valley (Cunningham, 1994). Exposed in a stream in this valley at 750m above sea level are 4m of light grey, compact, massive, sandy fine to medium gravel with some cobbles, overlying bedrock. This has been interpreted by Cunningham (1994) as the Sugar Loaf and Queenstown Hill Till, and Wood (1962) included them in his Camp Hill Formation. The gravel was interpreted as a till deposit on the basis of its massive, compact nature, and the abundance of greywacke clasts. The arcuate ridges are interpreted as end moraines deposited as ice retreated towards the west (Cunningham, 1994).

The elevation of these tills between 720 and 900m suggests they may be comparable in age to the Gibbston (late Otiran Glaciation) glacial advance. Wood (1962) classified the Camp Hill Formation as contemporaneous with the Hawea Glacial Advance, which also took place in the Otiran Glaciation. Wood (1962) (in the Wakatipu Sheet 22), places Camp Hill Formation mainly in the Clutha Catchment, particularly around Wanaka and Lake Hawea, and outcropping as far south as Bannockburn.

Two advances are inferred to have surrounded and over-ridden Queenstown Hill, advancing from the southwest along Frankton Arm (figure 2.11). The first advance is presumed to have overridden the top of Queenstown Hill during the Kumara 2 (Gibbston Advance), forming the hanging valley. The second advance occurred during the Kumara 3 (Gibbston Advance), and was not as extensive as the previous advance thus only moved along the south face of Queenstown Hill. This advance led to the formation of ice-carved benches on the south face of Queenstown Hill at 500 and 700 metres above sea level. The arcuate transverse ridges of Cunningham (1994) represent a series of end moraines deposited as the ice retreated back to the southwest. Two major terminal moraines are situated at 840m elevation and an earlier moraine deposited at 880m above sea level (figure 2.10). A number of secondary end moraines exist in addition to the major moraines, and represent a temporary pause in glacial retreat towards the west. The deeply incised gully between Sugar Loaf Hill and K No. 2 trig represents a subglacial meltwater channel that drained the ice on top of Queenstown Hill. The gully between Queenstown Hill and Marina Heights also acted as a meltwater channel.

Figure 2.10: Glacial topography on Queenstown Hill showing various end moraines, relict drainage channels and outwash areas.

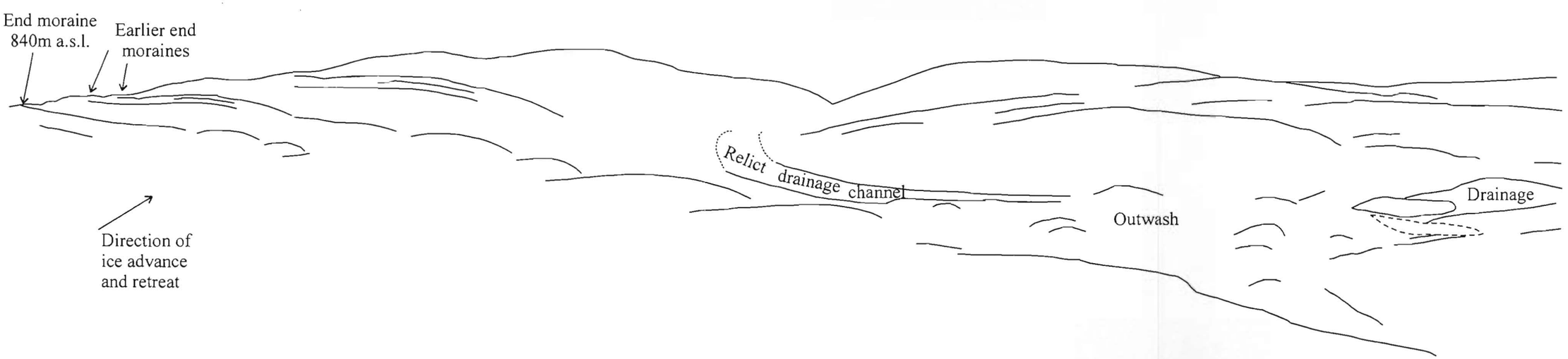

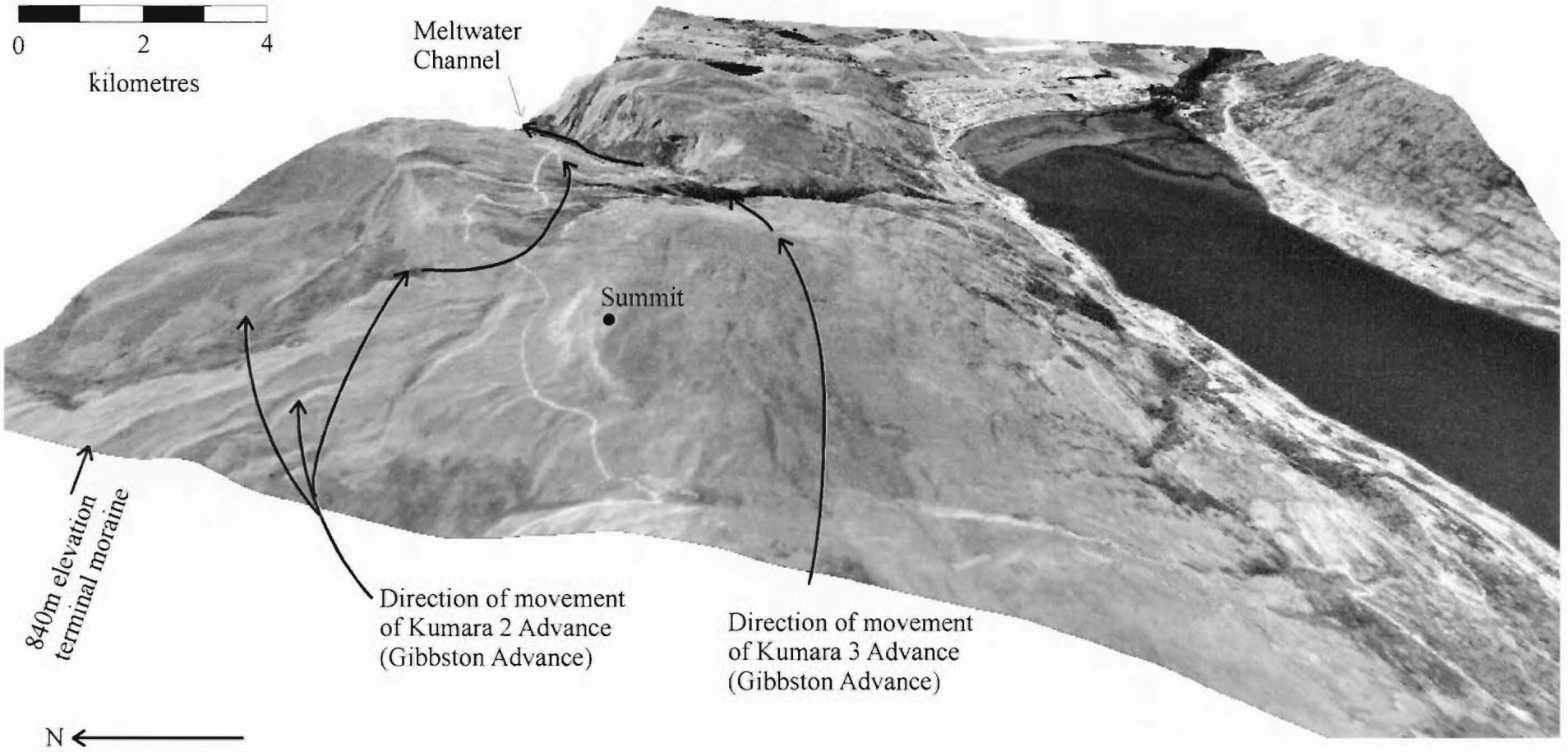

Figure 2.11: Computer-generated 3-dimensional oblique visualisation of Queenstown Hill showing glacial topography and directions of ice movement (generated by *Visual Explorer 98*).

An enlarged Lake Wakatipu formed during the early stages of ice retreat, depositing lake beach deposits at various elevations (42, 35, 27 and 23m) above the present lake level, with terraces forming by wave action, and these are extensively developed along the northern side of Frankton Arm (see figure 2.7). These shorelines represent the progressive lowering of the lake as the Kawarau outlet downcut from the prominent +48m lake level in the last 10000 years (Bell, 1982). Tributary streams draining into the lake at this higher elevation formed fan-delta complexes, and the major Shotover delta (on which Frankton Airport is located) was also constructed at this time (figure 2.12; Bell, 1985a).

When the lake elevation reached the +25m level it is likely that the Kawarau outlet had become established, and subsequent lowering is therefore related to incision of the Kawarau River into the Shotover delta sediments. The abandonment of the Kingston outlet may have occurred as recently as 5000 years ago (Bell, 1985a).

2.6 SYNTHESIS.

- Otago Schist, formed in the Rangitata Orogeny, is composed of two rock types – quartzofeldspathic schist and green schist, representing metamorphosed sedimentary and volcanic rocks respectively.

- Within the Caples terrane, textural zones occur as bands, with zone IIIB occurring as a transition between the Caples and Torlesse terranes.

- Remnants of a mid-Tertiary marine transgression are preserved at Bobs Cove. These sediments contain fossils of marine origin. A paleogeographic and tectonic boundary has been inferred by Turnbull (1975) to run east of the Moonlight Fault Zone because at the same time Manuherikia Group lacustrine sedimentation continued unchanged on the schists to the east.

- Quaternary sediments are derived from schist and contain up to 30% Caples Group sediments incorporated by glacial action.

Figure 2.12: The Shotover River fan-delta with Lake Johnson in the left centre, and Coronet Peak in the background. Photo by L. Homer.

- Regional southeasterly structural trends in Otago and Southland reflect orientations resulting from the Rangitata Orogeny such as the Moonlight Fault Zone, whereas the northeasterly faults and folds represent Cenozoic deformation.

- Tectonic movements of the Kaikoura Orogeny resulted in differential uplift of the basement, producing the "basin and range" topography of Central Otago. The Wakatipu Basin is a downfolded area that has been cut into and modified by glacial action.

- There is evidence for at least four major periods of ice advance and retreat in the Wakatipu Basin (from approximately 500000 years BP to 15000 years BP), with deposits dating from the Waimean (180000 years ago) and Otiran Glacial Periods preserved.

- The Frankton Arm of Lake Wakatipu was excavated by the Kawarau Lobe of the Wakatipu Glacier during the late Otiran advance 18000 years ago (post-Gibbston). In earlier Gibbston advances the ice overrode the sides and summit of Queenstown Hill.

- Glacial till was deposited as a discontinuous veneer over schist bedrock before and during the retreat of the Wakatipu Glacier 15-10000 years ago.

- During and following ice retreat (about 15000 years ago), Lake Wakatipu was at a greater elevation and was more extensive than at present, as evidenced by high level beaches, extensive deposits of lacustrine silts and fine sands, and high level truncated fan-deltas and alluvial fans. Progressive lowering of the lake water level continued until the lake reached its present level sometime after 5000 years ago.

CHAPTER 3

ENGINEERING GEOLOGY INVESTIGATIONS.

3.1 INTRODUCTION.

The engineering geological field investigations and the results of the rock and soil characterisation carried out as part of this study are presented in this chapter. The fundamental aim of the field investigation was to obtain information that was relevant to landslide stability. Background studies such as aerial photograph interpretation, field investigation and laboratory testing were done in order to obtain representative properties of the bedrock and related instability along Frankton Arm. The focus was on bedrock properties because landsliding along Frankton Arm occurs within the schist bedrock.

The objectives of these investigations were to carry out:

1. Engineering geological mapping of the major failures along Frankton Arm at scales of 1:5000 and 1:10000, with subsequent construction of failure models;
2. Laboratory testing of intact schist bedrock and shear zone material collected during field work to provide strength characteristics to assist in the interpretation of the failure mechanisms of the landslides along Frankton Arm;
3. Defect surveys at the Commonage Subdivision, to analyse defect sets within the Otago schist bedrock, and to undertake Slope Mass Rating calculations for the Queenstown/Frankton Arm area.

3.2 INVESTIGATION METHODOLOGY.

3.2.1 Aerial Photograph Interpretation.

Aerial photograph enlargements covering the study area at scales of 1:5000 and 1:10000 were obtained from New Zealand Aerial Mapping Land Information Services. Photos used were Numbers 232477 and 232500, Run C, taken on the 23rd March 1956. Interpretation of these stereopairs and engineering geological mapping using air photo enlargements, were essential aids in identifying features on the ground surface, which in turn provide the key to understanding the details of landslide processes and causes.

3.2.2 Engineering Geological Mapping.

Field mapping had two main objectives:

1. To determine the distribution and extent of the landslides within schist bedrock; and
2. To establish failure mechanisms in bedrock for each landslide along Frankton Arm.

The engineering geological field data, including information obtained from aerial photograph enlargements and stereopairs, is given in figure 1.2 (map pocket). Mapping focused on landslide features such as scarps, cracks, bulges, disrupted topography and internal morphology. Attitudes of rock defects, such as foliation, joints and faults, were measured to determine the structure of the landslides. Defect spacing, roughness and continuity were also measured as a part of the defect survey.

Cadastral and topographic data were obtained from Terralink under license of Linz NZ Ltd to the University of Canterbury, and scales of 1:5000 and 1:10000 were taken off AutoCAD with contour intervals of 20 metres. The relevant NZMS 260 sheets are F41 (Arrowtown) and E41 (Queenstown).

In areas of dense vegetation, it was possible to infer landslide features, as the aerial photographs used were taken just over 40 years ago when vegetation was not as prolific. The vegetation hindered field investigation by preventing site access and obscuring landslide morphology, particularly on the lower slopes of Queenstown Hill and on Slide No. 3.

3.2.3 Field Investigation and Sampling.

Mapping of bedrock outcrops constituted the principal source of information on rock materials. Engineering geological descriptions of the various rock types were recorded in the field, and photographs were taken for future reference.

Bulk samples of selected rock and shear zone material were collected for laboratory analysis, including:

1. Point load strength of intact rock;
2. Shear strength of rock defects;

3. Residual strength of sheared rock material;
4. X-ray diffraction analysis for mineralogy of sheared rock material; and
5. Schmidt Hammer Hardness of rock defects;

The purpose of laboratory testing was to determine physical and mechanical properties that would help assess the stability and performance of these materials in the field. Schmidt Hammer readings were conducted in the field to determine approximate values for rock hardness, and thus joint wall compressive strength.

Six defect scan lines were carried out (in total just over 363m in length) along various exposures in the Commonage Subdivision, Queenstown (Section 3.5.2). These were used to obtain quantitative data on the defects within the Otago Schist that may contribute to the instability of the rock unit at this site.

3.3 GEOTECHNICAL CHARACTERISATION OF SCHIST BEDROCK.

3.3.1 Descriptions of Lithologies.

Three types of schist bedrock are present along Frankton Arm – quartzofeldspathic schist, pelitic schist and green schist. These rocks can generally be described as:

a. Slightly weathered; moderately strong; grey micaceous schist.

b. Fresh to slightly weathered; moderately strong to strong; grey quartzofeldspathic schist.

c. Fresh to slightly weathered; moderately strong to strong; green schist.

Schist bedrock outcrops discontinuously along Frankton Arm, and glacial till, alluvial fan gravels and sands, lake deposits, beach gravels, stream alluvium and schist colluvium all occur as a veneer overlying bedrock, in places with a thickness of up to about 5 metres (Bell, 1989). The rock mass is dominated by a pervasive schistosity with a mean foliation attitude of 107±30/25±5°SW for intact schist bedrock. For schist beneath the Queenstown Hill Landslide and the six smaller Frankton Failures, the strike parallels the arm of the lake (east-west), and variations in strike reflect the local warping and deformation of the bedrock. Bedrock typically dips to the south-southwest (down slope towards the lake) at low angles of 20±10°.

Master joint sets are well-developed in outcrop, and are typically open because of rock mass "relaxation" towards the free face by subsequent unloading. Two joint sets are present beneath the Queenstown Hill landslide, with attitudes of 145/85±5°SW and 220/90±5°NW. Along the entire length of Frankton Arm, four master joint sets exist, all of which are dipping sub-vertically (see Chapter 5).

3.3.2 Point Load Strength Testing.

Point load testing was carried out instead of uniaxial compressive strength because of the weak, highly foliated nature of the schist bedrock being tested. Coring of the samples was attempted in the Geological Sciences Rock Mechanics Laboratory, but as a result of low tensile strength the core kept breaking along the foliation, thus uniaxial compressive strength or triaxial testing could not be performed. The point load test was applied as smaller, more irregularly shaped samples could be used instead of core. $I_{s(50)}$ values obtained could then be correlated with those found elsewhere within the Otago schist.

Point load strength testing was undertaken following the method of Broch and Franklin (1972), and details of the test method and calculations are presented in Appendix F. Schist samples on which point load testing was performed consisted of square blocks and irregular lumps. Because of the anisotropic nature of schist, testing was carried out with the platens orientated parallel and perpendicular to the schistosity. The ratio of strength perpendicular to schistosity to that parallel to schistosity is the anisotropy index. The strength of intact rock specimens can vary by a factor of ten or more depending on the direction of loading relative to that of the weakness planes (Broch and Franklin, 1972). When load was applied parallel to foliation, failure occurred by splitting along the flat mica-rich foliation surfaces. In contrast, the failure of samples with load applied perpendicular to the foliation was highly irregular.

Test Results.

A summary of the point load test results is given in Table 3.1. $I_{s(50)}$ values ranged from 0.60MPa to 3.83MPa for samples tested perpendicular to schistosity, and from 0.11MPa to 0.92MPa for those tested parallel to schistosity. Using the point load strength classification proposed by Broch and Franklin (1972), these values would classify the rock as weak to strong. Average $I_{s(50)}$ values of 2.09MPa for samples tested perpendicular to foliation and

Sample	Test Type	W (mm)	D (mm)	P (kN)	$De^2(mm^2)$	De (mm)	I_s	F	$I_{s(50)}$(MPa)
1	Perpendicular	63	63	15.8	5053	71	3.12	1.17	3.66
2	Perpendicular	41	41	5.7	2140	46	2.67	0.97	2.58
3	Perpendicular	34.5	34.5	1.5	1515	39	1.02	0.89	0.91
4	Perpendicular	31	31	1.4	1224	35	1.11	0.85	0.95
5	Perpendicular	39	39	1.6	1937	44	0.81	0.94	0.76
6	Perpendicular	35	35	1	1560	39	0.67	0.9	0.6
~~7~~	~~Perpendicular~~	~~57.5~~	~~57.5~~	~~14.8~~	~~4210~~	~~65~~	~~3.51~~	~~1.12~~	~~3.95~~
8	Perpendicular	43	43	5.4	2354	49	2.28	0.99	2.25
9	Perpendicular	35	35	4.6	1560	39	2.92	0.9	2.62
10	Perpendicular	60	60	10.8	4584	68	2.36	1.15	2.7
11	Perpendicular	53.5	53.5	12.8	3644	60	3.52	1.09	3.83
~~12~~	~~Perpendicular~~	~~49~~	~~49~~	~~13.2~~	~~3057~~	~~55~~	~~4.32~~	~~1.05~~	~~4.52~~
13	Parallel	61.5	61.5	3.8	4816	69	0.79	1.16	0.92
14	Parallel	60	60	2	4584	68	0.43	1.15	0.49
15	Parallel	61.5	61.5	2.5	4816	69	0.51	1.16	0.6
16	Parallel	62.5	62.5	3.1	4974	71	0.63	1.17	0.73
~~17~~	~~Parallel~~	~~52.5~~	~~52.5~~	~~0.4~~	~~3509~~	~~59~~	~~0.1~~	~~1.08~~	~~0.11~~
18	Parallel	52.5	52.5	2.9	3509	59	0.81	1.08	0.88
19	Parallel	40	40	0.3	2037	45	0.14	0.95	0.13
20	Parallel	50	50	0.5	3183	56	0.15	1.06	0.16
21	Parallel	60	60	0.93	4584	68	0.2	1.15	0.23
~~22~~	~~Parallel~~	~~61~~	~~61~~	~~0.43~~	~~4738~~	~~69~~	~~0.09~~	~~1.15~~	~~0.1~~
23	Parallel	61	61	0.28	4738	69	0.06	1.15	0.07
24	Parallel	41	41	1.56	2140	46	0.73	0.97	0.7
25	Parallel	40	40	1.26	2037	45	0.62	0.95	0.59
26	Parallel	67	67	1.65	5716	76	0.29	1.2	0.35
27	Parallel	56	56	2.28	3993	63	0.57	1.11	0.63
28	Parallel	68	68	3.01	5887	77	0.51	1.21	0.62

Table 3.1: Point Load test results for Frankton Arm, Queenstown.

0.51MPa for samples tested parallel to foliation were obtained. The anisotropy index for Frankton Arm is calculated as 4.1 (using an average of the $I_{s(50)}$ values). These values correlated closely to those obtained at Macraes Gold Mine by Chapple (1998), however values obtained by Moody (1985) from Maniototo were higher (by, on average, just over 5MPa), indicating that the schist is generally stronger at Maniototo than Frankton Arm or Macraes. Moody's high strength values but low anisotropy index, indicates significant textural differences within the schist bedrock at Maniototo. However, the high values are unusual for tests conducted within Otago and outside the range of tests reported within the literature for strength of schist bedrock. Data from Chapple (1998) and Moody (1985) are given in table 3.2.

Table 3.2: $I_{s(50)}$ Values for Frankton Arm, Macraes Gold Mine and Maniototo.

	$I_{s(50)}$ Frankton Arm (MPa)	$I_{s(50)}$ Macraes (MPa)	$I_{s(50)}$ Maniototo (MPa)
Range	0.11-3.83	0.03-3.14	0.3-9.4
Perpendicular to schistosity	0.6-3.83	0.20-3.14	0.5-9.4
Parallel to schistosity	0.11-0.92	0.03-0.58	0.3-5.0
Anisotropy Index	4.1	7.3	2.3

3:3.3 Direct Shear Strength Testing of Fractured Schist.

Shear strength testing was undertaken on fractured schist block samples from Frankton Arm to determine characteristics and properties of weak foliation surfaces. The peak shear strength and basic friction angle were obtained. Fractured schist samples were tested because intact samples could not be used, as they broke apart along the foliation when preparing the samples for testing. Direct shear testing of intact rock and triaxial testing could not be undertaken as during coring the samples also kept breaking along foliation.

A Robertson Geologging Rock Shear Box was used in the Department of Geological Sciences' Rock Mechanics Laboratory. This apparatus allows a specific discontinuity to be sheared at different normal stresses to determine shear strengths under stress combinations reflecting overburden loads. An outline of the method is given in Appendix F.

Test Procedures.

The samples chosen for testing were trimmed to a cube (with a maximum size of 125mm) in the laboratory using a rock saw in order for each specimen to fit into one of the mould assemblies. In all but one case (when the sample remained intact), an artificially fractured sample was tested parallel to foliation, thus it was necessary to wire the two halves of the sample together using copper wire so that the faces on each side of the fracture stayed matched together. Each block was then fixed into one of the sample clamps so that the horizon to be tested is secured in the correct position and orientation. The perspex sides were attached to the mould assembly and then the encapsulating material was poured. After this had set, the other half of the specimen was encapsulated in a similar manner. The casts were then left overnight to cure.

Measurements of joint roughness profiles of jointed samples were made before testing began, and the samples wired together were cut so that there would be no artificial resistance to shearing. The cast was then placed into the lower housing of the shear box, with the upper housing put on the sample in order to commence testing. A constant normal force was added at this point, by means of hydraulic and air pressure. The normal forces applied covered the range of normal stresses present (using an inferred overburden load of approximately 2.7MPa from the equation $\sigma_{overburden} = \rho gh$). Shear force was then applied in a continuous manner in order to control the rate of displacement (~1mm/minute). The maximum displacement moved for each sample tested was never more than 10mm, so that the normal stress applied always acted at 90° to the sample. It has therefore been assumed that the contact area remained constant for displacements of less than 10mm. Once a peak value of shear strength was reached, shear displacement was stopped. A residual strength was not established during testing because it was necessary to undertake staged testing at differing normal loads. A reading of the peak shear strength was taken, and both shear and normal loads were removed. The sample was lifted off and moved back to the original position to begin testing again at higher normal stresses.

Test Results.

A summary of shear test data is given in table 3.3. Graphs of shear strength vs. normal stress are given in figures 3.1 and 3.2. Additional graphs are presented in Appendix F. Basic friction angles for schist samples artificially fractured parallel to foliation were obtained from the

Table 3.3: Direct Shear Test Data.
Location: Frankton Arm, Queenstown.
Rock tested: Slightly weathered; grey; quartzofeldspathic SCHIST.
Test orientation: parallel to foliation.

Sample Number	Applied Normal Force (kN)	Applied Shear Force (kN)	Contact Area (m^2)	σ_n (MPa)	τ (MPa)	JRC	ϕ_b	Estimated $\phi_b + i$
1	3	2.5	0.005	0.5875	0.5	4-6	36	57
	5	5		1	1			
	6	3		1.2	0.6			
	7	6		1.4	1.2			
2	5	2.25	0.005	1	0.45	4-6	20	30
	8	3.5		1.6	0.7			
	15	5.75		3	1.15			
	14	5		2.8	1			
	32	10		6.4	2			
	34	11.25		6.8	2.25			
3	5.5	4	0.0037	1.5	1.08	6-8	30	48
	11.5	6		3.1	1.62			
	18	10		4.9	2.7			
	22	12.5		5.9	3.38			
	23	10.5		6.2	2.84			
4	5	3.25	0.0043	1.16	0.76	6-8	28	45
	10	6		2.33	1.4			
	15	8		3.49	1.86			
	20	9.5		4.65	2.21			
	30	14		6.98	3.26			
5	5	5.5	0.0042	1.19	1.31	14-16	31	63
	15	10		3.57	2.38			
	25	13.5		5.95	3.21			
	35	17		8.33	4.05			
6	5	5.75	0.0047	1.06	1.22	8-10	31	73
	15	12.5		3.19	2.66			
	25	16		5.32	3.4			
	35	20		7.45	4.25			
7	5	2.5	0.0046	1.09	0.54	10-12	24	26
	15	6.5		3.26	1.41			
	25	11.5		5.43	2.5			
	35	15.5		7.61	3.37			

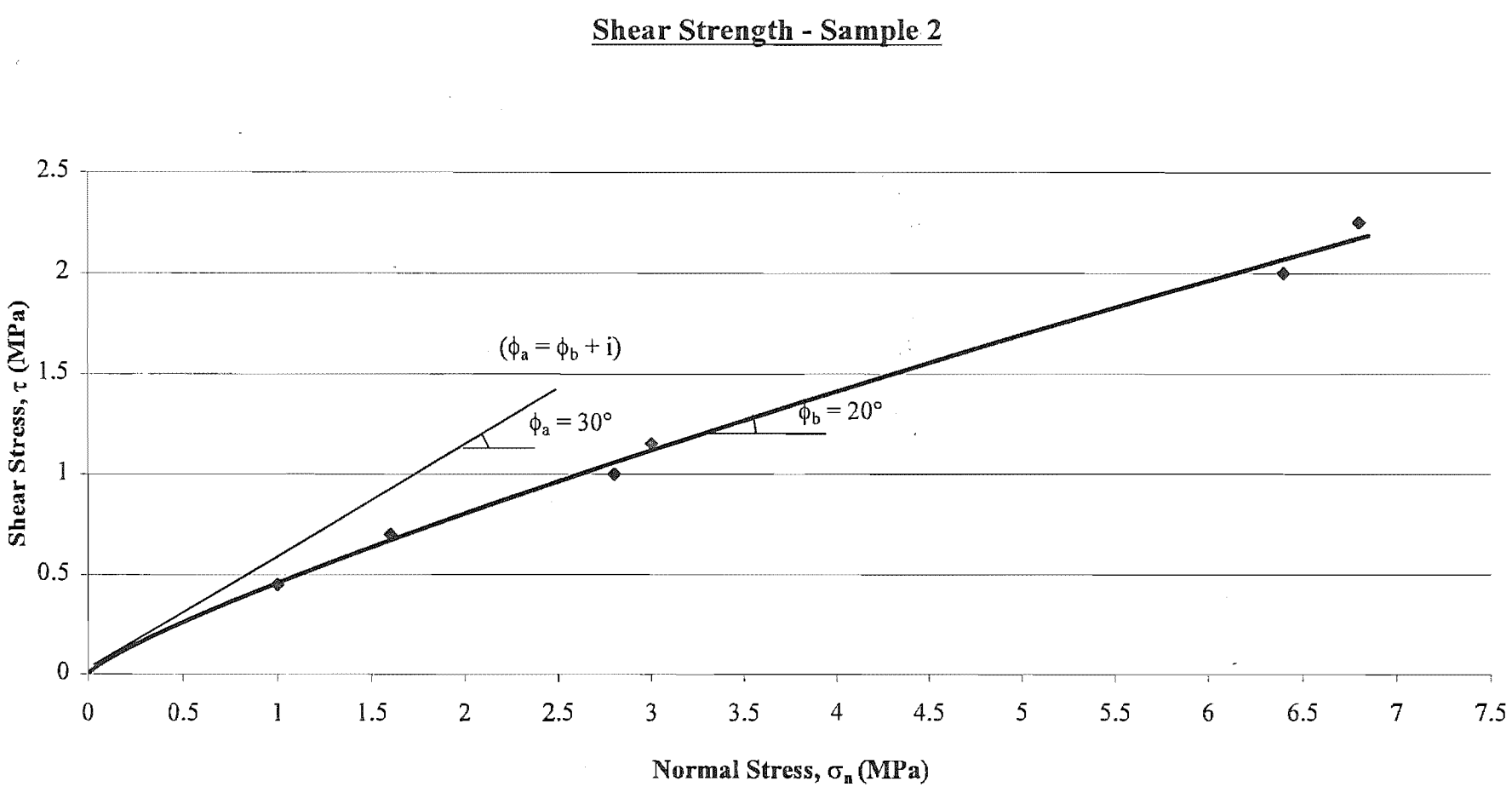

Figure 3.1: Graph of shear strength versus normal stress for Sample 2 (an artificially fractured schist block).

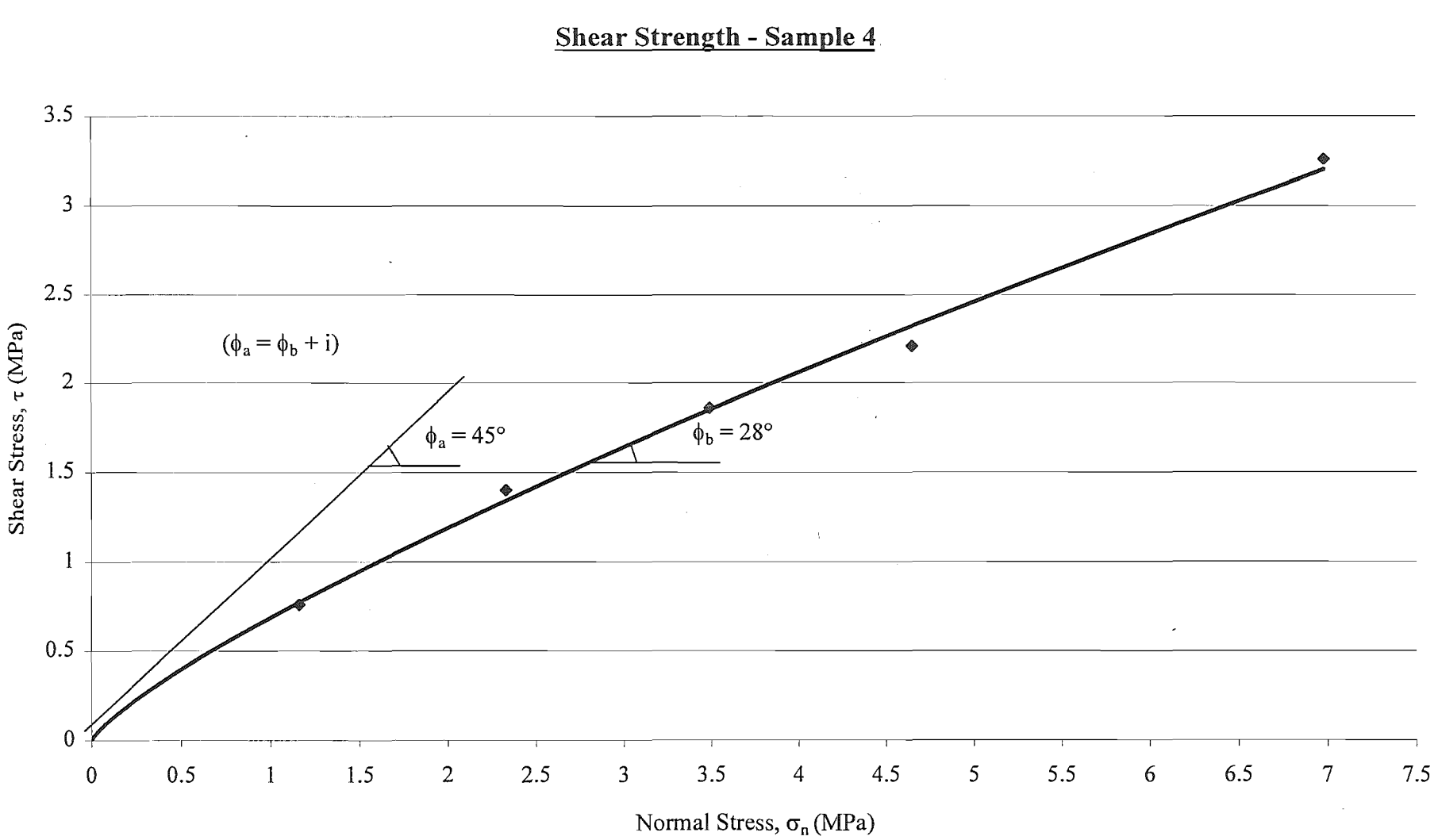

Figure 3.2: Graph of shear strength versus normal stress for Sample 4 (an artificially fractured schist block).

graphs and these values are summarised in table 3.4. Correlations of joint roughness with basic and apparent friction angle are displayed in figure 3.3 and show a linear trend, that is, as the friction angle increases, the joint roughness coefficient increases.

Table 3.4: Friction Values for Artificially Fractured Schist Samples.

Sample	Estimated $Ø_b + i$	$Ø_b$
1	57	36
2	30	20
3	48	30
4	45	28
5	63	31
6	73	31
7	26	24

The results for apparent friction angle can be regarded as approximate only, as the values are an artifact of the way the graphs in figures 3.1 and 3.2 have been drawn, as there were no low τ/σ_n points obtained during testing for subsequent graphing. Errors may have been incorporated during preparation of the samples after they had been artificially fractured. The initial friction angle (ϕ_b + i) is defined as the friction angle of initially undisturbed and interlocked samples. The asperities may become disturbed or even removed during preparation, unless great care is taken and once this has occurred, a reduced friction angle will be obtained (Wyllie and Norrish, 1996).

3.4 SHEAR ZONE DATA.

3.4.1 Ring Shear Testing.

The term 'residual strength' is applied to rock or soil that has been subjected to large strains so that the particles either side of the shearing surface will have rearranged to produce a more parallel orientation. As such, the strength is at a minimum value.

Samples tested for residual strength were either recompacted fault gouge or crushed and sheared rock material. The fault gouge sample was taken from Newman property (grid reference 2171425; 5567600) from a fault zone 3 metres wide. This fault zone can be traced

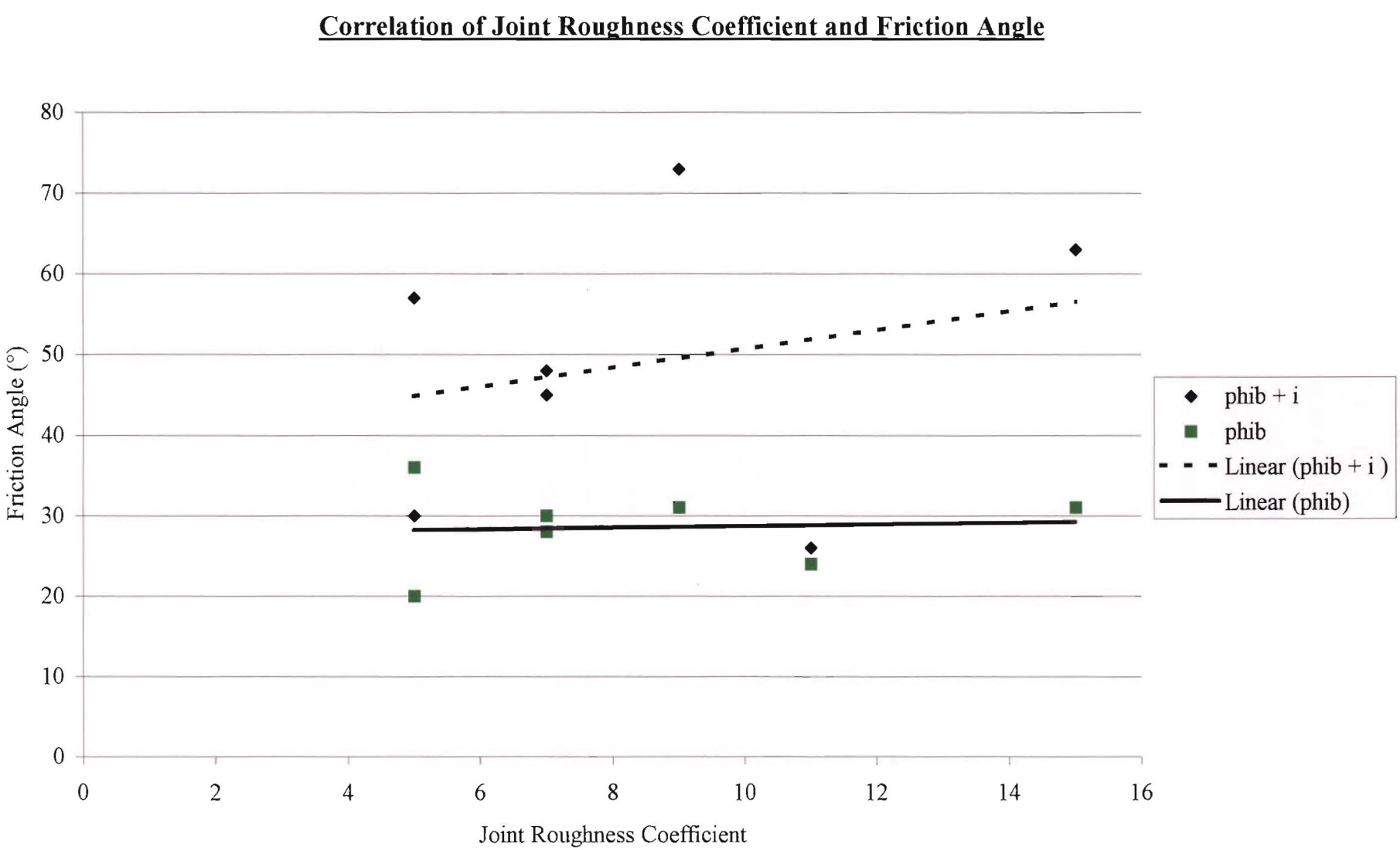

Figure 3.3: Graph correlating the joint roughness coefficient with basic friction angle and apparent friction angle.

to the northwest for more than 1km across the lower slopes of Queenstown Hill. The material is intensively folded and sheared schist with clay-rich "pug" zones up to 150mm wide. Crushed schist material was obtained from Goldfields subdivision (grid reference 2170650; 5567250). Intensely sheared and weathered schist was taken for testing from Hensman property (grid reference 2171700; 5567650). This area is a foliation shear zone up to 1m thick, occurring between competent strong quartzofeldspathic schist. Sample descriptions are given in Appendix E.

Residual shear strength was measured using a Bromhead ring shear apparatus according to the British standards BS1377: Part 7:1990. Testing was carried out at normal loads ranging between approximately 70kPa and 180kPa, with material tested at a moisture content just wet of the plastic limit. These low normal loads were chosen so that the sample would not be extruded from the test apparatus during testing, as would happen at higher loads. Applied normal loads were lower than inferred overburden pressure (a maximum of 2.7MPa) for the Queenstown Hill Landslide, however, in order to retain the sample and obtain any test results, low normal loads were adopted. The ring shear test methodology is outlined in Appendix F.

Test Results.

The results plots for each of the five samples tested are presented in figures 3.4 to figure 3.6. Residual friction angles ($Ø_r$) measured in this study ranged between $Ø_r = 6°$ and $Ø_r = 11°$. Cohesion values for crushed and sheared Otago Schist ranged from 0kPa to just over 4kPa for the same samples.

Table 3.5: Summary of Residual Shear Strength Parameters (for samples <2mm ϕ).

Sample Location	Cohesion (kPa)	Friction (°)
Goldfields Crush Zone Material	0	9
Goldfields Shear Zone Material	0	11
Hensman Mica Schist Shear Zone Material	0	6
Hensman Green Schist Shear Zone Material	0	6
Newman Fault Zone Material	0	7

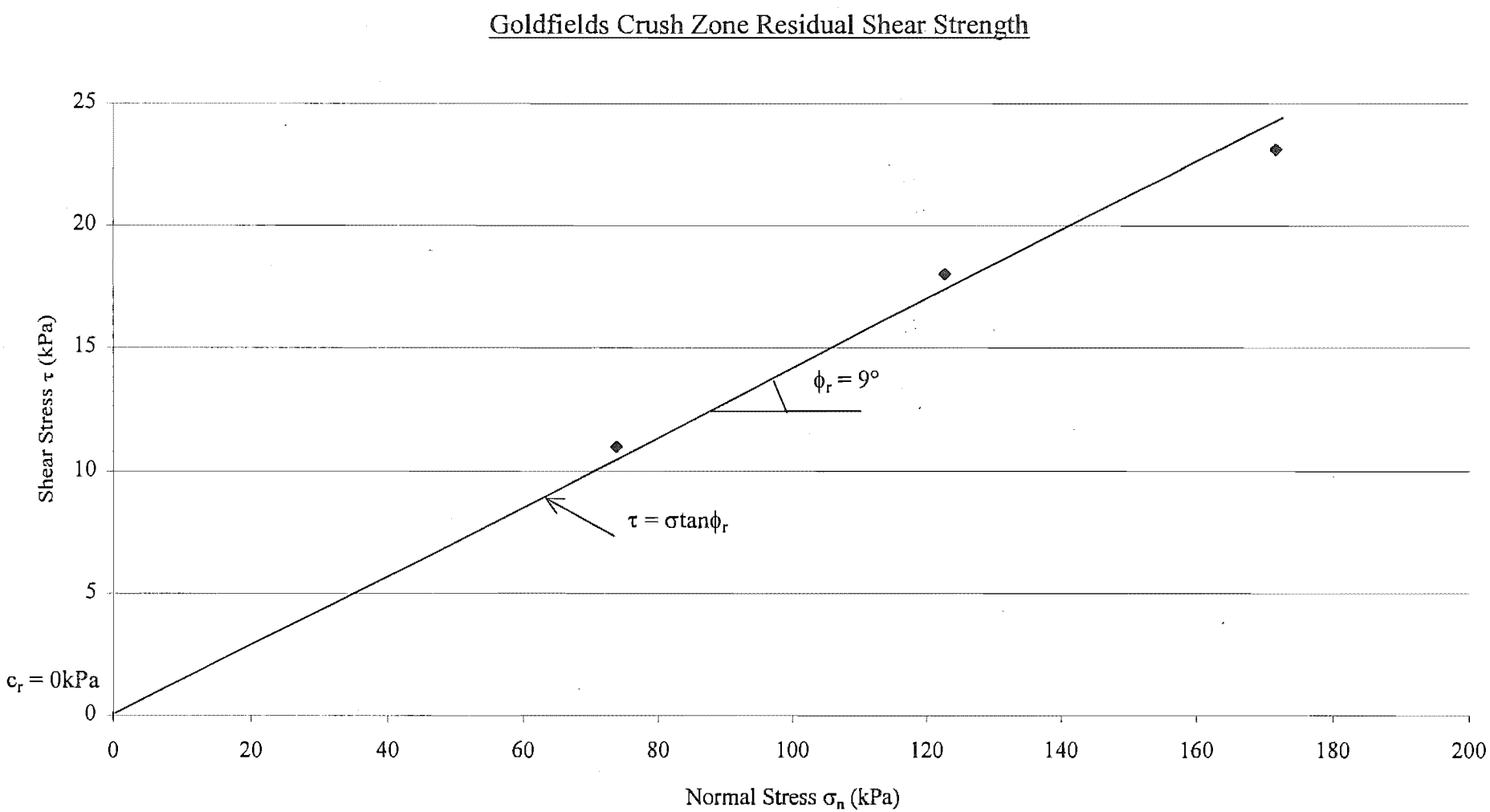

Figure 3.4a: A plot of normal stress (σ_n) versus shear stress (τ) for residual strength testing of Goldfields Subdivision crush zone material (for location refer to figure 1.2 - map pocket).

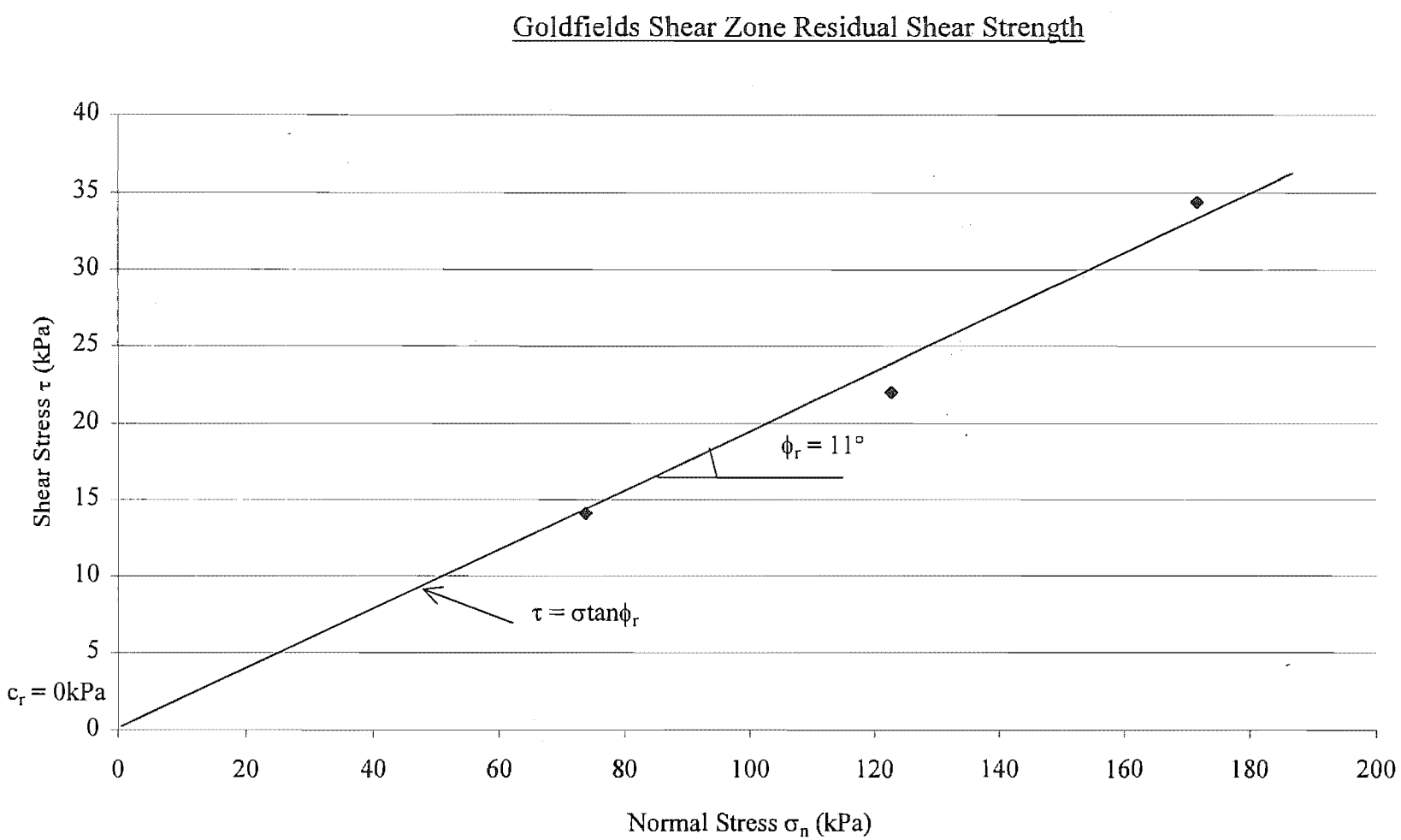

Figure 3.4b: A plot of normal stress versus shear stress for residual strength testing of Goldfields Subdivision shear zone material (for location refer to figure 1.2 - map pocket).

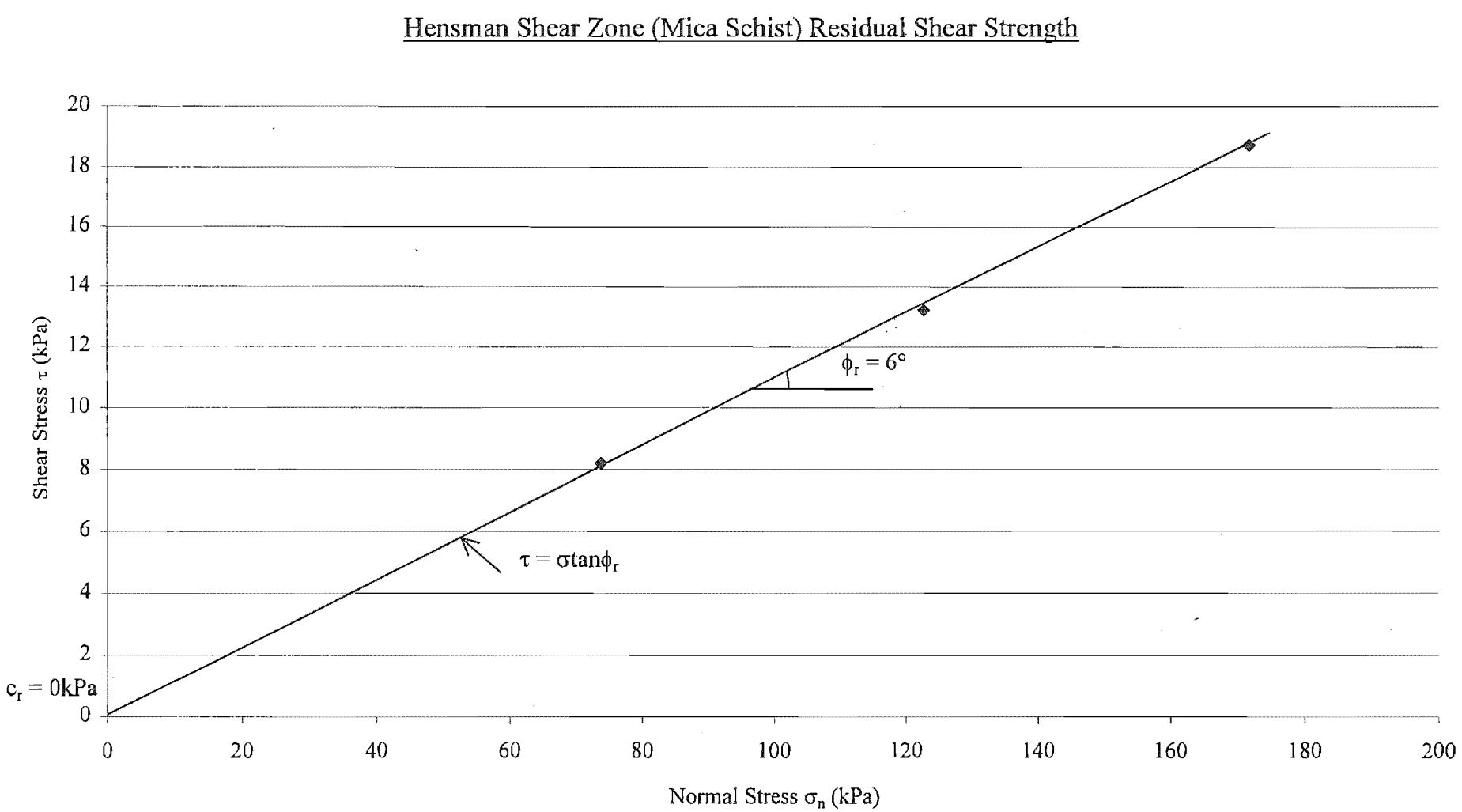

Figure 3.5a: Graph of normal stress versus shear stress for the Hensman Subdivision mica schist shear zone material.

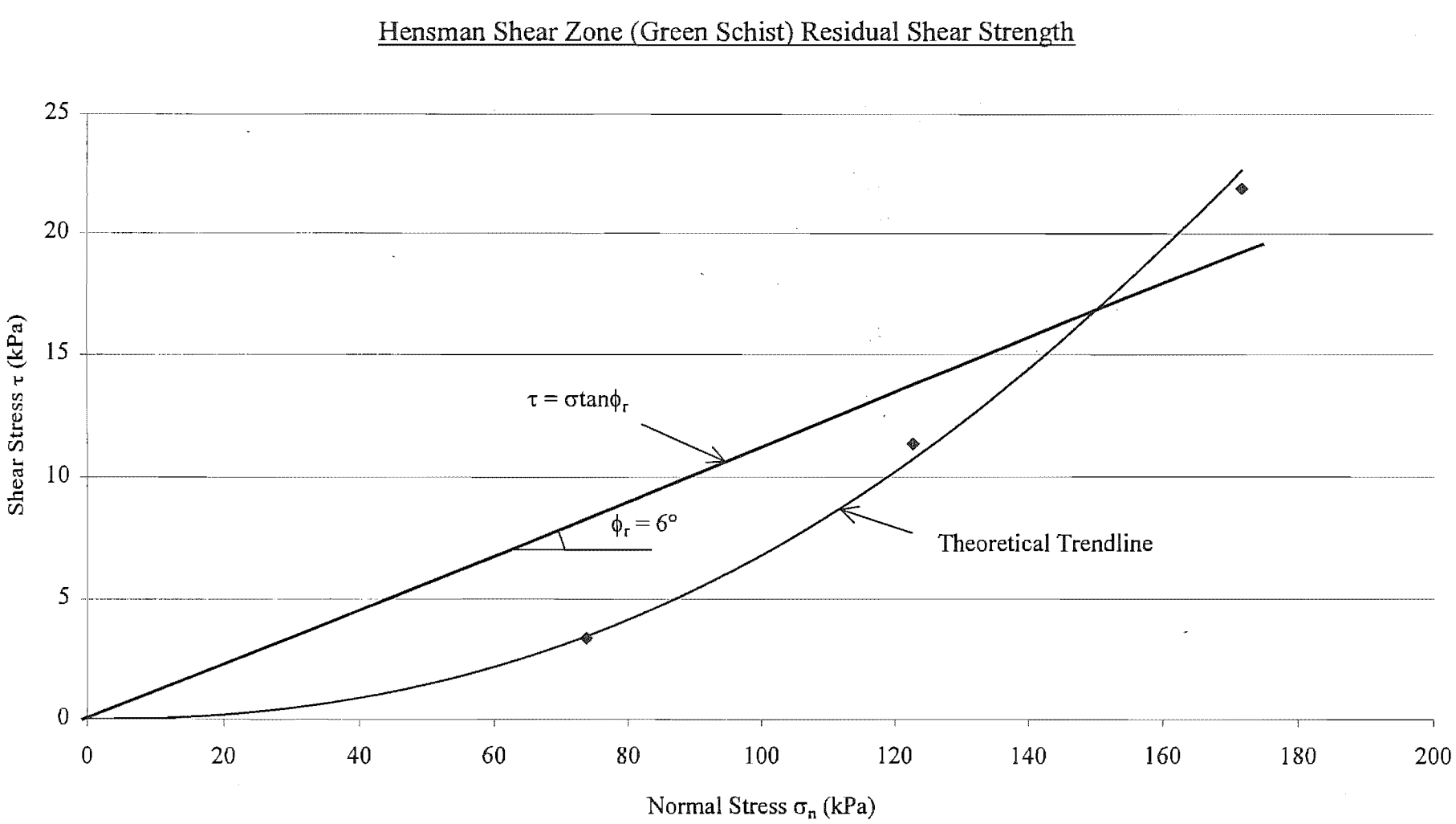

Figure 3.5b: Graph of normal stress versus shear stress for the Hensman Subdivision greenschist shear zone material.

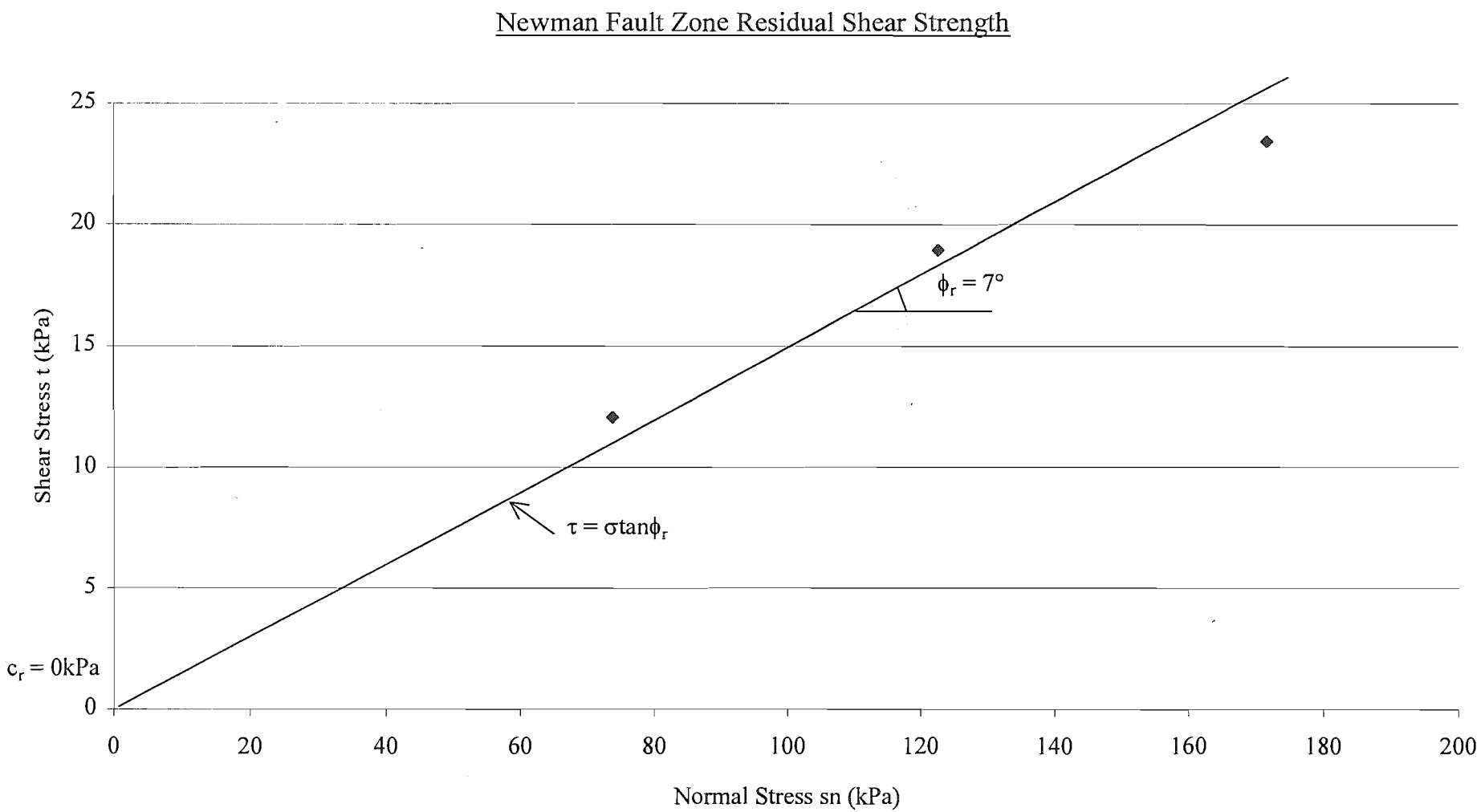

Figure 3.6: Graph of normal stress versus shear stress for residual strength testing of fault zone material from the Hensman Subdivision (for location see figure 1.2 - map pocket).

The proportions of platy particles to rounded particles present in the crushed or sheared rock material and the friction of the platy particles control the type of residual shearing mechanism which develops (Lupini et. al., 1981). The transition from one to the other is considered in terms of particle packing:

1. Turbulent mode: occurs in sheared/crushed rock with a high proportion of rounded particles or with platy particles with high friction of >25° (for example illites and kaolinites), in which preferred platy particle orientation does not occur.
2. Sliding mode: occurs when a low strength shear surface of strongly orientated low friction (5°-20°) platy particles forms, for example montmorillonites.
3. Transitional mode: no dominant particle shape, and involves turbulent and sliding behaviour in different parts of the shear zone.

The residual friction angles measured in this study are low, suggesting a sliding mode for residual shear behaviour for the material tested. XRD however, does not confirm this statement, as a high proportion of the material tested contained kaolinite (see section 3.4.2) – a high friction clay mineral. This mode of behaviour is the same as that found at Macraes Gold Mine by Chapple (1998), who also suggested a sliding mode for residual shear behaviour in Otago Schist at the mine site. He obtained slightly lower frictional values (ranging between $\emptyset_r$=3° and $\emptyset_r$=6°), but his results are overall consistent with results from Frankton Arm. Friction angles obtained are lower than should be expected within foliation shears, as only the fine fraction of the samples has been tested. Grains greater than 1mmϕ were removed, and this has caused a reduced frictional resistance. X-ray Diffraction revealed an abundance of swelling clay minerals (swelling chlorite/smectite) in the clay fraction at Macraes, while there are no swelling clays evident along Frankton Arm. In addition, a small fraction of quartz was identified in the samples during XRD testing, and this may also be the cause of higher friction values. As a result, friction angles for Frankton Arm are higher than those at Macraes Gold Mine, implying a higher percentage of clay-sized particles (particularly those with an expanding lattice) is present at Macraes Mine. The percentage composition of clay-sized particles for shear zone material along Frankton Arm averages just over 4%, consisting predominantly of sand-sized grains (Appendix K).

3.4.2 X-ray Diffraction Analysis.

X-ray Diffraction (XRD) analysis is a widely used technique for the identification of clay minerals that cannot be easily identified through more conventional methods such as

petrography. The same samples tested for residual shear were analysed for clay mineralogy, that is fault gouge, crushed and shear zone material, in order to correlate residual strengths with clay mineralogy. Percentages of each mineral were visually estimated as the proportion of the areas corresponding under each peak for each mineral to the total area encompassed under all peaks for all minerals. The XRD test technique used in this study is presented in Appendix F.

Test Results.

The diffractograms for each of the five gouge samples tested are presented in Appendix F, while table 3.6 and figure 3.7 present a summary of the constituent clay minerals identified in each of the samples tested. Clay-sized grains identified in all the samples were kaolinite, albite, muscovite and clinochlore. Trace amounts of quartz were discovered in all, except Hensman green schist, where hornblende was identified instead (a commonly occurring mineral in green schist). Table 3.7 presents X-ray Diffraction results from Chapple (1998) for material tested from Macraes Mine as a comparison for samples taken from another area within Otago Schist.

Table 3.6: Queenstown Hill XRD Analysis showing percentage composition of clay-sized minerals.

Crystalline Material	Hensman Greenschist (%)	Hensman Mica Shear Zone (%)	Goldfields Fine Grained Shear Zone (%)	Goldfields Coarse Grained Shear Zone (%)	Newman Culvert (%)
Clinochlore	10	5	5	5	5
Albite	5	30	25	35	40
Kaolinite	60	35	40	35	25
Muscovite	10	25	25	20	20
Hornblende	15	-	-	-	-
Quartz	-	5	5	5	10

Note: percentage composition is an estimate.
Analyst: Steven Brown, Department of Geological Sciences.

Figure 3.7: Queenstown Hill XRD Results

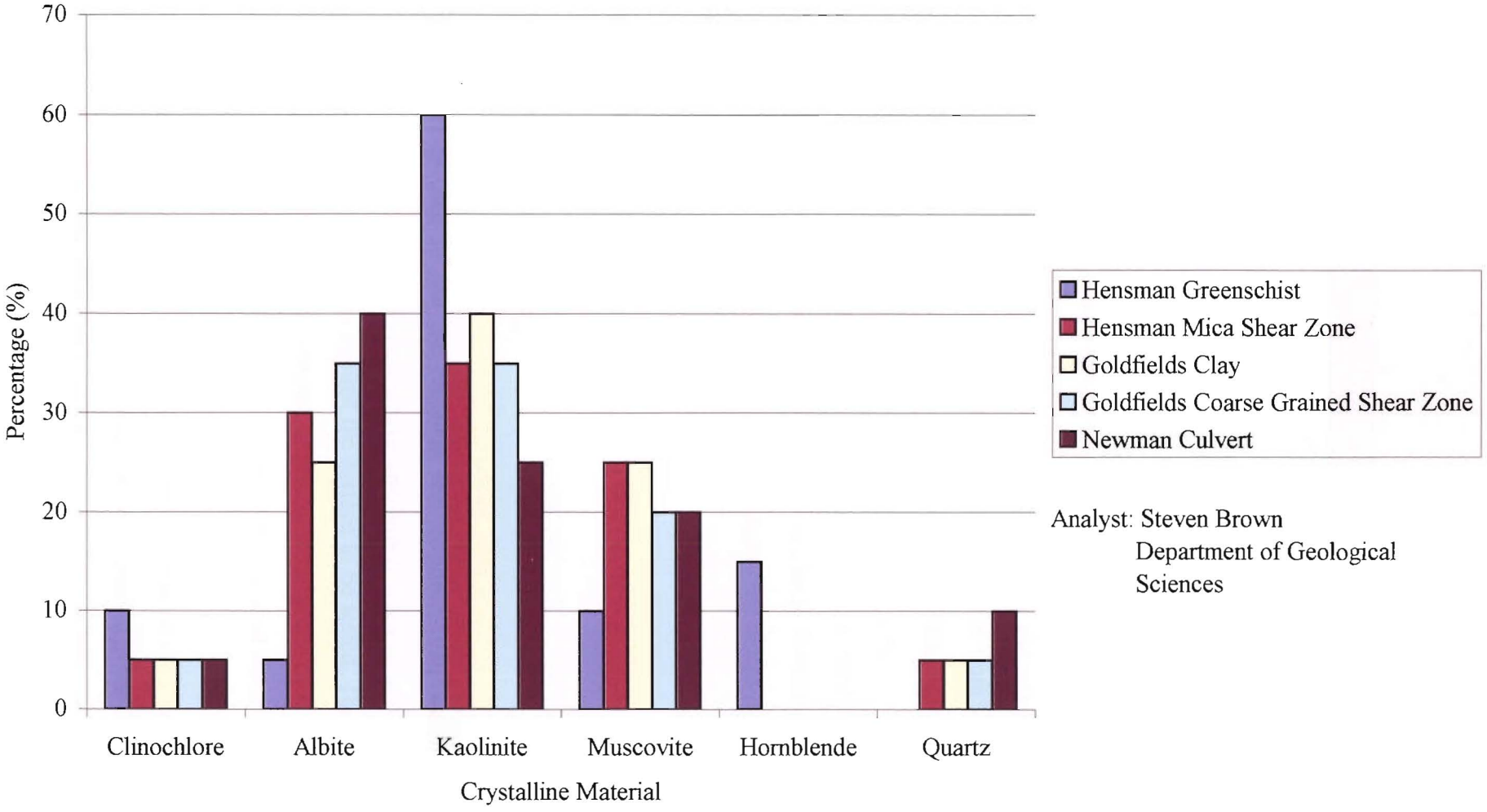

Table 3.7: Approximate percentages of the mineral composition for the clay mounts analysed at Macraes Mine by Chapple (1998).

	FG1	FG2	FG3	FG4	FG5	FG10
Chlorite (Non-swelling)	trace	10	trace	-	-	10
Kaolinite	20	30	25	25	20	30
Muscovite	35	35	30	40	35	35
Quartz	-	trace	trace	trace	trace	trace
Swelling Chlorite/Smectite	45	25	45	35	45	25
Total	100	100	100	100	100	100

There were no smectites or montmorillonites identified in any of the samples tested from Frankton Arm using X-ray Diffraction. In all other samples analysed from within the Otago Schist (such as Maniototo, Macraes and Clyde), these have been identified as the dominant clay minerals. Friction angles of sheared material obtained using Ring Shear testing are extremely low for samples containing kaolinite. Friction angles of around 20° are usual for kaolinite (Grim, 1962), whereas values of 5-11° were obtained. Further investigation is required in order to explain these results, but has not been attempted in this project because of time and other constraints.

3.5 JOINT PROPERTIES.

3.5.1 Schmidt Hammer Test.

The Schmidt Hammer is used to test the hardness and estimate compressive strength of jointed rock materials. The test is a non-destructive one which releases a certain amount of stored energy by pushing a steel plunger against the surface to be tested. The rebound of the hammer, after striking the surface, is proportional to the hardness of the rock and is measured by a dimensionless number. The harder the rock the higher the rebound number.

The test has the advantage of being quick and convenient and can be used on in situ rock as well as individual blocks in the laboratory. However, wide variations in the results can occur depending on the testing and recording techniques used. An L-type hammer with an impact energy of 0.74Nm was used on in situ rock as only large block specimens in the field were to

be tested. The equation by Deere and Miller (1966) was used to estimate joint wall compressive strength.

At least 20 individual tests were conducted on each rock sample, with the test locations separated by at least the diameter of the plunger. All readings were taken on dry rock surfaces, normal to schistosity. Testing was done in the same locations as samples were taken for shear testing, tests were also done at Marina Heights (grid reference 2172475; 5568250). Results of Schmidt Hammer Rebound Hardness are presented in table 3.8. Average joint wall compressive strength was calculated as 39MPa.

Moody (1985) obtained readings parallel to schistosity in Otago Schist at the Paerau Diversion Works at Maniototo, but not without difficulty. It was found the rock being tested was fractured or partially detached along a foliation plane, as occurs along Frankton Arm, and this resulted in an underestimation of the rebound values. Moody found only a small difference between readings obtained from testing parallel to and those obtained normal to schistosity within pelitic schist. This showed that despite the rock having highly anisotropic strength characteristics, it is still relatively hard parallel to schistosity. Moody emphasised the care required not to confuse rebound hardness with strength (the internal resistance of a body to stress), especially in anisotropic rocks.

Computed joint wall compressive strength values range from 21MPa to 54MPa for schist along Frankton Arm. These values are approximately half the uniaxial compressive strength of schist bedrock, as UCS test results obtained from within other areas of Otago schist, such as Clyde were 61-105MPa. Chapple (1998) and Moody (1985) acquired results of 5-61MPa and 9-46MPa respectively (see table 3.9).

3.5.2 Defect Surveys.

3.5.2.1 Purpose and Methods.

Scan lines were carried out along sections within the Commonage Subdivision for the purpose of obtaining quantitative information on the defects that affect schist bedrock stability for the Frankton Arm area. Engineering geological reports by Bell (1995) were available, and as the area had been recently developed, fresh exposures could be surveyed. The attitudes and

Rock Material Description	Rock Mass Description	Test Location	Test Orientation	Number of Tests	Rebound Number			Computed Joint Wall Compressive Strength (MPa)
					Standard Deviation	Range	Mean	
fresh to slightly weathered; strong; grey-green quartzo-feldspathic schist.	Pervasive, planar schistosity, dipping south at 20+/- 5°; prominent joint sets are subvertical, striking E-W and N-S.	446m above sea level at end of Goldfield Heights Road. 2170650E; 5567250N	Normal to schistosity.	20 20 20 20 20	4.9 5.5 2.9 3.8 5.4	34 - 47 22 - 44 20 - 32 41 - 55 24 - 45	39 37 27 48 36	46 44 35 54 43
fresh to slightly weathered; moderately hard to hard; moderately strong to strong; olive grey quartzo-feldspathic schist.	Planar schistosity dipping 20-25° south west; joints are very closely to moderately spaced; low to highly persistent.	2172473E 5568184N (Marina Heights Rd)	Normal to schistosity.	20 20	7.0 4.3	19 - 44 14 - 32	32 21.5	40 30
strong to moderately strong; slightly weathered; grey quartzofeldspathic schist.	Schistosity dipping 25-35°WSW; locally sub-vertical joints open to ~10mm; zone of intensely sheared and weathered schist 150mm wide.	Hensman Subdivision 438m above sea level off the west end of Perkins Road. 2171700E; 5567650N	Normal to schistosity.	21 20 20	1.7 5.3 3.3	10 - 15 23 - 39 28 - 40	13 31.5 36	21 39 43

Joint wall compressive strength calculated using $\log_{10}\sigma_c = 0.88\gamma R + 1.01$ (Barton and Choubey, 1977).

Table 3.8: Summary of Schmidt Hammer Rebound Testing.

properties of the defects were recorded, along with foliation attitudes. Defect data summary tables are presented in Appendix D. A Rock Mass Rating analysis was applied by using the subdivision data and subsequent Slope Mass Ratings were obtained.

The analysis (following Hoek and Bray, 1981) of 363 defects sampled from a total scan line of 151m (figure 3.8) revealed the following defect populations:

$F_1 = 104\pm32/86\pm4°S$

$F_2 = 101\pm23/76\pm14°SW$

$F_3 = 099\pm20/66\pm17°S$

$F_4 = 194\pm38/63\pm27°W$

Foliation attitude for the Commonage Subdivision = 105±5/25-30°S.

These are regarded as the major defects within the schist. To assess the validity of the data obtained, it was necessary to statistically analyse the data using confidence intervals. This revealed that the four defect sets were 99% statistically significant.

3.5.2.2 Analysis.

Data sets from all subdivision lots have been integrated in Figure 3.8. Using a friction angle of 30° (obtained from shear strength testing of artificially fractured schist – section 3.3.3), a zone of instability according to Markland's Test is produced. Only a small grouping of poles (<2%) falls within this area. The in situ schistosity falls within the daylight envelope, indicating schistosity daylights in the slope face. Pole concentrations of up to 4% daylight in the slope face. It can therefore be assumed from kinematics that this slope would be unstable because of this structural condition, and further detailed investigations or the implementation of stability measures would be necessary. Data and stereonets for individual subdivisions are presented in Appendix D.

A histogram of discontinuity spacings for the Commonage Subdivision is given in Figure 3.9. Priest (1993) defines discontinuity spacing as the distance between a pair of discontinuities measured along a line of specified location and orientation. Figure 3.9 is of total spacing – the spacing between a pair of immediately adjacent discontinuities. The mean discontinuity spacing provides a direct measure of rock quality, and a histogram plot provides a good illustration of the distribution of defect spacing. Figure 3.9 shows a negative exponential

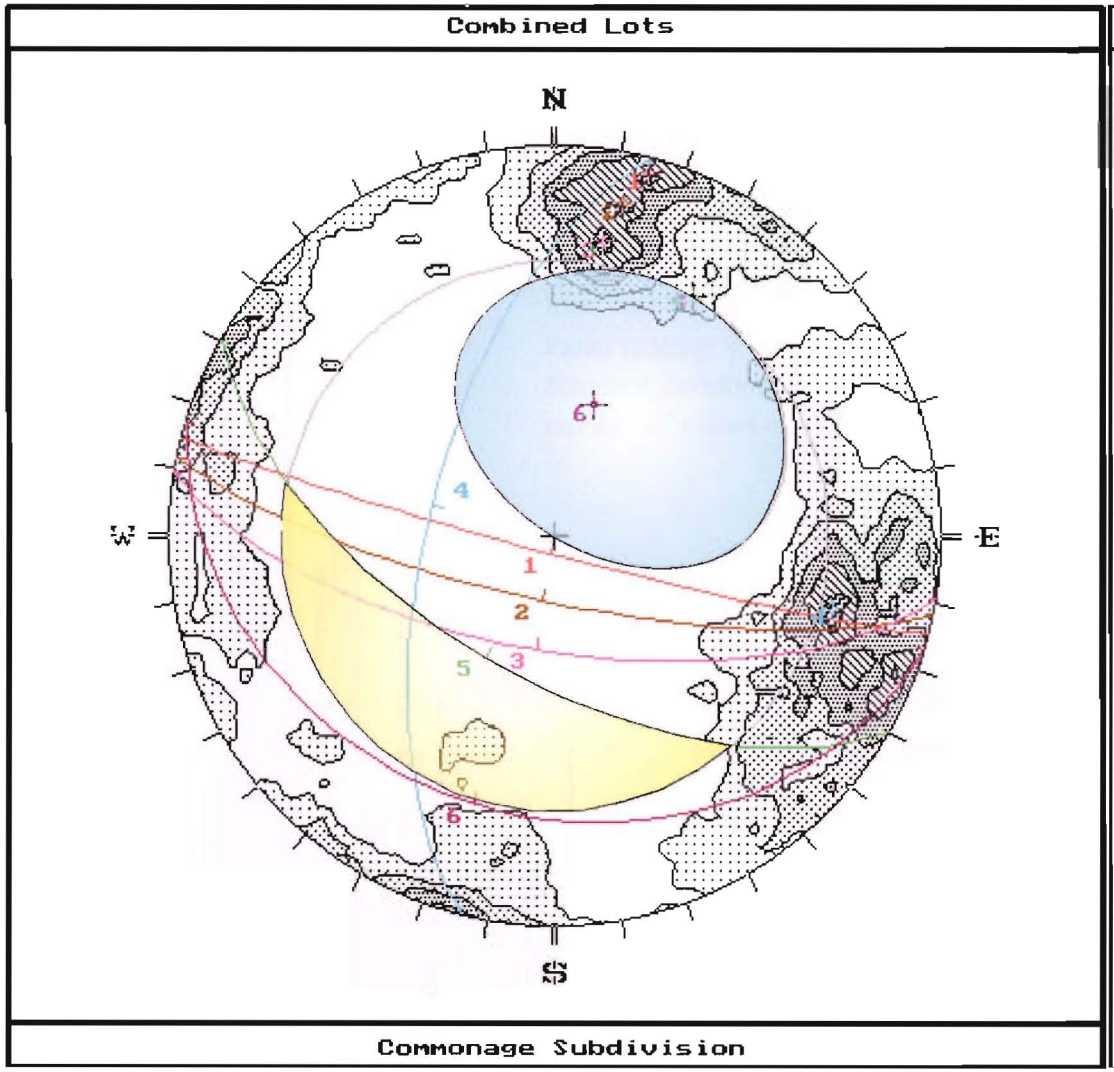

CONTOUR PLOT

SCHMIDT POLE CONCENTRATIONS
% of total per 1.0 % area

< 0 %
< 1 %
< 2 %
< 3 %
< 4 %
< 5 %
< 6 %
< 7 %

EQUAL AREA
LWR. HEMISPHERE

363 POLES
363 ENTRIES

NO BIAS CORRECTION

1 = great circle representing plane corresponding to centre of pole concentration of joint set 1
104± 32/86 ± 4SW

2 = great circle representing plane corresponding to centre of pole concentration of joint set 2
101±23/76±14SW

3 = great circle representing plane corresponding to centre of pole concentration of joint set 3
099 ± 20/66±17S

4 = great circle representing plane corresponding to centre of pole concentration of joint set 4
194±38/63±27S

5 = great circle representing slope face-120/60S

6 = great circle representing plane corresponding to undisturbed schist -106/29S

Friction Angle = 30°

Daylight Envelope

Zone of instability according to Marklands Test

Direction of Sliding

Figure 3.8: A combination of all joints on Commonage Subdivision showing master joint sets, daylight envelope and zone of instability.

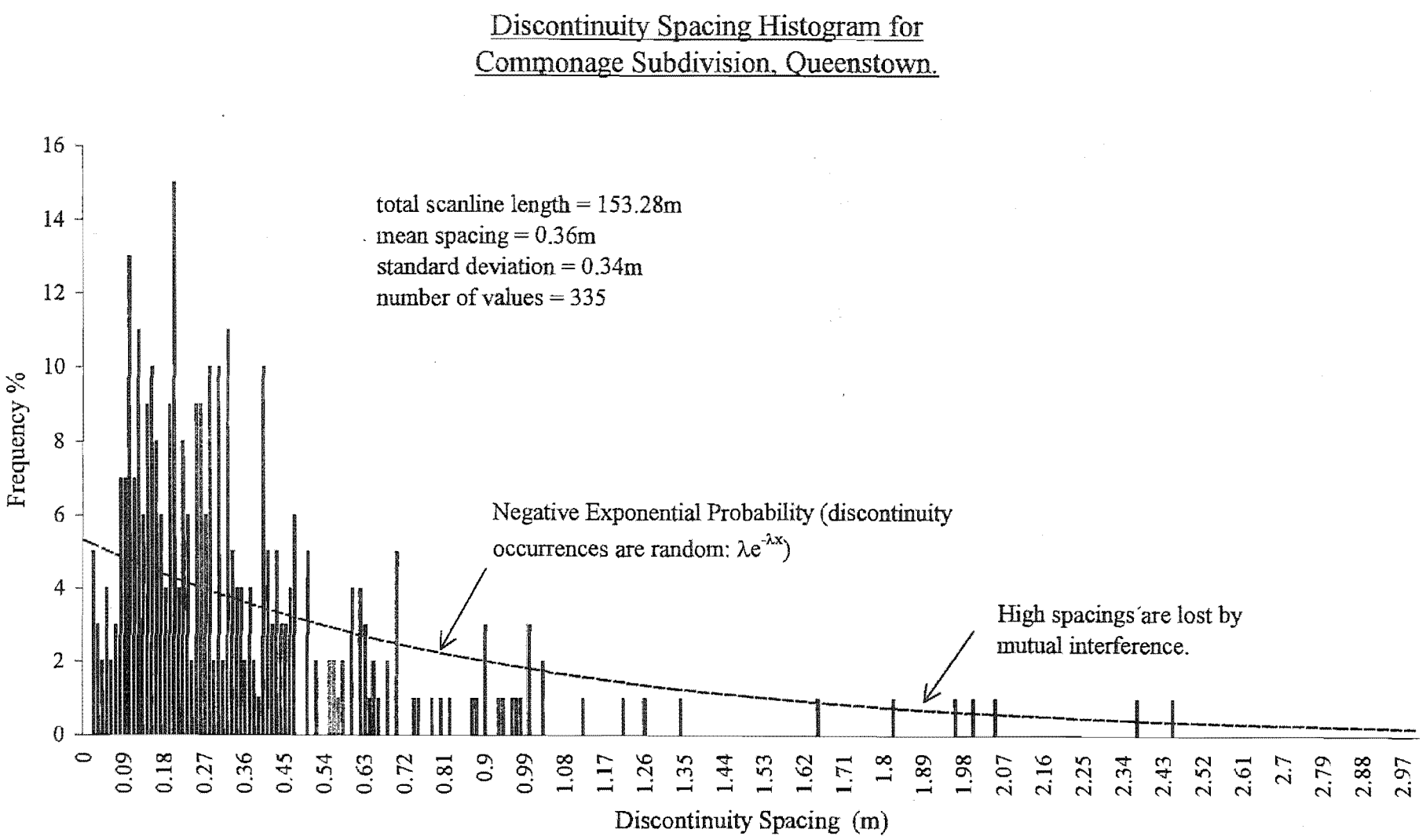

Figure 3.9: Histogram of discontinuity spacings for the Commonage Subdivision, Queenstown.

probability distribution, which Priest (1993) indicates is the case for a variety of igneous, sedimentary and metamorphic rocks. The fact that the discontinuity spacing obeys a negative exponential distribution is an important implication in the analysis of the rock structure using the Rock Quality Designation (RQD). The distribution illustrates that discontinuities with highly variable orientations will mutually interfere because defects occur randomly along a scanline. RQD is a measure of discontinuity spacing, and the link between the two is given in the following section.

3.5.2.3 Rock Mass Rating.

The RQD numerical value can be applied to the Rock Mass Rating Classification System (Bieniawski, 1973). This classification includes eight rock parameters, however emphasis was given by Bieniawski (1973) to the use of this in regards to tunneling. Therefore Romana (1985b) used the Rock Mass Rating (RMR) to develop the Slope Mass Rating (SMR) in order to assess slope instability risk parameters. SMR is a preliminary prediction of slope stability, and will not predict the absolute stability of a slope, but it can identify areas where stability problems may occur (McKenzie, 1993). This classification may be used during the feasibility stages of site investigations, but does not replace site-specific engineering geological investigations.

The SMR parameters cover attitude of discontinuities and slope, failure modes (plane and toppling) and slope excavation methods. The classification system takes into account the following parameters:

- Rock mass characterisation (including joints frequency, state and water inflow).
- Differences in strike between slope face and prevalent joints.
- Differences between joints dip angle and slope dip angle – which control the daylighting of a joint in the slope face (a necessary condition for plane and/or wedge failure.
- Relationship of joints dip angle with normal values of joint friction (for plane and/or wedge failure).
- Relationship of tangential stresses, developed along joint, with friction (for toppling failure).

The slope mass rating of Romana (1985b) is as follows:

$$SMR = RMR + (F_1.F_2.F_3) + F_4$$

3.5.2.4 Determination of Slope Mass Rating.

Rock Mass Rating:-

Parameter 1: Strength of Intact Rock Material.
Point Load Strength Index = 0.11 – 3.83MPa
Total Mean = 1.17
∴ Rating = 4

Parameter 2: Drill core Quality RQD% = 95.7% [using $RQD_t = 100e^{-\lambda t}(1+\lambda t)$]
∴ Rating = 20

Parameter 3: Spacing of discontinuities = 360mm
∴ Rating = 10

Parameter 4: Condition of discontinuities
Slightly rough, separation <1mm, highly weathered wall rock
∴ Rating = 20

Parameter 5: Groundwater
Summer = Completely dry ∴ Rating = 15
Winter = Wet ∴ Rating = 7

Rating Adjustment for Discontinuity Orientation
Length: 1-3m ∴ Rating = 4
Separation: 1-5mm ∴ Rating = 1
Roughness: Slight ∴ Rating = 3
Infilling: None ∴ Rating = 6
Degree of weathering: Moderate ∴ Rating = 3

Slopes Adjustment Rating = -17
A favourable/fair case

TOTAL RMR: Summer = 52
Winter = 44
Class No. III Described as Fair Rock.

Slope Mass Rating (Romana, 1985):

$F_1 = (1 - \sin A)^2 = (1 - \sin 16)^2 = 0.52$, where A = angle between slope face and joint strike.

$F_2 = 1.00$ (joints dip greater than 45°)
$F_3 = 1.00$ (joints dip more than slope dip)
$F_4 = 15$ (a natural slope)

McKenzie (1993) has stated that the SMR Classification does not consistently and accurately assess the stability of natural slopes in schist, so he proposed additional adjustment ratings for natural slopes containing landslides. By using his suggested adjustments, the SMR classes were consistent with site-specific investigations (from within the Cromwell Gorge where he completed his study). The F_4 adjustment factors as applied to failed slopes are as follows (after McKenzie, 1993):

Natural Slopes	Rating
In situ Rock	15
Inactive Landslide	0
Active Landslide	-8

As this survey was conducted from within the Commonage Subdivision where there are no naturally occurring landslides, the above adjustment ratings were not implemented. This adjustment rating would need to be applied to the slopes along Frankton Arm, however, due to the limited availability of bedrock exposure in this area the analysis could not be completed in this project.

$SMR = RMR + (F_1.F_2.F_3) + F_4$
$= 52 + (0.52 * 1 * 1) + 15$
$SMR = 67.5$ (for summer conditions)

$SMR = 59.5$ (for winter conditions)

An SMR of 67.5 was calculated for summer conditions, a class IIb rating. This class is classified as 'stable' by Romana (1991) and implies support measures involving the installation of toe ditches or fences; spot or systematic bolting or anchoring may be necessary. This choice would be made during site-specific engineering geological investigations, not just using SMR analysis; however, the analysis gives a basic prediction of the possible site conditions. Winter conditions would result in an SMR value of 59.5, a class III rating. SMR makes the broad prediction of classifying the slope as 'partially stable', with some joint failures and multiple wedge failures. McKenzie (1993) reported SMR values of >60 for in situ schist and <60 for rock situated within unstable masses for within the Cromwell Gorge. Bell (1995, unpubl.) reported minor groundwater seepages were present at the till-bedrock interface during winter field investigations, but most investigation trenches were dry. Significant overland flows were present on parts of the upper slopes where bedrock is present at shallow depths. These are evident in figure 3.10. The significant difference in values obtained for winter and summer may be attributed to local ice-plugged drainage during very heavy frosts in the winter. In addition, increased infiltration as a result of heavy rainfall or snow may add to the decrease in stability however, a result of development is the control of storm water. Romana (1991) indicates some slopes are stable with an SMR of 65, but each

Figure 3.10: The Commonage Subdivision, showing significant overland flows. This photo was taken in January 1999.

slope must be assessed and analysed individually, along with site-specific investigations, to obtain realistic conclusions. SMR should be used as a broad predictor only.

Both qualitative and quantitative information on rock mass defects has been obtained for the schist bedrock in the Queenstown area. Conventional models for modes of failure could not be used for the Commonage Subdivision. As can be seen in figure 3.11, what would seem to be a classic wedge failure, is instead a plane failure. This failure has formed as a result of undermining beneath the main block, with lateral release on one joint and sliding taking place along the foliation. As can be seen in figure 3.11, wedge failure can not take place, as the intersection between the two planes is too steep does not daylight. Ravelling of minor schist blocks has taken place (figure 3.12), resulting in undercutting of the larger schist blocks. This process may lead on to larger wedge failures, as support has been removed by unravelling, along with the subsequent daylighting of the line of intersection (figure 3.11-top centre).

It is inferred that unravelling was initiated once blasting had been completed (in order for development of sections to proceed within the subdivision), as this process would have removed support. Daylighting of intersecting planes was a result, creating a series of minor wedge failures. Prior to any blasting, the rock faces would have been stable.

Joint set 4 (figure 3.8) shows a highly variable strike, indicating the mode of failure by this joint set is mixed. Figure 3.13 shows a series of sub-vertically dipping joints (joint set 4) which in this instance are acting as releasing surfaces for simple planar sliding along schistosity. However, the wide range in strike infers this set also acts as a potential wedge surface, but a result of the steeply dipping intersecting plane is that the wedge will be stable. Unravelling and the removal of support must take place to form a daylighting surface in order for failure to occur. Small wedges have formed as a result of this process (figure 3.14).

Undermining has been taking place both during excavation and since the formation of the rock cuts, as is suggested by the large volume of rock debris present at the base of the rock faces (figure 3.14). Unravelling is expected to continue if stabilisation measures are not implemented. Planar sliding along foliation is inferred to be the dominant failure mechanism, with joint release provided by joint set 4. Future development within the subdivision will make use of rock stabilisation measures (such as rock bolts), resulting in the cessation of unravelling and any other unstable or loose schist blocks.

Figure 3.11: A wedge failure (a consequence of blasting) that may not have taken place under natural conditions as the intersection of the two faces (directly above the hammer) is dipping too steeply. A classic small wedge failure has occurred in the top centre, a result of the removal of support of the underlying schist blocks. The intersection between these two planes has a much shallower dip, thus would have occurred naturally.

Figure 3.12: Ravelling of minor schist blocks (immediate right of the hammer), which may continue if left unsupported, and result in the formation of larger wedge-type failures.

Figure 3.13: A series of sub-vertically dipping joints which have acted as releasing surfaces for simple translational planar sliding parallel to the foliation.

Figure 3.14: Unravelling and undermining of the rock face has left the overlying rock unsupported. A small wedge failure has resulted in the top left of the photo. The intersection between the two planes of the wedge failure has a shallow dip (out of the slope) and has subsequently failed (towards the viewer).

3.6 STABILITY IMPLICATIONS.

A summary of results obtained from various engineering projects throughout Otago is summarised in Table 3.9.

Table 3.9: Summary data table from projects around Otago.

		Frankton Arm (This Work)	Clyde (Macfarlane et. al., 1991)	Macraes (Chapple, 1998)	Maniototo (Moody, 1985)	Gibbston (Johnson, 1986)
Friction (degrees)	Intact/Fractured Schist	20-36	23-32		22-33	29
	Sheared Schist	6-11	8-28	3-6	8-12	15-32
Point Load Strength (Range $I_{s(50)}$) MPa		0.11-3.83	0-3.63 (McKenzie, 1993)	0.65-3.14	0.3-9.4	-
Anisotropy Index		4.1	3-8	7.3	2.3	-
Dominant Clay Mineral		Kaolinite	Mica-smectite	Swelling Chlorite/ Smectite	Montmorillonite	-
% Clay-sized Particles in Sheared Material		4.5	30	-	2-18	20-30
Cohesion (MPa)	Intact Schist	-	10-90	-	2	0.34
	Sheared/Fractured Schist	0	0	0	0	0
UCS (MPa)	Parallel to foliation	-	61-105	5-61	9-46	-
	Perpendicular to foliation	-	33-72	-	28-86	-

Data obtained for along Frankton Arm correlates well with data from Clyde damsite investigations. Friction angles for intact schist from all other locations and the artificially fractured schist tested in this study are very similar. Clyde investigations obtained greater ranges of values for friction in sheared schist than were found from Frankton Arm, however this may be attributed to the limited number of samples tested in this study, compared with Clyde Damsite Investigations. Cohesion values are zero for shear zone material for all areas studied in Otago Schist.

Point Load strengths correlate well with data from Clyde and Macraes, although Moody (1985) has obtained higher point load strengths for Maniototo. Anisotropy Indexes are similar for Frankton Arm and Clyde, but vary for Macraes and Maniototo.

The dominant clay mineral for along Frankton Arm (kaolinite) differs from the clay minerals found in other areas (smectites and montmorillonite). The X-ray Diffraction Analysis completed in this project did not identify any smectites (although there may be <5%), even though the glycolated test was run twice, looking for swelling clays.

Results of laboratory work for this project appear higher than values from Macraes, although this is probably because the mine is situated within a mineralised shear zone, whereas Frankton Arm and Clyde are not. Work conducted at Maniototo was undertaken within pelitic schist and quartzofeldspathic schist, whereas testing in this project was only done in quartzofeldspathic schist, thus variations are to be expected. Overall, there are significant variations between each individual project within the Otago Schist.

3.7 SYNTHESIS.

- $I_{s(50)}$ values obtained from point load strength testing ranged from 0.60MPa to 3.83MPa (for samples tested perpendicular to schistosity), and from 0.11MPa to 0.92MPa for samples tested parallel to schistosity. This classifies the rock as weak to strong.

- Friction values for artificially fractured rock ranged from 24° to 36° for ϕ_b and estimated values of 26° to 73° for (ϕ_b + i) values.

- Friction values for shear zone material ranged from 6 to 11°, with zero cohesion, and residual shear behaviour is inferred to be by a sliding mode.

- X-ray Diffraction analyses revealed kaolinite, albite, muscovite, clinochlore, quartz and hornblende as the clay-sized minerals present in the shear zone material, with kaolinite as the dominant mineral in the samples tested.

- Schmidt Hammer hardness testing indicated joint wall compressive strengths ranging from 21MPa to 46MPa for tests conducted normal to schistosity. It is inferred from results obtained in this project that joint wall compressive strength is approximately half that of the uniaxial compressive strength of intact schist bedrock (using results from Clyde).

- Stereographic analysis illustrated four major defect sets within the schist bedrock, and these features contribute to destabilisation of the rock mass. SMR values ranging from 52 (summer conditions) to 44 (winter conditions) were calculated, and implies the rock is marginally stable, and support measures should be implemented. However, specific site investigations would be necessary to confirm this statement, as SMR only makes general predictions about stability conditions, and cannot be used for detailed quantitative assessment of the failure parameters of a slope.

- Data obtained from geotechnical testing was similar to values obtained from Clyde. This may indicate failure models for Frankton Arm are similar to those obtained in the Cromwell Gorge for example, failure may occur along foliation shear zones as it does in some of the slides at Clyde, which normally occurs within schist bedrock.

CHAPTER 4

QUEENSTOWN HILL LANDSLIDE.

4.1 INTRODUCTION.

This chapter examines the Queenstown Hill Landslide along Frankton Arm as determined by engineering geological investigations of the area. The primary objectives of this chapter are to:

1. Discuss possible failure mechanisms in schist bedrock, as determined by previous investigations from other areas in schist terrain.
2. Describe the Queenstown Hill Landslide in terms of surface morphology;
3. Examine the failure in terms of aerial photographs, field evidence and kinematics to determine an engineering geological failure model;
4. Conduct factor of safety sensitivity analyses to determine parameters necessary to promote failure;
5. Discuss the geotechnical failure models;
6. Consider any implications of the landslide for the residential area below the landslide.

Studies of the Queenstown Hill Landslide have been conducted without subsurface investigations, due to budget limitations. Information has been obtained from aerial photograph interpretation and surface engineering geological mapping.

4.2 FAILURE MECHANISMS IN SCHIST BEDROCK.

4.2.1 General.

Slope development is strongly influenced by the nature of the schist bedrock as the foliation provides continuous planes of weakness along which sliding may occur. Because of the strongly directional character of the schistosity, failure is favoured where slopes are developed parallel or sub-parallel to it with a dip at a shallow angle out of the slope at approximately 20-30°. The pattern of jointing and shearing (faulting) provides further

conditions favourable to the development of often large ($\geq 10^8 m^3$) slope failures; however, many smaller ($<10^6 m^3$) landslides involve only plane- or wedge- sliding on joint sets. The detailed geomorphology of Frankton Arm is the result of the lithological characteristics of the area, while the glacial processes may have acted as natural triggering mechanisms for slope failure (Bell, 1982).

Initial development of slope instability in schist terrain occurs by three predominant modes:
1. Planar sliding in which down dip movement along foliation or foliation shear zones is the predominant type. Planar sliding may also occur along suitably oriented crushed and sheared zones (faults) that cross-cut foliation;
2. Wedge failures, which may involve intersecting joint-joint or joint-foliation release of unfavourably oriented blocks;
3. Toppling failures generally in the head scarp area controlled by high-angle, slope-parallel jointing (figure 4.1; Beetham et. al., 1991).

4.2.2 Toe Buckling.

Bell (1987) introduces the concept of gravitational spreading and toe buckling as a probable precursor slope movement to observed major foliation-controlled landslides in schist terrain. He observed that the toe buckling and the infilled topographic depressions above the K9 landslide head scarp provide evidence for slope movements prior to and as a consequence of large-scale failure. The triggering of the K9 and Roaring Meg landslides then required some mechanism of toe support removal, such as river incision or glacial over-deepening. The former was the final initiating factor in the K9 landslide. Initial slope movements may have involved creep on schistosity surfaces or foliation shears, and pelitic schist horizons provide the most common sites for shear failure, as micaceous schist is a comparatively ductile rock material which deforms readily by creep movement (Bell, 1987).

The evidence for both toe "buckling" and gravitational "spreading" in the K9 Landslide is summarised in figure 4.2. Buckling of the toe and partial over-riding by displaced blocks from up slope is represented by schist block rotation. Graben features have developed as a result of toe "buckling" and rock mass displacements of possibly as much as 100m, and have

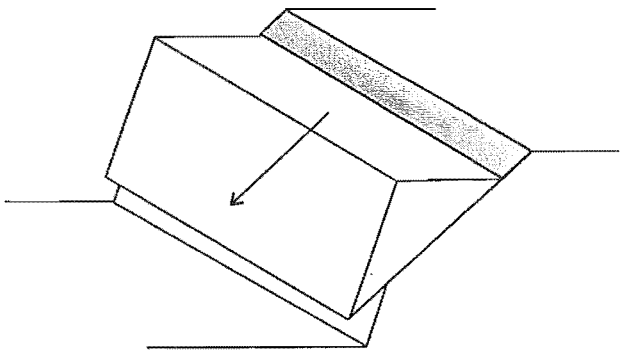

Planar Failure in rock in which a discontinuity (such as foliation) "daylights" the slope face.

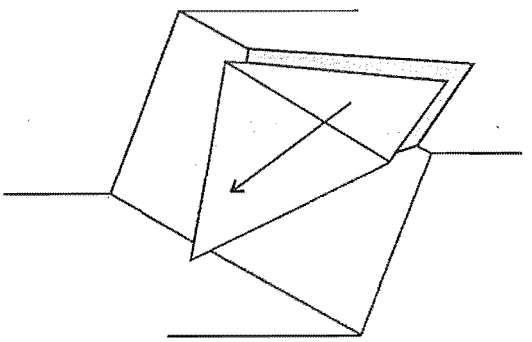

Wedge Failure on two intersecting discontinuities with a line of intersection (such as foliation and a major joint set) which "daylights" the slope.

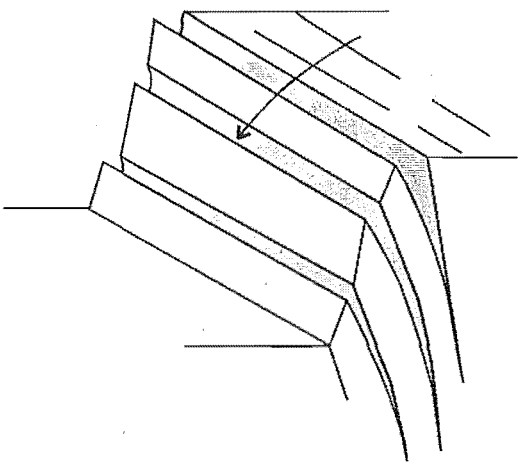

Toppling Failure in hard rock with slabs or columns defined by discontinuities that dip steeply into the slope.

Figure 4.1: Types of rock slope failures in schist terrain (from Hoek and Bray, 1981; and Norrish and Wyllie, 1996).

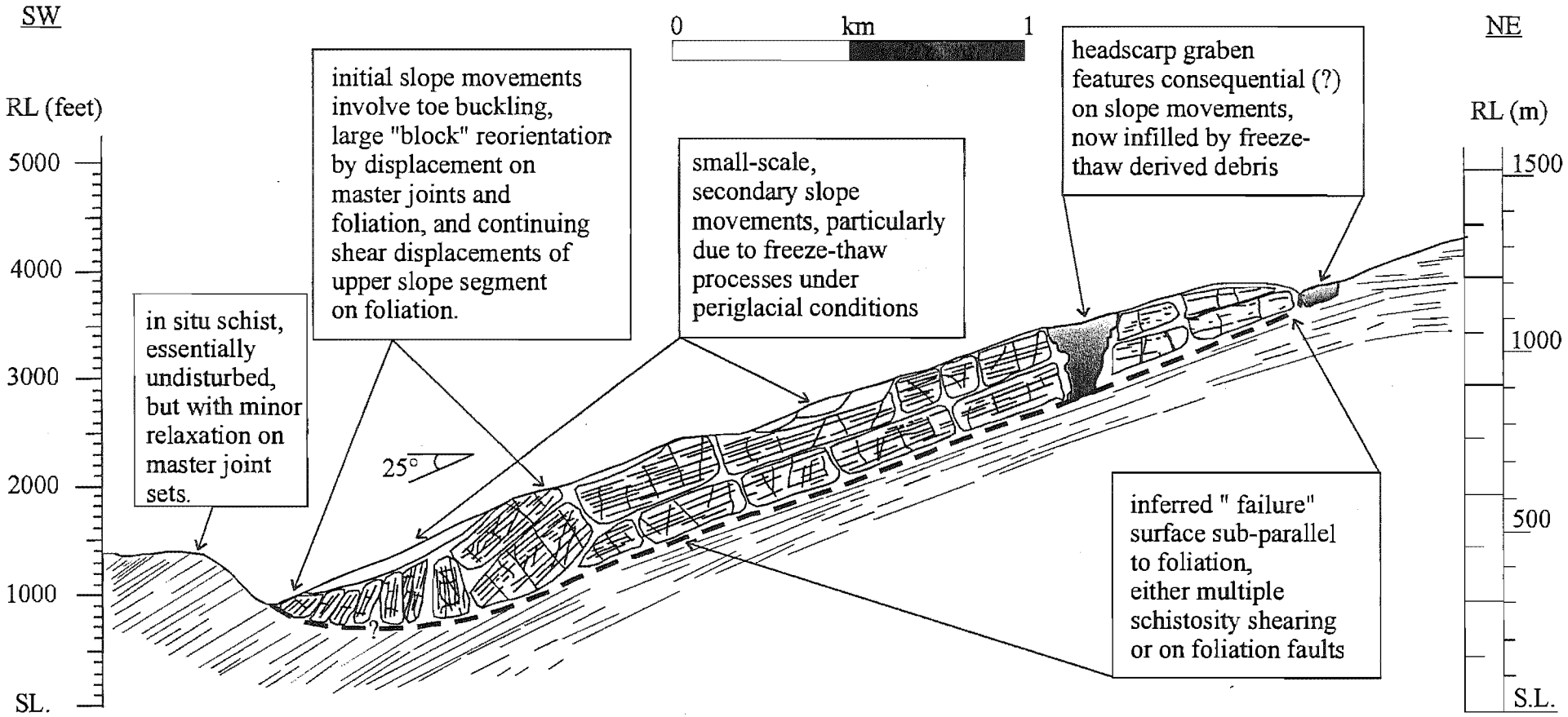

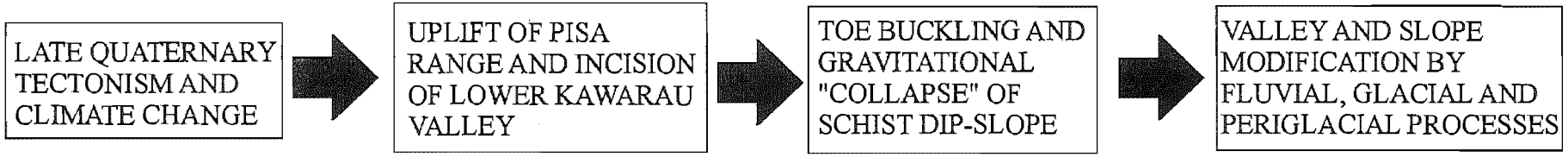

POSSIBLE CONTRIBUTING FACTORS

foliation attitude and geotechnical properties of schist; creep on foliation shear zones; earthquake shaking due to Pisa Fault movements; valley deepening by ice.

Figure 4.2: K9 Landslide, Kawarau Valley, Central Otago, showing toe buckling and gravitational spreading. Note the obvious schist block rotation in the lower part of the section. (From Bell, 1983).

subsequently been infilled by periglacial material. Movement probably took place along foliation shear zones, and shear displacement has occurred on steeply dipping joints approximately normal to the slope, if "buckling" has taken place (Bell, 1987).

Textural Zone IV schist rocks are found in the steep mountainous areas of Central Otago, New Zealand, and have deformed by slow bedrock creep over long periods of time. The variable foliation attitude in combination with the prominent jointing and localised shearing of the rock mass provides an important control of slope stability, and hence of landform development (Bell, 1982). The buckling observed by various authors (such as Beetham and Moody et. al., 1991; and Bell, 1987), has generally developed into landsliding on the flanks of steep slopes (about 20-30°). Areas such as the Cromwell and Kawarau Gorges show extensive development of toe buckling adjacent to the valley floor (Beetham et. al., 1991).

4.2.2.1 Kawarau Gorge.

The basement rocks in the Cromwell and Kawarau Gorge areas are similar to those found in the Wakatipu Basin. Grey schist is the predominant lithotype (similar to Frankton Arm), with a well-developed foliation of light (quartz-feldspar) and dark mica (muscovite) minerals segregated into thin (mm) layers of variable thickness and planarity. Green schist, a subordinate rock type is of two end varieties, a massive, dark green, poorly foliated, strong epidote schist and weaker foliated chloritic schist (Beetham et. al., 1991).

Multiple slide failures triggered by fluvial or glacial undercutting of slopes and extensive derivation of mass movement debris under periglacial conditions have occurred in the Kawarau Gorge. In addition, smoothing by mudflow activity and terracette development following glaciation, and in some localities renewed slope instability and mass movement has taken place (Bell, 1987).

4.2.2.2 Cromwell Gorge.

Extensive deep-seated landslides, formed mainly in schist bedrock, border approximately 25% of the shoreline of Lake Dunstan. Many of the slides have a relief of 300-500m and

slope lengths of one to several kilometres. Landsliding in the Cromwell Gorge has developed gradually over time in response to the erosion of the gorge by the Clutha River and tributary streams through the uplifting Dunstan-Cairnmuir Ranges.

A feature of the central Cromwell Gorge is the semi-continuous zone of steepened to overturned (sub-vertical) schist that outcrops predominantly on the left bank. These rock structures are consistent with deformation by toe buckling (figure 4.3). The rock mass is closely to moderately jointed and has numerous crushed and sheared zones sub-parallel to foliation, consistent with post-metamorphic, flexural slip deformation (Beetham et. al., 1991).

An example of toe buckling deformation without development of a basal failure zone has been found in drillholes and tunnels in the mid Nine Mile landslide area (figure 4.3). The subsurface evidence indicates that the schist was folded into an upstream plunging, gentle antiform structure (interlimb angle 140°) during the Jurassic-Cretaceous Rangitata Orogeny and the Kaikoura Orogeny (Miocene to Recent). This zone was later deformed by toe buckling in the near-surface zone (0-100m depth), so that the hinge and down slope limb have been over-steepened to form an accentuated, asymmetric fold with an interlimb angle of 90° (Beetham et. al., 1991).

4.2.3 Foliation Shear Zones.

4.2.3.1 Terminology.

Foliation shear zones are narrow (commonly less than 100mm wide) schistosity faults that have developed during folding and deformation of the schist in the Central Otago area. They are associated with clay-rich material of low shear strength and cohesion, along which slope failure may readily occur if the zones are appropriately orientated. These shears may have formed by stress within a weak pelitic/micaceous layer contained in the schist rock, as the platy minerals will readily align and subsequently form failure surfaces, particularly if water has become concentrated along the zone. An example of this is the Gibbston Slide, where movements accompanied by over-steepening, rotation and deformation of schist blocks have occurred on weak, micaceous foliation laminae and unfavourably oriented rock mass defects (Johnson, 1986).

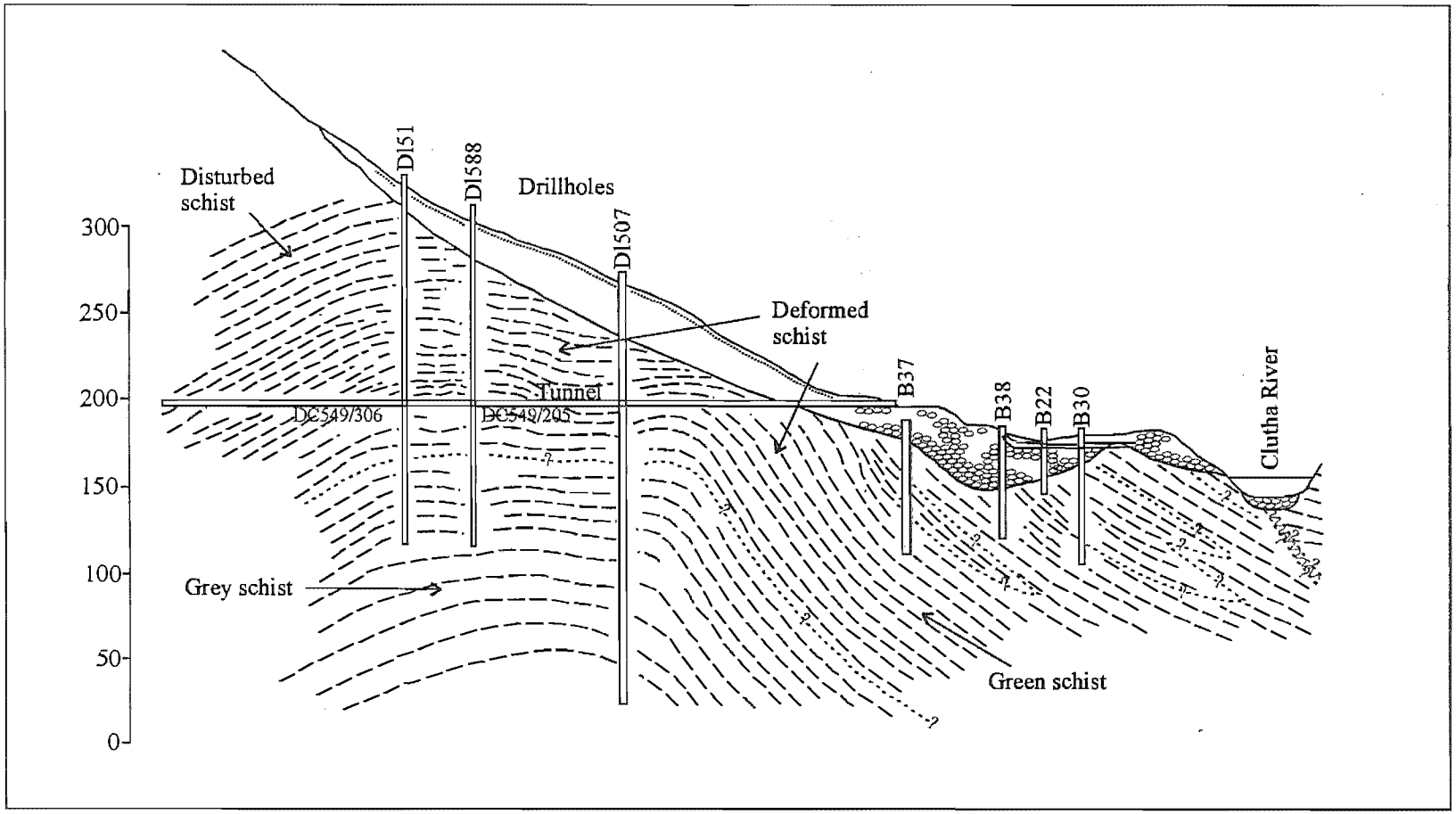

Figure 4.3: An example of toe buckling deformation without development of a basal failure zone in the mid Nine Mile Landslide area, Cromwell. Subsurface evidence indicates the schist is folded into an upstream plunging, gentle antiform structure (interlimb angle 140°) which has been later deformed by toe buckling in the near-surface zone (0-100m depth, so that the hinge and downslope limb have been oversteepened to form an accentuated, asymmetric fold (interlimb angle 90°). (Redrawn after Beetham et. al., 1991).

4.2.3.2 Kawarau Gorge.

From geological observation of natural slopes by Bell (1987) along the Kawarau Gorge, foliation controlled movements occur on schist slopes dipping between about 20 and 30°. For steeper dips the foliation is "buttressed" (as the foliation will not daylight) and toppling may become a factor for dips exceeding 70°. Most commonly slope failures occur by displacements on foliation shear zones (or schistosity faults), for example the K9 Landslide, which may be a few millimetres in width and tens of metres in length. Lateral and head scarp release takes place along near-vertical master joint sets that are sub-parallel to the dip and strike of the foliation, and slide "blocks" of variable proportions have a tendency to break up along joints and schistosity during slope movement (Bell, 1987).

4.2.3.3 Cromwell Gorge.

Most of the slides in schist bedrock and colluvium within the Cromwell Gorge are considered to be creeping translational rock and chaotic debris slides developed along foliation surfaces, foliation shears, fault crush and shear zones and joints. The chaotic debris is often very thick (tens of metres), and overlies gravitationally displaced schist bedrock, which is underlain by a basal shear zone. Crushed and sheared zones within the slide mass typically have low shear strengths, and are commonly controlled by thin gouge seams consisting of moderately to highly plastic clay with persistent slickensided surfaces. The zones range from 0.5mm to approximately 1 metre thick. Highly plastic clay gouge seams (with friction angles of 8-14°) are presumed to be derived from original tectonic crushed zones, and lower plasticity gouges are thought to be due solely to gravitational processes (Macfarlane et. al., 1992).

As well as forming failure zones, many defects also act as ground water barriers (aquicludes or aquitards) below and within landslides. This often results in complex ground water systems, which include multiple perched aquifers within slides. Confined ground water systems exert significant uplift pressures, which can have a major influence on landslide stability (Macfarlane et. al., 1992).

4.3 QUEENSTOWN HILL LANDSLIDE.

4.3.1 Description.

4.3.1.1 Distribution and Extent.

An initial reconnaissance of the Queenstown Hill Landslide by stereographic viewing of vertical aerial photographs was undertaken using numbers 232477 and 232500, Run C, taken in 1956. Enlargements of these aerial photos covered by the northern side of Frankton Arm were produced by New Zealand Aerial Mapping Limited, Hastings, at scales of 1:5000 (figure 1.2 – map pocket) and 1:10000 (figure 4.4), and subsequently used for engineering geological mapping.

The author also took oblique aerial photos of the site during November 1998. A topographic basemap of the field area was produced by Terralink on AutoCAD. Clark, Fortune, McDonald and Associates assisted by conducting a GPS survey of Goldfields Track and the associated power lines.

Geological mapping of the site was carried out at a scale of 1:5000. This involved collecting data on bedrock geology, surficial geology, slope morphology and slope movement features. Geomorphic data, including shear cracks, ridges, major and secondary scarps were also noted and added to the base plan.

The Queenstown Hill slide is 1500m in length (from head to toe) and 1600m in width, with a vertical elevation of 400m from head scarp to toe area and an estimated volume of 240 x $10^6 m^3$ (figure 1.2 - map pocket). A deeply incised stream originating from behind the head scarp runs down the eastern lateral margin, with a prominent joint-controlled lateral scarp existing on the western margin of the landslide. Aerial photographic interpretation showed a well defined but degraded head scarp situated 20m below the summit of Queenstown Hill trending northeast-southwest. The toe of the slide was difficult to detect using aerial photographs, and in addition difficult to find in the field as a result of regenerating vegetation and steep slopes. It is however, inferred to occur approximately at the level of the power lines (trending east-west) then changes to trend northeast southwest (figure 1.2 – map pocket).

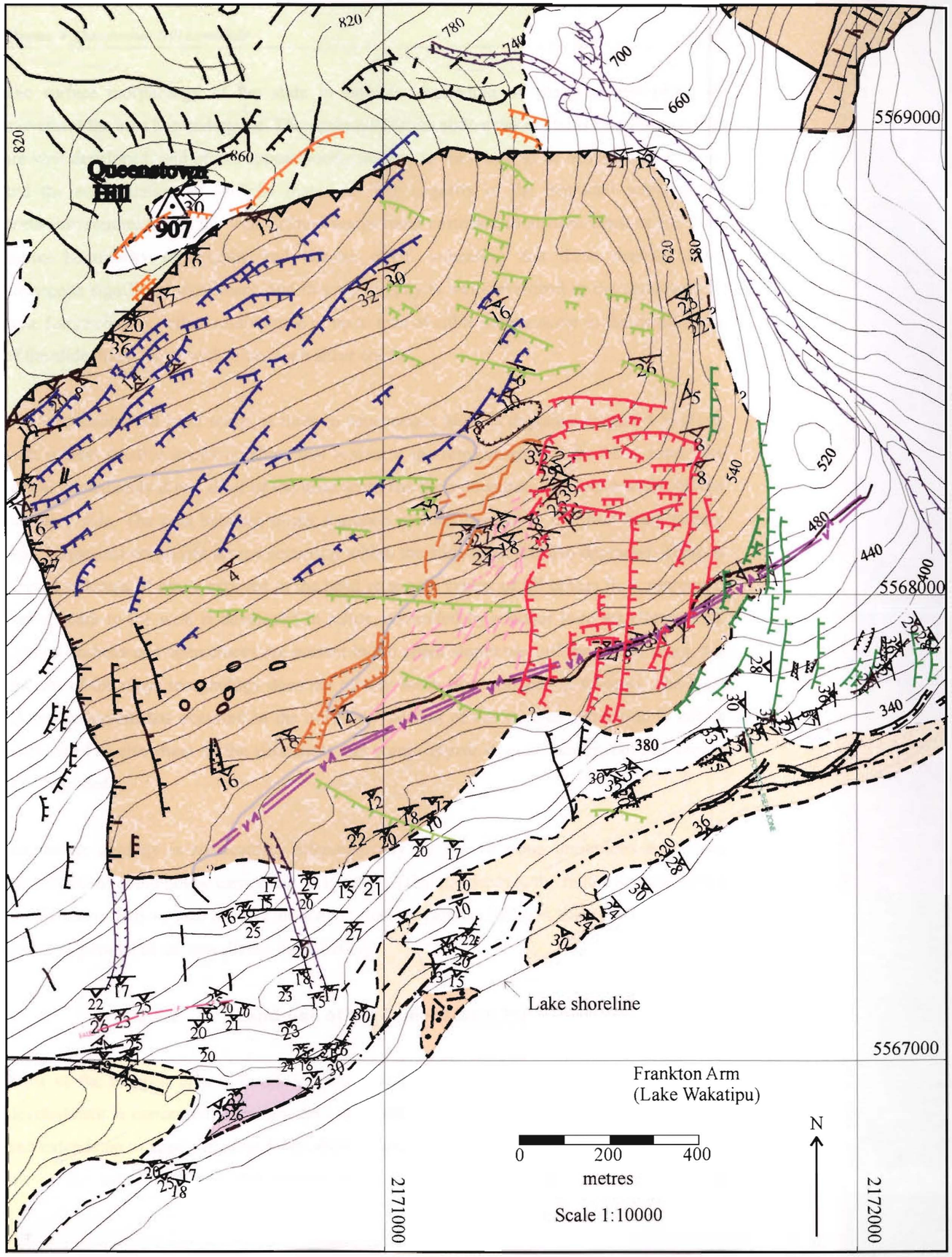

KEY

- Raised Beach Terrace (+48m above lake level)
- Eroded Gully
- Lineament (interpreted from aerial photographs).
- State Highway 6A
- Area of Sinkholes
- Depression
- 4WD Track
- Power lines
- Zone of shear cracks and voids (area of maximum compression and bulging).
- Scarps from last (most recent) phase of movement. Relaxation into void left by green scarps, subsequently forming a shallow compressional zone in the toe area.
- Degraded scarps formed during the second phase of movement, after the removal of support by the first phase of movement.
- Scarps from the earliest phase of movement caused by glacial undercutting or preferential removal of the weaker pelitic schist horizons.
- Area of joint-controlled release scarps.
- Lateral margins daylight to provide area of release for movement to occur.
- Retrogressing head zone
- Glacial Moraines
- Approximate limit of slide (toe).
- Lateral scarp (joint-controlled).
- Head scarp (degraded).

SURFICIAL GEOLOGY
(Modified from Cunningham, 1994).

- Landslide Material
- Otiran-age Glacigenic Deposits
- Terrace Alluvium
- Alluvial Fan Deposits
- Fan Delta Deposits
- Queenstown Hill and Sugar Loaf Till
- Schist Bedrock

For more detailed descriptions see Figure 1.2 (Map Pocket).

Figure 4.4: 1:10000 geomorphological map of the Queenstown Hill Landslide.

The surface morphology of the slide is variable, depending on the type and phase of movement the area has undergone. The upper half of the slide mass contains many scarps that are well developed, and others appear poorly defined as they tend to be obscured by erosion and the accumulation of surficial materials. The majority of the degraded scarps trend northwest-southeast, and the well-defined scarps trend northeast-southwest. Most of the slide shows hummocky topography and chaotic relief, indicating that these deposits have undergone significant movement, and this topography is well-developed in the southwestern area. Large chasms with a void volume of up to tens of cubic metres occur in the central area of the slide mass, along with wide, open shear cracks.

The joint-controlled head scarp, at three to four metres high, is degraded (figure 4.5) along with several smaller scarps up slope that represent the retrogressing of the head zone. The region immediately down slope of the head scarp has been downthrown relative to the blocks on either side. The area between forms a graben running parallel to the head scarp (figure 4.5). Numerous secondary scarps occurring within the slide mass are also degraded. There is limited outcrops of schist exposed in the head zone as a veneer of till covers it. A prominent lateral scarp to the west is developed in schist, controlled by a major joint set (figure 4.6). Several grabens and open cracks are present in the upper slopes west of the lateral scarp, but the rest of the slope morphology does not clearly show slope movement features. The most recent movement has occurred in the northwest portion of the slide as vegetation is not as established as elsewhere on the slide mass and scarps appear slightly fresher, but this area is still degraded.

Subsurface geology is restricted to inference only, as due to many limitations subsurface investigations could not be carried out. It is inferred that the depth to the failure surface occurs at 100-150m. This surface follows the schist foliation, perhaps foliation shears, or along schist fractured parallel or sub-parallel to the foliation.

4.3.1.2 Land-use of the Queenstown Hill Landslide.

Most of the mapped area is farmland, predominantly for sheep and cattle grazing. Urban development is concentrated immediately surrounding the Frankton Arm of Lake Wakatipu and extends up to approximately 440m above sea level. State Highway 6A crosses below the toe of the landslide. Grass and tussock cover the upper half of the slopes, with sparse

Figure 4.5: The Queenstown Hill Landslide degraded head scarp, showing the graben running parallel to the head scarp.

Figure 4.6: The prominent western lateral scarp of the Queenstown Hill Landslide. Photo taken looking west.

(~4m high) pine trees; while the density of pine trees and other native and introduced scrub is much higher in the lower half of the slope (figure 4.7).

Prior to the 1950's the majority of the slope was clear of vegetation, except for a sparse covering on the lower western corner of the slide mass. In addition, the power line access road was not constructed until the 1970's, with the 4WD track (Goldfields Track) leading to the summit of Queenstown Hill not established until later by the landowner.

4.3.1.3 Bedrock and Surficial Deposits.

Bedrock consists of Otago Schist (psammitic and pelitic greyschist with a bedding attitude of approximately 283/23S) with a thin band (100m) of green schist occurring about 1km west of the landslide area. Bedrock is described as:

> *Fresh to weathered; moderately hard to hard; moderately strong to strong; closely foliated; grey quartzofeldspathic and pelitic SCHIST (Haast Schist Textural Zone 4).*

Deposits of schist-derived bouldery debris, and displaced schist masses, have been mapped within the slide area. Landslide debris consists mainly of schist-derived materials (angular schist blocks up to 10m in dimension) and minor amounts of brown-grey gravelly sandy silts with some clay.

The large displaced schist blocks are separated in places by open and/or infilled joints and zones of sheared and crushed material (figures 1.2.1 and 1.2.2 – map pocket). The foliation within the slide mass is sub-parallel to the underlying undisturbed rock and the basal failure surface, and slide blocks have been only slightly rotated relative to one another. Blocky debris occurs where disruption is greatest; that is, where there is hummocky topography (table 4.1; terminology follows Macfarlane et al., 1992).

A fault zone can be traced on aerial photographs for more than 1km across the lower slopes of Queenstown Hill (figure 1.2 - map pocket). In a test pit on Newman Property (Bell, 1985b) intensively folded and sheared schist is present, with clay-rich "pug" zones up to 150mm wide: this is considered to form part of the same fault zone, which trends in a general NW-SE direction and controls the stream alignment above the property (figure 1.2 - map pocket). This

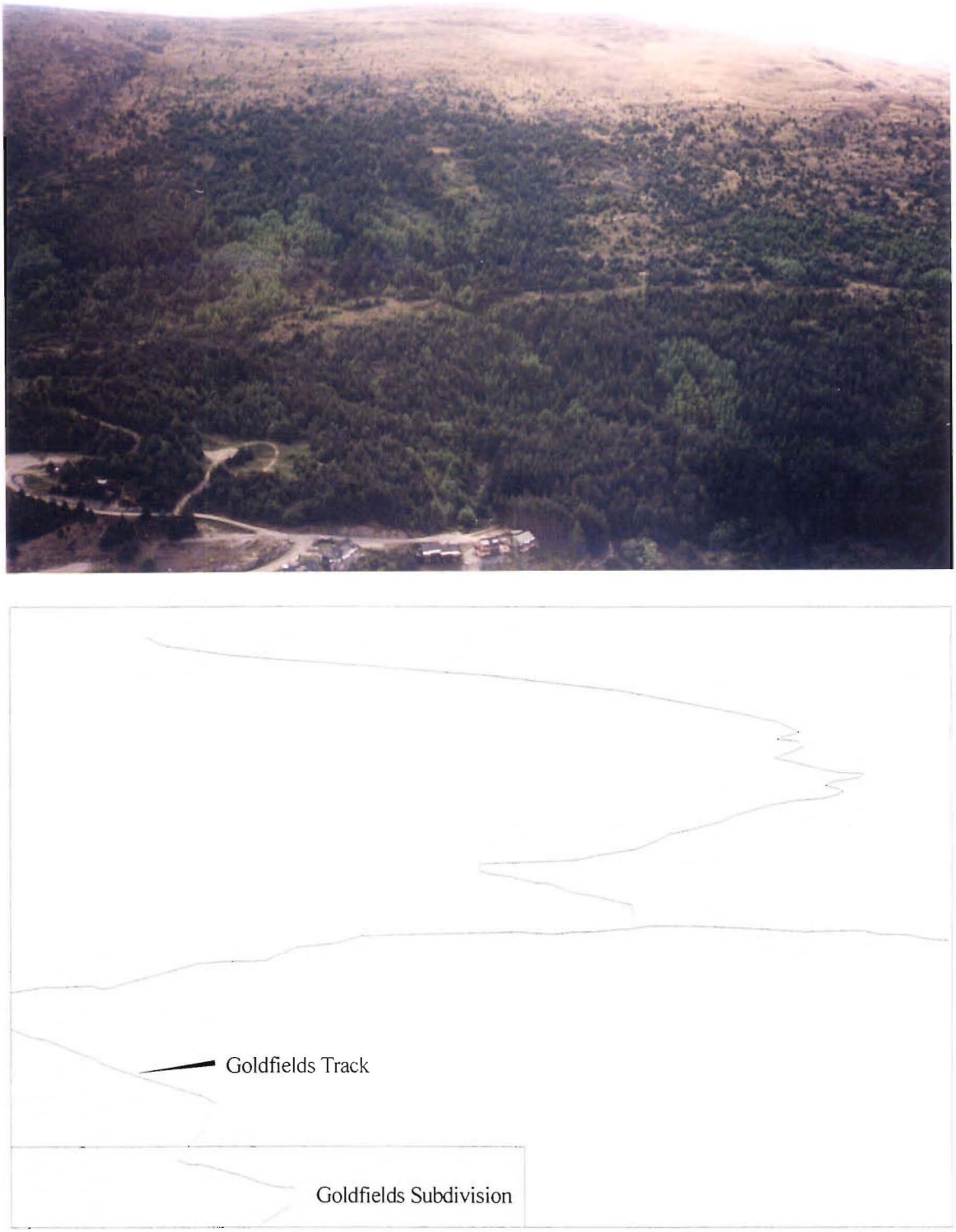

Figure 4.7: Queenstown Hill Landslide, showing Goldfields Subdivision in relation to the landslide area, and the 4WD track to the summit. Note the prominent lateral scarp to the left (west) and the concentration of vegetation on the lower slopes. The head scarp is at the skyline.

Term	Mass Description	Surface Characteristics	Type of Movement	Degree of Displacement
Chaotic Debris	Gradation from large competent rock blocks to fine grained material (commonly intensely sheared and crushed schist) with gouge seams. Foliation attitudes of blocks normally highly variable. Slickensided downslope-dipping internal or basal failure zones.	Laterally impersistent breaks in slope (i.e. hummocky). Well-developed slide scarps where active. Blocks on surface.	Rotational, translational, or complex slide.	10's to 100's of metres.
Displaced Schist	Large competent rock blocks either in contact or separated by open and/or infilled joints or by zones of sheared/ crushed material. Foliation either parallel or oblique to undisturbed rock, and adjacent blocks may be slightly rotated relative to one another. Slickensided near downslope-dipping internal or basal failure zones, typically sub-parallel to foliation or pre-existing rock defects (Also termed "Blocky Debris", where disruption is greatest).	Laterally persistent breaks in slope (i.e. broadly irregular). Forms outcrops locally.	Translational slide.	metres to 10's of metres.
Basal Failure Zone	Crushed zones and gouge seams with some sheared and shattered schist of variable thickness. Fabric may be sub-parallel to boundaries, contorted, or totally disrupted. Gouge seams typically thin but persistent with slickensides, orientated downslope.	Outcrops rare.	Slide.	mm's to 100's of metres.
Disturbed Schist	Sub-slide rock mass with partly open defects often infilled. Typically quartz-rich massive and laminated schist. (Termed "Relaxed Schist" in near-surface situations).	Relaxed schist forms prominent outcrops similar to undisturbed schist.	Stress relief processes.	mm's to metres.
Deformed Schist	Sub-slide rock mass, fissile with discrete sheared and crushed zones sub-parallel to flexurally deformed ("buckled") foliation, steepened to overturned locally. Typically mica-rich laminated schist.	Prominent outcrops with foliation dipping at moderate to high angles to undisturbed schist.	Bedrock flow, by stress relief and/or gravitational processes.	mm's to 10's of metres.
Undisturbed Schist	In situ rock mass with closed defects.	Forms prominent outcrops.	None.	None.

Table 4.1: Terminology used in slope movement interpretation, Cromwell Gorge (Macfarlane et. al., 1992).

clay-rich zone is concealed beneath glacial till and/or high-level (approximately +48 metres) lake beach gravels: this indicates that there has been no movement on the fault for at least 10000 years (and probably much longer than this period). The schist bedrock itself is weakened by past fault movements and subsequent weathering (Bell, 1985).

In places, a thin veneer of glacial till covers the slopes and this may be described as:

> *Fresh to slightly weathered; dry to wet; compact; greenish-grey; massive; medium gravelly SAND; sandy medium GRAVEL and gravelly SILT; SP-GP.*

Along the lower slopes – below the landslide feature - fan-delta (gravels and sands) and beach deposits are extensively developed around the lake shoreline, which formed as Lake Wakatipu lowered some 45m between 9000 and 5000 years ago.

The Queenstown Hill Landslide is the largest landslide present in the study area. Field evidence suggests the landslide is a translational planar slide at least several thousand years old. Investigations by Bell (1997b, unpubl.) at the Marina Heights Subdivision noted the presence of a weathering profile 800mm thick in landslide deposits from Slide No. 3 (Section 5.5.1). From this he has implied the deposits are at least several thousand years old. This may also be the case for Queenstown Hill. The slide base is inferred to be 100-150m below the surface interpreted by the construction of cross sections and the fact that the depth to length ratio is approximately 0.1 for a translational slide (Cruden and Varnes, 1996).

4.3.2 Failure Models.

4.3.2.1 Possible Failure Model.

For toe buckling to take place on Queenstown Hill, the schistosity must be parallel to the slope. In this case, taking into account that there has been no subsurface investigation, the failure surface, foliation and slope face may not be parallel. If the slope angle is steeper than the foliation, the foliation will daylight in the slope, causing a simple planar slide. Furthermore, all previous investigations conducted in landslides with a toe buckling mechanism, slopes have been greater than 1500m in length and dipping at a steeper angle,

which possibly creates enough mass and driving force necessary for deep-seated toe buckling to take place. Toe buckling occurs along the Kawarau and Cromwell Gorges, and the slopes in these places have an average dip of 25 – 40° (whereas Queenstown Hill is approximately 19°), and are just over 2km in length.

In all previous studies that have concluded toe buckling to be the failure mechanism for the landslide studied, deep valley incision has been a dominant factor in the history of slope deformation. In the case of Frankton Arm, glacial oversteepening has taken place, but not the deep valley incision that has taken place over thousands of years in areas such as the Cromwell and Kawarau Gorges. The slope on Queenstown Hill is concluded as being too flat for toe buckling to take place (figure 1.2.1 – map pocket). Toe buckling or valley bulging implies a more deep seated failure surface, and if this were the case, the failure surface would extend out beyond the lake. Subdivision reports by Bell (1985a, 1985b, 1989, 1994, 1995, 1997a, 1997b, 1997c) completed along the lower slopes of Queenstown Hill, have indicated that the schist is in situ, thus the failure surface cannot extend below lake level, but must be shallower, placing the toe at a higher elevation.

4.3.2.2 Preferred Failure Model.

The preferred failure model consists of a classic translational slide, with the toe forming a shallow compressional bulge instead of a toe buckle (as toe buckling infers a more deep-seated deformation within the schist). In map view, the orientation and placement of shear cracks (figure 4.8) were an indication of schist compression. Deep, open fractures of 3-4m are common, with some up to 20m in depth and 3m in width. Trenches along strike and parallel to the slope represent preferential removal of weaker pelitic schist by ice scouring. In the translational slide model (figure 4.8; figures 1.2.1 and 1.2.2 - map pocket), compression in the toe area has resulted from a slow creep of the rock mass.

The upper part of the slide mass, with no support, moved down slope, acting as an overriding block, cutting off the drainage channels of the lower slopes, and forming a compressional zone from gravitational relaxation on to the undisplaced material on the lower slopes. The middle block (figure 4.9) is still acting as a compressional zone with the upper block having thrust into it as field and aerial photograph evidence shows numerous tension features and

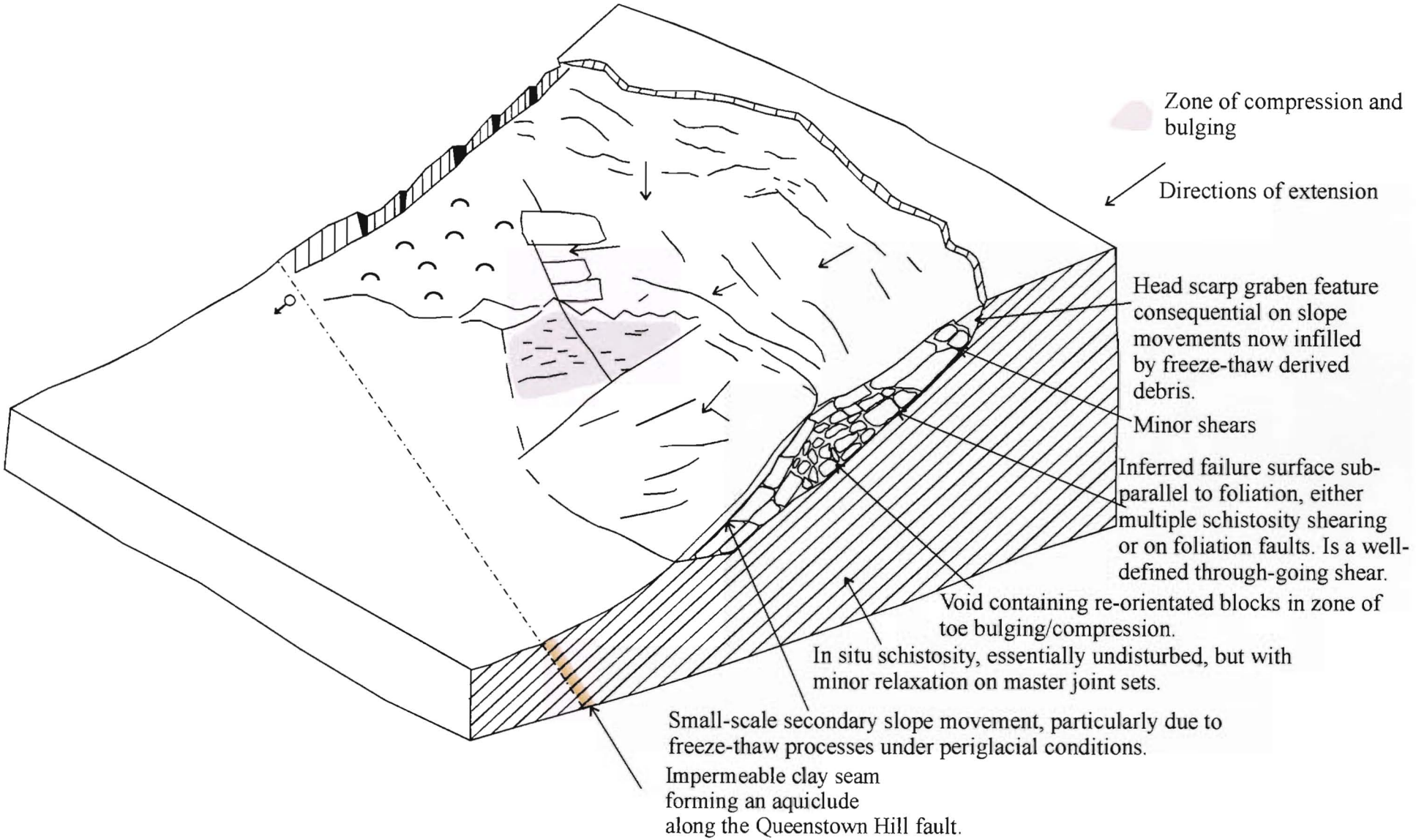

Figure 4.8: Schematic block diagram of the Queenstown Hill Landslide preferred toe compression model.

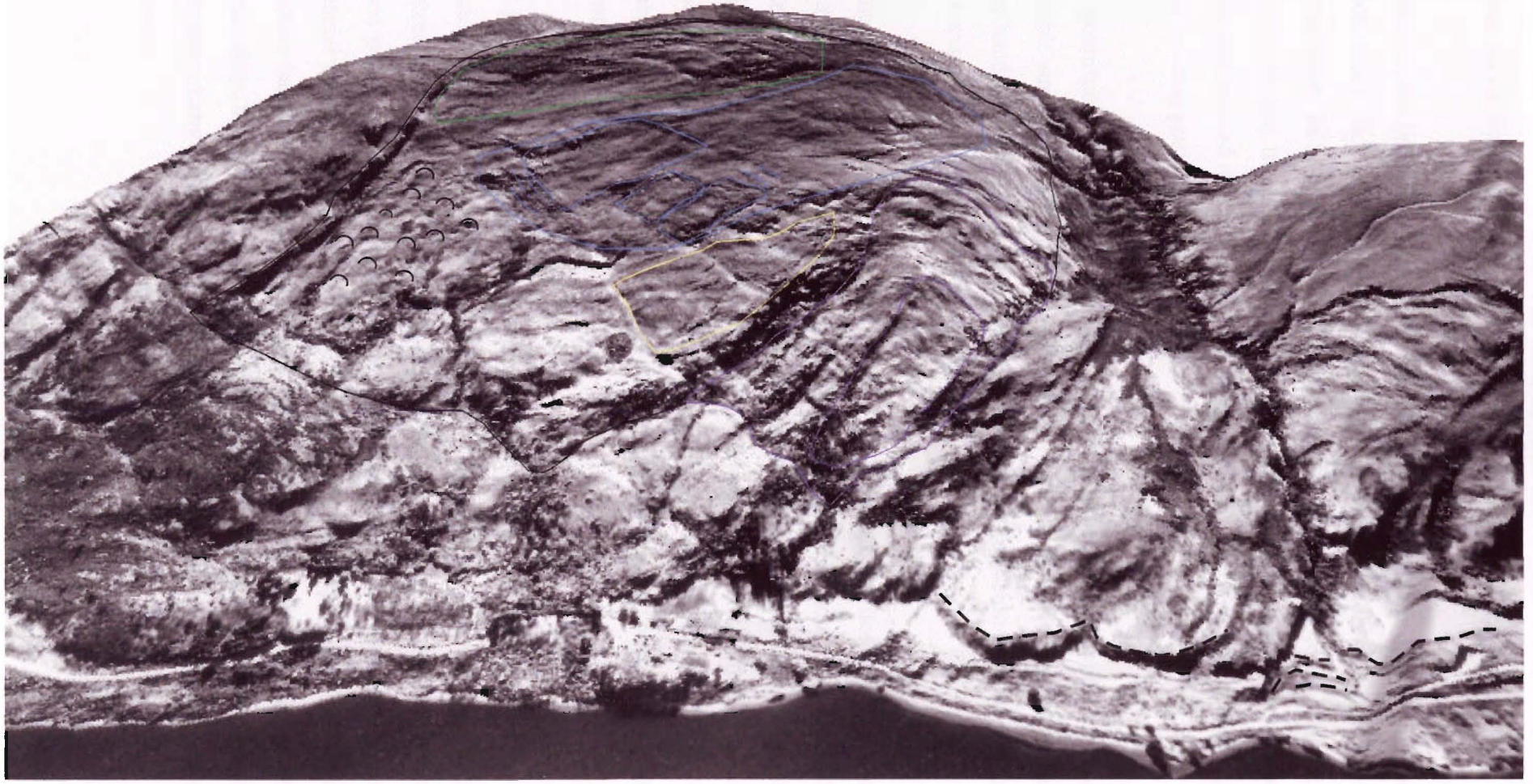

First phase of movement

Second phase of movement

Third phase of movement

Zone of compression

Hummocky Topography

Beach Terraces

Figure 4.9: Computer-generated 3-d visualisation of the Queenstown Hill Landslide facing north, showing various phases of movement (generated using *Visual Explorer 98*).

open voids within this area. The limit of slide debris occurs where the drainage gullies have been cut off by the down slope movement of the upper block (figure 4.9).

Geomorphic features therefore indicate that the Queenstown Hill Landslide is a translational rock block slide according to Varnes' (1978) classification system. The surface of rupture presumably follows foliation and steps across foliation along joints. The failure plane follows a discontinuity that is parallel to the slope, and the toe of the mass forms a wedge that ploughs into undisplaced material causing compression beyond the toe of the surface of rupture (figure 1.2.1 – map pocket).

Hutchinson (1988) has drawn attention to confined movements that have a scarp but no visible surface of rupture in the toe of the displaced mass. He suggested that displacements in the head of the displaced mass are taken up by compression and slight bulging in the foot of the mass as is the case on Queenstown Hill.

The activity of the Queenstown Hill Landslide can be described as retrogressive, as the surface of rupture extends in the direction opposite the movement of the displaced material. Geomorphological features indicate the failure is a multiple landslide in that it shows repeated movements of the same type, often following enlargement of the failure surface. This may mean the original head scarp was located at a lower elevation on the slope. The newly displaced masses are in contact with the previously displaced masses and share a failure surface with them.

It is inferred that three phases of movement have taken place within the Queenstown Hill landslide mass (figure 4.8 and figure 4.9). These phases have been determined by stereographic analysis of aerial photographs and engineering geological mapping. During the first phase of movement a small translational failure has occurred, perhaps as a result of glacial erosion and undercutting of foliation shears within weak pelitic schist layers. This feature has no lateral support on its eastern margin, and this would have contributed to overall instability. Several retrogressive scarps have formed up slope of this shallow failure. With the absence of any subsurface data, it is inferred that movement has occurred along foliation shear zones.

The second phase of movement has formed a series of degraded scarps trending northwest-southeast, in the north east area of the slide. A small series of translational planar slides have occurred during this phase of movement (as they are trending in the same direction as the degraded scarps) in the central area of the slide. The main degraded scarps may have formed as a result of retrogression of these smaller translational failures. Bulging of the toe area is evident on the aerial photos in the larger of the secondary failures. Down slope of this zone, the topography is very hummocky, (figure 4.10) with displaced schist blocks.

The third phase of movement has taken place in the northwestern section of the failure. The scarps have formed as a series of retrogressive features striking northeast-southwest, and the mass moving down slope has come into contact with a large in situ schist block that has acted as a buttress. A series of tension cracks and large voids (of more than $10m^3$) have resulted, forming sub-parallel to the scarps. This area of tension represents the zone of maximum compression of the toe area for the slide mass. The toe has formed a 'roll over' structure, as the schist block down slope has acted as a buttress restricting any further movement.

4.3.3 Kinematic Analysis.

Stereographic analysis of the foliation data obtained from the Queenstown Hill Landslide is shown in figure 4.11. The figure shows a pole plot of geological conditions likely to lead to a planar failure (Hoek and Bray, 1981). Foliation within the slide is dipping at 16°S and the slope is dipping at 19°.

The following factors indicate failure on Queenstown Hill is kinematically possible:

- Poles lying within the daylight envelope may daylight in the slope face, thus represent discontinuities along which planar failure is kinematically possible.
- The strike of the planar discontinuities (the foliation) is within 20° of the strike of the slope face (figure 4.11), and the dip of the foliation is within 20° of the dip of the slope face, indicating landsliding may be taking place because schistosity is sub-parallel to the slope.
- The lateral extent of the failure mass is defined by a lateral release surface that does not buttress or restrict movement of the mass.

Figure 4.10: Hummocky topography of the Queenstown Hill Landslide, taken from the western lateral scarp looking east. The Crown Terrace is in the distance, with the Shotover River flowing at the base of The Remarkables.

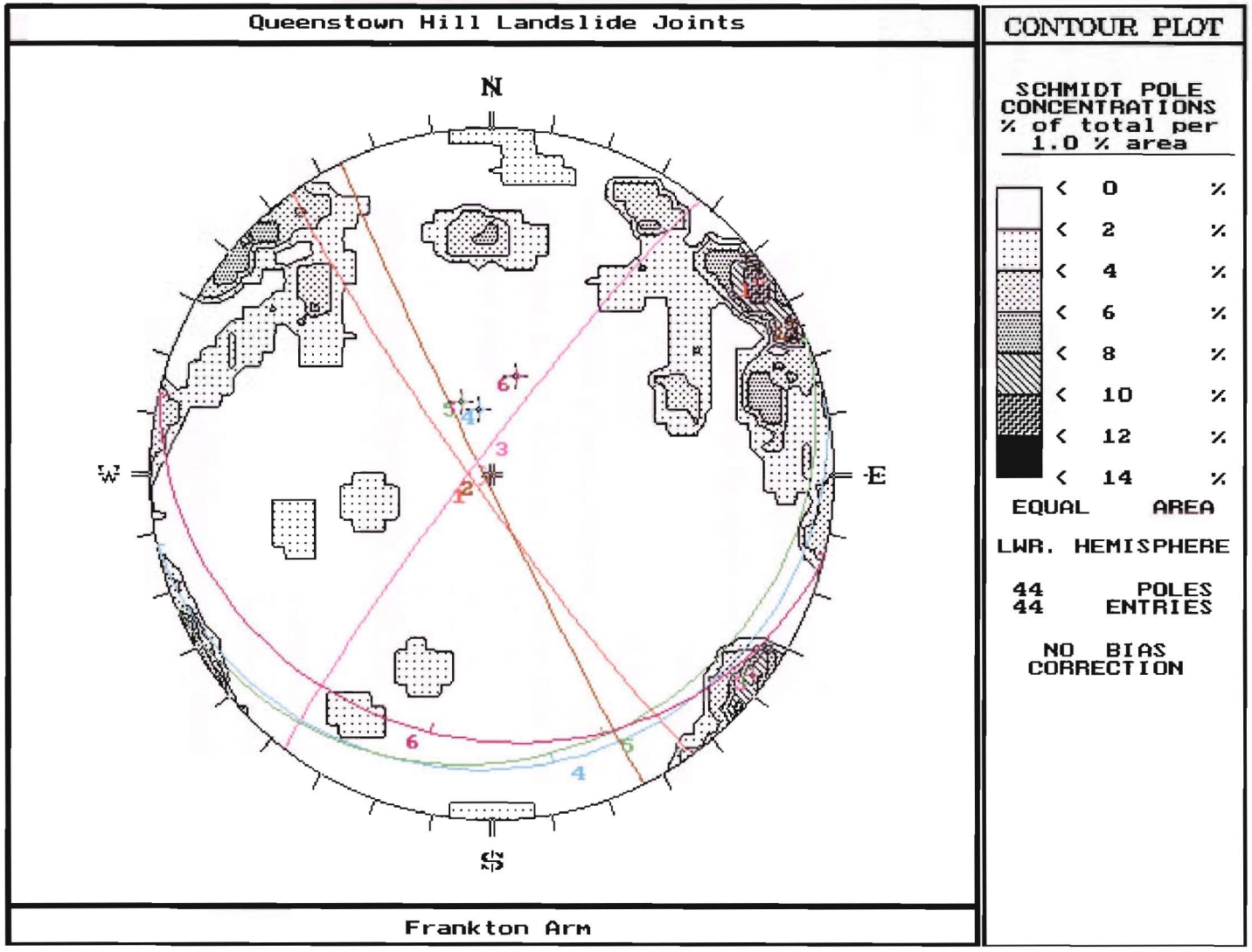

1 = 144/85SW] master
2 = 153/88SW] joint
3 = 217/85NW] sets

4 = Great circle representing plane corresponding to centre of pole concentration 078/16S

5 = Great circle representing slope face 066/19SE

6 = Great circle representing plane corresponding to undisturbed schist (from outside landslide area) 103/24S

Figure 4.11: Queenstown Hill data showing the master joint sets and major structural features.

- The presence of significant pore water pressures (during and immediately following glaciation) along the failure surface can in some cases alter the possibility that planar failure will take place, even if the above-mentioned conditions are met.

Kinematic analysis concludes that a friction angle of 30° (a value obtained during shear testing of artificially fractured rock) will, using kinematics, not initiate sliding, as the plunge of the slope face is less than the angle of friction (figure 4.12). A complex step-like failure surface is therefore interpreted if the failure surface is situated along the foliation, which would increase the dip of the surface of rupture to greater than the residual friction angle. Small steps formed by schistosity defects are connected by fractures which exist in the crushed rock mass and these define a failure surface that has a dip steeper than schistosity but less than the slope angle. Figure 4.13 shows the structure of the Queenstown Hill Landslide using a friction angle of 8°. This would be the kinematic situation if failure occurs completely on foliation shear zones. A zone of instability according to the Markland Test forms, and the intersection of the displaced schist foliation and the slope face fall in this area. Kinematically, these intersecting planes may be a cause of instability within the slope.

Failure is inferred to have occurred along pre-existing defects such as foliation shear zones or along the weaker pelitic layers within the schist. As can be seen in Figure 4.11, kinematics illustrates that the orientation of the foliation within the slide mass is very similar to the orientation of the slope face, a major factor contributing to slope instability. The major defects are also recognised as controlling lateral margins. In figure 4.13 joint sets one and two are orientated at right angles to the foliation, suggesting these defect sets have formed the prominent western lateral scarp.

4.3.4 Factor of Safety Sensitivity Analysis.

The main objective of the stability analysis was to determine if instability and parameters in place during movement of the Queenstown Hill Landslide could be predicted using a model constructed from known and inferred topographic and geotechnical data. Inferred values used were geologically and geotechnically reasonable, in order to indicate the minimum conditions required for failure (factor of safety of 1.0) to provide a sensitivity indication of the various failure parameters, and to determine a likely trigger mechanism for the landslide. The analysis

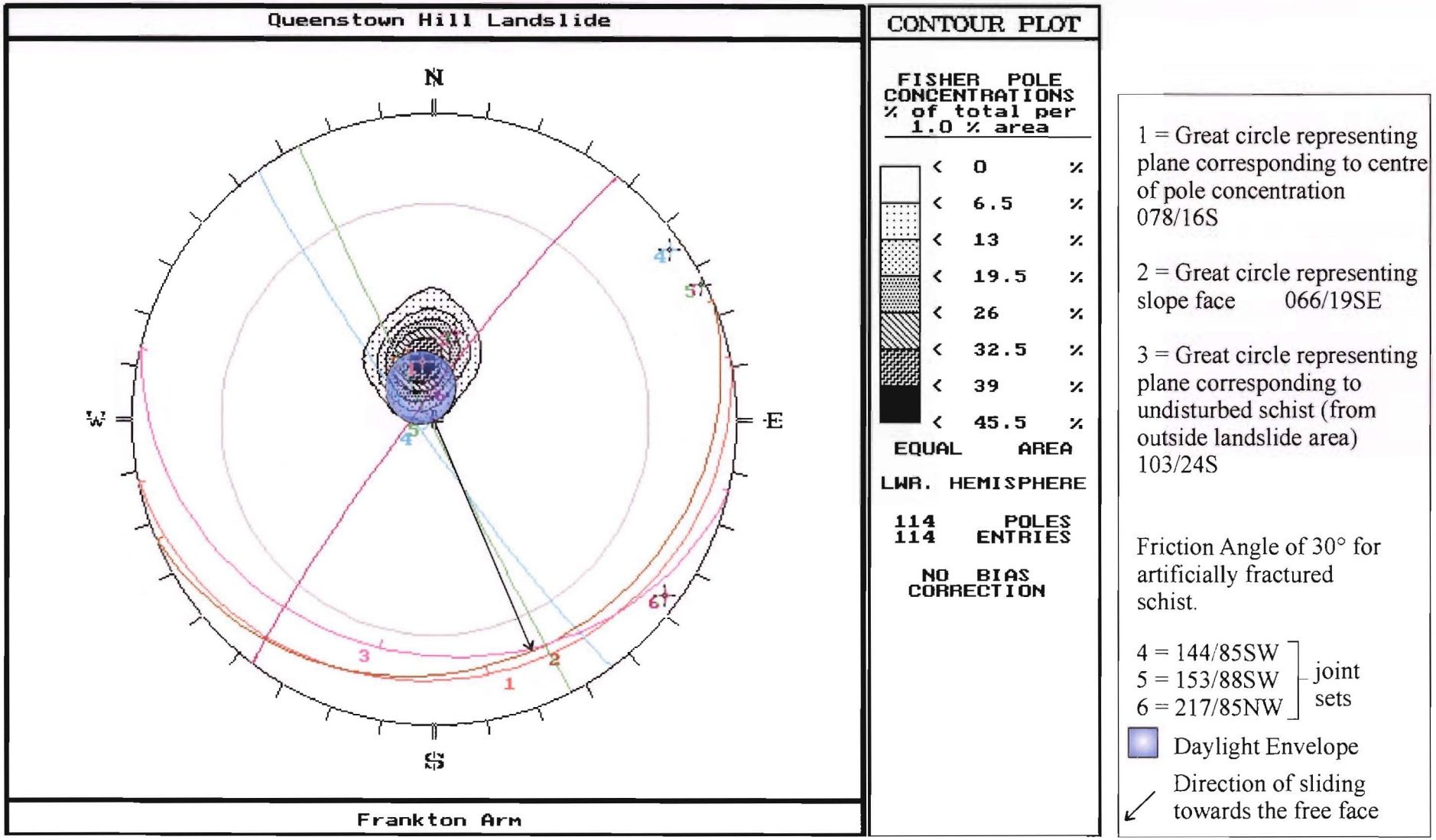

Figure 4.12: Stereonet showing major structural controls of the Queenstown Hill Landslide, using a friction angle of 30°, a value obtained from laboratory testing of artificially fractured schist collected from outside the slide area. There is no Markland's zone of instability formed.

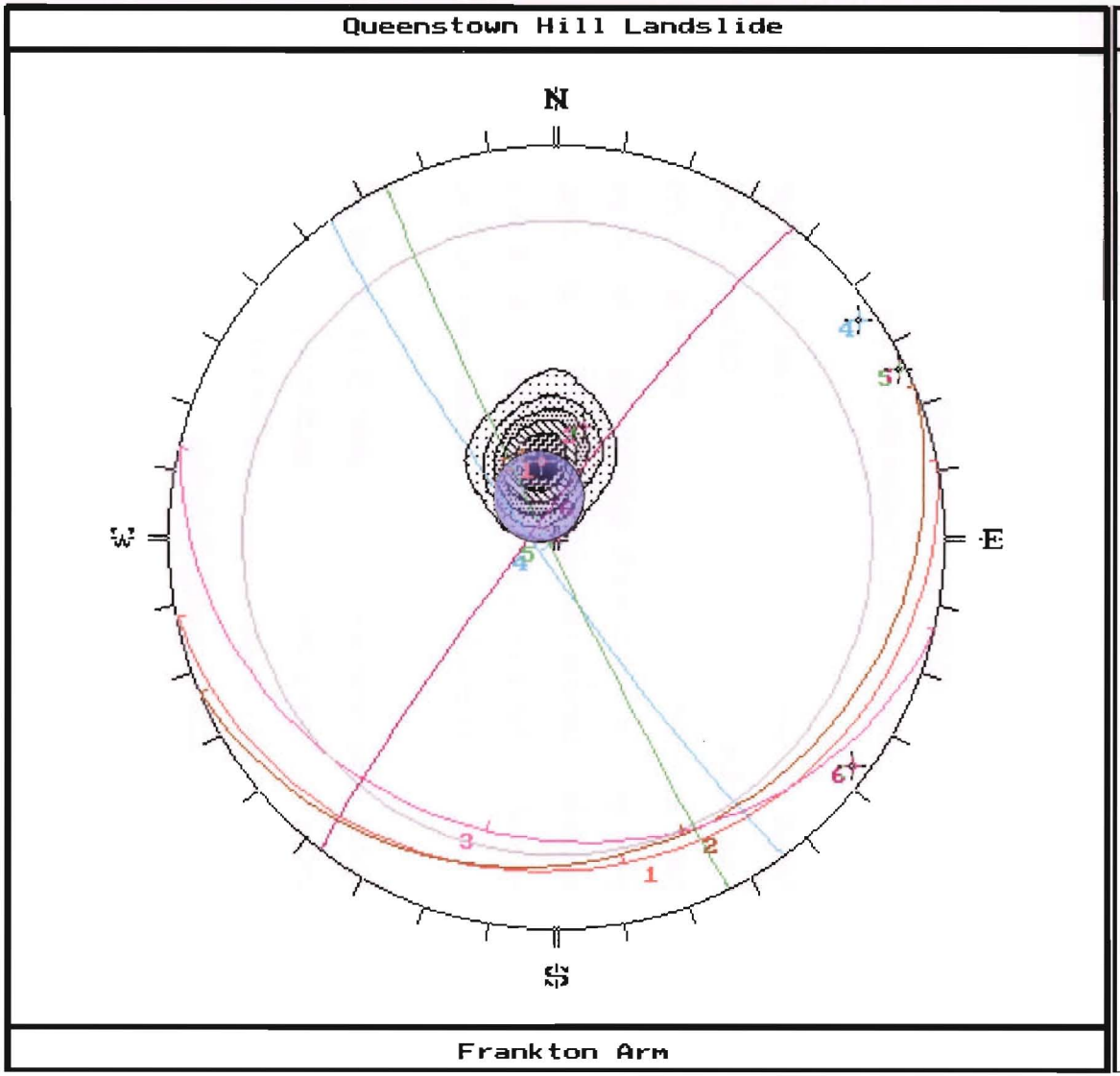

CONTOUR PLOT

FISHER POLE CONCENTRATIONS
% of total per 1.0 % area

< 0 %
< 6.5 %
< 13 %
< 19.5 %
< 26 %
< 32.5 %
< 39 %
< 45.5 %

EQUAL AREA
LWR. HEMISPHERE

114 POLES
114 ENTRIES

NO BIAS CORRECTION

1 = Great circle representing plane corresponding to centre of pole concentration 078/16S

2 = Great circle representing slope face 066/19SE

3 = Great circle representing plane corresponding to undisturbed schist (from outside landslide area) 103/24S

Friction Angle of 20° for fractured and/or sheared schist.

4 = 144/85SW
5 = 153/88SW
6 = 217/85NW
} joint sets

Daylight Envelope

Direction of sliding towards the free face

Figure 4.13: Stereonet showing major structural controls of the Queenstown Hill Landslide, using a friction angle of 20°, a value assumed for foliation shear zone material collected from outside the slide area.

considered the shear strength along the failure surface, the effects of pore water pressures, and the influence of seismic accelerations.

4.3.4.1 Sensitivity Analysis Assumptions and Results.

Results of the stability analysis (geometric model from Norrish and Wyllie, 1996) are summarised in table 4.2. A single failure plane extending the length and width of the entire slide mass was assumed for simplicity, however in reality this would not be the case. A uniform slide base is inferred for this study, but would not actually be the case. The failure surface would be highly irregular, with foliation shear zones in some places, interlocking blocks causing increased friction in other places, and points where the failure plane steps across the foliation. Values with a friction angle of 30° (for fractured schist) and 8° (for foliation shear zone material) were used to obtain realistic values for the Queenstown Hill Landslide. A 20° friction angle has been assumed for a realistic value for failure through crushed schist, or a maximum value of frictional resistance for failure through foliation shears zones. A 35° friction angle was assumed for a failure surface that steps across the foliation along joints. The analysis made many assumptions, however, the parameters that have the greatest effect on stability are still indicated in the analysis.

The sensitivity analysis has given an indication of possible triggering mechanisms for the Queenstown Hill Landslide. Cohesion values of up to 10kPa were used in the analysis, with varying depths of water within the slide mass. The preferred value would be 0kPa as with increasing displacement along foliation shear zones or along schistosity, the cohesion will decrease to zero. The analysis shows that with cohesion values of less than 10kPa, and a friction angle of 8°, the slide mass can fail along foliation shear zones, rather than through intact schist or schist that is fractured parallel to foliation.

Friction angles from 8° to 35° were used as input parameters. Laboratory testing indicated an 8° friction angle for clay-rich shear zone material, and this is the lowest value assumed if the failure surface is situated along foliation shear zones. Using a dip angle of 16° for the failure surface (obtained from the construction of cross-sections), with ground water levels within the slide mass anywhere from dry to at the ground surface, the variable values of the friction angle will have a major effect on stability. Using a friction angle of 20° (for failure occurring within crushed schist) the slope is sensitive to the depth of the perched water table within the

Table 4.2: Factor of Safety values for Queenstown Hill Landslide.
(Geometric model from Norrish and Wyllie, 1996)

Cohesion.						
when:			$z_w/z = 1$	$z_w/z = 0.5$	$z_w/z = 0$, $\phi = 8°$	$z_w/z = 0$, $\phi = 20°$
	c' = 0kPa	FS =	0.87	1.45	0.49	1.27
$\phi = 30°$	c' = 2kPa	FS =	0.88	1.46	0.5	1.28
$\varphi_p = 16°$	c' = 5kPa	FS =	0.89	1.47	0.51	1.29
$\alpha = 0$	c' = 10kPa	FS =	0.91	1.5	0.53	1.32

Friction Angle					
when:			$z_w/z = 1$	$z_w/z = 0.5$	$z_w/z = 0$
c' = 0kPa	$\phi = 8°$	FS =	0.21	0.35	0.49
$\varphi_p = 16°$	$\phi = 20°$	FS =	0.55	0.92	1.27
$\alpha = 0$	$\phi = 25°$	FS =	0.7	1.17	1.63
	$\phi = 30°$	FS =	0.87	1.5	2.01
	$\phi = 35°$	FS =	1.06	1.76	2.44

Depth of Perched Water Table				
	z_w/z	FS	when $\phi = 8°$	when $\phi = 20°$
when:	0	2.01	FS = 0.49	FS = 1.27
c' = 0kPa	0.5	1.45	0.35	0.87
$\phi = 30°$	0.75	1.16	0.28	0.67
$\varphi_p = 16°$	1	0.87	0.21	0.47
$\alpha = 0$	1.1	0.76	0.18	0.39
	1.25	0.6	0.15	0.28

Seismic Acceleration				
when:	α	FS	$z_w/z = 0$, $\phi = 8°$	$\phi = 20°$, $z_w/z = 0$
$z_w/z = 0.5$	0	1.45	FS = 0.49	1.29
c' = 0kPa	0.1	1.4	0.48	1.25
$\phi = 30°$	0.25	1.31	0.45	1.2
$\varphi_p = 16°$	0.5	1.17	0.42	1.11

Angle of Failure Plane				
when:	φ_p	FS	$z_w/z = 0$, $\phi = 8°$	$\phi = 20°$, $z_w/z = 0$
$z_w/z = 0.5$	15	1.54	FS = 0.52	1.34
c' = 0kPa	16	1.45	0.49	1.27
$\phi = 30°$	20	1.18	0.39	1
$\alpha = 0$	25	0.95	0.3	0.78
	27	0.88	0.28	0.71
	30	0.79	0.24	0.63

slide mass. Instability is achieved with the ratio $z_w/z = 0.5$. Low friction angles can trigger instability while high frictional resistance may promote more stable conditions.

It is concluded from the analysis of friction angles in the sensitivity study that a possible triggering mechanism is along foliation shears or perhaps crushed schist with a friction angle value of up to 20°. The slope is very sensitive to friction, particularly when the depth to the perched water table is above half the depth of the slide base.

Depth of the water table within the failure mass was taken at six different depths – from dry to artesian water pressure (a possibility immediately following ice retreat). Failure can be triggered if the slide material has a friction angle of 35°, and the perched water table is close to the ground surface. At a ratio of $z_w/z = 0.5$, a maximum friction angle of 22° will promote failure. The slide will not take place (when $z_w/z = 0.5$) if the failure surface is situated in fractured schist (along foliation), especially if the slide base steps across the foliation along joints (35° friction angle assumed in this case). This statement assumes a uniform slide base across the entire landslide complex, and in reality, the surface would be highly irregular, and failing in a number of ways. If the water table is at the ground surface (as is inferred following ice retreat), then failure is possible through fractured schist (parallel to foliation).

Failure through fractured schist blocks is possible if the ratio of depth of water in the tension crack to depth of the tension crack is 0.75. Failure can be initiated at any water level (from dry to at the ground surface) along foliation shears. The evidence suggests high ground water levels have a great influence on stability, that is, the slope is sensitive to changes in ground water levels. A value of $z_w/z = 1$ could have been achieved during retreat of the Last Glaciation. A possible failure mechanism during ice advance on Queenstown Hill may be by ice plugged drainage, where fractures and joints within the bedrock may have become blocked by ice, inhibiting internal drainage. The water percolates into the ground or forms ice wedges in joints or rock crevices thereby creating and sustaining high pore water pressures. An artesian water system may have existed, as hydrostatic pressure exerted on the saturated mass may have been high enough to cause water levels to rise. The slope would have been extremely active with ice advancing and retreating along Frankton Arm a number of times. It is therefore concluded that high ground water levels on the failure surface during final retreat of the glacier, acted as a possible triggering mechanism on the Queenstown Hill Landslide.

Gravitational accelerations from 0 to 0.5g (MM IX) were used as input parameters for this analysis, as they took into account pseudo-static conditions, up to possible maximum accelerations predicted for the area (table 4.3). These are regarded as realistic estimates for the Frankton Arm area. Seismic accelerations will trigger failure if the base of the slide occurs through foliation shear zones. Seismic activity may have been the cause of landslide activity, but it is considered more likely that other factors, which acted over thousands of years (such as glaciation), than an earthquake, would have been involved in destabilising the slope. The analysis has taken into account the maximum possible earthquake for Frankton Arm, and at seismic accelerations of 0.5g, failure would not be triggered though fractured schist. However, the possibility that a large earthquake triggered instability cannot be disregarded, as more detailed investigations would need to be carried out to confirm this statement.

During this project, it was not possible to obtain any subsurface information on the landslides along Frankton Arm, therefore for this sensitivity analysis, the angle of the failure plane has been varied (from 15° to 30°). However, the preferred angle (obtained from kinematics, engineering geological mapping and construction of cross-sections) is 16°, sub-parallel to the slope. The analysis has used both friction values (30° and 8°) in order to include all possible failure mechanisms.

According to the model, sliding can take place with the failure surface angle as low as 15° along foliation shears, however, through fractured schist parallel to the foliation (with a friction angle of 30°), the failure plane must be at least 20-25° for sliding to be initiated. The angle of the failure plane would need to be confirmed by subsurface investigations, as it would have a variable angle of dip throughout the slope.

4.3.5 Queenstown Hill Preferred Failure Model.

The formation of glacial ice on the slope, while itself initially tending to support the landslide, would have elevated ground water levels in the area, resulting in increased hydrostatic pressure within the unstable mass. When the glacier retreated it would have removed lateral support, increased pore water pressures and reduced the shear strength of the slope. Ice may have moved along a weak foliation shear or pelitic schist horizon, causing increased undercutting at the level of the power lines (figure 1.2 – map pocket). The undercutting may have formed a lateral bench, and with the added influence of water (that

Table 4.3: Summary of data on active faults in the region (Gillon and Hancox, 1992).

Active Fault	Estimated MCE (Ms) [1]	Probability of Occurring (in 150 yrs) [2]	Recurrance Interval (yrs)	Time Since Last Event (yrs)	Distance From Frankton Arm (km)
Alpine	8.5	36 - 80%	500	< 800	80
Dunstan	7.5	2 - 7%	8000	c. 5000	40
Moonlight	7.5	4 - 21%	2000 - 4000	uncertain	10
Nevis	6.6	< 4%	c. 4000	c. 4000	30
NW Cardrona	7.4	2 - 8%	6500	> 4000	25
Old Man	c. 7.3	< 1%	> 35000	-	50
Ostler	7.5	4 - 21%	2800 - 4500	3000 - 3500	130
Pisa	7.4	< 1%	unknown	> 23000	35
Teviot	7.2	< 2%	> 16000	-	80

[1] MCE (Maximum Credible Earthquake) estimates derived using Fault Displacement Relationships of Siemmons, 1982.
[2] Faulting probabilities have been derived using the method of Rhodes and Miller (NZ Geological Survey, 1983).

Estimates of MM Intensity Return Periods in the Queenstown area:

Queenstown [1]	mean PGA (g) [2]
MM VI - 12 yrs	0.06
MM VII - 54 yrs	0.1
MM VIII - 250 yrs	0.18
MM XI - 1100 yrs	0.32

[1] From Smith and Berryman, 1986.
[2] Peak horizontal ground acceleration (PGA) from Murphy and O'Brien, 1977.

would cause weathering and alteration to ultimately form foliation shear zones), may have initiated failure.

Deep ground freezing during the Last Glaciation along Frankton Arm would have widened existing bedrock joints and opened up foliation. On the slope, whole jointed blocks may have become separated and moved downhill. Movement is inferred to have been by translational planar sliding by slow rock creep, possibly along foliation shear zones and a stepped failure surface immediately following glacial retreat. Small minor slides began in the south west area of the slide, causing an additional removal of support for the areas up slope. Translational sliding then began in the western side of the mass, with movement towards the southwest. This caused retrogression in the northeastern area.

Preferential removal of the weaker pelitic schist, along with other highly weathered schist blocks would have occurred during ice coverage as a result of ice scouring and initiated instability in the southeastern area of the slide. Movement of the slide mass has followed pre-existing discontinuities in the schistose rock, some of which may have been widened by the increased pore water pressure or ice blockage within the rock mass defects during glaciation.

4.3.6 Origin and Movement History.

It has been established in earlier chapters that the Kawarau Lobe of the Wakatipu Glacier advanced and retreated along Frankton Arm a number of times during past glaciations. During the last phase of glacial retreat, the Queenstown Hill slope would have been highly active geomorphically. Water levels within the slope will have fluctuated, and ice-plugged drainage within schist bedrock fractures would have existed during ice advances. Elevated ground water levels within the slide mass on glacial retreats would have weathered, altered and eroded the platy micaceous minerals contained within the pelitic schist horizons. These areas would have ultimately formed the foliation shear zones failure is inferred to have taken place along. Rock mass relaxation due to unloading after the retreat of the glacier has formed opened joints within Queenstown Hill and these have acted as lateral and head scarp release structures. Movement has been accompanied by oversteepening, rotation and deformation of schist bedrock that has occurred on weak, foliation shear zones, and unfavourably oriented rock mass defects. Possible seismic triggers could have been the initiating failure mechanism, and created enough inequilibrium within the slope to cause failure.

Three phases of movement are suggested for the Queenstown Hill Landslide:

1. Translational sliding in the southeastern area of the slide, a result of increased glacial undercutting at the level of the power lines (~460m above sea level) along weak pelitic schist horizons or foliation shear zones. The eastern lateral release structure would have added to the instability.
2. Movement down slope towards the southwest to a depth of 100-150m has occurred in the northeast area as a result of the removal of support in the southeast (phase 1). A series of small, very shallow translational slides formed along with compression and bulging of the toe areas. Hummocky topography formed during this phase. The failed area continued to retrogress up slope, with continued enlargement of the failure surface at the same time.
3. Extension then took place in the northwestern area to a depth of 100-150m as a result of the removal of support directly down slope, with movement towards the southeast. The in situ schist block immediately down slope below the power lines has formed a buttress, restricting further gravitational creep movement. A compressed zone has resulted in the mid slope area, containing large open chasms and shear features. This phase would have formed the retrogressive head scarp and graben.

4.3.7 Age and Present Activity.

The age of the landslide is likely to have been after the Last Glaciation approximately 14000 years before present. During the Kumara 2 advance in the Otiran Glaciation, the ice over-rode the summit of Queenstown Hill, thus depositing the Camp Hill Formation. The exact age of the landslide remains unknown, however it is estimated to have occurred soon after retreat of the Last Glaciation (approximately 18-14000 years ago).

Comparison of 1950's aerial photographs with the author's fieldwork indicates that no visible movement within the last 50 years has taken place. There is no evidence for changes in surface morphology, which indicates the slope is quasi-stable with a factor of safety close to one. The landslide is classed as 'relict' in that it developed under different climatic conditions than at present. It may be reactivated, for example by development (creating increased stormwater run-off), road construction, etc. but precise details on possible future movement remain unknown.

4.4 IMPLICATIONS FOR RESIDENTIAL DEVELOPMENT.

There is minimum risk to residential development, as no movement has been visually detected for within the last 50 years, however further investigation is necessary to confirm this statement. The slide is inferred to currently be in equilibrium (with a factor of safety just above 1), however possible future development may affect the slide, thus site-specific geotechnical investigations (including detailed sub-surface investigation) would be necessary before any development within the slide area is initiated. If residential development were to proceed, storm water discharge must be well-controlled and confined as it could induce further movement on a landslide that is currently stable. Sewage tanks should not be constructed on the slide mass, they must be built elsewhere. It would however, be more appropriate to prevent future development on the slide mass, to ensure long-term stability. Existing residential development (such as Goldfields) is located on in situ schist thus is not under any threat of movement.

In comparing aerial photographs taken fifty years ago with field work done in 1998, there has been no evidence of any changes in surface morphology. Vegetation has become well-established obscuring a lot of the surface morphology, however establishment of vegetation is in itself an indication of stability.

4.5 FURTHER WORK REQUIREMENTS.

Additional work (such as one or two drill holes) is required to accurately locate the depth, shape and angle of inclination of the failure surface of the landslide, as the model presented in this work is a preliminary one only.

A surface movement monitoring network would need to be established to confirm the rate of movement (or even if there is any at all). Firstly, monitoring for surface displacement using instruments such as inclinometers, and secondly, monitoring of tension cracks at the maximum extent of compression using extensometers. This would give measurements of both horizontal and vertical movement within the unstable zone.

Determination of ground water movement and depth by the installation of a piezometer network at various points within the failure is an important measurement as ground water is a major cause or triggering mechanism of many landslides. Pore water pressure should be examined at the failure surface so that effective stress analyses may be performed or to assess to adequacy of internal drainage.

Determination of the rate of possible sliding (velocity) to provide information on stability measures necessary for future development within the slide mass.

4.6 SYNTHESIS.

- Toe buckling and foliation shear zones commonly occur in schist bedrock within the Otago region, for example the Cromwell and Kawarau Gorges.

- A possible failure model for Queenstown Hill is translational sliding with toe buckling, but this model has been dismissed as the slope does not meet the conditions necessary for toe buckling to take place.

- The preferred failure model for the Queenstown Hill Landslide is a simple translational slide with compressional bulging in the toe, with the formation of large open chasms, voids, and shear features.

- Three phases of movement have been interpreted from aerial photograph interpretation and engineering geological mapping, forming variable surface morphological features.

- The landslide has been classed as relict, as it developed under different climatic conditions (soon after the retreat of the Last Glaciation) than exist at present, and no visible movement has taken place within the last 50 years.

- The glacial ice on Queenstown Hill is inferred to have widened existing bedrock joints and elevated ground water levels which occurred following ice retreat. The water has weathered, altered and eroded the weak pelitic schist horizons, forming foliation shear zones, along which failure is inferred to have taken place.

- Seismic triggers may have been the final factor acting to initiate failure on Queenstown Hill. The maximum credible earthquake for the area would have been necessary, but this would not have been the only initiating factor in triggering instability.

- Simplified stability analyses concluded that pore water pressures have significant influence on the stability on Queenstown Hill. Low cohesion and friction values also contribute to instability on the slope.

- Results from the sensitivity analysis indicate that failure could have been triggered along foliation shears or crushed schist, with friction angle values of up to 20°

- With the perched water table for the slide mass at ground surface level, failure is possible with a friction value of 35° - an assumed value if the failure plane steps across foliation on joints (causing increased frictional resistance).

- The Queenstown Hill slope is sensitive to changes in ground water levels. Failure is possible through fractured schist if the ratio of the depth of water in the tension crack to the depth of the tension crack (depth to slide base) is greater than 0.75.

- It is recommended that detailed site-specific engineering geological and geotechnical investigations (including sub-surface investigations) be conducted if residential development is to proceed further up slope on to the slide mass, however no development is the preferred option.

CHAPTER 5

OTHER FRANKTON ARM FAILURES.

5.1 INTRODUCTION.

The primary objectives of this chapter were to:

1. Describe the Frankton Arm bedrock failures in terms of surface morphology;
2. Examine the failures using aerial photographs, field evidence and kinematics to determine engineering geological failure models;
3. Conduct factor of safety sensitivity analyses to determine parameters necessary to promote failure;
4. Discuss geotechnical and engineering geological failure models for each of the slides.

The surface morphology was mapped at a scale of 1:5000 (figure 1.2 - map pocket) and 1:10000 (figure 5.1) to obtain adequate detail and an overall view of the failures along Frankton Arm. Engineering geological mapping, aerial photograph interpretation and kinematic analysis was conducted in order to determine the structure of each landslide and its failure mechanisms. Input parameters for the sensitivity study were determined from laboratory testing, which has been discussed in Chapter 3.

5.2 GENERAL SETTING.

5.2.1 Distribution and Extent.

All of the failures along the Frankton Arm of Lake Wakatipu occur within the mid-shoulder area of ice coverage during the Last Glaciation (15000 years ago). Overall, elevations range from 310 to 680 metres above sea level. The Marina Heights Failure (the largest) covers approximately 11.25 hectares and Failure No. 2 area of instability extends over 5.25 hectares (the smallest failure).

Field evidence suggests that Slide No. 3 is the most active and unstable of all the failures along Frankton Arm with an area of instability covering 9 hectares. Slide No. 4 may extend

GEOLOGY

SLOPE DEPOSITS.
- Landslide
- Colluvium

STREAM, RIVER AND LAKE DEPOSITS.
- Recent Floodplain
- Fan
- Fan/Delta
- Lake
- Beach
- Terrace
- Alluvium:

GLACIAL DEPOSITS.
- Various Till Deposits
- Queenstown Hill and Sugar Loaf Till

BASEMENT GEOLOGY.
- Schist
- Geological Contact

GEOMORPHOLOGY
- Roads
- Powerlines
- Schist Attitude (dip indicated)
- Lateral Scarp
- Head Scarp
- Swampy Ground
- Lake
- Eroded Scarp
- Topographic Contour
- Schist Bluffs
- Approximate limit of landsliding
- Schist boulders
- Scrub Cover
- Incised Scarps

Contour Interval 20m

0 200 400 600 800 1000

1:10000

N

DRAWN: D STOSSEL.
DRAUGHTED: D STOSSEL.
GEOLOGY: D STOSSEL.
SURFICIAL GEOLOGY: V CUNNINGHAM; D BELL.

FIGURE 5.1

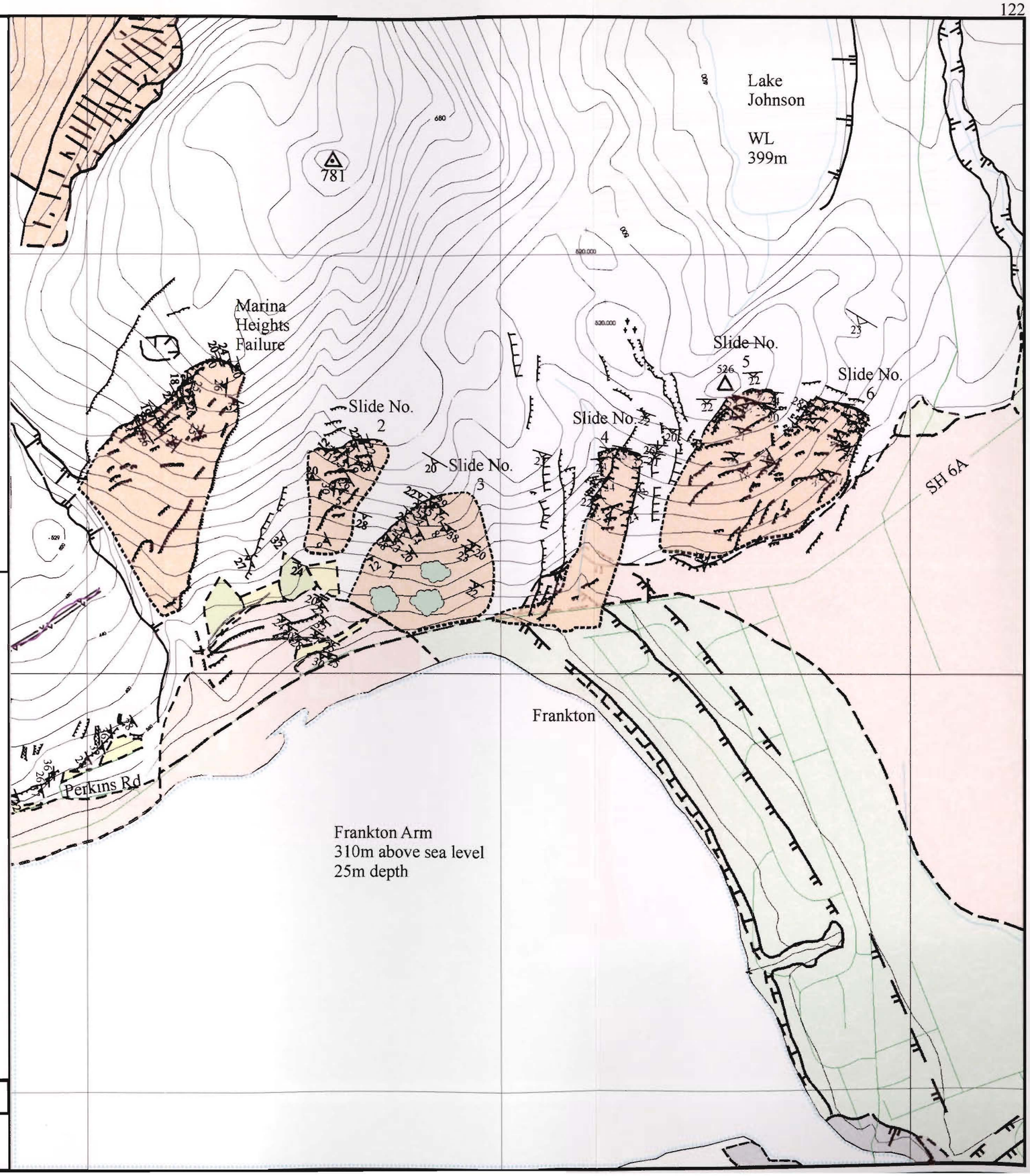

across to the southern side of the highway, but because of residential development dating back to the 1950's the true extent could not be determined.

Subsurface geology was obtained by the construction of cross-sections and engineering geological mapping. Due to budget limitations, no sub-surface investigations were carried out, therefore the depth and angle of the failure surface is an estimate only.

Table 5.1: Physical dimensions of the Frankton Arm Failures:

Landslide	Length (m)	Width (m)	Depth (m)	Volume (m^3)
Marina Heights	450	250	25	$2.8x10^6$
Slide No. 2	350	150	6	$3.1 x10^5$
Slide No. 3	325	300	20	$1.9 x10^6$
Slide No. 4	425	100	15	$0.6 x10^6$
Slide No. 5	400	200	8	$6.4 x10^5$
Slide No. 6	400	175	10	$7.0 x10^5$

5.2.2 Geological and Geomorphological Setting.

Engineering geological mapping was carried out at a scale of 1:5000 (Figure 1.2 – map pocket). This map was compiled using:

1. aerial photographic interpretation (enlargements to a scale of 1:5000); and
2. engineering geological field mapping.

Rock and soil descriptions are given according to the procedure of Bell and Pettinga (1983); see Appendix A.

All of the failures along Frankton Arm are located in the Jurassic-Cretaceous Otago Schist. The bedrock can be described as:

> *Fresh to slightly weathered; moderately hard to hard; moderately strong to strong; olive grey quartzofeldspathic and pelitic SCHIST; foliation spacing 1-5mm (Haast Schist Group Textural Zone IV).*

In places, a thin veneer of glacial till locally up to 5m in thickness covers the slopes and can be described as:

> *Light grey-green; slightly weathered to fresh; sandy medium GRAVEL; medium gravelly SAND and gravelly SILT (SP/GP).*

All of the slides are characterised by steep joint-controlled lateral and head scarps. The lateral margins of each act as lateral release structures, allowing movement or relaxation to take place. Subdued hummocky topography occurs on all slides, indicating that the schist blocks within the mass have been displaced.

The head scarps for each slide show varying states of activity, with the least active head scarp subsequently the most eroded (figure 5.2). Slide No. 5 is the most degraded, however still shows retrogressive movement and hummocky topography (figure 5.3). There has been some back rotation and relaxation within the slide masses. Secondary scarps are present within the slide masses, especially around the head scarp regions, possibly as a result of retrogressive movement. Scarps in the southern part of Slide No. 6 are less degraded (estimated using aerial photographs) than those in the northern part of the slide and those situated on Slide No. 5 (figure 5.4). All eastern margins are lateral release structures, and Slide No. 3, No 4, and Marina Heights have prominent western (or north western) lateral scarps. Loose, chaotic debris covers the top part of Slide No. 3 and No. 4, and minor wedge failures have proceeded to become dislodged from the head scarp on each slide. Most of the slides (except No. 3 and No. 6) have deeply incised streams flowing along their southwestern margin.

5.2.3 Land-use of the Frankton Failures.

The area within the landslide masses is used for farming, particularly sheep grazing. Urban development is concentrated along the area immediately surrounding Frankton Arm. Residential development does not occur on the actual slide masses, although to the west of Slide No. 3 a subdivision was built in 1997 adjacent to the landslide debris (figure 5.5).

Grass and tussock cover most of the slopes, along with various scrub such as matagouri and gorse. Slide No. 3 is the most densely vegetated, with the lower section of the failed mass completely obscured (figure 5.2). Schist blocks litter the mid to upper body of the slide masses, with fewer on the lower slopes/toe.

Figure 5.2: Slide No. 3 (top) and Slide No. 4 (bottom) showing the large wedge failures coming from the head scarps. Marina Heights Extension subdivision is shown in the middle left of the top photo.

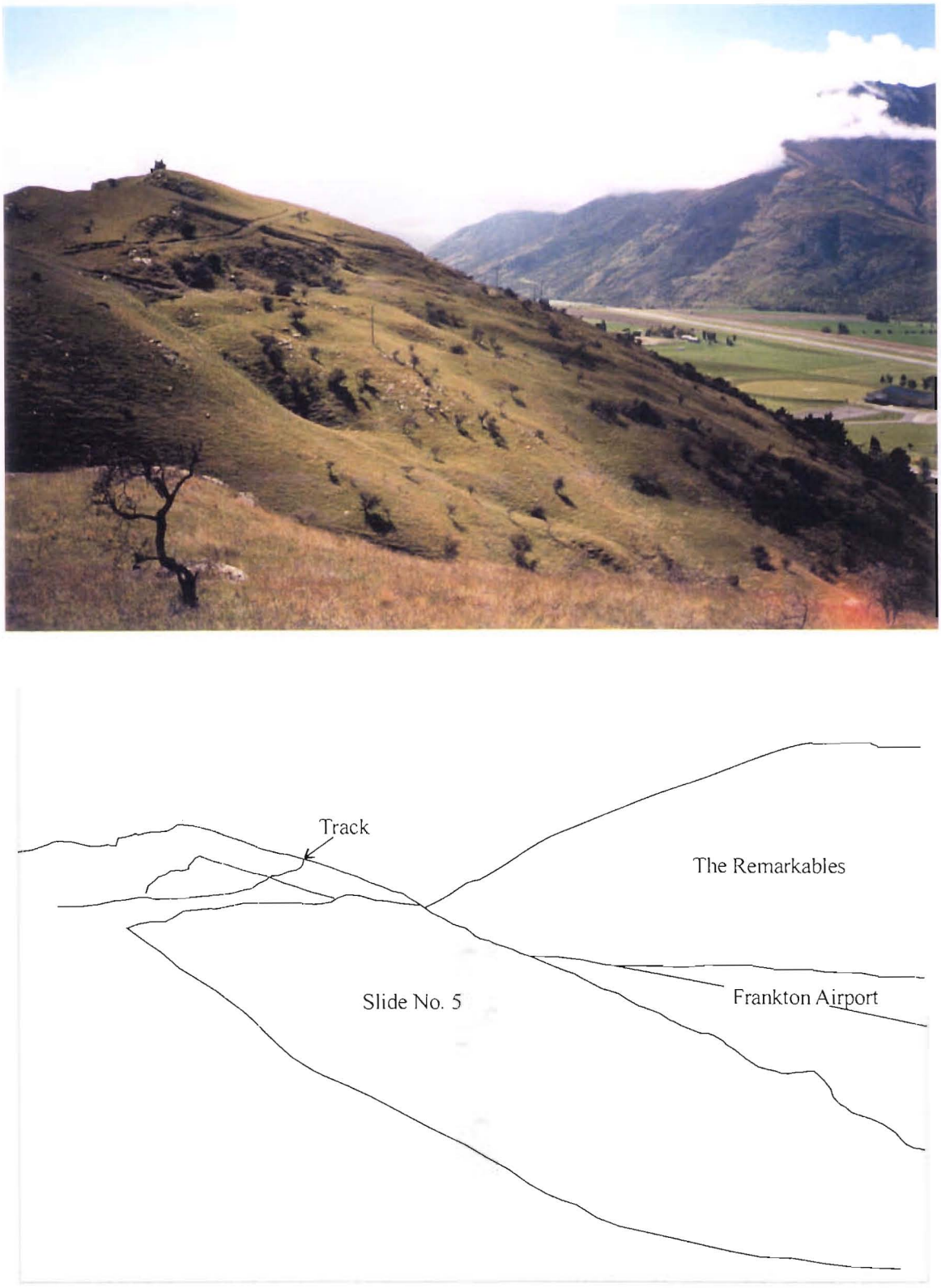

Figure 5.3: Photo looking east over Slide No. 5 with The Remarkables in the distance. This failure shows hummocky topography and a retrogressive head scarp.

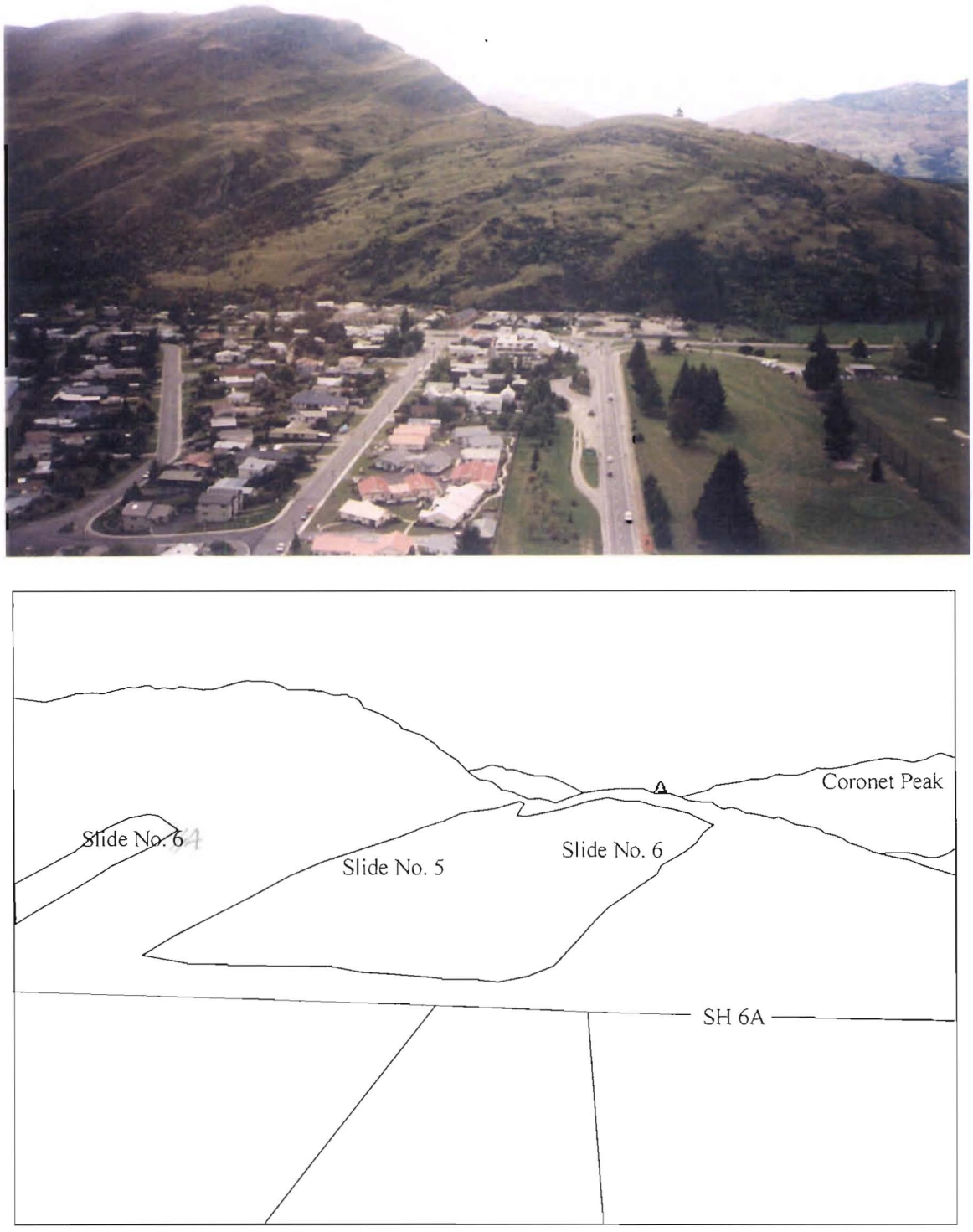

Figure 5.4: Photo showing Slide No.'s 5 and 6 taken facing north. Note variable degradation between the scarps within the slide masses.

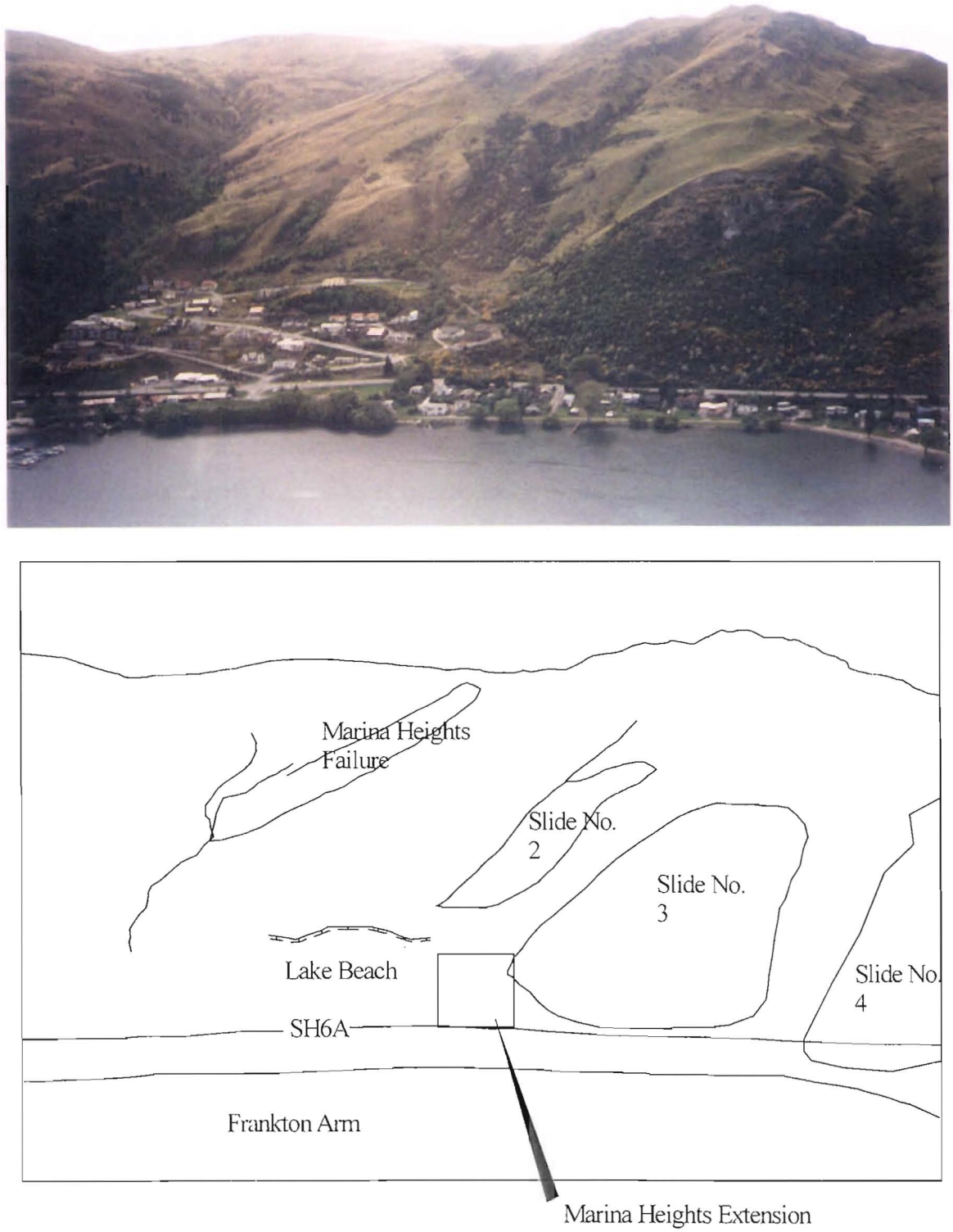

Figure 5.5: Photo looking north over Frankton Arm at the Marina Heights and No. 2 failures in relation to the subdivision. Note Marina Heights Extension Subdivision in relation to Slide No. 3.

5.2.4 Possible Failure Models.

The failure models for these landslides are based on field investigations and aerial photograph interpretation of the slides. A translational failure mechanism has been adopted, with the failure planes assumed to be parallel to the schistosity, and possibly along foliation shear zones. Lateral and head releasing is occurring along master joint sets within the schist. The subdued hummocky topography sub-parallel to foliation (figure 5.4) and the weak pelitic schist exposures all suggest the major control is foliation planes in weak schist. Initial slope movements may have involved creep on schistosity surfaces or foliation shears formed by erosion and weathering by the Kawarau Lobe of the Wakatipu Glacier, within weak pelitic schist horizons.

The failures have formed along two discontinuities (foliation and master joint sets) that have caused the contained rock mass to displace down their line of intersection forming wedge-type slides (figures 1.2.3 – 1.2.9 – map pocket). The shape of the displaced masses are bound by a joint set that forms the main scarp of the slide and foliation or foliation shear zones form the failure surface. The landslides along Frankton Arm formed by wedge movements involving displacements on the schist foliation dipping at 25-30° with joint release, with sub-vertical joints acting as head and lateral release features. The low tensile strength in the head zone forms a pull-apart under gravity down slope. A stepped rupture surface may result in some cases if two or more sets of discontinuities, such as foliation and joint sets, penetrate the rock mass. One set of discontinuities forms the risers of the steps (the joint set) and the other forms the treads (the foliation), creating a stepped slide.

The state of activity for most of the slides along Frankton Arm can be classed as relict, as they developed under different climatic conditions. Vegetation has become established on the main head scarps of Marina Heights, Slide No. 5 and No. 6 (figure 5.4), thus the slides can be classed as dormant. Drainage extends across Slide No. 2 without obvious offset, thus is considered to be relict. Slide No.'s 3 and 4 would be classed as inactive as they show minor movement and retrogression within the head scarp areas. This type of movement is inferred to be a continual process, with small wedges collapsing off the head scarps on to the slopes immediately below. The distribution of activity is retrogressive in all cases as the failure surface extends in the direction opposite to the movement of the displaced material. Several minor retrogressive scarps exist up slope of the main head scarps of the slides which are

evident on aerial photographs. Retrogressive movement implies enlargement of the failure surfaces has taken place for each slide. It is therefore inferred that the head scarps for the slides were originally situated further down slope, and subsequent retrogression has resulted in an up slope migration of the head scarp. This would have taken place as continual gravitational creep was occurring. Scarps within each slide are sub-parallel to the head scarps, and due to post-glacial weathering and erosion, have been reduced to minor scarps. The style of movement is classified as multiple landsliding as they show repeated movements of the same type.

Comparing 1950's aerial photographs with recent photographs, no movement has been visually detected. There is no evidence for changes in surface morphology, and scarps within the slide area have only become more degraded due to erosion.

5.2.5 Kinematic Analysis.

Figure 5.6 shows the main joint sets present along Frankton Arm. Joint sets one and two are orientated sub-parallel to the strike of the undisturbed schist along Frankton Arm, and it is inferred that this joint set acts as a head scarp release structure for the failures. Joint set three is striking at right angles to the in situ schist bedrock, and it is suggested that this set has provided a surface for lateral release for each of the failures. Plots of each slide are presented in the following sections. Having determined that a planar failure is possible, an indication of possible triggering mechanisms in place at the time of failure can be gained for each failure using sensitivity analyses.

5.2.6 Sensitivity Analyses.

If the kinematic analysis indicates that the requisite geologic structural conditions are present, stability is evaluated by a limit-equilibrium analysis, which considers the shear strength along the failure surface obtained from laboratory testing (see Chapter 3), the effects of pore-water pressures, and the influence of external forces such as seismic accelerations and reinforcing elements (Norrish and Wyllie, 1996). The shear strength of the rock material composing slopes has a considerable effect on slope stability.

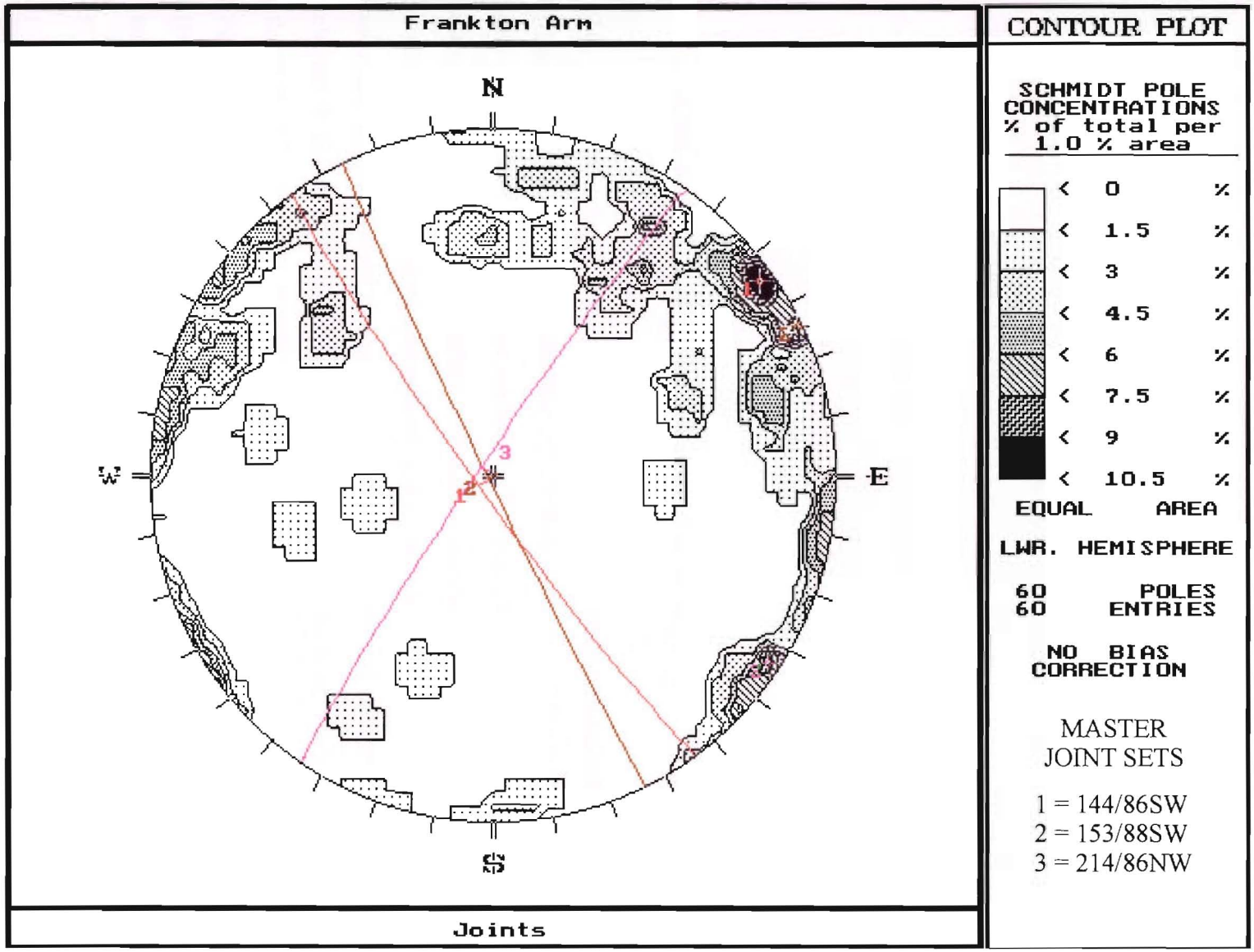

Figure 5.6: Stereoplot showing master joint sets along Frankton Arm.

The three broad types of landslide triggering mechanisms for failures along Frankton Arm are:

1. Increased shear stress – this can be achieved by processes that lead to the removal of lateral support (in this case by glacial processes); the addition of surcharges (the addition of water by rain, snow or the growth of glaciers) and changes in transitory stresses such as from earthquakes.
2. Low strength – rock material within the landslide may be naturally weak or become weak as a result of natural processes such as saturation with water, or by chemical weathering to form clays and the rock mass may be weakened by discontinuities such as faults, foliation, joints and shear zones.
3. Reduced shear strength – rock may disintegrate under cycles of freezing and thawing or thermal expansion and contraction, in addition, wet weather may dissolve natural rock cements which in turn reduces effective granular pressure and friction (Cruden and Varnes, 1996).

5.2.6.1 Sensitivity Analysis Assumptions.

The analyses conducted in this thesis were aimed at obtaining contributing factors or possible triggering mechanisms for instability, rather than solutions to the problem of unstable land, thus reinforcing elements were excluded. The resolution of forces was carried out in two dimensions, in which the stability formulation considers a unit thickness of the slope. For simplicity, a single failure plane extending the entire length and width of each slide has been assumed, but this would not occur in reality. The same assumptions made in the previous chapter in regard to the Queenstown Hill Landslide sensitivity analysis have been made for the following analyses. Evaluation of the stability of the slope requires solution of the equations and computations shown in Appendix L. A geometric case with the tension crack (head scarp) present in the slope face relative to the crest of the slope was considered (Norrish and Wyllie, 1996) and the resulting factor of safety values for various conditions are present in tables 5.2 to 5.7.

The following input parameters were used in the analysis:

a. Cohesion values ranging from 0kPa up to 10kPa were put into the analysis, however 0kPa is the preferred value, as with increasing displacement of the unstable mass, cohesion will become zero.

b. Friction angles of 30° (for fractured schist parallel to foliation – a value obtained from shear strength testing) and 20° (for shear zone material) were used in order to get realistic values for the slides along Frankton Arm. 25° is the suggested value for the failure surface to be in crushed schist, and 35° was used for a failure surface that is occurring along the foliation and stepping across on joint sets (which would add resistance to sliding).

c. Depth to the perched water table within the slide mass was taken at variable depths – from dry ($z_w/z = 0$) up to artesian water pressure ($z_w/z = 1.5$), a possibility immediately following retreat of the Kawarau Lobe of the Wakatipu Glacier. The ratio of depth of water in the tension crack to depth of the slide mass is assumed to be uniform throughout the slope. In reality, the ground water system would be highly compartmentalised and variable, as rock mass defects within the mass would act as barriers or paths for flow. The ground water systems in the slides would likely be highly complex.

d. Seismic acceleration was considered as a possible triggering mechanism. Seismic activity is likely to be one of a number of factors (such as ground water, friction and the effects of ice scouring) acting on the slopes at the time of failure, and it is unlikely to have acted in isolation. Values of seismicity used in the analysis were considered as those most likely to occur along Frankton Arm. Gravitational accelerations of up to 0.5g (MMIX – the maximum possible earthquake for the area) were put into the analysis, and zero acceleration was used for pseudo-static conditions.

e. The angle of the failure surface has also been varied, as limited budget during this investigation did not allow for sub-surface investigations to determine the exact angle of the failure planes. Values ranging from 10° (to take account of possible local warping of the schist bedrock) up to 30° were used, however certain values are preferred, as determined from kinematics and the construction of cross-sections (figures 1.2.1 – 1.2.9 – map pocket).

5.3 MARINA HEIGHTS FAILURE.

5.3.1 Geology and Failure Mechanisms.

The Marina Heights Failure is interpreted to be a simple translational slide, and a failure plane that may be situated along foliation shear zones. In places it may follow fractures parallel to the foliation, and step across foliation on major joint sets. A smaller translational slide has occurred in the southwestern area of the main slide and scarps appear to be less degraded in

this zone than the rest of the failure (interpreted using aerial photographs). Both main head and lateral scarps show retrogressive features, and small minor scarps are evident up slope indicating the retrogression.

Aerial photographs from the 1950's have shown that there has been no visual changes in landslide morphology since then. The head scarp runs northwest southeast (figure 5.7) and then trends northeast southwest forming the lateral scarp (figure 5.1). The scarps within the failure are all degraded, and a small minor failure towards the west in the southern corner also appears in the 1950's aerial photographs, thus cannot be attributed to recent movement. The entire slide mass has hummocky topography, indicating most of the slide mass is made up of displaced schist blocks that have moved down slope towards the west (figure 5.8).

Residential development does not occur on the landslide mass (which extends from 440m above sea level to 680m above sea level), however, directly down slope the Marina Heights residential area occurs, with development extending from lake level up slope to approximately 390m above sea level (figure 5.5).

The southern boundary of the failure acts as a lateral release structure, thus movement has been accommodated towards the south as well as down slope towards the incised gully towards the west. This joint-controlled gully acts as the eastern margin of the much larger Queenstown Hill Landslide.

The failure is assumed to have taken place several thousand years ago. Similar triggering mechanisms as the Queenstown Hill Landslide are thought to have occurred at the Marina Heights Failure. Following retreat of the glacial ice, elevated ground water levels, and the preferential removal of weak pelitic schist horizons, would have been the main causes of instability. In addition, the ice retreat would have removed lateral support, creating further instability.

5.3.2 Kinematic Analysis.

Figure 5.9 shows a contoured plot of poles to displaced schist foliation from within the Marina Heights failure using a friction angle of 30° for schist artificially fractured parallel to foliation. Most poles (up to 45%) daylight in the slope face, a factor that contributes towards

Figure 5.7: the Marina Heights head and lateral scarps. Photo taken looking east.

Figure 5.8: Hummocky topography of the Marina Heights landslide.

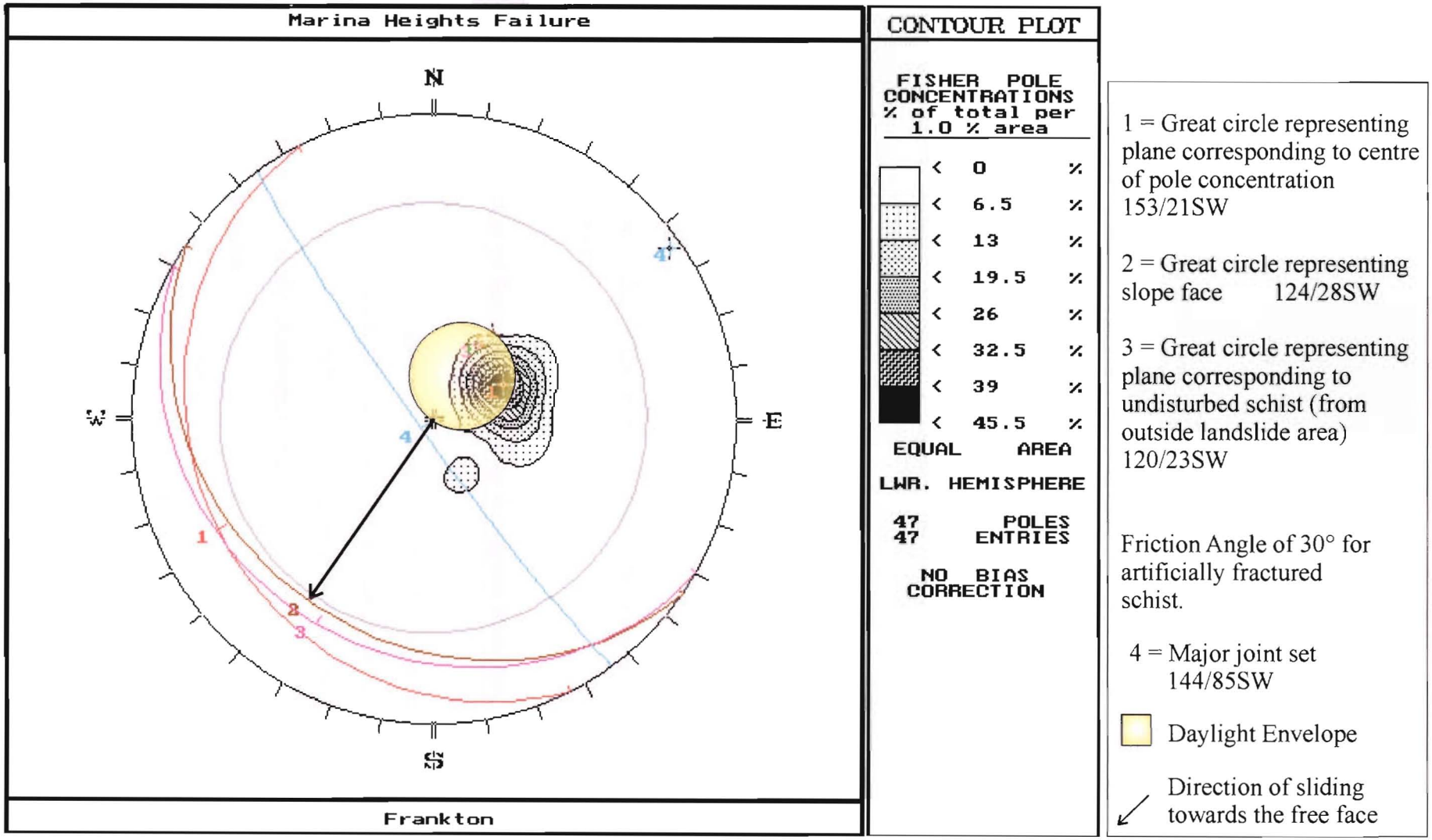

Figure 5.9: Stereonet showing major structural controls of the Marina Heights Failure, using a friction angle of 30°, a value obtained from laboratory testing of artificially fractured schist collected from outside the slide area. There is no Markland's zone of instability formed.

the failure model. Using a friction angle of 20° (figure 5.10), an area Markland area of instability exists. Sliding along the line of intersection of the foliation and the master joint set is kinematically possible because the plunge of this line is less than the dip of the slope face, measured in the direction of sliding (Hoek and Bray, 1981).

Figure 5.9 shows the close correlation of slope face, in situ foliation and displaced schist from within the slide mass. When schistosity dips sub-parallel to the slope face, this contributes to instability, particularly when weak foliation shear zones are present.

The four necessary structural conditions for planar failure within the Marina Heights Failure occur as follows:

1. The strike of the main joint set occurs 20° from the slope face, thus acts as a kinematically viable failure surface.
2. The schist foliation measured from within the landslide area has a dip 7° less than the slope face, thus it daylights, and is a kinematically viable failure surface.
3. The main joint set on the Marina Heights failure dips 55° steeper than the angle of friction, therefore is a kinematically viable failure surface (that is, it may act as a head scarp release surface).
4. The lateral extent of the failure mass is defined by a lateral release surface that occurs along the southern boundary of the failure.

5.3.3 Factor of Safety Sensitivity Analysis Results.

Results of the sensitivity analysis are given in table 5.2. For simplicity, a single failure plane extending the length and width of the entire slide mass with a failure mass of uniform thickness was assumed, but an indication of the possible triggering mechanisms within the slope is given in the study. Accompanying sensitivity graphs (presented in Appendix L) illustrate these conditions.

Table 5.2 shows that varying cohesion values do not have a marked effect on stability, even when the depth of the perched water table within the slide mass is increased from dry to $z_w/z = 0.5$.

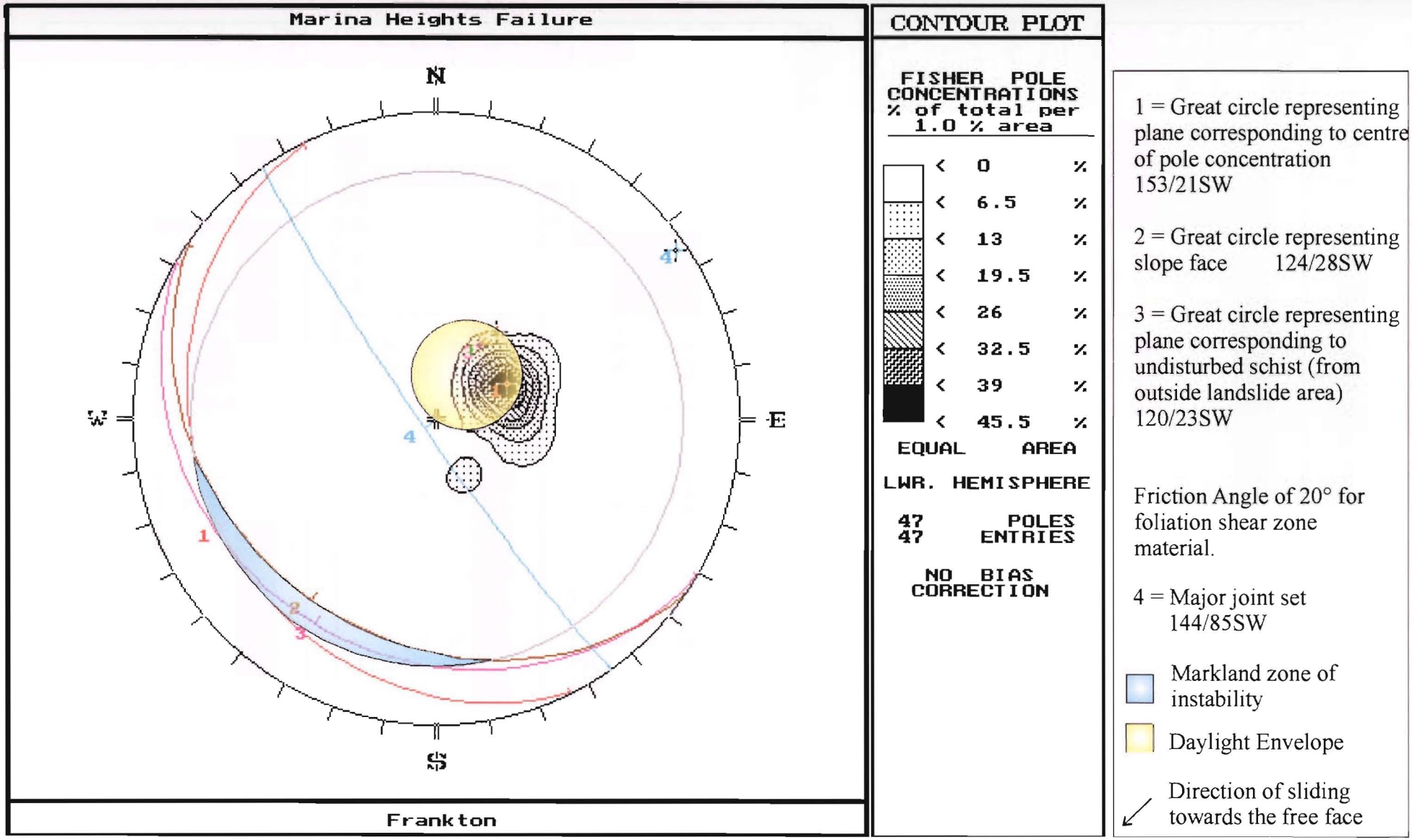

Figure 5.10: Stereonet showing major structural controls of the Marina Heights Failure, using a friction angle of 20°, a value assumed for foliation shear zone material. There is a Markland's zone of instability formed.

Table 5.2: Factor of Safety values for Marina Heights slope instability.

Cohesion						
when:		$\phi = 30°$	$\phi = 8°$	$z_w/z = 0, \phi = 30°$	$z_w/z = 0, \phi = 8°$	$z_w/z = 0, \phi = 20°$
$z_w/z = 0.5$	c' = 0kPa	1.27	0.31	1.5	0.37	0.95
$\varphi_p = 21°$	c' = 2kPa	1.28	0.32	1.51	0.37	0.95
$\alpha = 0$	c' = 5kPa	1.29	0.32	1.52	0.38	0.96
	c' = 10kPa	1.3	0.34	1.53	0.39	0.98

Friction Angle			$z_w/z = 0$
when:	$\phi = 8°$	FS = 0.31	FS = 0.37
$z_w/z = 0.5$	$\phi = 15°$	FS = 0.59	FS = 0.7
c' = 0kPa	$\phi = 20°$	FS = 0.8	FS = 0.95
$\varphi_p = 21°$	$\phi = 25°$	FS = 1.03	FS = 1.21
$\alpha = 0$	$\phi = 30°$	FS = 1.28	FS = 1.5

Depth of Perched Water Table				
when:	z_w/z	$\phi = 30°$	$\phi = 8°$	$\phi = 20°$
c' = 0kPa	0	1.5	0.37	0.95
$\varphi_p = 21°$	0.5	1.28	0.31	0.8
$\alpha = 0$	1	1	0.24	0.63
	1.25	0.86	0.21	0.54
	1.5	0.72	0.18	0.45

Seismic Acceleration						
when:	α	$\phi = 30°$	$\phi = 8°$	$z_w/z = 0, \phi = 30°$	$z_w/z = 0, \phi = 8°$	$z_w/z = 0, \phi = 20°$
$z_w/z = 0.5$	0	1.28	0.31	1.5	0.37	0.95
c' = 0kPa	0.1	1.22	0.3	1.45	0.35	0.91
$\varphi_p = 21°$	0.25	1.13	0.28	1.36	0.33	0.86
$\alpha = 0$	0.5	0.99	0.24	1.21	0.3	0.77

Angle of Failure Plane						
when:	φ_p	$\phi = 30°$	$\phi = 8°$	$z_w/z = 0, \phi = 30°$	$z_w/z = 0, \phi = 8°$	$z_w/z = 0, \phi = 20°$
$z_w/z = 0.5$	10°	2.86	0.69	3.27	0.79	2.06
c' = 0kPa	15°	1.85	0.45	2.16	0.52	1.36
$\alpha = 0$	20°	1.35	0.33	1.59	0.39	1
	21°	1.28	0.3	1.5	0.37	0.95
	25°	1.05	0.25	1.24	0.3	0.78
	30°	0.85	0.21	1	0.24	0.63

The Marina Heights Failure is very sensitive to friction. At perched water table levels of below the slide base, frictional values of 20°-25° (for crushed schist) are likely to have caused failure. These values represent a critical point between stability and instability. The frictional resistance of the failure surface would be highly variable, and if failure occurs partly along foliation shear zones, failure would certainly take place. Using an input value of 8° (a minimum value used if failure is occurring on foliation shear zones), failure is certainly triggered, even when slopes are dry. The analysis infers failure may not take place through fractures along foliation.

When the perched water table is at ground surface level, and if the failure surface is through fractured schist, the slope would be in equilibrium. Failure through foliation shear zones (with possible friction angle values of 8°-20°) could take place at any water table levels (from dry to artesian water pressure).

A gravitational acceleration value of 0.5g (the maximum acceleration assumed for Frankton Arm) would cause instability with a failure plane situated through fractured schist and foliation shear zones, if the perched water table is at half the depth of the slide mass. Any level of seismicity will initiate failure along foliation shear zones (using values of between 8° and 20°). Seismicity would not cause instability if the failure mass was dry with a slide base in fractured schist (parallel to the foliation).

If the angle of the failure surface is as low as 10°, failure can still take place through sheared material (at any perched water table level). A dry slope will be in equilibrium with a failure surface angle of 30°. The preferred angle of failure surface is 21°, as obtained from kinematic analysis and the construction of cross-sections. This suggests failure is occurring sub-parallel to the foliation and sub-parallel to the slope face – a major cause of instability within a slope. With water levels at half the depth of the failure, the slope is sensitive to dip angles of 25°-30°. Failure would certainly be triggered if the slide base is situated within foliation shear zones.

It can be concluded from this sensitivity study that failure of the Marina Heights Slide took place along crushed schist and foliation shear zones, therefore does not disprove the translational failure model presented earlier. The simplest case, when the slope is dry, and external forces are not present, the factor of safety is 1.5 – considered in this analysis to be a

stable slope if failure is occurring through fractured schist parallel to the foliation, however, detailed (subsurface) investigations are necessary before this can be confirmed.

5.4 SLIDE NO. 2.

5.4.1 Geology and Failure Mechanisms.

It is implied that this is a translational slide taking place along foliation shear zones, with head and lateral release along major joint sets. The head scarp runs approximately east west for 150m, with a small stream draining through the middle of the head scarp at 90° to it. When drainage extends across a landslide (as it does in this case) without any obvious offset, the landslide is considered to be relict. The western margin consists of a joint-controlled deeply incised gully with a stream (figure 5.11).

Vegetation covers most of the lower half of the landslide, especially in the proximity of the incised gully. A single well-established pine tree has grown in the centre of the slide mass, and is at least 30 years old.

The slide mass contains degraded scarps and hummocky topography. The failure appears to be a smaller version of the Marina Heights failure, and small retrogressive scarps have formed up to 25m above the main head scarp (figure 5.1).

The failure mechanism is similar to that for the Marina Heights Failure with a simple translational slide taking place along foliation shear zones or possibly on fractured schistosity. Head and lateral scarps have formed as a result of extension across master joint sets.

5.4.2 Kinematic Analysis.

Figure 5.12 shows a plot of poles to displaced schist foliation using a friction angle of 30°, and the grouping indicates planar failure. The main concentration does not fall within the daylight envelope, however a small percentage does daylight. Using a friction angle of 30° (obtained from shear testing of fractured schist – Chapter 3), no zone of instability exists according to Marklands Test. However, sliding along the intersection of the foliation with the

Figure 5.11: Slide No. 2 (in the centre of the photo) with the head scarp at the sky line. Note well-established pine tree in the lower part of the slide. Slide No. 4 is at far right.

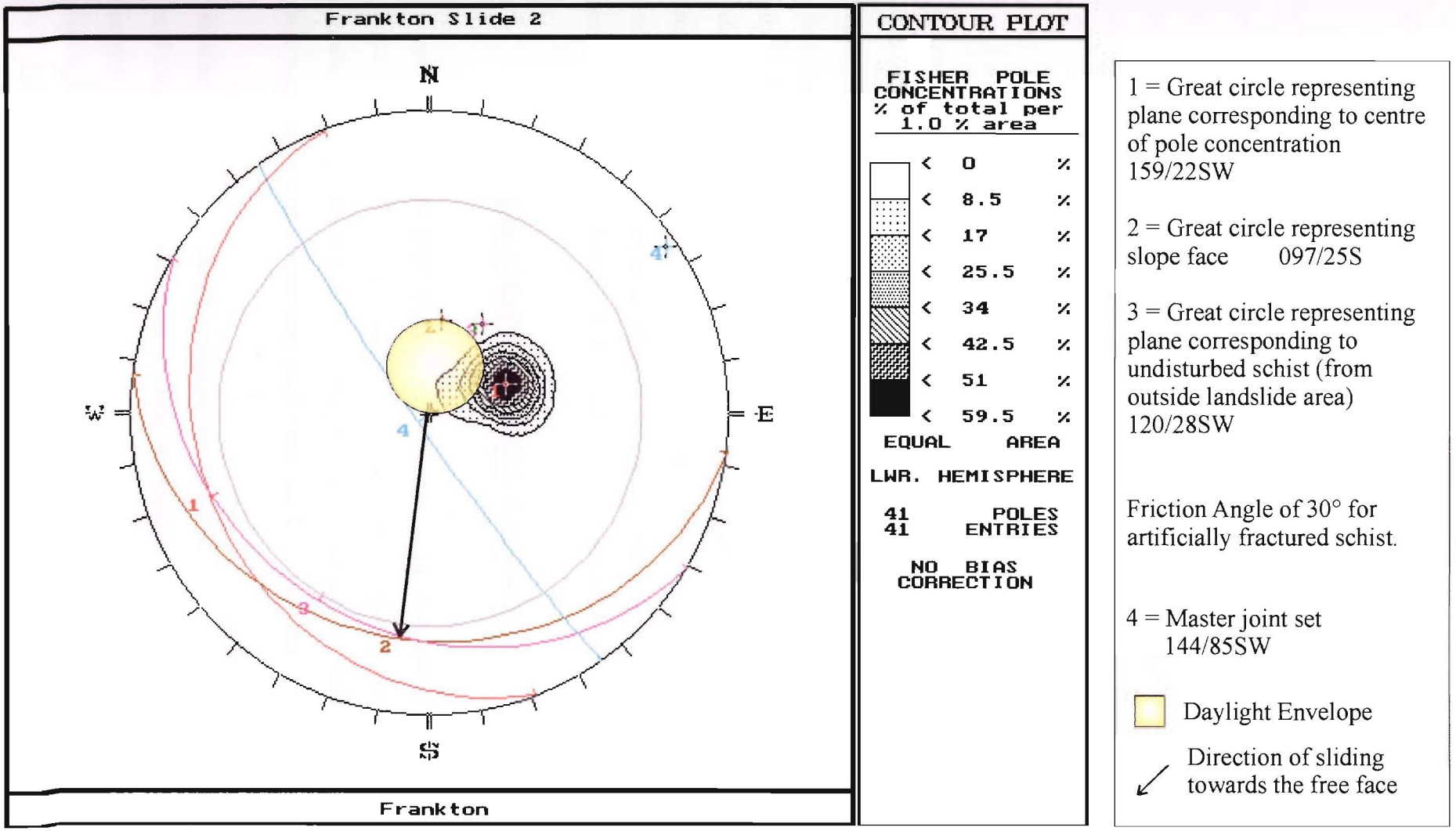

Figure 5.12: Stereonet showing major structural controls of Slide No. 2 Failure, using a friction angle of 30°, a value obtained from laboratory testing of artificially fractured schist collected from outside the slide area. There is no Markland's zone of instability formed.

master joint set is possible because the plunge of this line is less than the dip of the slope face, measured in the direction of sliding.

Figure 5.13 shows a plot of poles to displaced schist foliation using a friction angle of 8° (a minimum value used for failure taking place along foliation shear zones), together with the major planes. Sliding is inferred to be taking place obliquely down slope, not directly down the dip of the foliation as the strike of the displaced schist foliation is not within 20° of the strike of the in situ foliation.

The four kinematic conditions necessary for failure (as listed in section 5.2.4) do not all occur in the case of Slide No. 2. The strikes of the master joint set and the displaced schist foliation are not within 20° of the strike of the slope face. The dip of the displaced schist foliation is less than the dip of the slope face, but as the values are only three degrees apart, more detailed engineering geological and subsurface investigations are necessary to confirm if failure is occurring parallel to the slope face. The master joint set dips 55° steeper than the angle of friction, thus acts as a kinematically viable failure surface, by forming a head scarp release surface. If failure took place along foliation shear zones, the friction angle may have a minimum value of 8° (figure 5.13), and the displaced schist foliation would then become a viable failure surface as well. The last structural condition necessary for failure is the presence of a lateral release surface, which on Slide No. 2, is situated on the eastern side of the failure.

5.4.3 Factor of Safety Sensitivity Analysis.

A result of the kinematic analysis of Slide No. 2 was that not all structural conditions for failure were met. Thus, a factor of safety sensitivity analysis was undertaken to determine conditions that were necessary to trigger failure. Results are summarised in table 5.3 with computations and accompanying graphs presented in Appendix L.

Similar to the Marina Heights Failure, variable cohesion values do not have a marked effect and thus cannot be considered a major triggering mechanism for failure. Various friction angles were used (from 8° to 30°). The depth of the perched water table within the slide mass has a strong influence on stability. A perched water table at half the depth of the slide mass will bring the slide close to equilibrium, thus anything greater than this may trigger failure. Seismic accelerations can trigger failure in fractured schist or foliation shear zones, but it is

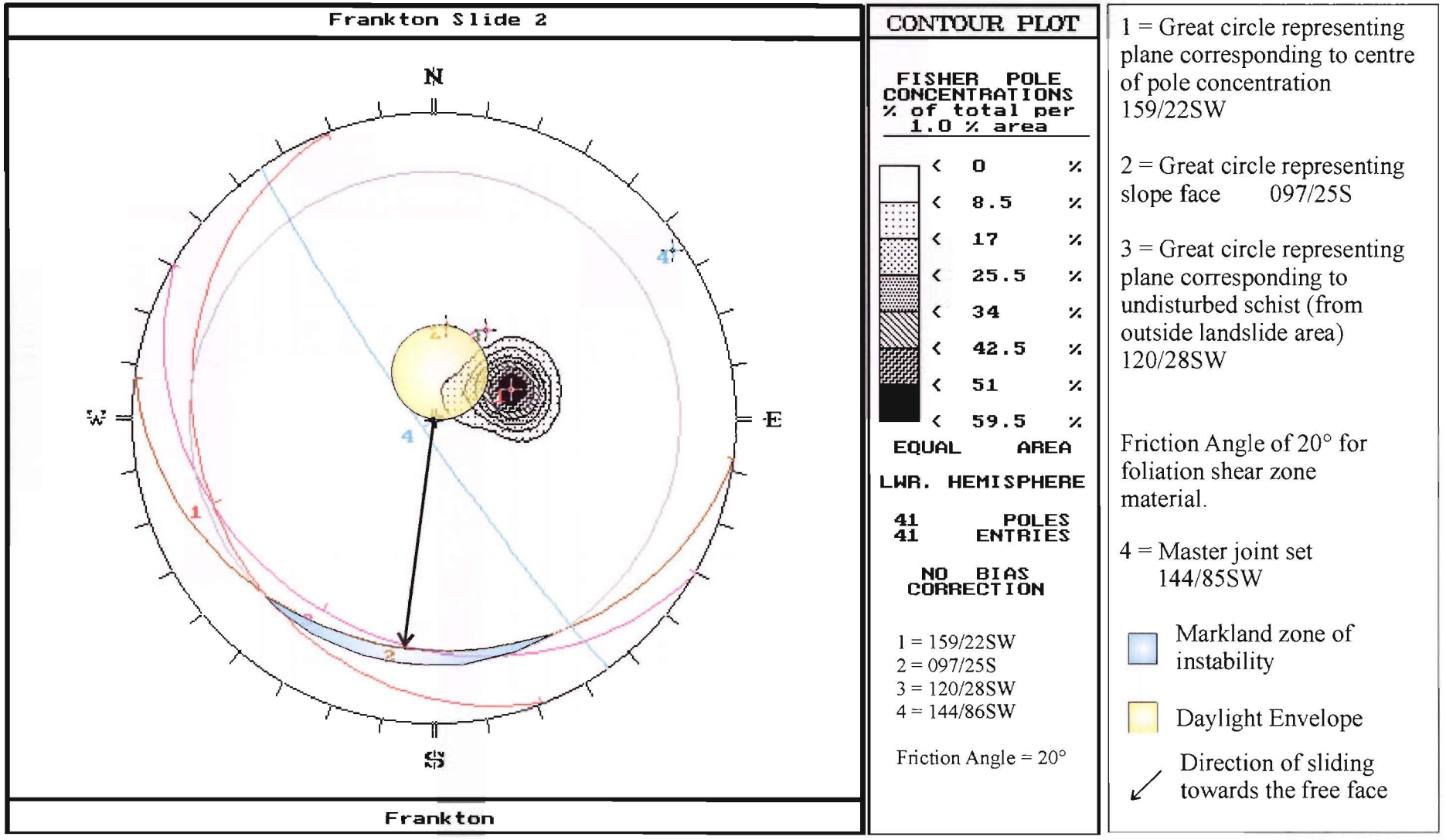

Figure 5.13: Stereonet showing major structural controls of Slide No. 2 Failure, using a friction angle of 20°, a value assumed for foliation shear zones. There is a Markland's zone of instability formed.

Table 5.3: Factor of Safety values for Slide No. 2 slope instability.

Cohesion.						
when:		$\phi = 30°$	$\phi = 8°$	$z_w/z = 0, \phi = 30°$	$z_w/z = 0, \phi = 8°$	$z_w/z = 0, \phi = 20°$
$z_w/z = 0.5$	c' = 0kPa	1.07	0.26	1.43	0.35	0.9
$\varphi_p = 22°$	c' = 2kPa	1.09	0.28	1.45	0.37	0.92
$\alpha = 0$	c' = 5kPa	1.13	0.31	1.48	0.4	0.96
	c' = 10kPa	1.18	0.37	1.54	0.46	1.01

Friction Angle			$z_w/z = 0$
when:	$\phi = 8°$	FS = 0.26	FS = 0.35
$z_w/z = 0.5$	$\phi = 15°$	FS = 0.5	FS = 0.66
c' = 0kPa	$\phi = 20°$	FS = 0.68	FS = 0.90
$\varphi_p = 22°$	$\phi = 25°$	FS = 0.87	FS = 1.15
$\alpha = 0$	$\phi = 30°$	FS = 1.07	FS = 1.43

Depth of Perched Water Table				
when:	z_w/z	$\phi = 30°$	$\phi = 8°$	$\phi = 20°$
c' = 0kPa	0	1.43	0.35	0.9
$\varphi_p = 22°$	0.5	1.07	0.26	0.68
$\alpha = 0$	1	0.7	0.17	0.44
	1.25	0.51	0.13	0.32
	1.5	0.34	0.08	0.21

Seismic Acceleration						
when:	α	$\phi = 30°$	$\phi = 8°$	$z_w/z = 0, \phi = 30°$	$z_w/z = 0, \phi = 8°$	$z_w/z = 0, \phi = 20°$
$z_w/z = 0.5$	0	1.07	0.26	1.43	0.35	0.9
c' = 0kPa	0.1	1.02	0.25	1.37	0.33	0.86
$\varphi_p = 22°$	0.25	0.93	0.23	1.28	0.31	0.81
$\alpha = 0$	0.5	0.79	0.19	1.14	0.28	0.72

Angle of Failure Plane						
when:	φ_p	$\phi = 30°$	$\phi = 8°$	$z_w/z = 0, \phi = 30°$	$z_w/z = 0, \phi = 8°$	$z_w/z = 0, \phi = 20°$
$z_w/z = 0.5$	15°	1.56	0.38	2.15	0.52	1.36
c' = 0kPa	20°	1.18	0.29	1.59	0.39	1
$\alpha = 0$	25°	1.24	0.3	1.24	0.3	0.78
	30°	0.78	0.19	1	0.24	0.63
	35°	0.66	0.16	0.82	0.2	0.52

suggested that other triggering mechanisms in addition to gravitational acceleration would be necessary for any initiation of failure.

The preferred angle for the failure surface for this analysis is 22° as determined from kinematics and cross-sections, and failure is assumed to occur parallel or sub-parallel to the schistosity. If this is correct, failure will not take place in fractured schist, but rather through foliation shear zones. For a slope angle of 30°, the slide mass would be in equilibrium if the failure plane was through fractured schist parallel to the foliation.

In the simplest case, when the surface is cohesionless, the slope is dry, and external forces are disregarded, the factor of safety is 1.43 if the failure surface is through fractured schist, and 0.90 if the slide base is along foliation shear zones (assuming foliation shears have a frictional resistance of up to 20°).

5.5 SLIDE NO. 3.

5.5.1 Geology.

The location of Slide No. 3 is to the immediate east of the Marina Heights subdivision (figure 5.1, figure 1.2 – map pocket). It has an estimated volume of 1.9 x $10^6 m^3$ and an area of $9.75 km^2$. The slide is very densely vegetated, with gorse, matagouri, bush lawyer, etc., which made accessibility very difficult (figure 5.2). This highly dense growth indicates the water table is close to the surface, or seepage through the landslide blocks takes place near the surface. Data obtained from the report by Bell (1997) on the Marina Heights Extension states the water table at 3.8m from a trench situated within the landslide deposits.

The head scarp has formed along joints dipping about 60° to the south and in places is sub-vertical to overhanging (figure 5.14). An area immediately below the head scarp contains a number of displaced schist blocks (>10m^3 and some up to 20m in length). Within the head scarp the dip of the schist is variable (ignored in simplified analyses), and large wedge failures have taken place from within the head scarp. Various seepage zones are present in this area, however no vegetation has become established within the displaced blocks, as the most recent failures have been approximately 100 years ago (estimated from the amount of vegetation that has become established – such as lichen, and by the freshness of cracks and

Figure 5.14: Slide No. 3 sub-vertical to over-hanging head scarp. Note prominent displaced schist blocks and down slope relaxation. Photo taken looking east.

surfaces within the head scarp). Open "pull-apart" cracks also appear within the head zone. At 450m above sea level, an area of collapsed schist deposits occurs, with blocks up to $10m^3$.

The eastern boundary of the slide mass is acting as a lateral release surface, allowing movement to take place. The head scarp runs northeast-southwest and is a very prominent 8m high joint-controlled feature. The western boundary is a continuation of the head scarp and extends down into the Marina Heights Extension subdivision development at 360m above sea level.

Air photo and field evidence indicates that a lobe of failed debris has extended down the western side of the failure. Bell (1997) logged these landslide deposits situated on the subdivision boundary as overlying beach gravels to a maximum depth of 2.3m. The materials consist of brown-grey gravelly sandy silts with some clay and rare angular schist blocks to 1m in dimension, and these deposits represent the outer limit of the failure (Bell, 1997). The nature of the landslide materials suggests a derivation of a single movement event accompanying the latter stages of lake lowering or possibly following a major earthquake. Since this event, there has been head scarp retrogression taking place within the last 100 years. The extent of weathering in the upper part of the profile in the test pit mentioned above suggests that the original landslide is probably several thousand (3-5000) years old. Bell (1997) therefore concluded that the slope failure has been marginally stable for this period of time, and that seismic and climatic triggers have not caused any significant reactivation (after Bell, 1997).

The field and air photo evidence does not indicate any significant activity in the past 40 years, and this is supported by the 800mm (+/-) depth of post glacial weathering observed in one of the test pits excavated through the margin of the landslide debris and into the underlying lake beach deposits (Bell, 1997). Thus, the landslide can be described as being "presently inactive"(last moved more than one annual cycle of seasons ago), but the mass of debris must also be only "marginally stable" given its origin as a multiple wedge rock slide. However Bell (1997) suggests that any excavation into landslide material during property development should be retained so as at least to reinstate existing marginal stability. Furthermore, he recommends specific engineering design is required, with subsurface drainage, retention of cut and fill ground, and rockfall protection for any house constructed on the lot nearest the landslide (after Bell, 1997). The author agrees with these recommendations.

5.5.2 Kinematic Analysis.

Figure 5.15 shows a plot of poles to displaced schist foliation of Slide No. 3 using a friction angle of 30°, and again, the grouping indicates a planar failure. The main concentration (~56% of poles) falls within the daylight envelope, demonstrating that most of the foliation will daylight in the slope, and this implies there is the opportunity for instability if the slide is foliation-controlled. In the figure, a friction angle of 30° has been applied (as this value was obtained during shear testing of fractured schist bedrock) and no zone of instability forms. Figure 5.15 demonstrates the close correlation of strike and dip between the slope face and average foliation. Sliding is taking place obliquely down slope, not down the dip of the foliation.

Figure 5.16 uses a friction angle of 20°, a value that is possible if failure occurs along foliation shear zones. The intersection of the displaced schist foliation with the master joint set does not fall in the Markland zone of instability however, sliding along these intersecting planes is kinematically possible because the plunge of the line of intersection is less than the dip of the slope face, measured in the direction of sliding (Hoek and Bray, 1981).

The four structural conditions in place that are necessary for failure in Slide No. 3 are as follows:

1. The strike of the master joint set is within 20° of the strike of the slope face;
2. The dip of the displaced schist foliation is less than the dip of the slope face, thereby daylighting in the slope face. The displaced schist foliation has a dip 7° less than the slope face (the same as the Marina Heights failure) thus the foliation acts as a kinematically viable failure surface.
3. The dip of the master joint set is greater than the friction angle. If failure is taking place on a foliation shear zone, then the displaced schist foliation also acts as a viable failure surface.
4. The lateral extent of the failure mass is defined by a lateral release surface on the eastern boundary.

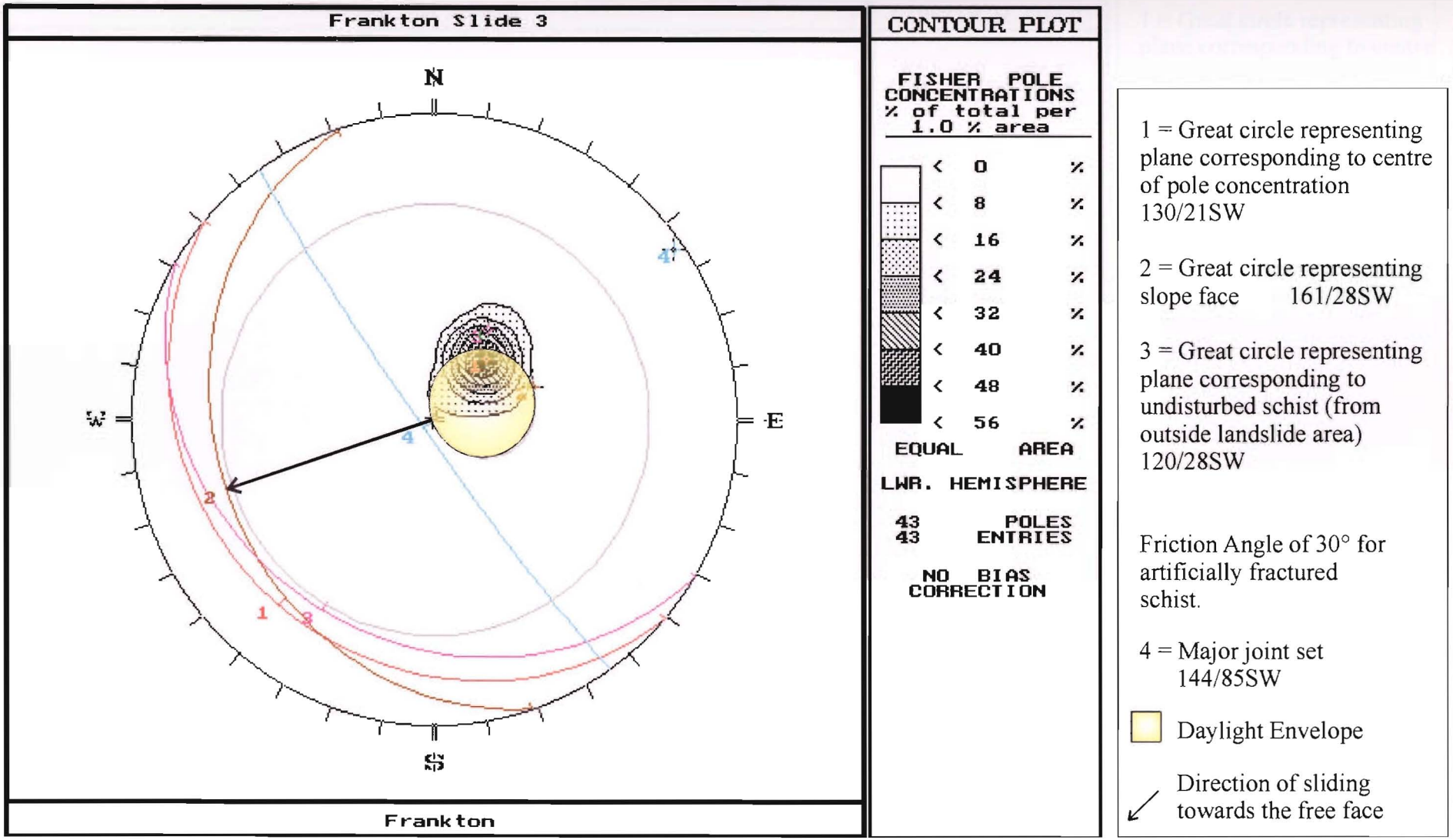

Figure 5.15: Stereonet showing major structural controls of the No. 3 Failure, using a friction angle of 30°, a value obtained from laboratory testing of artificially fractured schist collected from outside the slide area. There is no Markland's zone of instability formed.

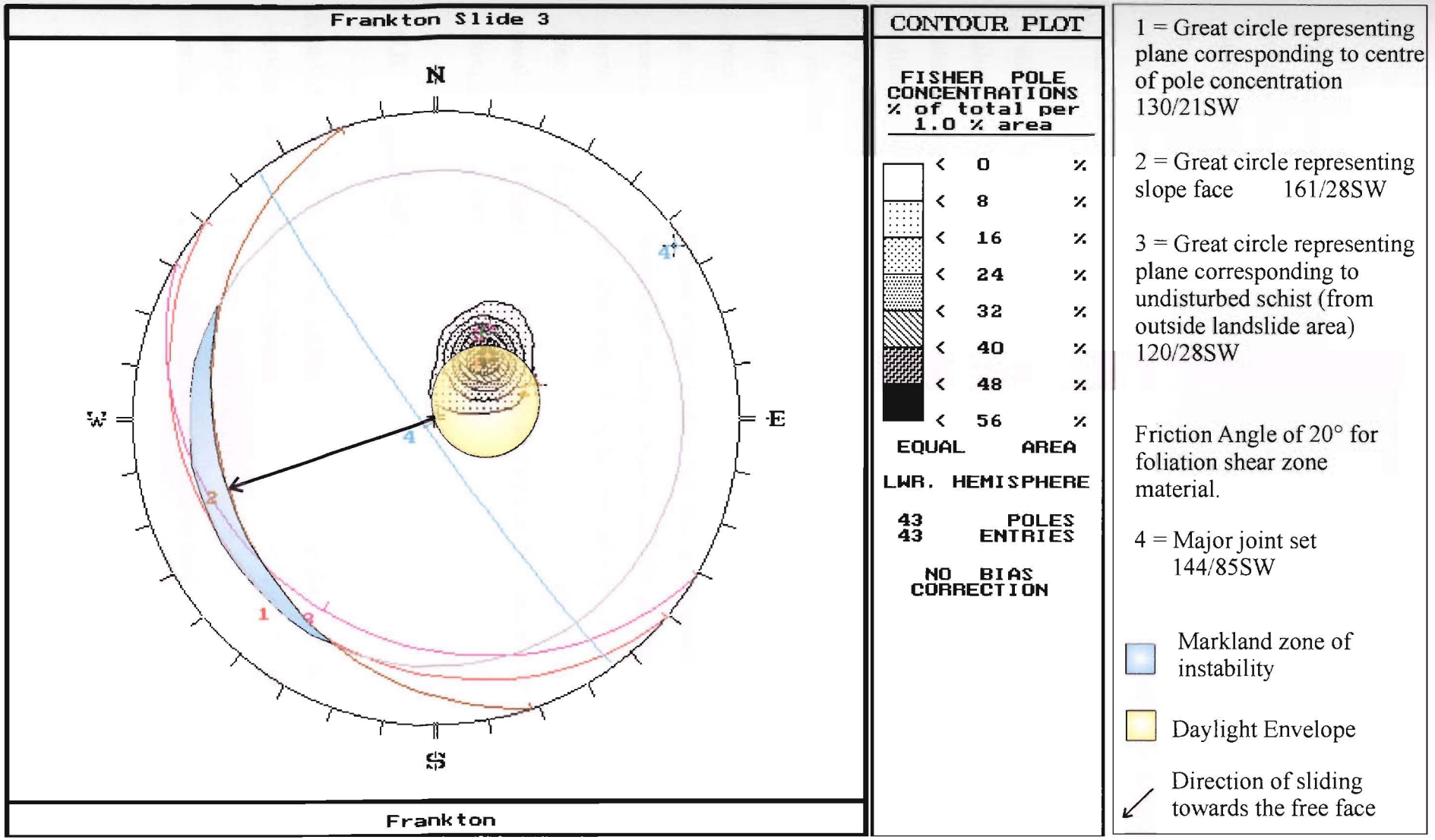

Figure 5.16: Stereonet showing major structural controls of the No. 3 Failure, using a friction angle of 20°, a value assumed for foliation shear zone material. There is a Markland's zone of instability formed.

5.5.3 Factor of Safety Sensitivity Analysis.

The kinematic analysis outlined in section 5.5.2 indicates that the required geologic structural conditions are present for failure to take place. An evaluation of stability was undertaken by limit-equilibrium analysis (as outlined in section 5.2.6.1), considering the shear strength along the failure surface, the effects of pore water pressure, and the influence of seismic acceleration. Computations and graphs of sensitivity results are displayed in Appendix L, and a summary of factor of safety values are shown in table 5.4.

Table 5.4 illustrates, as with all of the previous mentioned failures, that changing cohesion values do not have a major effect on instability, therefore the slope may not be sensitive to cohesion. Frictional resistance does have an effect, and a value of 20° for failure along foliation shear zones, at any perched water table level, can cause failure. When the slope is dry, a cohesionless surface is applied and external forces are ignored a factor of safety of 1.5 is reached if the failure surface is situated within fractured schist. To reduce the factor of safety to instability (a value of close to 1), the level of the perched water table must reach the ground surface if failure is taking place along fractured schist. The slope can be dry and still be unstable if the friction value is 20°. Seismic accelerations of at least 0.25 would be necessary if failure is through fractured schist, and the perched water table was at half the depth of the slide mass. The angle of the failure surface for this slide is 21° (concluded after kinematic analysis and drawing of cross-sections). Failure would be triggered on shear zones parallel to foliation if the slide base is inclined at 21°, and is 0.95 if failure has taken place along foliation shear zones.

5.6 SLIDE NO. 4.

Slide No. 4 has an area of 4.25km^2, and a possible depth to the failure surface of 15-20m (concluded from the construction of cross-sections – figure 1.2.7 – map pocket). The western lateral scarp, approximately 7m in height (figure 5.17), is retrogressing to the northwest, resulting in an additional scarp 2m in height. It is made up of a large relatively intact schist block (figure 5.18), and has formed along a prominent continuous joint set dipping about 80° to the west (underhang). The slide area extends across to the southern side of state highway 6A (concluded from aerial photograph interpretation; figure 1.2 – map pocket), however the toe is presently obscured by residential development.

Table 5.4: Factor of Safety values for Slide No. 3 slope instability.

Cohesion						
when:		$\phi = 30°$	$\phi = 8°$	$z_w/z = 0, \phi = 30°$	$z_w/z = 0, \phi = 8°$	$z_w/z = 0, \phi = 20°$
$z_w/z = 0.5$	c' = 0kPa	1.21	0.29	1.5	0.37	0.95
$\varphi_p = 21°$	c' = 2kPa	1.22	0.3	1.51	0.37	0.96
$\alpha = 0$	c' = 5kPa	1.23	0.31	1.52	0.39	0.97
	c' = 10kPa	1.25	0.33	1.54	0.41	0.99

Friction Angle			$z_w/z = 0$
when:	$\phi = 8°$	FS = 0.29	FS = 0.37
$z_w/z = 0.5$	$\phi = 20°$	FS = 0.76	FS = 0.95
c' = 0kPa	$\phi = 25°$	FS = 0.98	FS = 1.21
$\varphi_p = 21°$	$\phi = 30°$	FS = 1.21	FS = 1.50
$\alpha = 0$	$\phi = 35°$	FS = 1.47	FS = 1.82

Depth of Perched Water Table				
when:	z_w/z	$\phi = 30°$	$\phi = 8°$	$\phi = 20°$
c' = 0kPa	0	1.5	0.37	0.95
$\varphi_p = 21°$	0.5	1.21	0.29	0.77
$\alpha = 0$	1	0.87	0.21	0.55
	1.25	0.7	0.17	0.44
	1.5	0.54	0.13	0.34

Seismic Acceleration						
when:	α	$\phi = 30°$	$\phi = 8°$	$z_w/z = 0, \phi = 30°$	$z_w/z = 0, \phi = 8°$	$z_w/z = 0, \phi = 20°$
$z_w/z = 0.5$	0	1.21	0.29	1.5	0.37	0.95
c' = 0kPa	0.1	1.15	0.28	1.45	0.35	0.91
$\varphi_p = 21°$	0.25	1.07	0.26	1.36	0.33	0.86
$\alpha = 0$	0.5	0.93	0.23	1.21	0.3	0.77

Angle of Failure Plane						
when:	φ_p	$\phi = 30°$	$\phi = 8°$	$z_w/z = 0, \phi = 30°$	$z_w/z = 0, \phi = 8°$	$z_w/z = 0, \phi = 20°$
$z_w/z = 0.5$	20°	1.27	0.27	1.59	0.39	1
c' = 0kPa	25°	1	0.24	1.24	0.3	0.78
$\alpha = 0$	30°	0.81	0.2	1	0.24	0.63
	35°	0.68	0.17	0.82	0.2	0.52

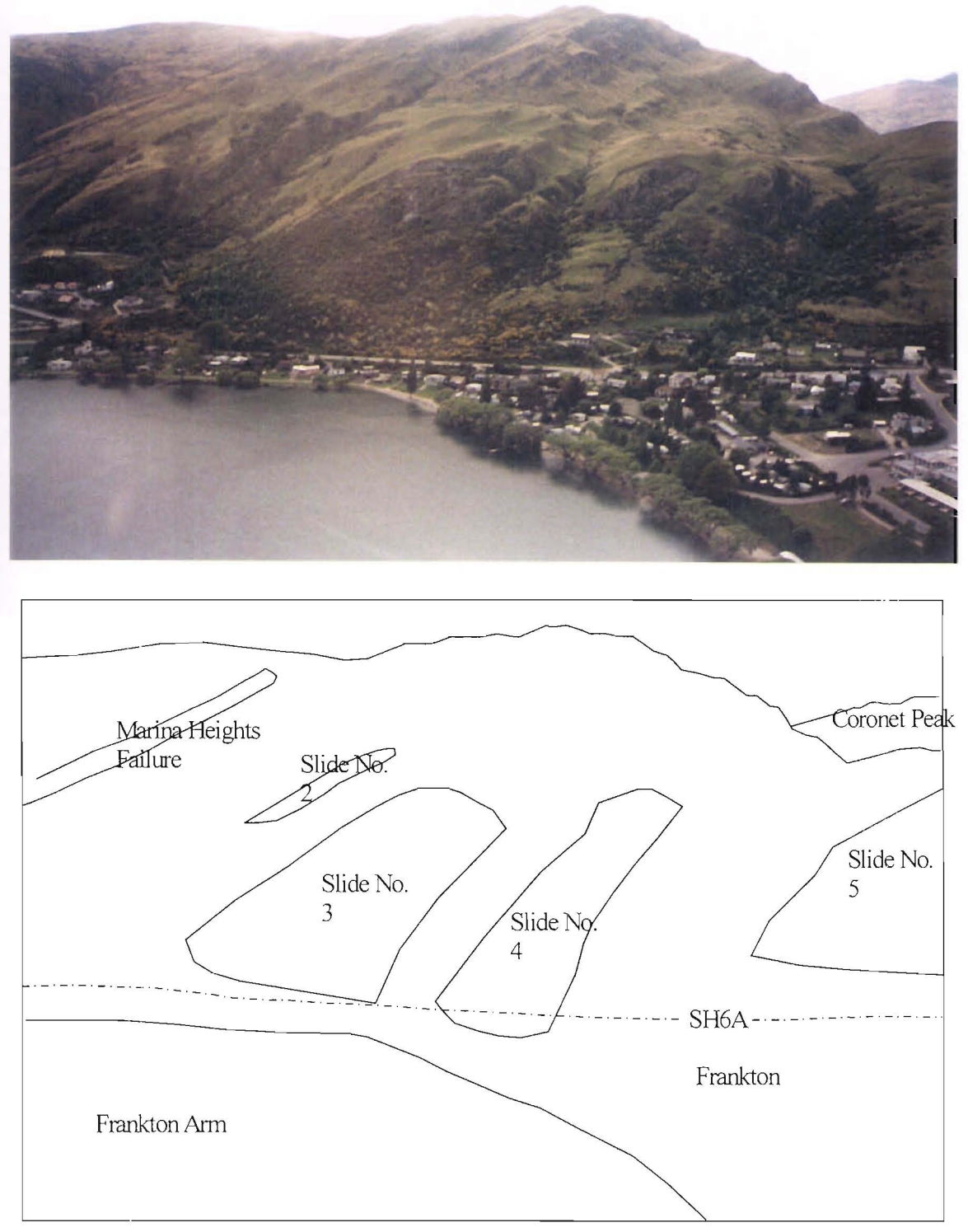

Figure 5.17: Photo looking north at the Marina Heights Failure and Slide No.'s 2 - 5.

Figure 5.18: Slide No. 4 western lateral scarp. Note the hammer for scale.

5.6.1 Geology.

Bedrock consists of quartzofeldspathic schist, with an in situ foliation attitude of 120/28SW. The average foliation attitude within the landslide area is 084/19S. Due to limited bedrock exposure within the landslide, geological information was only attainable from the margins of the zone of failure, that is, the head and lateral scarps.

The unstable area is densely vegetated in the area adjacent to the main highway, and extends up to about 380m elevation. Across the mid-slopes, vegetation consists predominantly of grass, tussock and sparse matagouri scrub. Dense scrub then occurs in the northern quarter of the slide, particularly along the eastern side.

Rock falls have taken place from the head scarp within the last 100 years (evident from the lack of vegetation and the freshness of rock surfaces within the head scarp), however a high frictional interlock prevents any hazard to residential areas below (figure 5.2 and figure 5.17). A major open joint (figure 5.19) oriented into the lateral scarp has resulted in a large part of the scarp moving down slope on a foliation surface at the base of the scarp by gravitational relaxation down slope. Minor collapse and rock fall has occurred within the last 100 years along the exposed edge of this lateral scarp. The head scarp runs westnorthwest-eastsoutheast and joints within it have caused significant wedge failures (figure 5.2). Minor scarps within the failure are all degraded (contrary to the head scarp activity) and the surface shows hummocky topography.

5.6.2 Kinematic Analysis.

Figure 5.20 shows a plot of poles to displaced schist foliation using a friction angle of 30° (for artificially fractured schist), and the grouping indicates planar failure. For this condition, no Markland zone of instability emerged. Sliding along the intersection of the displaced schist foliation with the master joint set is possible because the plunge of this line is less than the dip of the slope face (measured in the direction of sliding). Figure 5.21 uses a friction angle of 20° (a value assumed for foliation shear zone material) and no Markland zone of instability forms.

Figure 5.19: Open joint at the base of the western lateral scarp of Slide No. 4. This joint can be seen in Figure 5.18 to the right of the hammer.

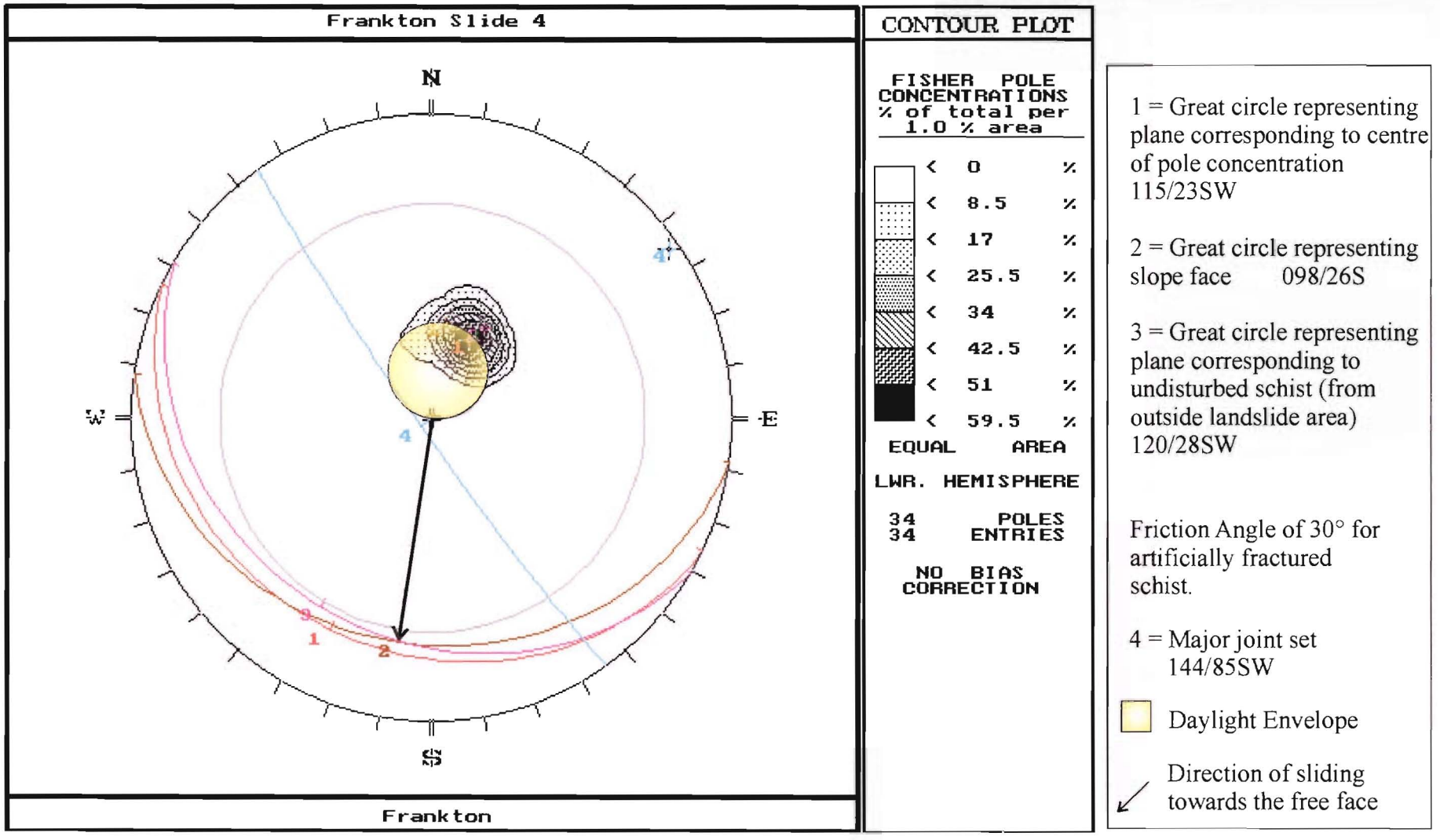

Figure 5.20: Stereonet showing major structural controls of the No. 4 Failure, using a friction angle of 30°, a value obtained from laboratory testing of artificially fractured schist collected from outside the slide area. There is no Markland's zone of instability formed.

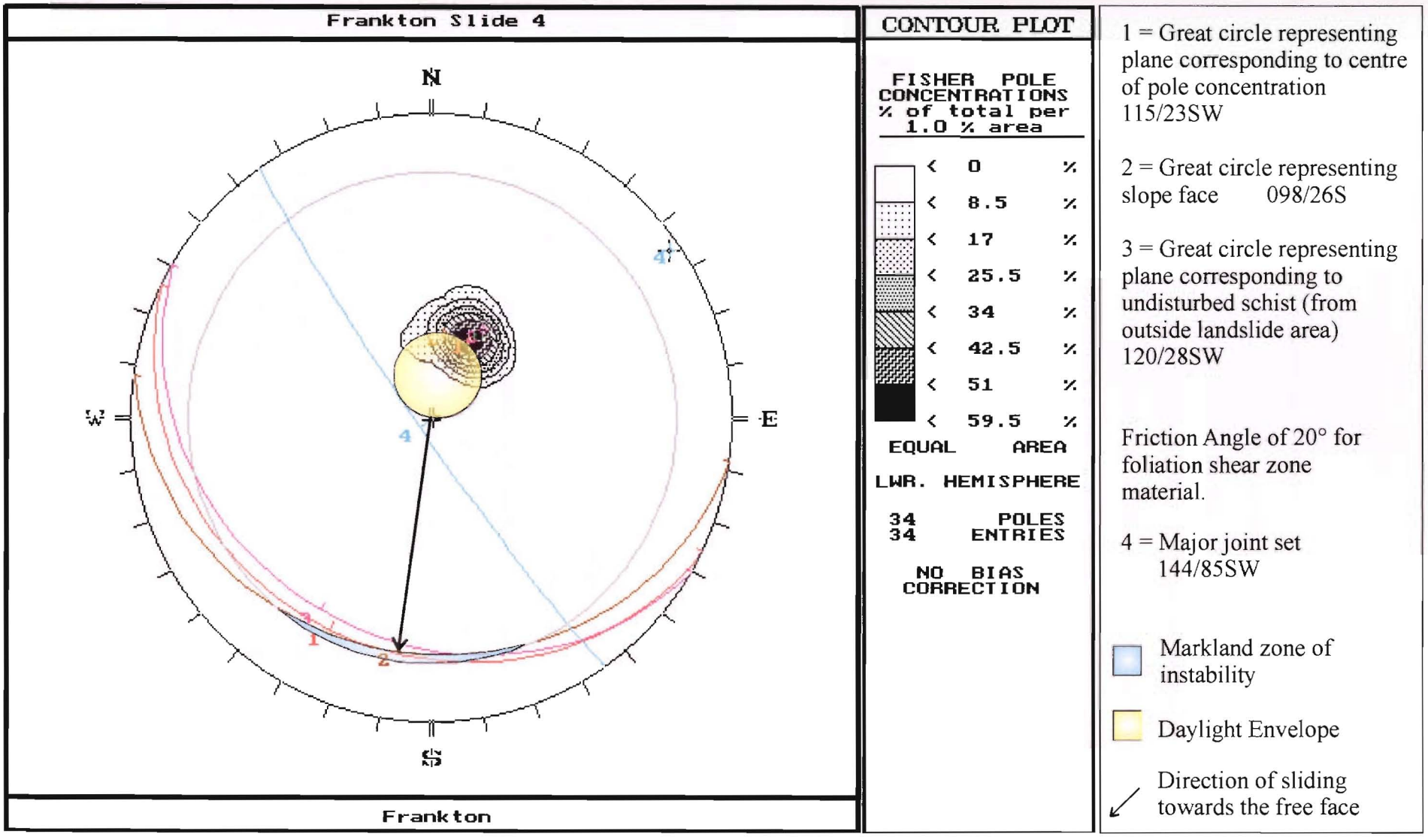

Figure 5.21: Stereonet showing major structural controls of the No. 4 Failure, using a friction angle of 20°, a value assumed for foliation shear zone material. There is a Markland's zone of instability formed.

The four structural conditions necessary for failure (see section 5.2.4) occur as follows in Slide No. 4:

1. The strike of the displaced schist foliation is within 20° of the strike of the slope face, thus acts as a kinematically viable failure surface;
2. The dip of the displaced schist foliation is the same as the dip of the slope face;
3. The dip of the master joint set is greater than the angle of friction by 55° thus the joint set behaves as a kinematic failure surface (possibly acting as a head scarp release structure);
4. The lateral extent of the failure mass is defined on the eastern side by a lateral release surface that does not contribute to the stability of the mass.

5.6.3 Factor of Safety Sensitivity Analysis.

Stability has been evaluated by limit-equilibrium analysis because kinematic analysis has indicated the required structural conditions are present to cause failure. The same input parameters as the previous failures were applied to this failure: shear strength along the failure surface, the effects of pore water pressures, and the influence of seismic acceleration. Results of this analysis are presented in table 5.5 and computations and graphs are shown in Appendix L.

Table 5.5 illustrates that the slope is sensitive to cohesion if the slide base occurs in fractured schist. If the slope has a ratio $z_w/z = 0.5$, failure may have been triggered through either fractured schist or foliation shear zones. High seismic accelerations would have initiated slope failure within the slope at any level of perched water table (even dry conditions) through either shear zones or fractured schist. The angle of the failure plane in the case of Slide No. 4 is considered to be 25° (from kinematics), which would trigger failure across foliation shears – the inferred mode of failure. In the simplest case of a cohesionless surface, dry slope, and external forces not present, the factor of safety is 1.24 if failure is to be considered through fractured schist. For the factor of safety to be reduced to 1, increased levels of the water table would be necessary ($z_w/z = 0.5$) and the friction angle must be less than 30°. The factor of safety is 0.78 if (as is considered in this case) failure occurs along foliation shear zones.

Table 5.5: Factor of Safety values for Slide No. 4 slope instability.

Cohesion						
when:		$\phi = 30°$	$\phi = 8°$	$z_w/z = 0, \phi = 30°$	$z_w/z = 0, \phi = 8°$	$z_w/z = 0, \phi = 20°$
$z_w/z = 0.5$	c' = 0kPa	0.9	0.22	1.24	0.3	0.78
$\varphi_p = 25°$	c' = 2kPa	0.96	0.28	1.3	0.36	0.84
$\alpha = 0$	c' = 5kPa	1.05	0.37	1.39	0.45	0.93
	c' = 10kPa	1.2	0.52	1.54	0.6	1.08

Friction Angle			$z_w/z = 0$
when:	$\phi = 8°$	FS = 0.22	FS = 0.3
$z_w/z = 0.5$	$\phi = 20°$	FS = 0.42	FS = 0.57
c' = 0kPa	$\phi = 25°$	FS = 0.57	FS = 0.78
$\varphi_p = 25°$	$\phi = 30°$	FS = 0.73	FS = 1.0
$\alpha = 0$	$\phi = 35°$	FS = 0.9	FS = 1.24

Depth of Perched Water Table				
when:	z_w/z	$\phi = 30°$	$\phi = 8°$	$\phi = 20°$
c' = 0kPa	0	1.24	0.3	0.78
$\varphi_p = 25°$	0.5	0.9	0.22	0.57
$\alpha = 0$	1	0.56	0.14	0.35
	1.25	0.39	0.1	0.25
	1.5	0.23	0.05	0.14

Seismic Acceleration						
when:	α	$\phi = 30°$	$\phi = 8°$	$z_w/z = 0, \phi = 30°$	$z_w/z = 0, \phi = 8°$	$z_w/z = 0, \phi = 20°$
$z_w/z = 0.5$	0	0.9	0.22	1.24	0.3	0.78
c' = 0kPa	0.1	0.85	0.21	1.18	0.29	0.74
$\varphi_p = 25°$	0.25	0.76	0.19	1.09	0.27	0.69
$\alpha = 0$	0.5	0.62	0.15	0.95	0.23	0.6

Angle of Failure Plane						
when:	φ_p	$\phi = 30°$	$\phi = 8°$	$z_w/z = 0, \phi = 30°$	$z_w/z = 0, \phi = 8°$	$z_w/z = 0, \phi = 20°$
$z_w/z = 0.5$	10°	2.01	0.49	3.27	0.8	2.06
c' = 0kPa	15°	1.44	0.35	2.15	0.52	1.36
$\alpha = 0$	20°	1.11	0.27	1.59	0.39	1
	25°	0.9	0.22	1.24	0.3	0.78
	30°	0.76	0.18	1	0.24	0.63

5.7 SLIDE NO. 5.

5.7.1 Description.

Bedrock consists of quartzofeldspathic schist, with an average foliation attitude of 110/29S. This slide is the most degraded of all the slides along Frankton Arm, but still shows marked hummocky topography (figure 5.22). The head scarp is poorly developed and not broken through the soil cover, or has been re-vegetated with a prominent retrogressive scarp situated above the main head scarp (figure 5.3 and figure 5.4). A 4WD track has been cut across the slide mass and scarps with apparently no reactivation or movement. There is no sign of tilting of the power poles placed on the slide mass. Exposures of weak pelitic schist occur in the 4WD track cuttings.

Vegetation is sparse, with mainly small matagouri scrub, however, down slope in the proximity of the incised gully, it becomes much more established. Most of the slopes are covered with grass and tussock, and small powerlines cross the landslide at 460m above sea level.

The toe area has formed along the +48m beach terrace, which is easily distinguished from aerial photographs. An irrigation canal, constructed by the 1950's, runs along the top of this beach terrace (see figure 5.22). The lower section of the western lateral margin consists of a deeply incised stream (figure 5.1 and figure 1.2 – map pocket).

This failure is considered to be a shallow retrogressive translational slide, with a failure plane orientated along foliation shear zones or fractured schist, and head and lateral release taking place on master joint sets.

5.7.2 Kinematic Analysis.

Figure 5.23 is a structural analysis of Slide No. 5 poles to displaced schist foliation, and the grouping indicates planar failure, perhaps bordering on wedge failure according to Hoek and Bray (1981). Again, no zone of instability is produced using a friction angle of 30°. Sliding is not possible along the line of intersection of the foliation with the master joint set because the plunge of this line is greater than the dip of the slope face (Hoek and Bray, 1981).

Figure 5.22: Slide No.'s 5 and 6 showing hummocky topography. Note the prominent sunlit beach terrace at the base of Slide No. 5.

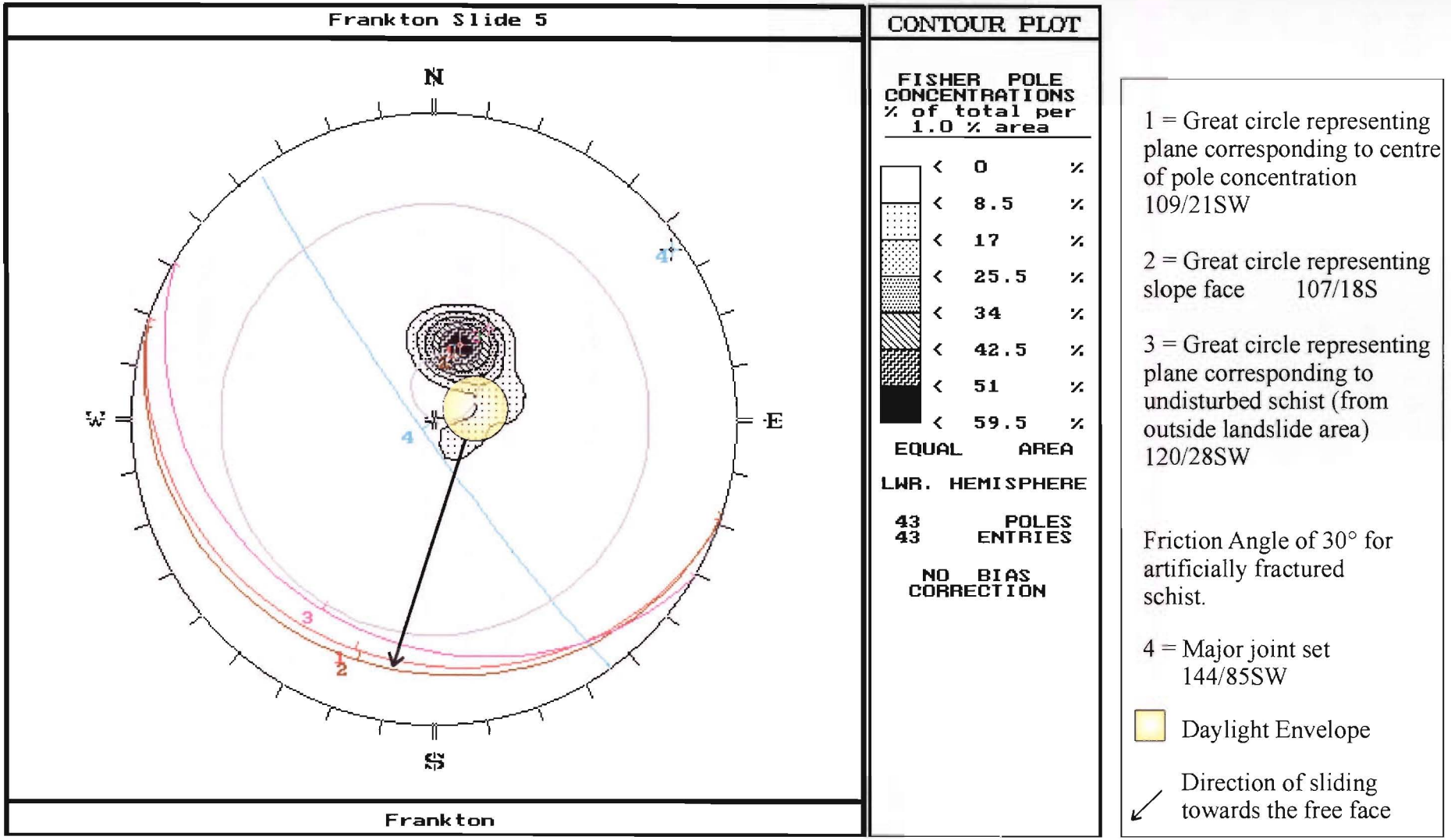

Figure 5.23: Stereonet showing major structural controls of the No. 5 Failure, using a friction angle of 30°, a value obtained from laboratory testing of artificially fractured schist collected from outside the slide area. There is no Markland's zone of instability formed

Figure 5.24 shows a plot of poles to displaced schist foliation with the major planes using a friction angle of 20° - a value assumed for failure occurring along foliation shear zones. One reason for failure in this case is that the in situ and displaced schist foliation has a very similar orientation to the slope face. This indicates sliding is taking place down the dip of the schistosity on foliation shear zones or perhaps through fractured schist. The intersection of the landslide foliation with the master joint set with the slope face does not quite fall in the Markland zone of instability, however with minor variations in orientation of the foliation occurring over the slope, in places, the foliation may in fact daylight.

The four structural conditions for Slide No. 5 necessary for failure occur as follows:

1. The strike of the displaced schist foliation is within 20° of the strike of the slope face;
2. The dip of the displaced schist foliation is more than the dip of the slope face by 3°, therefore, does not daylight in the slope face. An extended study would be required to confirm this statement because the values are so close. For this investigation it is presumed the dip of the foliation and the dip of the slope face are sub-parallel.
3. The dip of the master joint set is greater than the angle of friction.
4. The lateral extent of the failure mass is defined by a lateral release surface to the east of the unstable area.

5.7.3 Factor of Safety Sensitivity Analysis.

A result of the kinematic analysis of Slide No. 5 was that not all structural conditions necessary for failure were met. Thus, a factor of safety sensitivity analysis was undertaken, to obtain contributing factors or possible triggering mechanisms for instability.

Once again, the same input parameters to those used previously were applied. Results are presented in table 5.6 and computations and graphs are shown in Appendix L. Table 5.6 illustrates the slope is not sensitive to changes in the cohesion. In the simplest case, where the failure surface is along fractured schist, cohesionless, the slope is dry and there is no seismic acceleration, the factor of safety is 1.78 (for a failure plane situated within fractured schist). In order for the slope to fail, the friction angle must be reduced to less than 20° - a possibility if foliation shear zones are present at the slide base. Another method of creating instability would be to increase the level of the perched water table to half the depth of the slide mass. The factor of safety will be reduced to approximately one. If failure took place along foliation

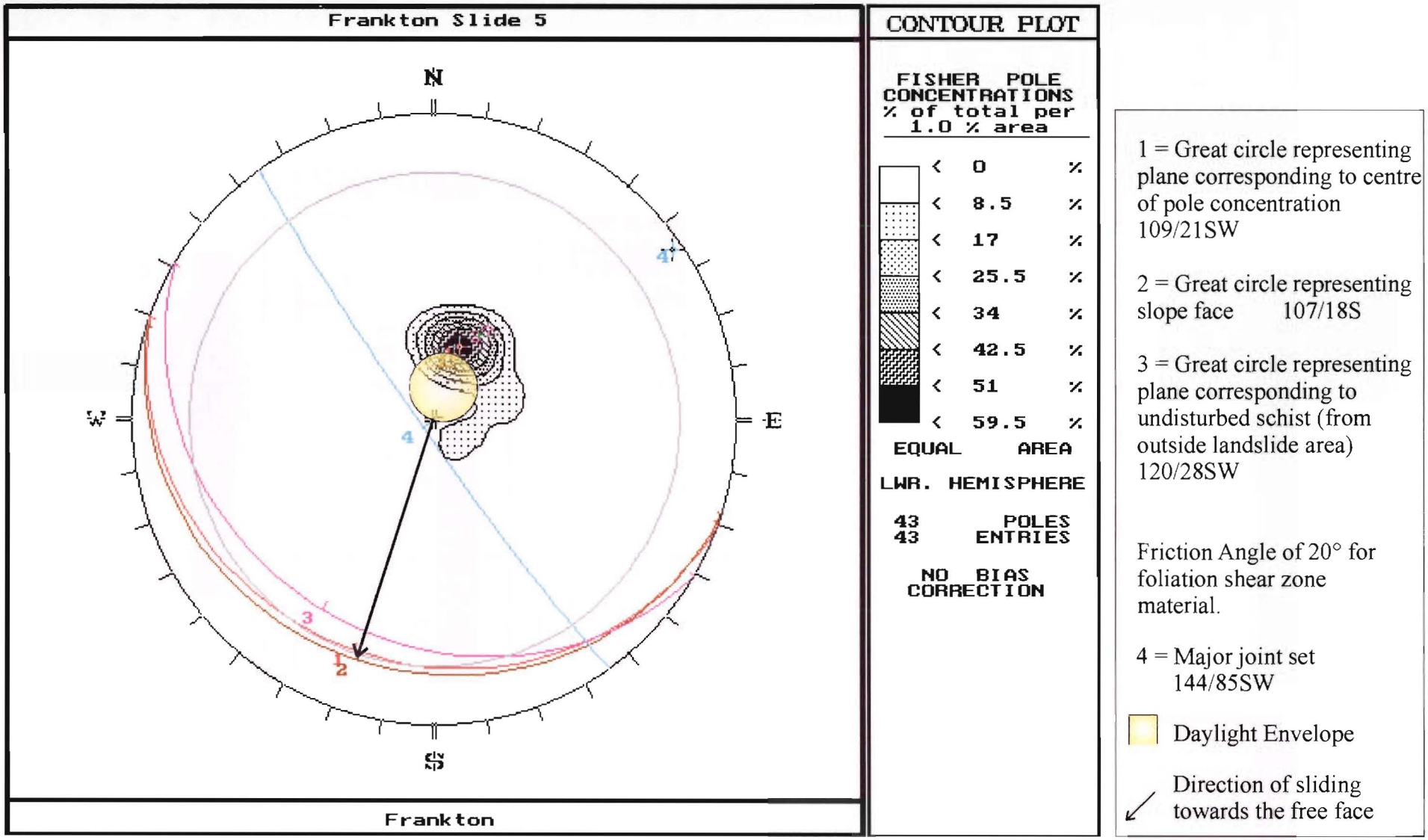

Figure 5.24: Stereonet showing major structural controls of the No. 5 Failure, using a friction angle of 20°, a value assumed for foliation shear zone material. There is no Markland's zone of instability formed

Table 5.6: Factor of Safety values for Slide No. 5 slope instability.

Cohesion						
when:		$\phi = 30°$	$\phi = 8°$	$z_w/z = 0, \phi = 30°$	$z_w/z = 0, \phi = 8°$	$z_w/z = 0, \phi = 20°$
$z_w/z = 0.5$	c' = 0kPa	1.32	0.32	1.78	0.43	1.12
$\varphi_p = 18°$	c' = 2kPa	1.36	0.36	1.81	0.47	1.16
$\alpha = 0$	c' = 5kPa	1.41	0.41	1.87	0.53	1.21
	c' = 10kPa	1.5	0.5	1.96	0.62	1.3

Friction Angle			$z_w/z = 0$
when:	$\phi = 8°$	FS = 0.32	FS = 0.43
$z_w/z = 0.5$	$\phi = 20°$	FS = 0.61	FS = 1.12
c' = 0kPa	$\phi = 25°$	FS = 0.83	FS = 1.44
$\varphi_p = 18°$	$\phi = 30°$	FS = 1.07	FS = 1.78
$\alpha = 0$	$\phi = 35°$	FS = 1.32	FS = 2.15

Depth of Perched Water Table				
when:	z_w/z	$\phi = 30°$	$\phi = 8°$	$\phi = 20°$
c' = 0kPa	0	1.78	0.43	1.12
$\varphi_p = 18°$	0.5	1.32	0.32	0.83
$\alpha = 0$	1	0.85	0.21	0.54
	1.25	0.63	0.15	0.39
	1.5	0.41	0.1	0.26

Seismic Acceleration						
when:	α	$\phi = 30°$	$\phi = 8°$	$z_w/z = 0, \phi = 30°$	$z_w/z = 0, \phi = 8°$	$z_w/z = 0, \phi = 20°$
$z_w/z = 0.5$	0	1.32	0.32	1.78	0.43	1.12
c' = 0kPa	0.1	1.27	0.31	1.72	0.42	1.08
$\varphi_p = 18°$	0.25	1.18	0.29	1.63	0.4	1.03
$\alpha = 0$	0.5	1.04	0.25	1.49	0.36	0.94

Angle of Failure Plane						
when:	φ_p	$\phi = 30°$	$\phi = 8°$	$z_w/z = 0, \phi = 30°$	$z_w/z = 0, \phi = 8°$	$z_w/z = 0, \phi = 20°$
$z_w/z = 0.5$	10°	2.28	0.56	3.27	0.8	2.06
c' = 0kPa	15°	1.57	0.38	2.15	0.52	1.36
$\alpha = 0$	20°	-	-	-	-	-
	25°	0.96	0.23	1.24	0.3	0.78
	30°	0.8	0.19	1	0.24	0.63

shear zones, gravitational accelerations of 0.1g would bring the slide very close to failure. 0.5g would certainly cause failure. If the slide mass is dry, and the friction angle is 30° the slope would fail (factor of safety is reduced to 1). If the failure surface occurs within shear zones parallel to foliation, the simplified factor of safety falls to 1.12, a stable slope.

5.8 SLIDE NO. 6.

5.8.1 Geology.

Slide No. 6 has a volume of 7.0 x $10^5 m^3$ and an area of $7km^2$. The landslide is situated on the northeastern edge of Frankton Arm (figure 5.1; figure 1.2 – map pocket). The head scarp trends northwest-southeast, similar to the other slides, and is prominently joint-controlled. Again, the +48m beach terrace cuts across the toe of the slide along with the irrigation canal. The scarps of this slide are not as degraded as they are on Slide 5, and this may be attributed to the change in strike of the slope face which causes the strike of the foliation to be a lot similar in orientation to the strike of the slope face, a factor contributing to increased levels of instability. However, the head scarp has still not broken through the soil cover. The western lateral margin coincides in places with the eastern margin of Slide No. 5 and the eastern margin acts as a lateral release structure on which movement can occur (figure 5.22).

The head scarp (figure 5.25) contains a concentration of vegetation (predominantly matagouri) at its base; whereas any scrub-like vegetation is absent on the mid to upper slopes, contains mostly grass and sparse tussock. Vegetation is more established along the lower slopes, indicating perhaps the water table is closer to the surface than elsewhere within the failure mass.

The land making up the slide is used for sheep grazing. No residential development occurs on the slide, although on the flat land immediately south of the irrigation canal, houses have been built adjacent to the main highway (figure 5.4). These houses are not considered to be at risk from any movement of this landslide.

Figure 5.25: The head scarp of Slide number 6 (at the sky line) showing degradation and the establishment of vegetation.

5.8.2 Kinematic Analysis.

Figure 5.26 shows a stereoplot of poles to displaced schist foliation for Slide No. 6, using a friction angle of 30°. Many of the poles fall within the daylight envelope, denoting most daylight in the slope face. The plunge of intersection of the foliation and the master joint set is less than the angle of friction, if the failure surface is placed within artificially fractured schist, indicating sliding cannot take place (Hoek and Bray, 1981). Sliding along the line of intersection of the foliation and the master joint set is kinematically possible because the plunge of this line is less than the dip of the slope face. Figure 5.27 uses a friction angle of 20°, possible if failure is through foliation shears. There are no intersecting planes within the area of instability, therefore, it is assumed from kinematics, that this slope is currently in equilibrium.

The following kinematic conditions have acted as failure initiators in Slide No. 6:

1. The strike of the displaced schist foliation is within 20° of the slope face, thus acts as a kinematically viable failure surface;
2. The dip of the displaced schist foliation is greater than the dip of the slope face, therefore is not a viable failure surface. This would have to be confirmed by a more involved study, as the difference is only 2° - a margin of error would be greater than this, so the possibility of displaced schist foliation dipping less than the slope face is still valid especially as the slope before failure would have been steeper than it is post-failure. It is assumed for this study that the foliation within the landslide and the angle of the slope face are sub-parallel;
3. The dip of the master joint set is greater than the friction angle by 55°;
4. The lateral extent of the failure mass is defined by a lateral release surface that does not contribute to the stability of the mass.

5.8.3 Factor of Safety Sensitivity Analysis.

A limit-equilibrium analysis was undertaken to determine conditions necessary to cause failure of Slide No. 6. The kinematic analysis concluded that not all structural conditions necessary for failure were in place, thus another means of acquiring conditions in place at the time of failure was necessary. Results of the factor of safety sensitivity analysis are presented in table 5.7, and computations and graphs are supplied in Appendix L.

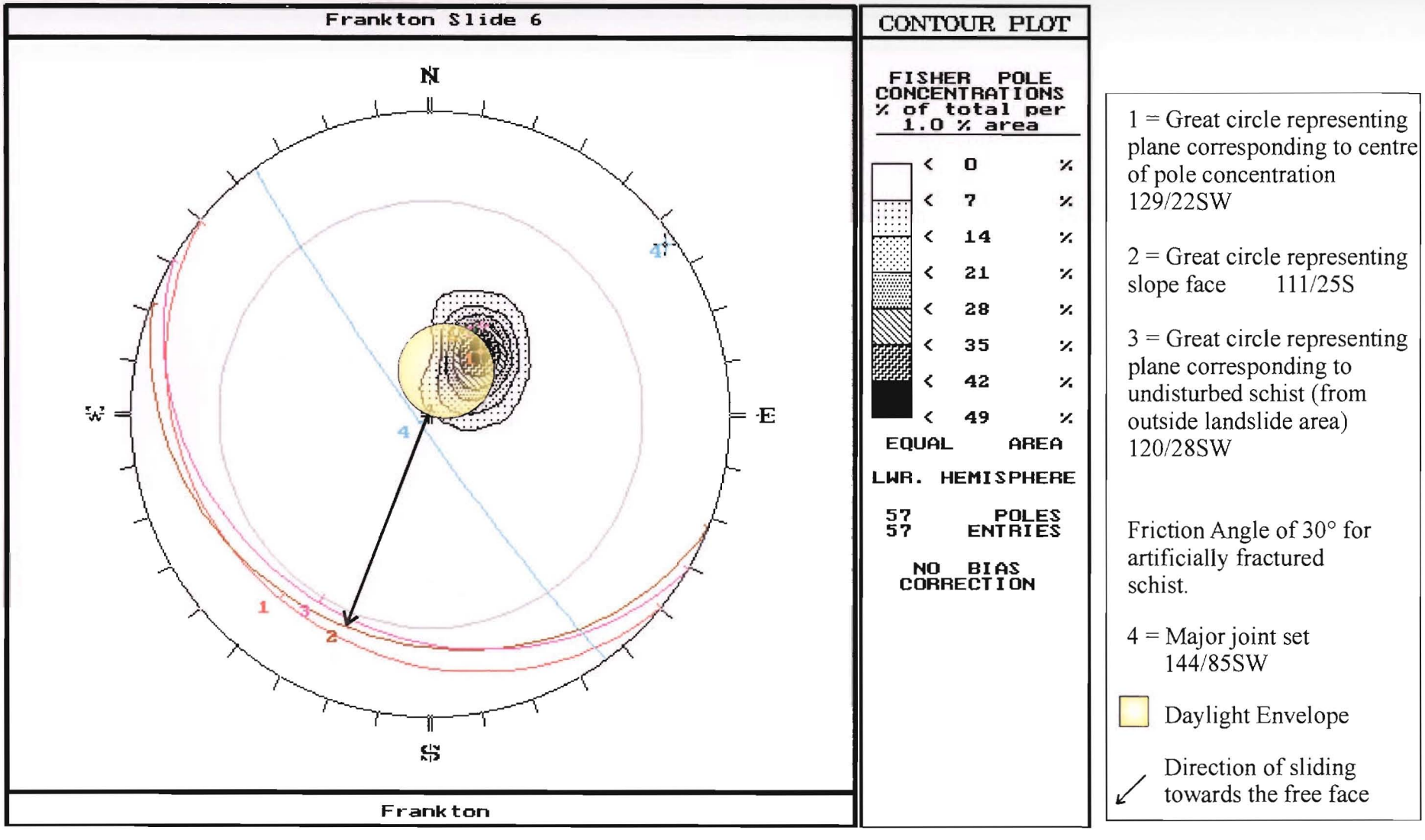

Figure 5.26: Stereonet showing major structural controls of the No. 6 Failure, using a friction angle of 30°, a value obtained from laboratory testing of artificially fractured schist collected from outside the slide area. There is no Markland's zone of instability formed.

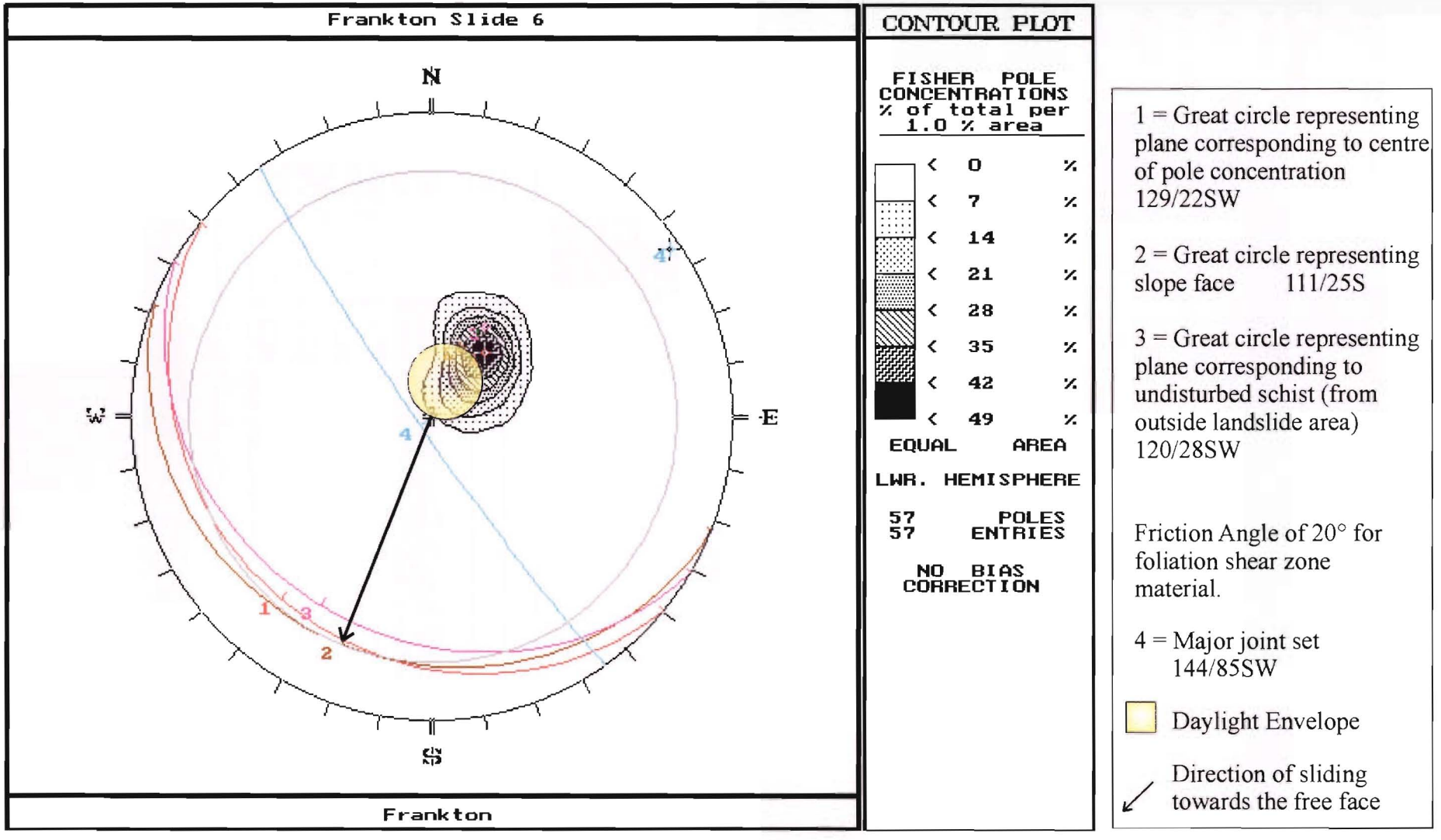

Figure 5.27: Stereonet showing major structural controls of the No. 6 Failure, using a friction angle of 20°, a value assumed for foliation shear zone material. There is no Markland's zone of instability formed.

Table 5.7: Factor of Safety values for Slide No. 6 slope instability.

Cohesion						
when:		$\phi = 30°$	$\phi = 8°$	$z_w/z = 0, \phi = 30°$	$z_w/z = 0, \phi = 8°$	$z_w/z = 0, \phi = 20°$
$z_w/z = 0.5$	$c' = 0$kPa	1.45	0.35	1.78	0.43	1.12
$\varphi_p = 18°$	$c' = 2$kPa	1.46	0.36	1.79	0.44	1.13
$\alpha = 0$	$c' = 5$kPa	1.48	0.38	1.8	0.46	1.15
	$c' = 10$kPa	1.5	0.41	1.83	0.49	1.17

Friction Angle			$z_w/z = 0$
when:	$\phi = 8°$	FS = 0.35	FS = 0.43
$z_w/z = 0.5$	$\phi = 20°$	FS = 0.67	FS = 0.82
$c' = 0$kPa	$\phi = 25°$	FS = 0.91	FS = 1.12
$\varphi_p = 18°$	$\phi = 30°$	FS = 1.17	FS = 1.44
$\alpha = 0$	$\phi = 35°$	FS = 1.45	FS = 1.78

Depth of Perched Water Table				
when:	z_w/z	$\phi = 30°$	$\phi = 8°$	$\phi = 20°$
$c' = 0$kPa	0	1.78	0.43	1.12
$\varphi_p = 18°$	0.5	1.45	0.35	0.91
$\alpha = 0$	1	1.07	0.26	0.67
	1.25	0.88	0.21	0.55
	1.5	0.7	0.17	0.44

Seismic Acceleration						
when:	α	$\phi = 30°$	$\phi = 8°$	$z_w/z = 0, \phi = 30°$	$z_w/z = 0, \phi = 8°$	$z_w/z = 0, \phi = 20°$
$z_w/z = 0.5$	0	1.45	0.35	1.78	0.43	1.12
$c' = 0$kPa	0.1	1.4	0.34	1.72	0.42	1.08
$\varphi_p = 18°$	0.25	1.31	0.32	1.63	0.39	1.03
$\alpha = 0$	0.5	1.17	0.29	1.49	0.36	0.94

Angle of Failure Plane						
when:	φ_p	$\phi = 30°$	$\phi = 8°$	$z_w/z = 0, \phi = 30°$	$z_w/z = 0, \phi = 8°$	$z_w/z = 0, \phi = 20°$
$z_w/z = 0.5$	10°	2.7	0.66	3.27	0.8	2.06
$c' = 0$kPa	15°	1.76	0.43	2.15	0.52	1.36
$\alpha = 0$	20°	1.3	0.32	1.59	0.39	1
	25°	1.24	0.3	1.24	0.3	0.78
	30°	0.83	0.2	1	0.24	0.63

As can be seen in table 5.7, the slope is not sensitive to varying values of cohesion, however it is sensitive to variable values of friction.. A factor of safety of 1.78 is obtained within fractured schist when the cohesion is zero, the slope is dry and seismic acceleration is disregarded. In order to make the slope fail, maximum friction values of 26° (with the ratio $z_w/z = 0.5$) and 21° (for a dry slope) need to be applied. Alternatively, for a landslide occurring along crushed schist, the perched water table need only be at a maximum of half the depth of the slide mass. If the slide base is following a fractured schist horizon, the ratio $z_w/z = 1$ would be necessary (that is, the perched water table is at the ground surface). Seismic accelerations of at least 0.25g are necessary to promote failure along crushed schist. If the angle of the failure plane is inclined at 20°, and the failure surface occurs within crushed schist (friction value of 20°) then the slope is considered to be at a factor of safety of 1. Using a friction angle of 20°, the simplified factor of safety is 1.12.

5.9 DISCUSSION.

5.9.1 Failure Mechanisms.

A translational failure mechanism has been adopted for the Frankton Arm landslides, with the failure planes assumed to be parallel to the schistosity, and along foliation shear zones or crushed schist. In places the failure surface may follow fractures and cross the foliation. This would create increased frictional resistance within the slope. Movement has been accommodated along the lateral release surfaces for each slide, as this boundary provides unrestricted movement.

The landslides along Frankton Arm formed by planar movements involving displacements on the schist foliation shear zones dipping at 25-30°, with sub-vertical joints acting as head and lateral release features. The schist contains a range of defects and the stability of the rock would decrease by pore water pressures from ice or water that exerts pressure on joint walls enhancing the likelihood of failures. This pressure would also decrease the friction component that resists shear along inclined defects, causing translational sliding on low shear strength foliation surfaces daylighting on natural slopes. Several of the landslides have, however, failed on to very young lake beaches, thus it is inferred that seismicity may be a more likely triggering mechanism. Detailed subsurface investigations are necessary to confirm the failure mechanisms suggested in this project.

5.9.2 Kinematics and Sensitivity.

The range of defects within the schist is conducive to the development of planar failures. Most of the failures show that sliding along the intersection of the foliation with the major joint set is possible.

All of the slides along Frankton Arm have a lateral extent that is defined by a lateral release surface that does not contribute to the stability of the mass. If failure were to take place along a foliation shear zone, then the foliation will act as a kinematically viable failure surface.

Table 5.8: Summary of Kinematic Analyses.

Condition	Marina Heights	Slide No. 2	Slide No. 3	Slide No. 4	Slide No. 5	Slide No. 6
Strike of the discontinuity is within 20° of the strike of the slope face	Yes	No	Yes	Yes	Yes	Yes
The discontinuity daylights in the slope face	Yes	Yes	Yes	Possibly	No	Possibly
The dip of the discontinuity is greater than the angle of friction	Yes	Yes	Yes	Yes	Yes	Yes
The lateral extent of the failure is defined by a lateral release surface	Yes	Yes	Yes	Yes	Yes	Yes

Some of the slides show that the foliation within the landslide is daylighting in the slope face. In cases where the foliation has a similar strike to the slope face, this has a considerable influence on the stability of the rock mass. This structural feature occurs in the Marina Heights and No. 5 failures. In all other cases, sliding takes place obliquely down slope (or obliquely down the dip of the foliation).

5.9.3 Failure History and Triggering Events.

The translational rock block slides along Frankton Arm are assumed to be generated by the processes produced during the Last Glaciation. Shear stress within the unstable masses was increased by the removal of lateral support by the glacier during subsequent periods of ice advance and retreat. The rock may have disintegrated under cycles of freezing and thawing producing possible instability. Steepening of the slopes was caused by ice scouring by the glacier and weathering and the addition of water to the slopes following glacial retreat would also have altered and removed pelitic schist, forming foliation shear zones and open voids within the rock mass. The addition of ice would have widened the fractures contained within the bedrock and added surcharges to the mass, causing an overall increase in shear stress. It is likely that ground accelerations associated with earthquakes would also have played a part in increasing the shear stress. It is likely initial failure of the slides was caused by ice-plugged drainage and other effects of glacial retreat (such as elevated water table levels), and then at a much later stage, after deposition of lake beaches during lake lowering, a possible seismic event triggered later failure, with the slides over-riding the lake beaches. The schist along Frankton Arm was made weak as a result of saturation by water, as rock such as schist can decompose to clay by chemical weathering. Saturation with water would have reduced the effective intergranular pressure and friction of the rock. The rock mass was also weakened by discontinuities such as faults, foliation, joints and sheared zones.

5.10 FUTURE STABILITY.

The only evidence for continuing movement within the last 100 years is on Slide No. 3 and Slide No. 4. Continual minor wedge failures are expected from the head scarps, but as a result of the high frictional interlock between the displaced schist blocks, there is minimal risk to residential areas if prudent engineering geological practices are implemented. It is recommended that detailed engineering geological and geotechnical investigations be conducted on these two slides if any future development is to be considered within or close to the slide areas.

Future work requirements would be as follows:

- Electronic Distance Measurement (EDM) devices can be used for long-term monitoring for subsequent movement on Slide No. 3 (the most active) to confirm if any change in surface morphology is currently taking place.

- Monitoring of any cracks on the failed masses is a critical part of investigation, as any found uphill and downhill of the slide mass indicate a possible increase in the size of the failure.

- Direct measurement of ground water conditions using a network of peizometers is necessary to determine the degree of saturation and sub-surface water flow through the mass. Increased saturation will lead to increased instability.

- Subsurface drilling is recommended to identify the position and depth of the slide base. Ground water data can be acquired by observing conditions encountered while drilling. Subsurface exploration allows the retrieval of representative samples to conduct laboratory tests. However, specific drilling methods are necessary if undisturbed samples are required, such as core drilling (McGuffey et. al., 1996).

5.11 SYNTHESIS.

- There are six minor landslides that occur near Frankton, Queenstown, with an average volume of 1 – 2 million cubic metres.

- Failure models based on field investigations and aerial photograph interpretation indicated the slides had a simple translational sliding mechanism, with the failure plane located parallel or sub-parallel to schistosity, and head and lateral scarps formed by joint release on master joint sets.

- It is suggested the slides formed as a result of ice-scouring and retreat. The Kawarau Lobe of the Wakatipu Glacier advanced and retreated along Frankton Arm a number of times, and the addition of water within the slide areas resulted in the preferential removal or weathering of weak pelitic schist horizons. This formed open voids or foliation shear zones (a result of the weathering), along which subsequent movement took place.

- Kinematic analysis showed that the dip of the foliation was similar to the dip of the slope face – a condition that creates instability. The grouping of poles to foliation on each stereonet indicated a planar failure mechanism for all of the slides.

- Sensitivity analyses for each slide were conducted to determine possible triggering mechanisms in place at the time of failure for each slide. They showed that a change in cohesion would not act as a major triggering mechanism. In order to promote failure within the slide masses, the frictional resistance needed to be between approximately 18° up to a maximum of 30°. Alternatively the perched water table was situated at least half the depth of the failure, or seismic accelerations of 0.25g or greater were necessary to initiate failure. The angle of inclination of the failure plane needed to be at least equal to the friction angle of the failure surface to reduce the factor of safety to one. Inclination of failure surfaces calculated from kinematic analysis and the construction of cross-sections are considered realistic if failure takes place along foliation shear zones.

CHAPTER 6

SUMMARY AND CONCLUSIONS.

1. Engineering geological mapping at a scale of 1:5000 and 1:10000, aerial photograph interpretation, and laboratory testing has been used to investigate landsliding along Frankton Arm near Queenstown. These investigations have been used to establish engineering geological and geotechnical failure models for the seven schist bedrock landslides identified, and to determine probable conditions during the triggering of these landslides.

2. Bedrock in the Frankton Arm area is entirely Haast Schist Terrane, belonging to textural zone IV chlorite schist. The bedrock along Frankton Arm has been subject to at least four major periods of ice advance and retreat (from approximately 500000 years ago to 15000 years ago) are recognised within the area, with ice retreat commencing about 14000 years ago. During and following the last ice retreat, Lake Wakatipu was at a greater elevation, as evidenced by high level lake beaches (+42, +35, +27 and +23m), extensive deposits of lacustrine silts and fine sands, and high level truncated fan-deltas and alluvial fans.

3. Geotechnical testing of intact and fractured schist bedrock and foliation shear zone material was carried out to provide strength characteristics to assist in the interpretation of the failure mechanisms for the bedrock landslides. Geotechnical testing conclusions are as follows:

   a) $I_{s(50)}$ values obtained from point load testing ranged from 0.60MPa to 3.83MPa for samples tested perpendicular to schistosity, and from 0.11MPa to 0.92MPa for samples tested parallel to schistosity. This classifies the rock as weak to strong according to Bell and Pettinga (1983).

b) Friction values for rock artificially fractured parallel to foliation ranged from 24° to 36°, and 26° to 73° for estimated apparent friction. Friction values for clayey silt foliation shear zone material ranged from 6° to 11° (when the coarser material is removed), with zero cohesion. Residual shear behaviour is inferred to be by a sliding mode.

c) X-ray Diffraction analyses revealed kaolinite, albite, muscovite, clinochlore, quartz and hornblende as the clay-sized minerals present in the shear zone material, with kaolinite as the dominant mineral in the samples tested. The typical percentage of clay-sized particles present in the samples was 4.5%. Other investigations from within the Otago Schist have identified smectites, however these clay minerals were not found in the samples from Frankton Arm.

4. Stereographic analysis indicated four major defect sets, which were 104±32/86±4°S; 101±23/76±14°SW; 099±20/66±17°S and 194±38/63±27°W within the schist bedrock along Frankton Arm, and these features contribute to destabilisation of the rock mass.

5. The Queenstown Hill Landslide is the largest bedrock failure along Frankton Arm, with an estimated volume of 240M m^3, and it is interpreted as being a simple translational slide with the toe forming a shallow compressional bulge. This compression is related to the slow gravitational relaxation into an in situ schist block situated along the lower slopes of Queenstown Hill. Three phases of movement are inferred to have taken place, with the earliest stage initiated by ice scouring and undercutting during the final stages of glacial activity. The movement of the landslide is classed as retrogressive, with evidence for repeated movements of the same type, following enlargement of the failure surface. This may indicate the landslide has propagated up slope.

6. Kinematic analysis shows that a major factor contributing to instability is the orientation of the foliation at the base of the slide, being sub-parallel to the slope face. The major joint defects, with a strike perpendicular or parallel to foliation, are recognised as controlling

the lateral margins of the failure, and defects oriented parallel to the strike of the foliation provide head releasing structures.

7. Sensitivity analyses were completed using simplified failure models to determine parameters in place during the initiation of movement for the Queenstown Hill Landslide. It was concluded that low friction angles within foliation shear zone material (below 20° - 25°) may trigger instability. Failure may be initiated along foliation shears and crushed schist, particularly when the water table is at half the depth of the slide mass. High ground water levels may have triggered failure through fractured schist blocks (with a friction angle of 30° - determined from shear testing of fractured schist samples) and this situation may have been in place immediately following retreat of the Last Glaciation. Water levels would have fluctuated and ice-plugged drainage within schist bedrock fractures would have existed following retreat of the last ice advance. Elevated ground water levels within the slide mass on glacial retreats would have weathered, altered, and eroded the platy micaceous minerals contained within the pelitic schist horizons, causing failure along the pre-existing foliation shear zones. Possible seismic triggers could have been the final initiating failure mechanism, and created enough driving forces within the slope to cause failure.

8. Six smaller bedrock failures of up to 1 1km^2 occur along Frankton Arm, and these failures are also considered to be retrogressive translational planar failures. The failures have occurred along two discontinuities with the schist foliation forming the slide bases, and the sub-vertical master joint sets having acted as head and lateral release structures. The failure surface may be stepped across the foliation on joints, and foliation shear zones were most probably situated along the failure surface. The head scarps show retrogressive features, with several small scarps present up slope of the main scarp. Subsequent enlargement of the failure surface has resulted from this retrogression and the head scarp has gradually extended up slope.

9. Slide No. 3 and Slide No. 4 are considered the most active of all the smaller failures. Small wedge failures have been taking place over the last 100 years, as evidence by the lack of vegetation and the freshness of the rock surfaces within the head scarps. These wedge failures have collapsed from the head scarp and fallen on to the slopes immediately below the scarp. Due to the high frictional interlocking between the blocks, they have not moved more than 20m from the base of the head scarp.

10. The remaining slides are hummocky but partly degraded, and there is no air photograph evidence for movement within the last 100 years.

11. Kinematic analyses for each slide have confirmed that the orientation of the schist foliation and the slope face is very similar. This indicates failure is likely to occur parallel to the schist foliation, forming a translational planar slide.

12. A limit equilibrium analysis was undertaken for each slide to identify contributing factors or possible triggering mechanisms for instability. The slopes were not sensitive to varying values of cohesion, but they were sensitive to friction. In order to initiate failure, friction angles of between 20° and 30° are necessary, along with the perched water table level at half the depth of the failure mass. The perched water table must have been at this level if each of the slide bases occur within crushed schist, as this condition gives a factor of safety less than 1. For each failure to have taken place along fractured schist (parallel to the foliation), the perched water table needed to be at ground surface level. The factor of safety will be close to 1 if the angle of each failure plane is equivalent to the friction angle and seismic accelerations are involved.

13. The Frankton failures were initiated as a result of effects from the Last Glaciation (similar to the larger Queenstown Hill Landslide). Steepening of the slopes caused by ice scouring and the addition of water to the slopes, would have altered and removed the weak pelitic

schist, forming open voids within the rock mass and causing failure along pre-existing foliation shear zones.

14. Several of the smaller Frankton failures have failed on to very young lake beaches, thus it is inferred that failure was triggered in a number of the slides at a much later stage after deposition and lowering of Lake Wakatipu.

15. There is minimal risk to housing near Slide No. 3 and Slide No. 4, but for any future development, it is recommended prudent engineering geological practices be implemented. There is no visual evidence for movement within the last 100 years for the Queenstown Hill Landslide.

16. This study has produced engineering geological maps of the Frankton Arm landslides without sub-surface information. Further work requirements would be to establish the depth, shape and angle of inclination of the failure surface by the installation of several drill holes. This method would determine if the slide base is occurring along foliation shear zones and/or schist fractured parallel to the foliation.

ACKNOWLEDGEMENTS.

The following people have my sincere thanks for their assistance during the preparation of this thesis:

My supervisor, Mr. D. H. Bell, for his guidance and encouragement during the last 18 months, and for reviewing the many drafts of this project. Also to Dr. J. McKean for the review of early chapters and Mrs J. Campbell for helpful discussions on stereographic analysis.

The Mason Trust Fund, for their contribution to accommodation and travelling costs.

The technicians of the Geological Sciences Department, especially Cathy Knight for all the help doing lab work, and Jane Guise for doing the grain size analysis at short notice. Thanks to Steven Brown for the XRD analyses, John Southward for helping solve all my computer problems and Lee Leonard for the drafting of cross-sections.

Clark Fortune McDonald & Associates, for the GPS surveying and the use of their offices in Queenstown. Royden Thomson for insights into the Cromwell and Kawarau Gorge areas, and discussions on the Frankton Arm landslides. Arnold Middleton for letting me traipse over his land, and for giving me some garden veges.

To all my colleagues, especially my roomies Lou, Rich and Melinda. Thanks Lou for all the talks – sorry for distracting you so many times! Thanks to you guys for all the laughs.

The biggest thanks of all to Rick, Mum, Sharee, Darren, and Jason. Thanks for all your support throughout my university years and the many meals on wheels!

REFERENCES.

Barrell, D.J.A., Riddolls, B.W., Riddolls, P.M. and Thomson, R. (1994), Surficial geology of the Wakatipu Basin, Central Otago, New Zealand. Institute of Geological and Nuclear Sciences Science Report 94/39: 31p, 2 maps.

Barton, N. and Choubey, V. (1977), The shear strength of rock joints in theory and Practice, **in:** Rock Mechanics, 10: p1-54.

Beetham, R.D., Moody, K.E., Fergusson, D.A., Jennings, D.N. and Waugh, P.J. (1991), Landslide development in schist by toe buckling, Bell, D.H. (ed), **in:** Landslides; Proceedings of the Sixth International Symposium, Balkema, Rotterdam, p17-23.

Beetham, R.D., Smith, G., Jennings, D.N. and Newton, C.J. (1992), The geology of Nine Mile Creek schist landslide complex, Bell, D.H. (ed), **in:** Landslides; Proceedings of the Sixth International Symposium, Balkema, Rotterdam, p25-31.

Bell, D.H. (1976a), Slope evolution and slope stability, Kawarau Valley, Central Otago, New Zealand. Bulletin of the International Association of Engineering Geology, 14: p5-16.

Bell, D.H. (1976b), Late Pleistocene glaciations of the Kawarau Valley, Central Otago, New Zealand. Geological Society of New Zealand Inc, Hamilton Conference Abstracts.

Bell, D.H. (1977), Quaternary and engineering geology of the Kawarau and Upper Clutha Valleys. Geological Society of New Zealand Inc., Queenstown Conference Field Trip Guide B, p1-24.

Bell, D.H. (1982), Geomorphic evolution of a valley system: the Kawarau Valley, Central Otago. Chapter 17, Soons, J.M. and Selby, M.J. (eds), **in:** Landforms of New Zealand, Longman Paul Ltd, Auckland, p317-341.

Bell, D.H. (1985a), Engineering geology report on proposed subdivision Bishop property – Frankton. Unpublished report to Clark Brewster McDonald & Associates dated 20 Feb 1985: 19pp + 1 fig.

Bell, D.H. (1985b), Engineering geology report on proposed subdivision Newman property – Frankton Road Queenstown. Unpublished report to P. Newman dated 2 Dec 1985: 11pp + 1 fig.

Bell, D.H. (1987), The K9 Landslide, Kawarau Valley, Central Otago. Proceedings of the International Symposium on Engineering Geological Environment in Mountainous Areas, Beijing, China.

Bell, D.H. (1989), Engineering geology assessment of Goldfields Stage IV Development, Queenstown. Unpublished report to Woodlot Villas Ltd dated June 1989: 9pp + 2 figs.

Bell, D.H. (1994), Mike Stone Subdivision – Frankton Road – Queenstown. Unpublished Canterprise Report CP/2307 to Clark Fortune McDonald & Associates dated 31 August 1994: 4pp + 2 figs.

Bell, D.H. (1995), Engineering geology assessment of Commonage Stage VIII Subdivision proposal. Unpublished Canterprise Report CP/2411 to Clark Fortune McDonald & Associates dated 6 October 1995: 14pp + 1 fig.

Bell, D.H. (1995), Maurice Jamieson Property – Larch Hill Place – Queenstown. Unpublished Canterprise Report CP/2393 to Clark Fortune McDonald & Associates dated 18 June 1995: 6pp + 1 fig.

Bell, D.H. (1997a), Engineering geology report on proposed Remarkables View subdivision P & G Hensman – Frankton Arm. Unpublished report to Clark Fortune McDonald Associates dated 8 August 1997: 14pp + 1 fig.

Bell, D.H. (1997b), Geotechnical evaluation of the Marina Heights Extension – Frankton. Unpublished Canterprise Report CP/2576 to Clark Fortune McDonald & Associates dated 19 August 1997: 13pp + 2 figs.

Bell, D.H. (1997c), Engineering geology report on proposed subdivision Kremer & Associates Frankton Road property – Queenstown. Unpublished report to Clark Fortune McDonald & Associates dated 21 August 1997: 4pp + 9 figs.

Bell, D.H. and Pettinga, J.R. (1983), Presentation of geologic data, **in:** Proceedings of the Symposium Engineering for Dams and Canals, IPENZ, Volume 9, Issue 4(G), p4.1-4.35.

Bell, D.H., Thomson, R. and McKellar, I.C. (1977), Tour B; Quaternary and engineering geology of the Kawarau and Upper Clutha Valleys. Geological Society of New Zealand, pB1-24.

Bieniawski, Z.T. (1973), Engineering classification of jointed rock masses. Transactions of the South African Institute of Civil Engineering 15; 12: p335-344.

Bishop, D.G. (1974), Stratigraphic, structural and metamorphic relationships in the Dansey Pass area, Otago, New Zealand. New Zealand Journal of Geology and Geophysics 17: p301-335.

Bishop, D.G., Bradshaw, J.D., Landis, C.A. and Turnbull, I.M. (1976), Lithostratigraphy and structure of the Caples terrane of the Humboldt mountains, New Zealand. New Zealand Journal of Geology and Geophysics 19; 6: p827-848.

Broch, E. and Frankin, J.A. (1972), The Point Load Strength Test. International Journal Rock Mechanic and Mining Sciences, 9: p669-697.

Brown, E.T. (1981), Rock Characterisation Testing and Monitoring, International Society of Rock Mechanics Suggested Methods, Pergamon Press.

Chapple, A.P. (1998), An Engineering Geological Investigation into Pit Slope Stability at Macraes Gold Mine, Macraes Flat, Otago, New Zealand. Unpublished M.Sc. Engineering Geology Thesis, University of Canterbury, Christchurch, New Zealand, 241pp.

Coombs, D.S., Landis, C.A., Norris, R.J., Sinton, J.M. and Craw, D. (1976), The Dun Mountain Ophiolite belt, New Zealand. American Journal of Science 276: p561-603.

Craw, D. (1984), Lithologic variations in Otago Schist, Mt Aspiring area, northwest Otago, New Zealand. New Zealand Journal of Geology and Geophysics 27: p151-166.

Cruden, D.M. and Varnes, D.J. (1996), Landslide Types and Processes, **in:** Landslides - Investigation and Mitigation, Transportation Research Board Special Report 247, National Academy Press, Washington, p36-75.

Cunningham, V.J. (1994), Land use planning and development suitability in Queenstown, New Zealand. Unpublished M.Sc. Engineering Geology Thesis, University of Canterbury, Christchurch, New Zealand, 164pp.

Deere , D.U. and Miller, R.P. (1966), Engineering classification and index properties for intact rock. University of Illinois Contract AF 29(601)-6319, Technical Report AFWL-TR-65-116.

Gage, M. (1958), Late Pleistocene glaciations of the Waimakariri Valley, Canterbury, New Zealand. New Zealand Journal of Geology and Geophysics 1: p123-155.

Gillon, M.D. and Hancox, G.T. (1992), Cromwell Gorge landslides, a general overview, Bell, D.H. (ed), **in:** Landslides; Proceedings of the Sixth International Symposium, Balkema, Rotterdam, p83-102.

Grim, R.E. (1962), Applied Clay Mineralogy. International series in the Earth and Planetary Sciences. McGraw-Hill Book Company, 422pp.

Hector, J. (1863), Geological explorations to the west coast of Otago. New Zealand Journal of Science and Technology 6: p123-128

Hoek, E. and Bray, J.W. (1981), Rock slope Engineering, revised third edition, Institute of Mining and Metallurgy, London, 358pp.

Hoek, E. and Diederichs, M. (1989), DIPS – A program for plotting, analysis and presentation of structural geology data using spherical projection techniques. Rock Engineering Group, University of Toronto, 138pp.

Hutchinson, J.N. (1988), General Report: Morphological and Geotechnical Parameters of Landslides in relation to Geology and Hydrogeology, Bonnard C. (ed), **in:** Proceedings of the Fifth International Symposium on Landslides, Balkema, Rotterdam, p3-35.

Hutton, C.O. and Turner, F.J. (1936), Metamorphic zones in North-west Otago. Transactions of the Royal Society of New Zealand 65: p405-406.

Hutton, F.W. (1872), On the date of the last great glacier period in New Zealand and the formation of Lake Wakatipu. Transactions of the New Zealand Institute 5: p384-396.

Irwin, J. (1972), Lake Wakatipu, Bathymetry, New Zealand Oceanographic Institute Chart, Lake Series, 1:63,360, Department of Scientific and Industrial Research, Wellington, New Zealand.

Jennings, D.N., Newton, C.J., Beetham, R.D. and Smith, G. (1992), Stabilisation of the Nine Mile Creek schist landslide complex, Bell, D.H. (ed), **in:** Landslides; Proceedings of the Sixth International Symposium, Balkema, Rotterdam, p759-764.

Johnson, J.D. (1986), The Gibbston Valley, Kawarau Valley, Central Otago. Unpublished M.Sc. Engineering Geology Thesis, University of Canterbury, Christchurch, New Zealand, 169pp.

Keaton, J.R. and Beckwith, G.H. (1996), Important Considerations in Slope Design, **in:** Landslides – Investigation and Mitigation, Transportation Research Board Special Report 247, National Academy Press, Washington, p429-438.

Lewis, D.W. (1962), Practical Sedimentology Apteryx Books.

Lupini, J.F., Skinner, A.E. and Vaughan, P.R. (1981), The drained residual strength of cohesive soils. Geotechnique 31;2: p181-213.

Macfarlane, D.F., Riddolls, B.W., Crampton, N.A. and Foley, M.R. (1992), Engineering Geology of schist landslides, Cromwell, New Zealand, Bell, D.H. (ed), **in:** Landslides; Proceedings of the Sixth International Symposium, Balkema, Rotterdam, p2137-2144.

McGuffey, V.C., Modeer, V.A. and Turner, K.A. (1996), Subsurface exploration, **in:** Landslides – Investigation and Mitigation, Transportation Research Board Special Report 247, National Academy Press, Washington, p178-230.

McKellar, I.C. (1960), Pleistocene deposits of the Upper Clutha Valley, Otago, New Zealand. New Zealand Journal of Geology and Geophysics 3: p432-460.

McKenzie, M.J. (1993), An Evaluation of the Rock Mass Rating (RMR) System and its Potential Applicability in the Prediction of the Stability of Natural Slopes. Unpublished M.Sc. Engineering Geology Thesis, University of Canterbury, Christchurch, New Zealand, 341pp.

McSaveney, M.J., Thomson, R. and Turnbull, I.M. (1992), Timing of relief and landslides in central Otago, New Zealand, Bell, D.H. (ed), **in:** Landslides; Proceedings of the Sixth International Symposium, Balkema, Rotterdam, p1451-1456.

Metcalf, P. (1993), Landslide Investigation and Hazard Zonation of the Greymouth Urban Area. Unpublished M.Sc. Engineering Geology Thesis, University of Canterbury, Christchurch, New Zealand, 184pp.

Moody, K.E. (1985), Engineering Geology Assessment of Batter Stability Paerau Diversion Works, Maniototo, Central Otago, New Zealand. Unpublished M.Sc. Engineering Geology Thesis, University of Canterbury, Christchurch, New Zealand, 199pp.

Mortimer, N. (1993), Geology of the Otago Schist and adjacent rocks. Scale 1:500000. Institute of Geological & Nuclear Sciences geological map 7.1 sheet. Institute of Geological & Nuclear Sciences Ltd, Lower Hutt, New Zealand.

Mortimer, N. (1993), Jurassic tectonic history of the Otago Schist, New Zealand. Tectonics 12; 1: p237-244.

Mortimer, N. and Roser, B.P. (1992), Geochemical evidence for the position of the Caples – Torlesse boundary in the Otago Schist, New Zealand. Journal of the Geological Society, London 149: p967-977.

Norris R.J. and Bishop, D.G. (1990), Deformed conglomerates and textural zones in the Otago Schists, South Island, New Zealand. Tectonophysics 174: p331-349.

Norrish, N.I. and Wyllie, D.C. (1996), Rock Slope Stability Analysis, **in:** Landslides – Investigation and Mitigation. Transportation Research Board Special Report 247, National Academy Press, Washington, p391-425.

Park, J. (1906), The geology of the area covered by the Alexandra Sheet. New Zealand Geological Survey Bulletin, new series 2, Government Printer, Wellington.

Park, J. (1908), The geology of the Cromwell Subdivision. New Zealand Geological Survey Bulletin, new series 5, Government Printer, Wellington.

Park, J. (1909), The geology of the Queenstown Subdivision, New Zealand Geological Survey Bulletin new series 7, Government Printer, Wellington.

Priest, S.D. (1993), Discontinuity Analysis for Rock Engineering. Chapman & Hall, London, 473pp.

Riemer, W., Locher, T. and Nuncz, I. (1987), Mechanics of deep-seated mass movements in metamorphic rocks of the Ecuadorian Andes, Bonnard, C. (ed), **in:** Landslides – Glissements de Terrain, Proceedings of the Fifth International Symposium on Landslides, Lausanne, p307-310.

Romana, M. (1985b), New adjustment ratings for application of Bieniawski classification to slopes. International Symposium on the role of Rock Mechanics ISRM. Zacatecas, p49-53.

Romana, M. (1988), Practice of SMR Classification for slope appraisal, Bonnard, C. (ed), **in:** Landslides – Glissements de Terrain, Proceedings of the Fifth International Symposium on Landslides, Lausanne, p1227-1232.

Romana, M. (1991), SMR classification, Wittke, W. (ed), **in:** Proceedings; Seventh International Congress on Rock Mechanics 7: p955-960.

Rosen, M.R., Reeves, R.R., Stewart, M.K. and Taylor, C.B. (1997), Groundwater quality of the Wanaka and Wakatipu Basins, Central Otago, New Zealand. Institute of Geological and Nuclear Sciences Science Report 97/1, 98pp.

Salt, G. and Yetton, M.D. (1985a), An Engineering Geological Appraisal of the Proposed Subdivision of part Section 51, Block XXI, Shotover Survey District, Lake County. Unpublished Report to Ralph Moir & Associates dated 11 March, 1985: 10pp + 1 fig.

Salt, G. and Yetton, M.D. (1985b), An Engineering Geological Appraisal of Stage II of the Proposed Subdivision of part Section 51, Block XXI, Shotover Survey District, Lake County. Unpublished Report to Ralph Moir & Associates dated 29 May 1985: 13pp.

Salt, G. and Yetton, M.D. (1985c), An Engineering Geological Appraisal of Stage II of the Proposed Subdivision of part Section 50, Block XX, Shotover Survey District, Lake County. Unpublished Report to Ralph Moir & Associates dated 4 August 1985: 12pp.

Salt, G. and Yetton, M.D. (1985d), A Preliminary Engineering Geological Report of part Section 17 and the northern half of part Section 15, Block XXI, Shotover Survey District, Lake County. Unpublished Report to Ralph Moir & Associates dated 7 August 1985: 9pp.

Salt, G. and Yetton, M.D. (1986), A Preliminary Engineering Geological Appraisal of the Proposed Subdivision of part Section 19, Block XXI, Shotover Survey District, Lake County. Unpublished Consultant Report to Royds Garden Ltd, Invercargill, dated 5 March, 1986: 8pp + 2 figs.

Smith, W.D. and Berryman, K.R. (1986), Earthquake hazard in New Zealand: inferences from seismology and geology. Bulletin of the Royal Society of New Zealand 24: p223-243.

Suggate, R.P. (1965a), The tempo of events in New Zealand geological history. New Zealand Journal of Geology and Geophysics 8: p1139-1148.

Suggate, R.P. (1965b), Late Pleistocene geology of the northern part of the South Island, New Zealand. New Zealand Geological Survey Bulletin 77. Government Printer, Wellington.

Suggate, R.P. (1990), Late Pliocene and Quaternary glaciations of New Zealand, Quaternary Science Reviews 9: p175-197, Pergamon Press, Oxford.

Thomson, R. (1994), Resta Road Slide: a re-evaluation of an area of hummocky terrain in the Gibbston Basin, Central Otago. Institute Geology and Nuclear Sciences science report 94/33: 29pp + 5 figs

Turnbull, I.M. (1979), Stratigraphy and sedimentology of the Caples Terrane of the Thomson Mountains, Northern Southland, New Zealand. New Zealand Journal of Geology and Geophysics 22; 5: p555-574.

Turnbull, I.M. (1981), Contortions in the schists of the Cromwell District, Central Otago, New Zealand. New Zealand Journal of Geology and Geophysics 24; 1: p65-86.

Turnbull, I.M. and Forsyth, P.J. (1988), Queenstown: a geological guide. Geological Society of New Zealand Guidebook No. 9, Geological Society of New Zealand, Lower Hutt, Wellington, 48pp.

Turnbull, I.M., Barry J.M., Carter R.M. and Norris R.J. (1975), The Bob's Cove Beds and their Relationship to the Moonlight Fault Zone. Journal of the Royal Society of New Zealand: 5; 4: p355-394.

Turnbull, I.M., Craw, D. and Norris, R.J. (1993), Pre-Miocene and post-Miocene deformation in the Bannockburn Basin, Central Otago, New Zealand. New Zealand Journal of Geology and Geophysics, 36; 1: p107-115.

Varnes, D.J. (1978), Slope movement types and processes, Schuster, R.L and Krizek, R.J. (eds), **in:** Special Report 176: Landslides: Analysis and Control, Transportation Research Board, National Research Council, Washington, D.C., p11-33.

Watts, C.R. (1988), Engineering geology roading investigations of the Wakatipu Basin. Unpublished M.Sc. Engineering Geology Thesis, University of Canterbury, Christchurch, New Zealand, 275pp.

Wood, B. L. (1962), Sheet 22 Wakatipu (listed) Geological Map of New Zealand, 1:250,000. Department of Scientific and Industrial Research, Wellington, New Zealand.

Wood, B.L. (1963), Structure of the Otago Schists. New Zealand Journal of Geology and Geophysics 6; 5: p641-680.

Wood, B.L. (1978), The Otago Schist megaculmination: its possible origins and tectonic significance in the Rangitata Orogen of New Zealand. Tectonophysics 47: p339-368.

Wyllie, D.C. and Norrish, N.I. (1996), Rock Strength Properties and their Measurement, **in:** Landslides – Investigation and Mitigation. Transportation Research Board Special Report 247, National Academy Press, Washington, p372-390.

Yetton, M.D. (1988), An engineering geological appraisal of the proposed subdivision of part sections 16, 29, and 35 (Nicols Block), Block XXI, Shotover Survay District, Lake County, Queenstown. Unpublished Consultant Report to Royds Garden Ltd, Invercargill, dated 28 April, 1988: 13pp + 2 figs.

APPENDICES.

APPENDIX A: ROCK AND SOIL CLASSIFICATION.

ENGINEERING GEOLOGICAL FIELD DESCRIPTION FOR ROCK MATERIAL

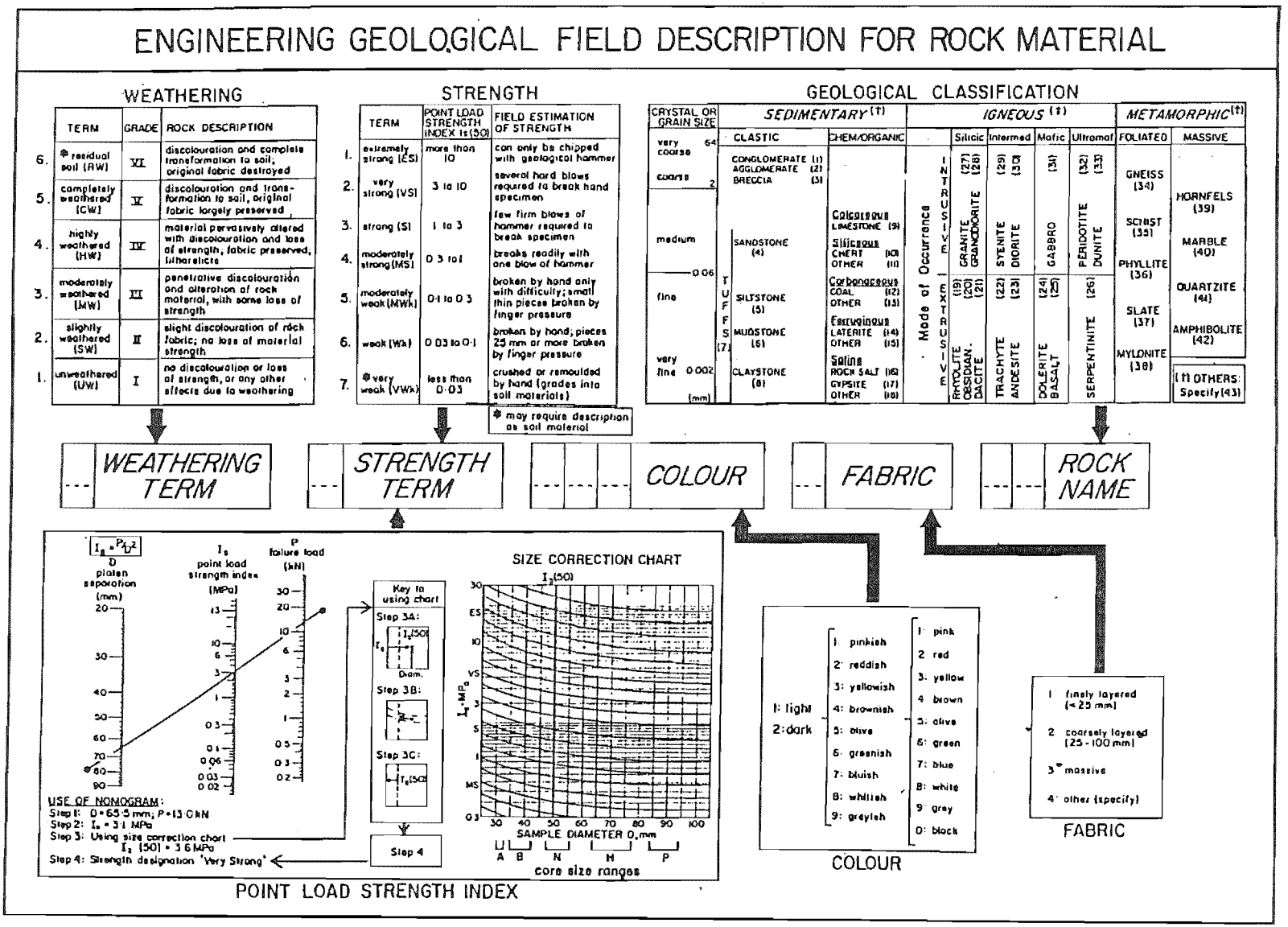

ENGINEERING GEOLOGICAL FIELD DESCRIPTION FOR ROCK MASS

FIELD SKETCH OR ANNOTATED PHOTOGRAPH

SCALE: ORIGINAL SCALE: 1: SKETCH ORIENTATION

GENERAL INFORMATION

PROJECT/AREA
LOCALITY:
REFERENCE MAP:
COORDINATES:
ELEVATION:
GEOLOGY BY:
DATE:
CHECKED:
Sheet No.: of

SHEET REFERENCE

ADDITIONAL DATA

GRAPHIC SYMBOL	ROCK UNIT No.	ROCK MATERIAL DESCRIPTION				
		WEATHERING	STRENGTH	COLOUR	FABRIC	ROCK NAME
	1					
	2					
	3					
	4					
	5					
	6					
		OTHER MATERIAL DESCRIPTIONS: (specify)				
	7					
	8					
	9					

TERMINOLOGY FOR COMMON DEFECTS IN ROCK MASS

DEFECT TYPE	LAYERING (1)			FRACTURES AND FRACTURE ZONES (1)		WEAK SEAMS OR ZONES (1)		
	BEDDING (1)	FOLIATION (2)	CLEAVAGE (3)	JOINT/FAULT (4)	SHEARED ZONE (5)	CRUSHED (6)	DECOMPOSED (7)	INFILLED (8)
DESCRIPTION	1) Arrangement in layers of mineral grains or crystals of similar size or composition 2) Arrangement of elongated or platy minerals, later parallel to one another and/or to the layers.	Usually fractures perpendicular which rocks may have formed (strength), parallel, curved, or irregular, open, closed or sometimes surface rough, smooth, or slickensided.		Zone of thickness greater than (> 100 mm) fracturing between, with roughly parallel planar boundaries, blocks of intact material within zone typically less weak or wedge shaped, fractures closely, open, usually cemented or not cemented		Zone with roughly parallel planar boundaries.- 1) Composed of fragmented, usually angular, rock fragments of non-cohesive size in a soil matrix. 2) Some weathering of fragments possible, with some either cohesive or non-cohesive 3) Lower shear strength parallel to zone boundaries, which are commonly slickensided	Zone of any shape, but commonly with roughly parallel planar boundaries:- 1) Various zone rock mechanically or completely weathered 2) All intermediate grades into fresher rock	1) Composed of soil thicknesses which may show layering roughly parallel to zone boundaries 2) Rock fabric not present in infill zone. NOTE: thicknesses forming zone require separate description as soil or rock
MAP SYMBOLS with strike and dip	075/75	80/064	37/246	027/86	045/043	Record width of zone as measured	76/072	064/20
								(1) OTHERS: Specify (9)

DEFECT DATA SUMMARY TABLE

ROCK UNIT No.	DEFECT SET No.	DEFECT TYPE	DEFECT SPACING	DEFECT PERSISTENCE	AV. UNIT BLOCK SIZE	DEFECT ORIENTATION: DIP DIRECTION	DEFECT ORIENTATION: DIP/VALUE	GROUND-WATER	REMARKS

DEFECT ORIENTATION DIAGRAM

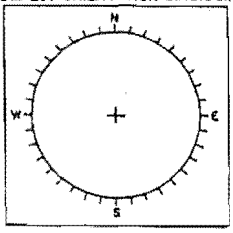

DEFECT SPACING

	TERM	SPACING (mm)
1	extremely wide	> 2000
2	very wide	600 — 2000
3	wide	200 — 600
4	moderate	100 — 200
5	close	25 — 100
6	very close	5 — 25
7	extremely close	< 5

DEFECT PERSISTENCE

	TERM	LENGTH (m)
1	very high	> 10
2	high	5 — 10
3	moderate	2 — 5
4	low	0.5 — 2
5	very low	< 0.5

AVERAGE UNIT BLOCK SIZE

	TERM	EQUIVALENT CUBE SIDE	APPROX. BLOCK VOLUME (m^3)
1	very large	1000 mm	> 1.0
2	large	500 mm	0.1 — 1.0
3	medium	100 mm	0.001 — 0.1
4	small	10 mm	< 0.001
5	very small		

GROUNDWATER

	TERM	FLOW RATE
1	dry	
2	seepage	< 1 ml s^{-1}
3	very low flow	1 — 10 ml s^{-1}
4	low flow	10 — 100 ml s^{-1}
5	moderate flow	0.1 — 1 l s^{-1}
6	large flow	1 — 10 l s^{-1}
7	very large flow	> 10 l s^{-1}

ENGINEERING GEOLOGICAL FIELD DESCRIPTION FOR SOIL MATERIAL

WEATHERING

	TERM	GRADE	SOIL DESCRIPTION
5	Completely Weathered (CW)	VI	completely discoloured and altered; no trace of original fabric
4	Highly Weathered (HW)	IV	mostly altered and weakened, little trace of original fabric
3	Moderately Weathered (MW)	III	large discoloured portions of original soil separated by more altered material, significantly weakened
2	Slightly Weathered (SW)	II	minor discolouration of some parts of the original soil, no loss of strength
1	Unweathered (UW)	I	original soil with no discolouration, loss of strength or other effects due to weathering
0	NOTE * in coarse-grained soils record weathering grade of DOMINANT fraction here and qualify weathering grade of subordinate and/or minor fractions if appropriate		

STRENGTH

	TERM	FIELD CRITERIA
1	loose	can be removed from exposure in disaggregated form by hand
2	compact	only removed from exposure by implement; material readily disaggregated by physical means
3	+ cemented	only removed from exposure by implement, material does not disaggregate
4	hard	may be removed from exposure with difficulty by implement or hand, softened on immersion in water and may be remoulded
5	stiff	indented by thumb pressure, but not moulded by fingers; softened on immersion in water, and may be remoulded
6	firm	moulded or indented only by strong finger pressure, easily moulded after immersion in water
7	soft	easily indented or moulded by finger pressure
8	very soft	exudes between fingers when squeezed
9	spongy	readily compressed by finger pressure, but cannot be remoulded

+ may require description of rock material

UNIFIED SOIL CLASSIFICATION SYSTEM

			FIELD IDENTIFICATION	GROUP SYMBOL	TYPICAL NAMES
COARSE-GRAINED SOILS	GRAVELS (more than 50% larger than 2mm)	clean gravels	wide range in grain size and substantial amounts of all interm. sizes	GW	well graded GRAVELS
			predom. one size or a range of sizes with some interm. sizes missing	GP	poorly graded GRAVELS
		gravels with fines	non-plastic fines (see ML below)	GM	poorly graded SILTY-GRAVELS
			plastic fines (see CL below)	GC	poorly graded CLAYEY-GRAVELS
	SANDS (more than 50% smaller than 2mm)	clean sands	wide range in grain sizes and substantial amounts of all interm. sizes	SW	well graded SANDS
			predom. one size or a range of sizes with some interm. sizes missing	SP	poorly graded SANDS
		sands with fines	non-plastic fines (see ML below)	SM	poorly graded SILTY-SANDS
			plastic fines (see CL below)	SC	poorly graded CLAYEY-SANDS

			SHINE	DILATANCY (1)	TOUGHNESS (1)		
FINE-GRAINED SOIL	SILTS AND CLAYS	LIQUID LIMIT < 50	none to very dull	quick to slow	none	ML	INORGANIC SILTS with slight plasticity
			moderate	none to very slow	medium	CL	INORGANIC CLAYS of low to medium plasticity
			none to very dull	slow	slight	OL	ORGANIC SILTS & CLAYS of low plasticity
		LIQUID LIMIT > 50	dull	slow to none	slight to medium	MH	INORGANIC SILTS of high plasticity
			very glossy	none	high	CH	INORGANIC CLAYS of high plasticity
			moderate to v glossy	none to very slow	slight to medium	OH	ORGANIC CLAYS of medium to high plasticity
HIGHLY ORGANIC SOILS			identified by colour, odour, spongy feel and fibrous texture			PI	PEAT and other highly organic soils

PROCEDURES FOR FINE-GRAINED SOILS OR FRACTIONS (1)

DILATANCY (reaction to shaking) -

1) Prepare pat of moist soil, adding water to make soft - but not sticky.

2) Place pat in palm of hand, shake horizontally by striking vigorously against other hand.

Positive Reaction: appearance of water on surface of pat, which becomes glossy. When squeezed between fingers, water and gloss disappear, pat stiffens and may crumble

TOUGHNESS: (consistency near plastic limit) -

1) Mould sample to consistency of putty, adding water or air drying as required

2) Roll to thin (3mm) thread, fold and reroll repeatedly until thread crumbles at plastic limit

3) Knead together and continue until lump crumbles

Dilatancy: a tough thread and stiff lump indicate high plasticity; a weak thread and lump low plasticity clays

GROUP SYMBOL CODINGS FOR USCS

COLUMN 1		COLUMN 2	
G:1	C:4	W:1	C:4
S:2	O:5	P:2	L:5
M:3	Pt:6	M:3	H:6

BOUNDARY CLASSIFICATIONS specify, enter 0.0

WEATHERING TERM | WATER CONTENT TERM | STRENGTH TERM | COLOUR | FABRIC | SOIL NAME | USCS SYMBOL

	TERM	FIELD CRITERIA
1	Dry	looks and feels dry; fine-grained soils usually hard, powdery or friable; coarse-grained soils may run freely through hands
2	Moist	soil feels cool and may be darkened in colour; particles tend to adhere in coarse-grained materials, fine-grained soils may be softened
3	Wet	soils feel cold and are darkened in colour; free water forms on hands when sample is disturbed
4	Saturated	restricted to wet soils below the water table or the static water level in excavations or drill holes

WATER CONTENT

1: light	1 pinkish	1 pink
2: dark	2 reddish	2 red
	3 yellowish	3 yellow
	4 brownish	4 brown
	5 olive	5 olive
	6 greenish	6 green
	7 bluish	7 blue
	8 whitish	8 white
	9 greyish	9 grey
		0 black

COLOUR

1: finely layered (< 2.5 mm)
2: coarsely layered (2.5 - 100 mm)
3: massive
4: other (specify)

FABRIC

*SUBORDINATE FRACTION 20-50% volume visual estimate

DOMINANT FRACTION >50% volume visual estimate

*MINOR FRACTION < 20% volume visual estimate

1	coarse gravelly
2	medium gravelly
3	fine gravelly
4	coarse sandy
5	medium sandy
6	fine sandy
7	silty
8	clayey
9	peaty

	SOIL TYPE TERM		PARTICLE SIZE (mm)	GRAPHIC LOG
1	coarse	gravel	> 60	
2	medium	gravel	20-60	
3	fine	gravel	2-20	
4	coarse	sand	0.6-2.0	
5	medium	sand	0.2-0.6	
6	fine	sand	0.06-0.2	
7	silt		0.002-0.06	
8	clay		< 0.002	
9	peat		NA	

PARTICLE SIZE

WITHSOME

1	coarse gravel
2	medium gravel
3	fine gravel
4	coarse sand
5	medium sand
6	fine sand
7	silt
8	clay
9	peat

APPENDIX B: MODIFIED MERCALLI SCALE.

Intensity	Description of characteristic effects	Maximum acceleration of the ground	Magnitude corresponding to highest intensity reached
MM I	Instrumental: detected only by seismographs	10	
MM II	Feeble: noticed only by some people	25	3.5
MM III	Slight: like the vibrations of a passing lorry; felt only by people at rest, especially on upper floors.	50	4.2
MM IV	Moderate: felt by people while walking; rocking of loose objects, including standing vehicles.	100	4.3
MM V	Rather strong: felt generally; most sleepers are awakened and bells ring.	250	- 4.8
MM VI	Strong: trees sway and all suspended objects swing; damage by overturning and falling of loose objects.	500	4.9 - 5.4
MM VII	Very strong: general alarm; walls crack; plaster falls.	1000	5.5 - 6.1
MM VIII	Destructive: car drivers seriously disturbed; masonry fissured; chimneys fall; poorly constructed buildings damaged.	2500	6.2 -
MM IX	Ruinous: some houses collapse where ground begins to crack, and pipes break open.	5000	6.9
MM X	Disastrous: ground cracks badly; many buildings destroyed and railway lines bent; landslides on steep slopes.	7500	7.0 - 7.3
MM XI	Very disastrous: few buildings remain standing; all services out of action; great landslides and floods.	9800	7.4 - 8.1
MM XII	Catastrophic: total destruction; objects thrown into air; ground rises and falls in waves.		>8.1 (maximum known 8.9)

The Modified Mercalli Scale of earthquake intensity.

APPENDIX C: CLIMATE DATA FOR THE QUEENSTOWN REGION.

Sourced from: National Institute of Water and Atmospheric Research, 1998

Queenstown Rainfall (mm) 1983-1998				
Month	Total Rainfall (mm)	Rain Days (no. of days with 0.1mm or more of rain)	Wet Days (No. of days with 1mm or more of rain)	Rainfall - 9am to 9am local time (mm)
Jan	65.8	10.1	7.3	22.6
Feb	55.0	7.9	5.6	21.9
Mar	65.0	11.7	8.3	18.8
Apr	65.7	11.3	8.5	19.1
May	69.3	12.8	8.3	21.8
Jun	74.3	13.4	8.9	25.1
Jul	60.3	12.4	7.4	20.6
Aug	72.9	12.1	9.7	26.8
Sep	47.3	10.5	6.8	16.7
Oct	67.7	12.1	7.9	26.9
Nov	65.1	11.8	8.8	19.1
Dec	81.5	13.0	10.0	25.6

Queenstown Wind Speed - 1991-1998					
Month	Mean Wind Speed (m/s)	Wind Gusts - Highest Speed (m/s)	Days of Wind Gusts >= 24 knots (day)	Days of Wind Gusts >= 33 knots (day)	Days of Wind Gusts >= 51 knots (day)
Jan	3.8	23.5	15.4	4.4	0.2
Feb	3.5	20.6	11.2	2.2	0
Mar	3.4	20.8	13.7	3.4	0
Apr	3	20.6	10.8	2.2	0
May	2.9	18.8	8.9	2.1	0
Jun	2.7	20	6	1.5	0
Jul	2.7	17.1	6.9	1	0
Aug	2.8	19.8	9.8	1.8	0
Sep	3.2	20.6	10.5	1.5	0.2
Oct	3.5	22.4	15	3.5	0
Nov	3.7	19.4	17.6	2.8	0
Dec	3.7	21.2	16.3	4.3	0.2

Month	Days of Occurrence: Screen Frost (day) 1991-1998	Days of Occurrence: Ground Frost (day) 1929-1996	Days of Occurrence: Screen Frost (day) 1969-1992	Days of Occurrence: Thunder (day) 1971-1992	Days of Occurrence: Gale (day) 1969-1992	Days of Occurrence: Fog (day) 1969-1992	Days of Occurrence: Hail (day) 1969-1992	Days of Occurrence: Lightning (day) 1972-1992	Days of Occurrence: Snow (day) 1969-1992
Jan	0.0	1.0	0.0	0.4	0.2	0.4	0	0.5	0
Feb	0.0	0.9	0.0	0.2	0.2	0.3	0	0.1	0
Mar	0.0	2.9	0.3	0.0	0.1	0.3	0.1	0	0.1
Apr	2.4	7.8	2.5	0.2	0.3	0.5	0.1	0.2	0.2
May	8.6	16.5	10.4	0.1	0.1	0.5	0	0	0.9
Jun	15.8	22.5	19.0	0.0	0.3	0.5	0	0	1.7
Jul	20.9	25.5	20.7	0.1	0.3	0.3	0.1	0	1.6
Aug	15.7	22.7	17.2	0.3	0.1	0.1	0.1	0.3	1.5
Sep	8.5	16.6	6.3	0.1	0.1	0.0	0	0.1	0.8
Oct	1.8	10.5	1.7	0.1	0.2	0.2	0	0.2	0.5
Nov	0.8	5.3	0.4	0.0	0.1	0.2	0	0.1	0.1
Dec	0.0	1.7	0.0	0.7	0.2	0.2	0	0.6	0.1

Queenstown Rainfall (mm) 1967-1994

Month	Maximum 10-minute Rainfall (mm)	Maximum 20-minute Rainfall (mm)	Maximum 30-minute Rainfall (mm)	Maximum 1-hour Rainfall (mm)	Maximum 2-hour Rainfall (mm)	Maximum 6-hour Rainfall (mm)	Maximum 12-hour Rainfall (mm)	Maximum 24-hour Rainfall (mm)	Maximum 48-hour Rainfall (mm)	Maximum 72-hour Rainfall (mm)
Jan	2.0	3.5	4.6	7.4	10.8	19.4	26.3	32.1	35.2	37.8
Feb	1.8	3.0	4.1	6.4	9.4	14.6	18.5	21.4	26.1	28.3
Mar	1.7	2.9	3.9	6.4	10.3	20.5	27.4	34.7	40.2	43.2
Apr	1.7	2.8	3.9	6.6	10.1	17.1	21.3	25.5	31.5	34.3
May	1.7	2.9	4.0	6.5	10.4	18.9	23.0	27.9	31.6	37.1
Jun	1.6	2.7	3.7	6.2	10	18.5	23.8	28.7	34.7	37.8
Jul	1.9	3.0	3.9	6.1	9.4	15.0	20.1	24.1	27.9	30.5
Aug	1.6	2.6	3.6	5.8	8.7	16.2	20.5	24.4	29.1	31.4
Sep	1.5	2.5	3.5	5.7	9.2	17.2	22.9	27.5	30.4	33.2
Oct	1.7	2.9	4.0	6.4	10.2	20.1	27.1	34.0	41.8	45.3
Nov	1.5	2.6	3.5	5.5	8.7	14.5	17.9	20.9	25.1	27.7
Dec	1.7	2.7	3.7	6.0	9.8	18.8	24.2	30.0	36.0	40.3

Month	Total Sunshine (Hours) 1930-1996
Jan	235.4
Feb	201.8
Mar	184.3
Apr	134.2
May	91.7
Jun	74
Jul	86.7
Aug	120.7
Sep	159.3
Oct	193
Nov	211.1
Dec	233.2

Month	Mean Vapour Pressure (hPa) 1979-1998	Mean Vapour Pressure (hPa) 1941-1996	Mean Vapour Pressure (hPa) 1971-1996
Jan	11	11.5	10.9
Feb	11.1	11.6	10.8
Mar	10	10.6	10.3
Apr	8.5	8.9	8.6
May	7.1	7.2	6.8
Jun	6	6	5.8
Jul	5.6	5.7	5.6
Aug	6.2	6.1	6.1
Sep	7.1	7.2	7
Oct	8	8.4	8
Nov	8.5	9.4	8.6
Dec	10.2	10.7	10

Month	Mean MSL Pressure at 9am (hPa) 1979-1998	Mean MSL Pressure at 9am (hPa) 1971-1996
Jan	1011.9	1011.5
Feb	1013.6	1014.1
Mar	1015.1	1015.4
Apr	1017.5	1016.4
May	1016.7	1015.3
Jun	1015.3	1015.4
Jul	1015.2	1013.7
Aug	1014.7	1013.4
Sep	1011.8	1011.7
Oct	1011.0	1010.5
Nov	1009.6	1010.9
Dec	1010.6	1009.3

Month	Mean Daily Grass Minimum Temperature (Celsius) 1930-1996	Extreme Grass Minimum Temperature (Celsius) 1930-1996	Mean Daily Grass Minimum Temperature (Celsius) 1984-1992	Extreme Grass Minimum Temperature (Celsius) 1984-1992
Jan	6.2	-0.3	7.3	0.4
Feb	6	-0.6	6.1	-0.9
Mar	4.4	-2	4.3	-3.3
Apr	1.9	-3.8	1.2	-4.5
May	-1	-6.4	-1.4	-7.1
Jun	-3.2	-8.1	-3.4	-8.4
Jul	-4	-8.7	-3.5	-8.2
Aug	-2.9	-7.5	-2.2	-7.4
Sep	-1.1	-6.2	-1	-6.3
Oct	0.9	-4.7	1	-4.9
Nov	2.8	-3.3	3.2	-4
Dec	5.1	-1.2	6.2	-0.6

Queenstown Rainfall - 1972-1992				
Month	Total Rainfall (mm)	Rain Days - No. of days with 0.1mm or more of rain (day)	Wet Days - No. of days with 1mm or more of rain (day)	Maximum 1-day rainfall - 9am to 9am (mm)
Jan	60.6	10.8	8	22.1
Feb	44	7.6	6	16.5
Mar	68.4	9.3	7.6	25.9
Apr	56.6	10.3	8	19.3
May	66.6	11.6	8.5	22.9
Jun	61	10.2	7.5	23.4
Jul	54.7	11	8.2	16.8
Aug	55.6	9.7	7.2	17.7
Sep	59.8	10.1	7.5	18
Oct	73.3	11.6	9	27.2
Nov	44.1	9.6	7	14.6
Dec	60.2	10.9	8.2	18.1

Queenstown Rainfall - 1977-1992										
Month	Maximum 10-minute rainfall (mm)	Maximum 20-minute rainfall (mm)	Maximum 30-minute rainfall (mm)	Maximum 1-hour rainfall (mm)	Maximum 2-hour rainfall (mm)	Maximum 6-hour rainfall (mm)	Maximum 12-hour rainfall (mm)	Maximum 24-hour rainfall (mm)	Maximum 48-hour rainfall (mm)	Maximum 72-hour rainfall (mm)
Jan	1.7	2.9	4	7	11.3	20.1	26.3	30.1	34.4	37.5
Feb	2.7	4.3	5.4	7.3	10.6	16	18.6	20.3	23	24.9
Mar	1.4	2.4	3.3	5.5	8.9	17.7	23.2	27.3	32	35
Apr	2	3.2	4.3	6.9	10.1	15	18.1	22	27	29.8
May	1.6	2.6	3.5	5.6	9	16.6	21.5	26.8	28.4	33.8
Jun	1.5	2.5	3.4	5.6	8.7	17.1	22	25.8	28.7	32.7
Jul	1.4	2.3	3.1	4.6	7	12.1	16.1	20.4	23.9	25.8
Aug	1.7	2.8	3.9	6.4	9	14.2	17.5	23.2	25.7	28.4
Sep	1.4	2.4	3.3	5.2	8.3	14	18.1	19.5	21.3	23.4
Oct	1.8	3	4	6.7	10.7	19.3	25.2	31.7	37.6	41.1
Nov	1.5	2.3	3	4.8	7.3	12.9	15.6	17.9	20.3	22.9
Dec	1.9	3	4	5.9	8.8	14.3	19.2	22	25.7	30

Queenstown Mean Temperature - 1991-1998

Month	Extreme Maximum Air Temperature (Celsius)	Mean Daily Maximum Air Temperature (Celsius)	Lowest Maximum Air Temperature (Celsius)	Highest Daily Mean Temperature (Celsius)	Mean Air Temperature (Celsius)	Lowest Daily Mean Temperature (Celsius)	Highest Minimum Air Temperature (Celsius)	Mean Daily Minimum Air Temperature (Celsius)	Extreme Minimum Air Temperature (Celsius)
Jan	27.5	21.4	13.1	20.2	15.6	10.1	16.1	9.9	3.1
Feb	27.5	21.3	12.9	20.4	15.4	10.2	14.9	9.5	3.1
Mar	24.7	17.7	10.7	17.4	12.1	7.7	12.4	6.5	1.4
Apr	20.3	14.5	8.6	15.0	9.4	4.8	10.3	4.2	-1.2
May	17.7	11.4	6.5	11.8	6.8	2.8	8.4	2.2	-2.8
Jun	13.3	8.1	2.9	8.5	4.0	-0.2	5.8	0.0	-4.5
Jul	13.0	7.4	2.6	7.3	2.9	-1.7	5.0	-1.6	-6.6
Aug	14.9	9.3	4.4	9.1	4.6	1.1	5.4	0.0	-4.2
Sep	17.3	11.9	6.0	11.4	6.9	2.7	7.8	2.0	-2.8
Oct	22.1	15.3	7.6	14.6	9.8	4.7	9.6	4.4	-1.3
Nov	22.5	16.4	9.5	15.9	11.1	6.4	11.3	5.8	-0.6
Dec	26.3	19.4	11.2	18.8	13.7	8.1	13.8	8.0	2.1

Queenstown Rainfall (mm) - 1983-1998

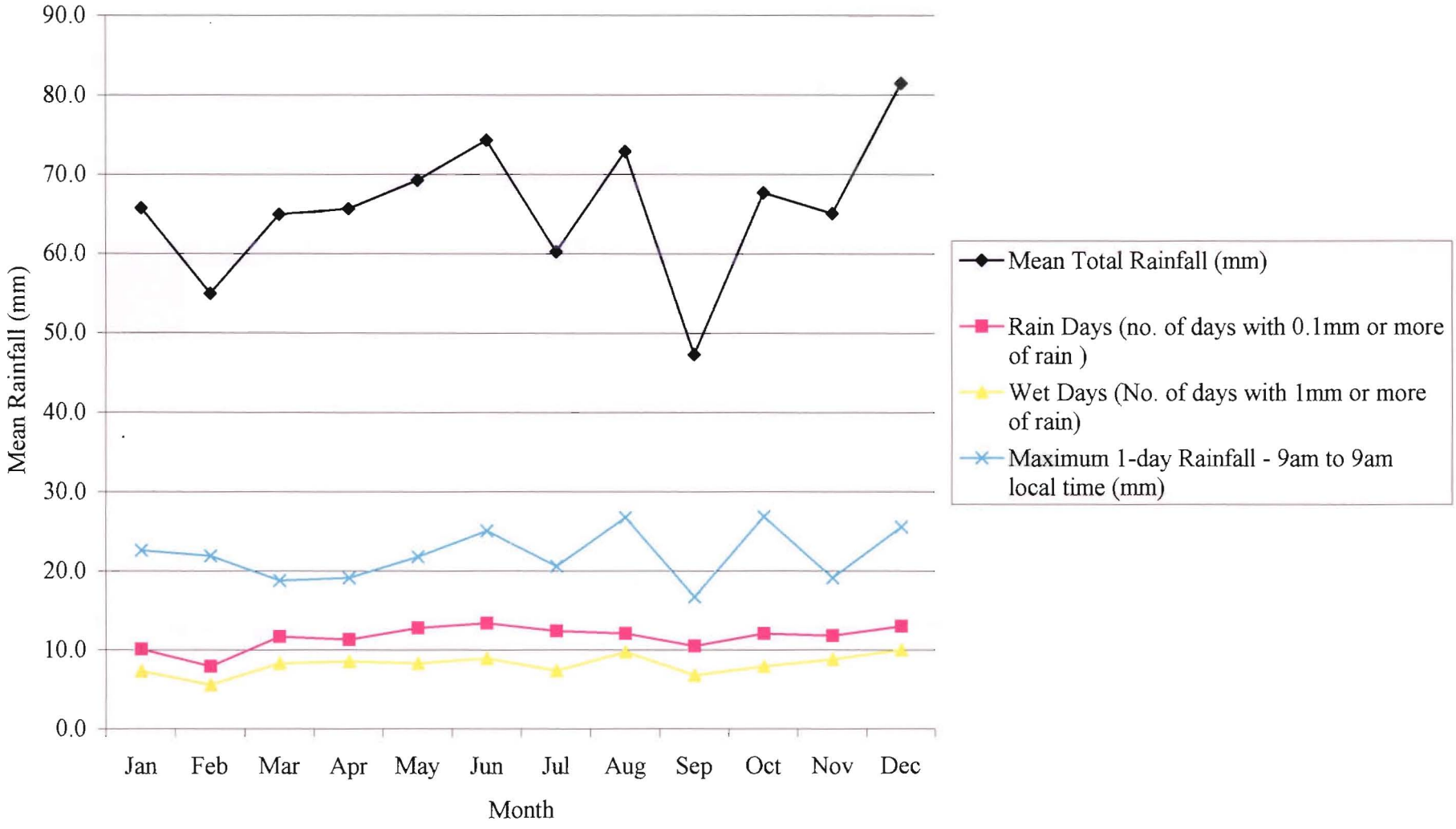

Mean Wind Speed and Highest Speed Wind Gust (1991-1998)

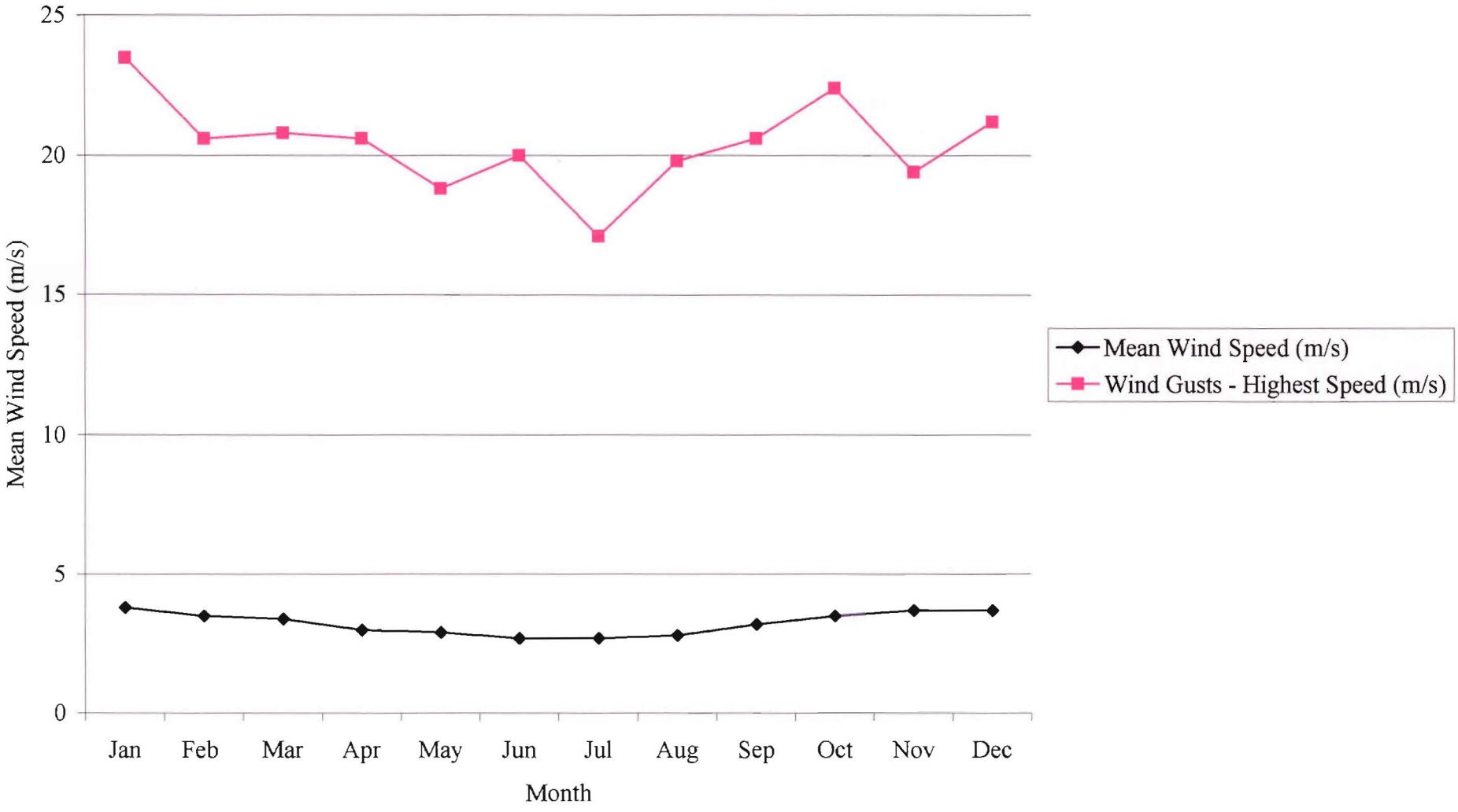

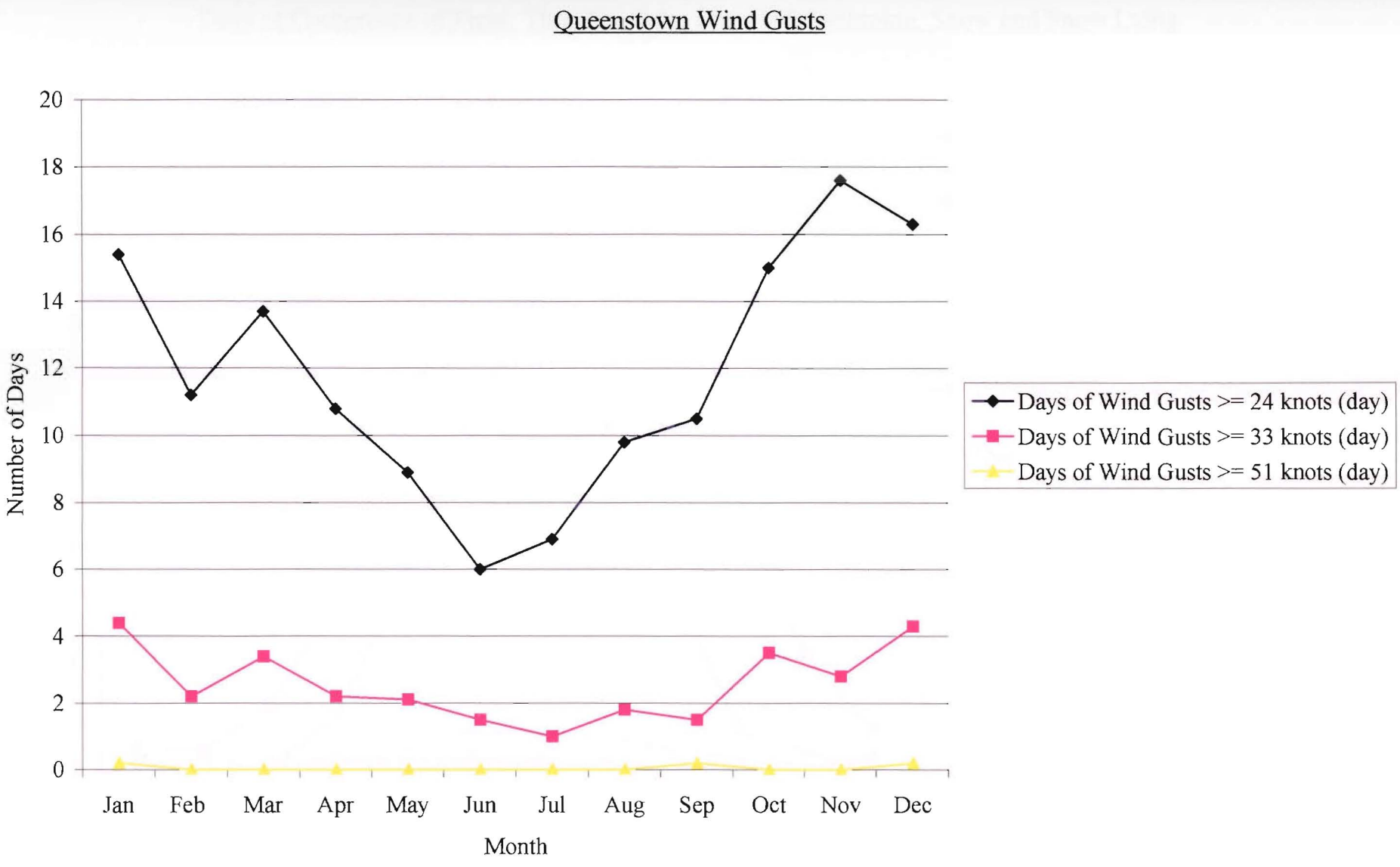
Queenstown Wind Gusts
Number of Days
20
18
16
14
12
10
8
6
4
2
0
Jan
Feb
Mar
Apr
May
Jun
Jul
Aug
Sep
Oct
Nov
Dec
Month
Days of Wind Gusts >= 24 knots (day)
Days of Wind Gusts >= 33 knots (day)
Days of Wind Gusts >= 51 knots (day)

Days of Occurrence of Frost, Thunder, Gale, Fog, Hail, Lightning, Snow and Snow Lying

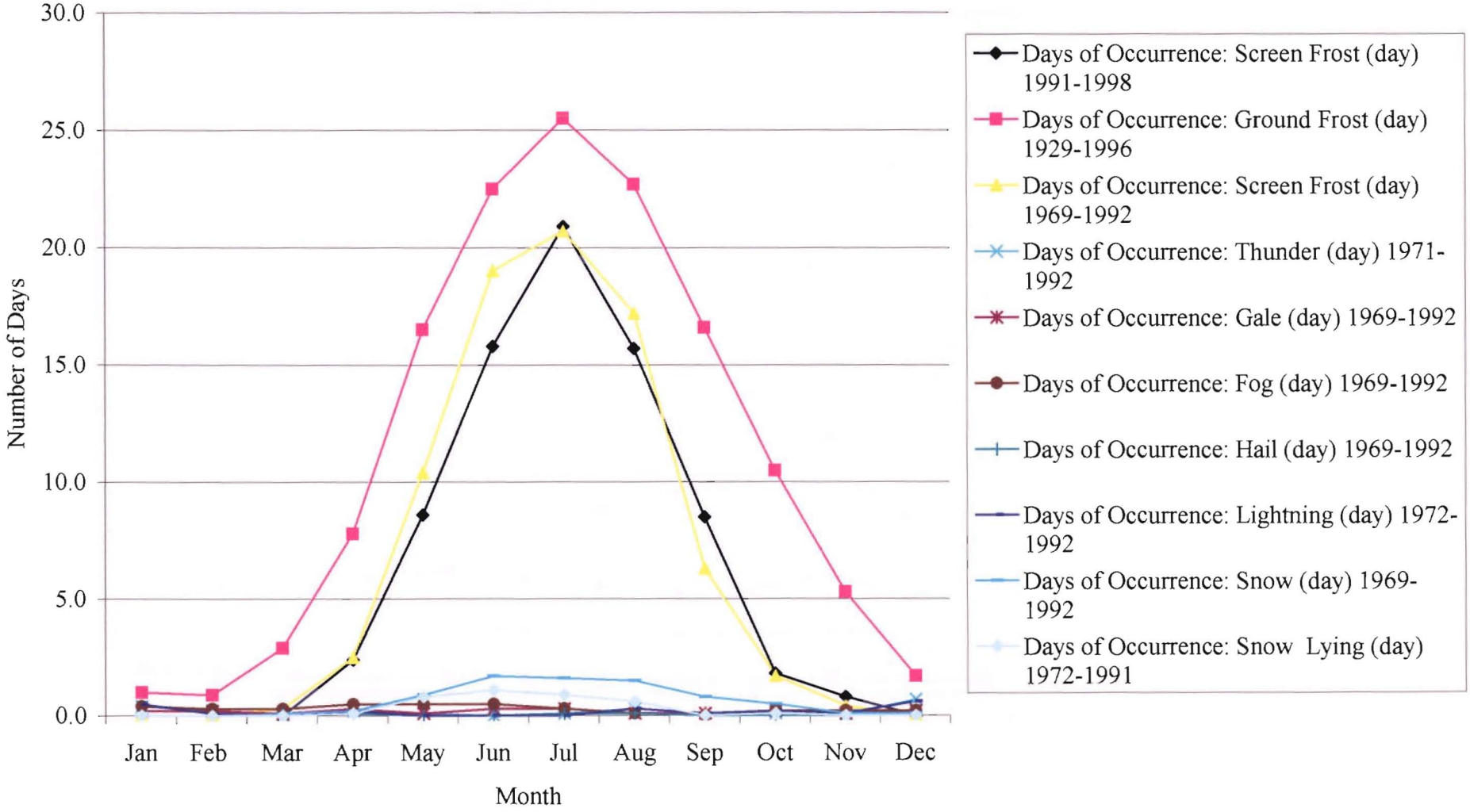

Queenstown Rainfall (1967-1994)

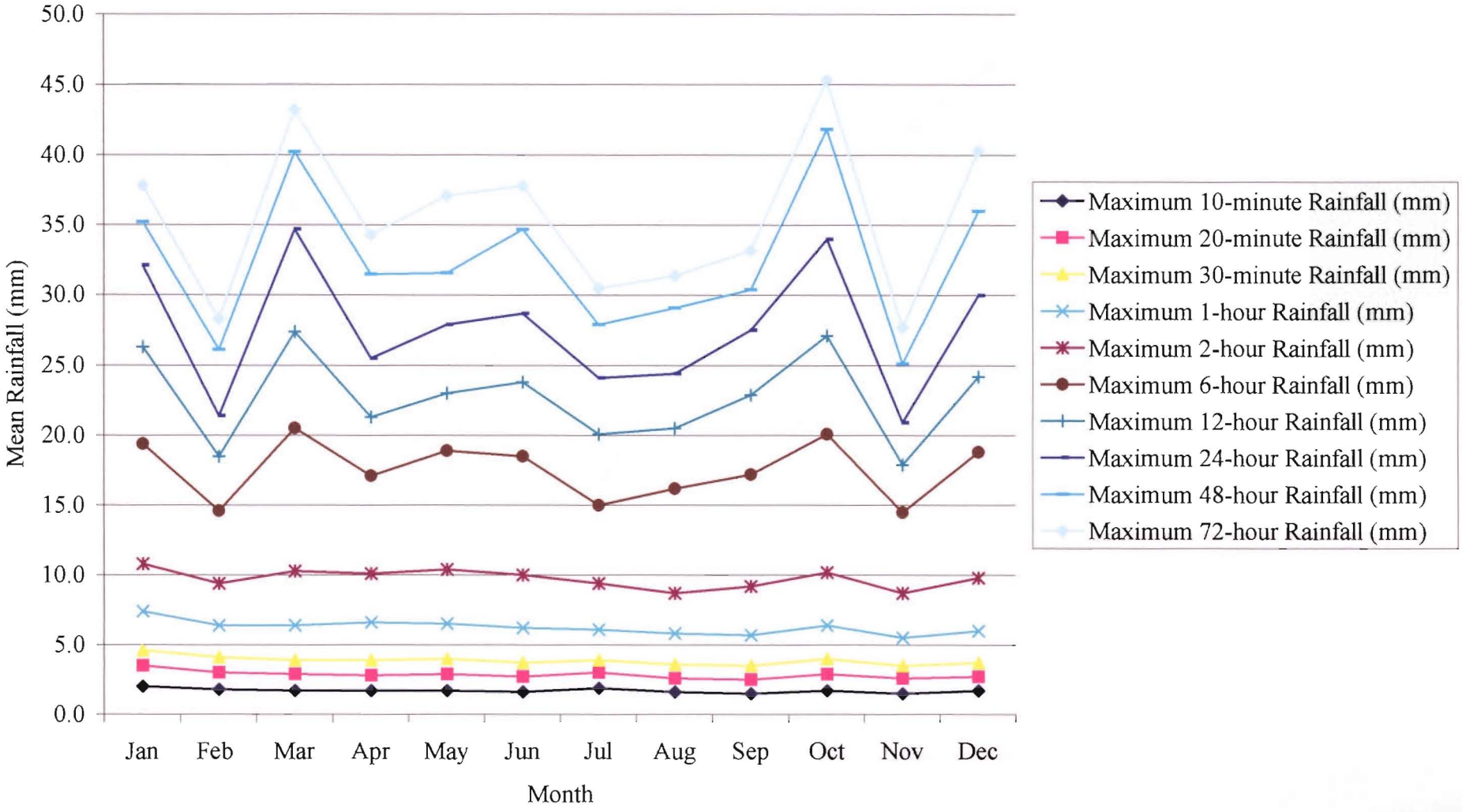

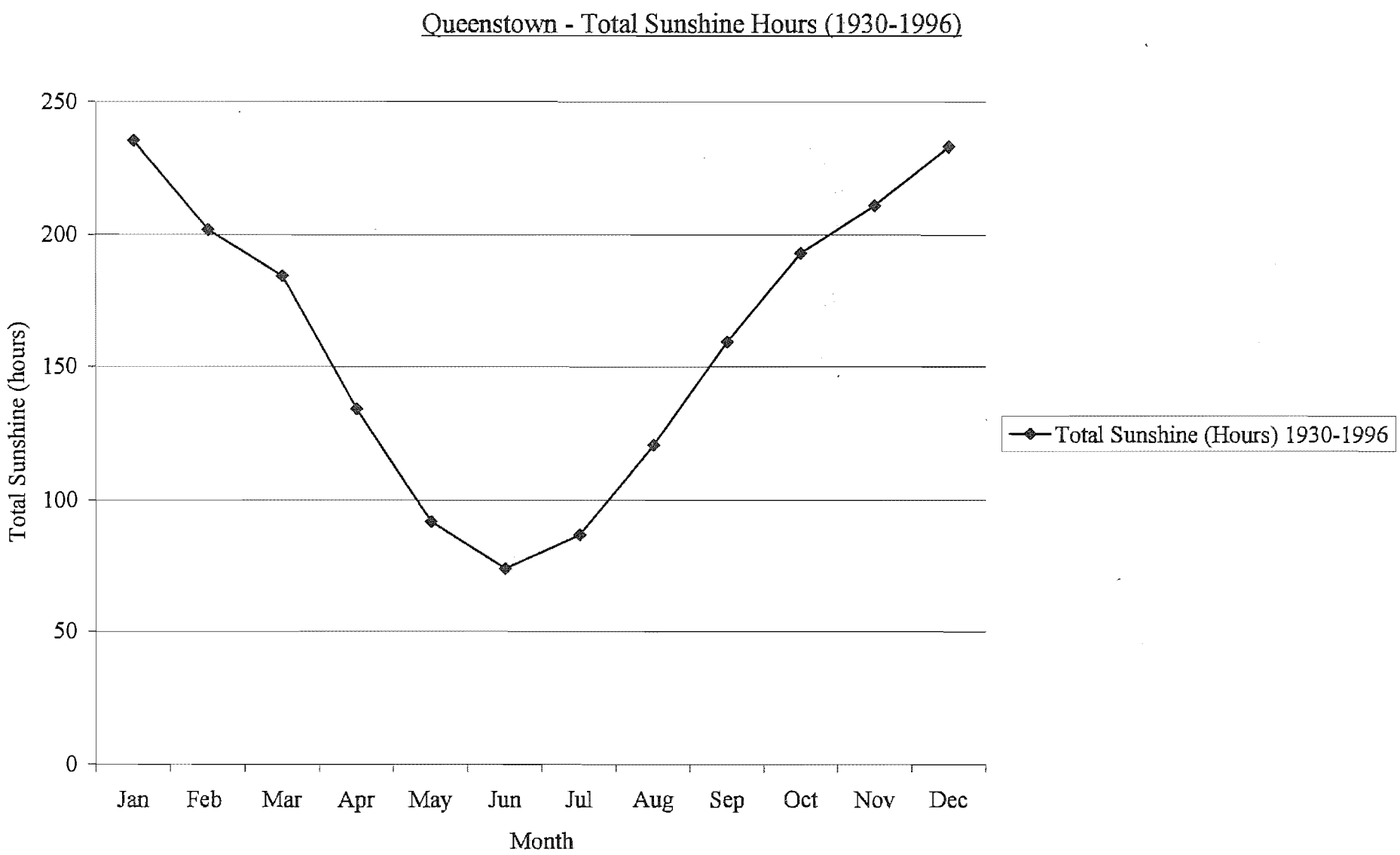
Queenstown - Total Sunshine Hours (1930-1996)
250
200
150
100
50
0
Total Sunshine (hours)
Jan
Feb
Mar
Apr
May
Jun
Jul
Aug
Sep
Oct
Nov
Dec
Month
Total Sunshine (Hours) 1930-1996

Queenstown Mean Vapour Pressure

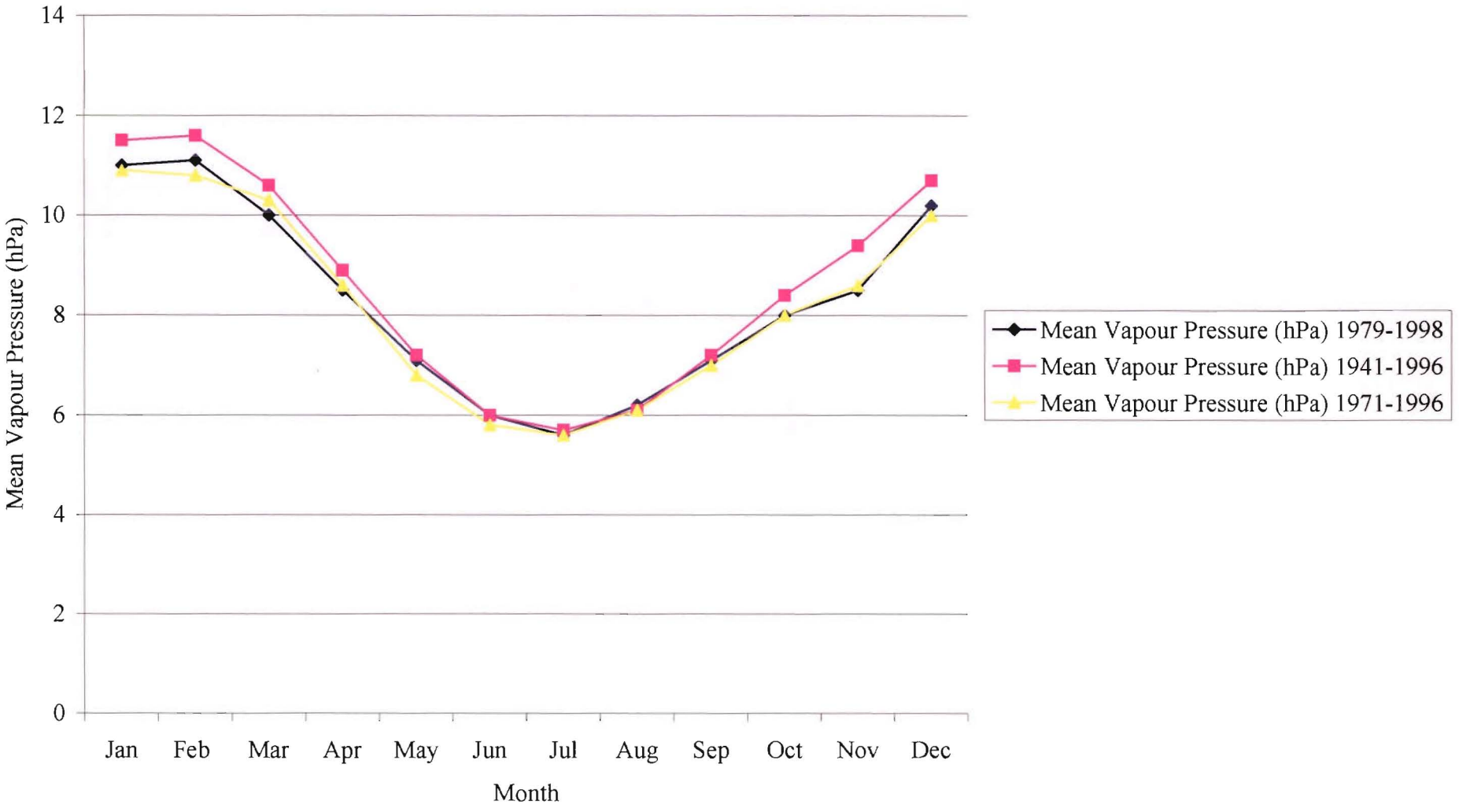

Queenstown Mean MSL Pressure

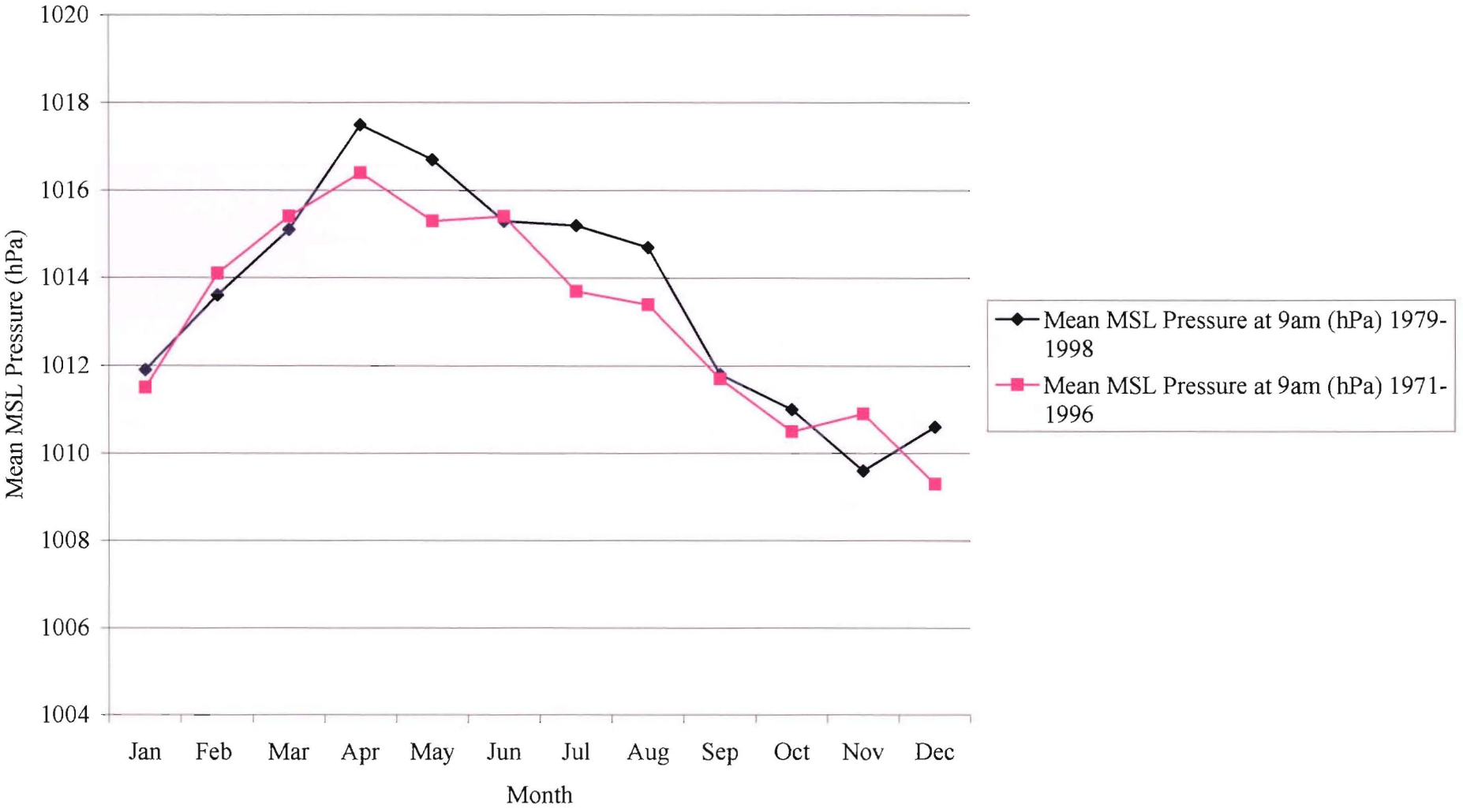

Mean and Extreme Daily Grass Minimum Temperature

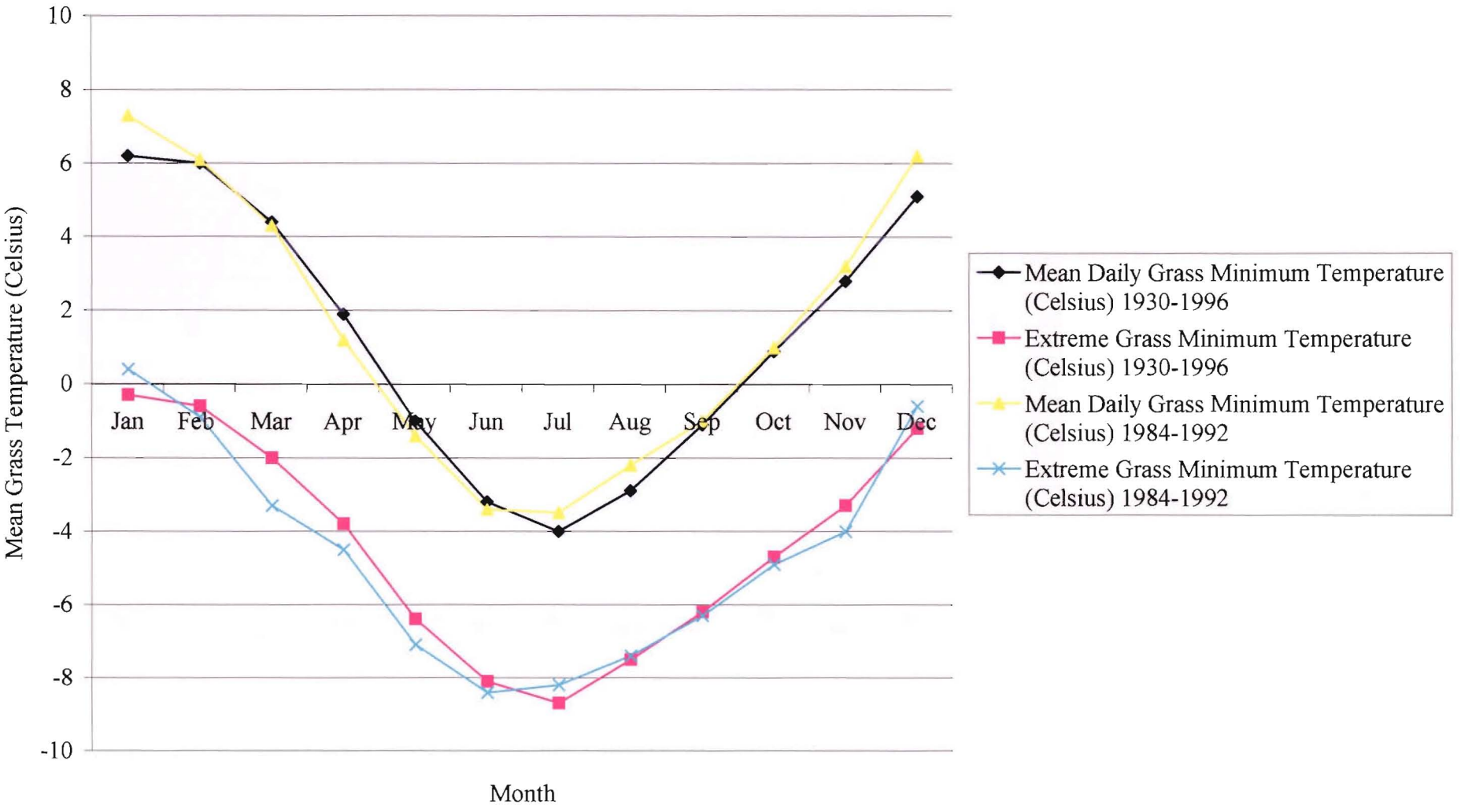

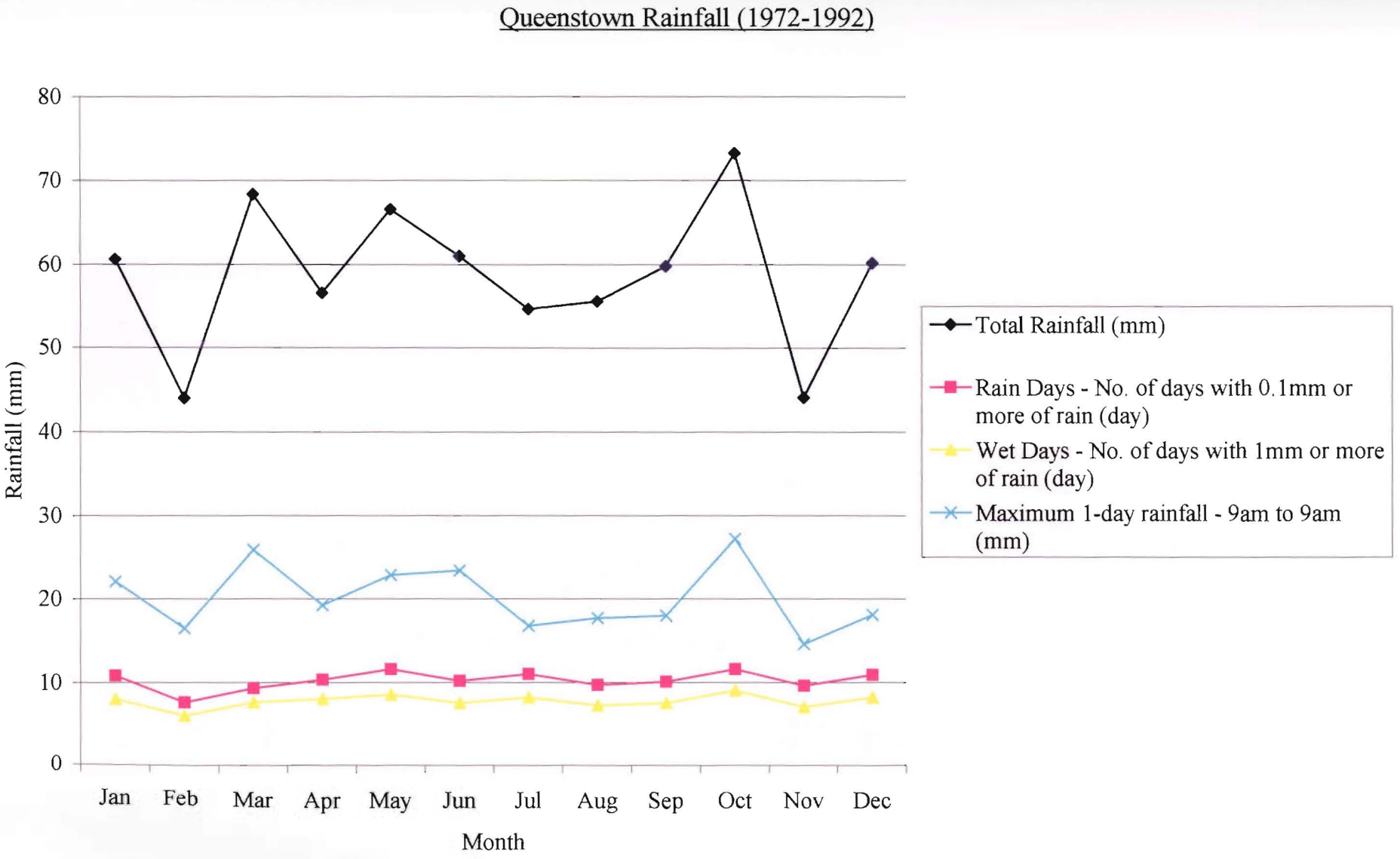
Queenstown Rainfall (1972-1992)
Rainfall (mm)
80
70
60
50
40
30
20
10
0
Jan
Feb
Mar
Apr
May
Jun
Jul
Aug
Sep
Oct
Nov
Dec
Month
Total Rainfall (mm)
Rain Days - No. of days with 0.1mm or more of rain (day)
Wet Days - No. of days with 1mm or more of rain (day)
Maximum 1-day rainfall - 9am to 9am (mm)

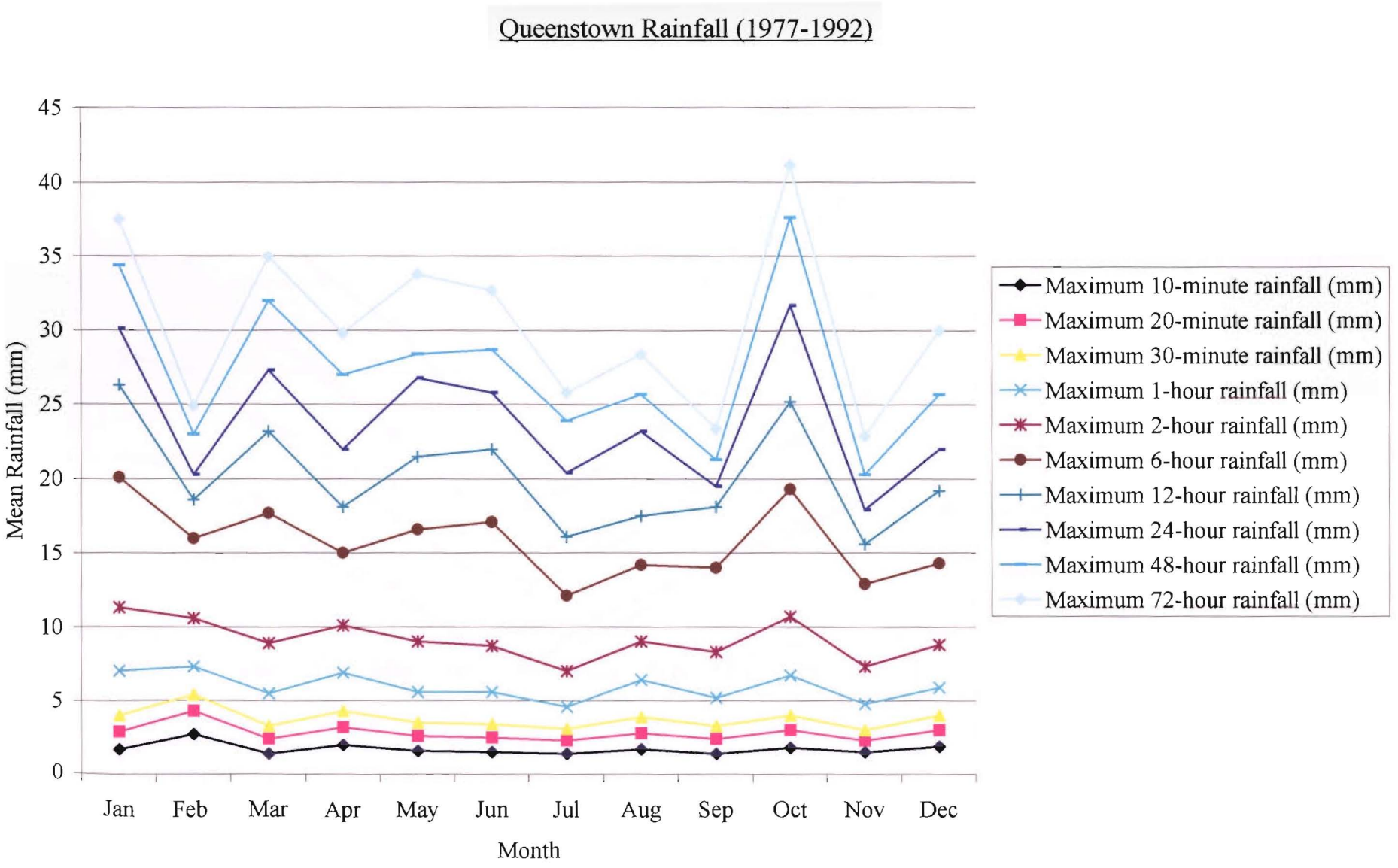
Queenstown Rainfall (1977-1992)
Mean Rainfall (mm)
45
40
35
30
25
20
15
10
5
0
Jan
Feb
Mar
Apr
May
Jun
Jul
Aug
Sep
Oct
Nov
Dec
Month
Maximum 10-minute rainfall (mm)
Maximum 20-minute rainfall (mm)
Maximum 30-minute rainfall (mm)
Maximum 1-hour rainfall (mm)
Maximum 2-hour rainfall (mm)
Maximum 6-hour rainfall (mm)
Maximum 12-hour rainfall (mm)
Maximum 24-hour rainfall (mm)
Maximum 48-hour rainfall (mm)
Maximum 72-hour rainfall (mm)

Mean Temperature - Queenstown (1991-1998)

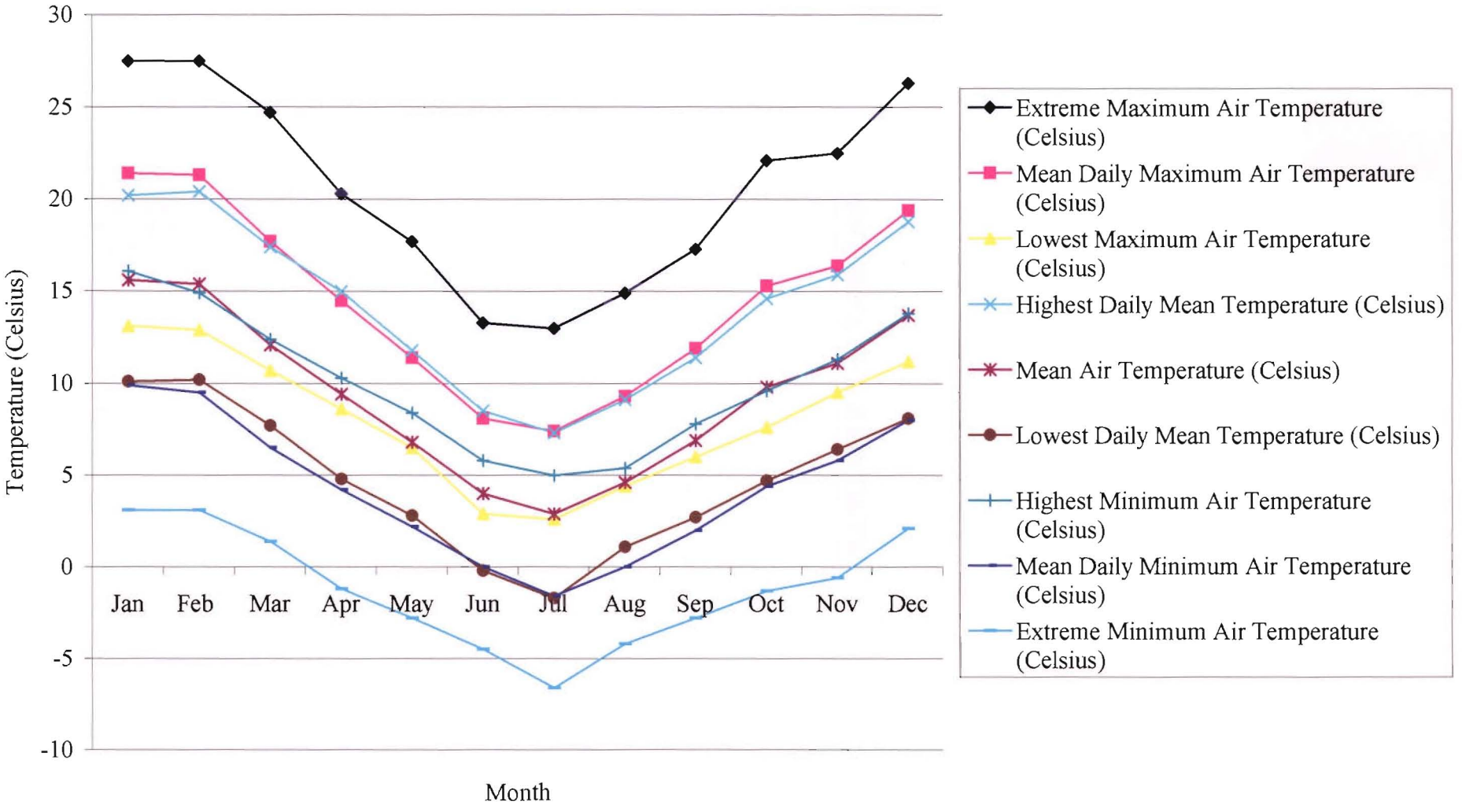

APPENDIX D: FIELD DATA.

APPENDIX D : DEFECT SURVEY SUMMARY TABLES

Distance Along Tape (Metres)	Defect Set No.	Defect Type	Defect Spacing	Defect Persistence	Av. Unit Block Size	Defect Orientation		Ground Water
						Strike	Dip	
LOT 98 (E) SLOPE HEIGHT = 6m								
0.80		4	7	4	1	036	60W	1
0.91		4	1	5	1	071	90	1
1.26		4	1	5	1	014	85W	1
1.35		4	1	5	1	000	69W	1
		Schist debris to 2.06m						
2.43		4	1	5	1	012	60W	1
2.85		4	1	4	1	026	43W	1
3.13		4	1	5	1	020	60W	1
3.55		4	1	5	1	088	86S	1
3.63		4	7	5	1	032	90	1
3.75		4	7	5	1	037	90	1
3.88		4	1	5	1	070	58S	1
4.09		4	1	4	1	029	50W	1
5.03		4	1	5	1	035	56E	1
5.10		4	1	5	1	000	60W	1
5.40		4	1	4	1	103	86S	1
		Schist debris to 7.8m						
8.4		4	1	4	1	135	50NE	1
		Schist debris to 9.4m						
9.4		4	1	5	1	342	60W	1
9.81		4	1	5	1	059	52SSE	1
10.06		4	1	5	1	072	90	1
10.08		4	1	4	1	106	90	1
10.20		4	1	3	1	109	52N	1
11.10		4	1	4	1	145	60SW	1
11.50		4	1	4	1	112	85S	1
12.0		4	1	3-4	1	109	82S	1
	Schist debris to 16.5m							
16.8		4	1	4-5	1	012	66W	1
16.8		4	4	4-5	1	126	26N	1
17.62		4	1	5	1	086	72S	1
17.85		4	1	3-4	1	160	75NE	1
19.67		4	1	5	1	100	82S	1
20		4	7	3-4	1	000	80W	1
20.30		4	1	4	1	312	90	1
20.34		4	1	5	1	088	80S	1
20.78		4	1	4	1	327	39N	1
21.23		4	1	4	1	303	90	1
21.78		4	1	4	1	326	72S	1
21.90		4	1	5	1	008	75E	1
22.06		4	1	4	1	030	83SE	1
22.80		4	1	4	1	314	56S	1
22.80		4	1	5	1	100	66S	1
23.15		4	1	5	1	321	50S	1
23.58		4	1	3	1	344	74NE	1
23.71		4	1	4	1	093	55S	1
25.67		4	1	3	1	326	74ENE	1
26.24		4	1	5	1	105	45N	1
26.35		4	1	5	1	013	72E	1

Distance Along Tape (Metres)	Defect Set No.	Defect Type	Defect Spacing	Defect Persistence	Av. Unit Block Size	Defect Orientation		Ground Water
						Strike	Dip	
26.63		4	7	5	1	042	80SE	1
26.72		4	7	5	1	106	62N	1
27.04		4	1	5	1	106	90	1
27.48		4	7	5	1	046	64SE	1
		Schist debris to 27.8m						
27.8		4	7	4	1	062	85W	1
27.99		4	7	4	1	054	64W	1
28.23		4	7	5	1	046	87W	1
28.63		4	7	4	1	028	83E	1
28.80		4	1	3	1	095	86S	1
29.27		4	1	5	1	058	24W	1
29.70		4	1	5	1	80	60SE	1
30.10		4	1	4	1	312	65N	1
30.43		4	1	4	1	316	72N	1
30.71		4	1	5	1	331	66S	1
30.83		4	1	5	1	010	68W	1
31.86		4	1	4	1	065	79E	1
		Schist debris to 33m						
LOT 102 (B) SLOPE HEIGHT = 5m								
0.2		4	1	5	1	302	82NE	1
0.8		4	3	5	1-2	064	74W	1
1.7		4	4	4	1	348	90	1
2.22		4	7	4	1	298	90	1
4.67		4	1	2	1	335	54NE	1
5.7		4	1	5	1	72	70N	1
6.91		4	1	5	1	334	90	1
7.2		4	1	5	1	018	68W	1
7.9		4	1	4	1	102	87N	1
8.1		4	1	5	1	016	71NW	1
8.8		4	7	5	1	125	545	1
9.4		4	7	4	1	101	80S	1
10.15		4	1	4	1	182	64W	1
10.58		4	1	5	1	110	85N	1
10.81		4	1	3	1	022	90 rregular surface	1
10.98		4	1	5	1-2	029	76NW	1
11.12		4	1	5	1	348	74E	1
11.4		4	1	2	1	026	8NW rregular surface	1
12.4		4	1	4	1	128	90 rregular surface	1
12.51		4	1	5	1	122	85S	1
12.7		4	1	3	1	007	75E	1
12.9		4	1	3	1	007	75E	1
13.5		4	1	2	1	024	90 rregular surface	1
14.46		4	1	2-3	1	037	78S	1
14.8		4	1	2	1	108	90	1
14.8		4	1	4	1	007	805	1
15.0		4	1	5	2-3	124	80SW	1
15.13		4	1	5	2-3	024	54NW	1
15.5		4	1	3-4	1	352	85E	1
16		4	1	4-5	1	100	74S	1

Distance Along Tape (Metres)	Defect Set No.	Defect Type	Defect Spacing	Defect Persistence	Av. Unit Block Size	Defect Orientation		Ground Water
						Strike	Dip	
16.4		4	1	4-5	1	022	90	1
17.4		4	1	5	1.3	106	85S	1
17.5		4	1	3	1	023	78NW	1
17.6		4	3-4	3	1	095	85N	1
18.0		4	3-4	3	1	095	74N	1
20.06		4	1	3	1	100	80S	1
20.1		4	1	5	1	013	90	1
20.73		4	1	4	1	108	54S	1
20.76		4	1	5	1	004	68W	1
20.88		4	1	5	1	024	85W	1
21.0		4	1	3	1	104	65NE	1
21.26		4	1	5	1-2	095	78S	1
21.40		4	1	3	1	099	68N	1
21.62		4	1	2-3	1	018	85W	1
22.0		4	7	3	1	092	72S	1
24.37		4	1	2-3	1	100	80S	1
24.57		4	1	5	1	006	66W	1
24.98		4	1	5	1	095	80N	1
25		4	1	4	1	026	80NW	1
25.87		4	1	4	1	094	80S	1
26.28		4	1	3	1	015	60W	1
LOT 107 SLOPE HEIGHT = 5m								
0.3		4	1	5	3-4	040	41NW	3 ater dripping
60		4	1	5	2-3	015	72WNW	3
1.16		4	1	5	1-2	012	90	3
1.27		4	1	3	2	354	75W	3
1.4		4	1	3	2	348	62W	3
2.65		4	7	5	3	091	84SSW	2
2.88		4	1	5	1	045	40NW	1
3.14		4	1	5	1	027	52W	1
3.22		4	1	5	2-3	328	77W	1
3.74	surface rough	4	1	3	1-2	002	78W	1
		Schist debris 1-5cm^2 blocks to 4.47m						
4.47		4	1	5	2-3	093	64S	1
4.49		4	1	5	2-3	045	80NW	1
4.63		4	1	5	2-3	036	70NW	1
4.71		4	1	5	2	042	66NW	1
4.83		4	1	4	2-3	026	79NW	1
5.2		4	1	3	1-2	028	72NW	1
5.90		4	1	5	1	357	84SW	1
6.12	surface rough water dripping	4	1	3 (5m)	1	325	50NE	2
6.4		4	7	5	2-3	108	80SW	1
6.57		4	1	5	1	058	90	1
		6.57-7m – schist blocks up to 10cm x 3cm						
7		4	3	5	2	084	76S	1
7.1		4	6	5	2-3	065	70S	1
7.2		4	1	3	1-2	339	84NE	1
		Schist debris from 7.2m-8.7m						
9.24	rough irregular surface	4	3	4	1	100	87S	1
9.44		4	1	4	1	351	86W	1

Distance Along Tape (Metres)	Defect Set No.	Defect Type	Defect Spacing	Defect Persistence	Av. Unit Block Size	Defect Orientation		Ground Water
						Strike	Dip	
10.1		4	1	5	1	099	70S	2
10.33		4	1	3	1	347	60E	2
11.1		4	7	5	1	094	82S	2
12.75		4	4	3	1	143	90	1
12.89		4	4	4	1	040	90	1
13.14		4	1	5	1	002	80W	1
13.64		4	1	4	1	058	30NW	1
13.8		4	3	4	1	086	64S	1
14.45		4	1	4	1	008	60W	1
14.75		4	1	5	1	047	74NW	1
14.9		4	1	5	1	006	80W	1
15.1		4	1	5	1	058	72NW	1
15.29		4	1	4	1	352	60E	1
15.75		4	1	4-5	1	045	60W	1
LOT 101 (C) SLOPE HEIGHT = 3m								
		0-1.2m topsoil; schist debris						
1.4	grey schist	4	1	5	1	348	76SW	1
2		4	1	5	1	004	42W	1
2.7		4	1	5	1	110	50S	1
2.8		4	2	5	1	032	80SE	1
2.9		4	1	5	1	063	80NW	1
3.15		4	1	3	1	110	90	1
3.37		4	1	5	1	024	40NW	1
3.8		4	1	5	1	113	60S	1
3.95		4	1	4	1	012	68W	1
4.08		4	7	4-5	1	060	90	1
4.23		4	1	5	1	328	73W	1
4.35		4	1	4-5	1	330	62W	1
4.5		4	1	5	1	100	90	1
4.96		4	1	4	1	345	62W	1
5.23		4	1	4-5	1	015	80NW	1
5.55		4	1	5	1	019	75W	1
5.73		4	7	5	1-2	066	76NW	1
6.05		4	1	5	1	108	64S	1
6.28		4	1	4-5	1	017	68W	1
6.6		4	1	4	1	110	85NE	1
6.86		4	7	5	1	042	85SE	1
7.33		4	1	5	1	345	72W	1
7.6		4	1	4	1	008	50W	1
8.26		4	4	4	1	114	45N	1
8.6		4	1	5	1	014	85W	1
8.96		4	1	4	1	033	78W	1
9.3		4	1 up slope to 7	5	1	006	90	1
9.4		4	1	5	1	112	72N	1
9.6		4	1	5	1	004	74E	1
		Schist debris up to 12m						
12.06		4	1	5	1	032	90	1
12.38		4	1	3-4	1	024	84W	1
13.35		4	1	5	1	150	80E	1
13.37		4	1	4	1	038	60W	1
14.3		4	7	5	1	130	70NE	1

Distance Along Tape (Metres)	Defect Set No.	Defect Type	Defect Spacing	Defect Persistence	Av. Unit Block Size	Defect Orientation		Ground Water
						Strike	Dip	
14.93		4	1	4	1	118	38N	1
14.98		4	1	4-5	1	023	80W	1 ed & blue pegs
15.4	grey schist	4	1	4	1	008	62W	1
15.5		4	1	5	1	017	62W	1
15.8		4	1	4	1	000	81E	1
16.06		4	1	4	1	350	80E	1
17.4		4	1	5	1	110	80S	1
18.4		4	1	4-5	1	142	58N	2 (damp)
19.02		4	1	5	1	097	62S	1
19.3		4	1	4-5	1	013	62W	1
20.56		4	1	5	1	086	74S	1
20.56		4	1	5	1	023	68NW	1
20.82		4	1	5	1	102	70S	1
20.82		4	1	5	1	008	57W	1
21.6		4	1	4-5	1	116	90	1
		Schist debris to 22.8m						
22.8		4	1	5	1	100	60S	1-2
23.07		4	1	5	1	090	74S	1
23.07		4	1	5	1	358	72W	1
23.4		4	1	5	1	102	80S	1
23.65		4	1	5	1	104	52N	1
25.7		4	1	5	1	078	88S	1
26.25		4	1	5	1	113	86S	1
26.83		4	1	5	1	331	90	1
LOT 100 (D) SLOPE HEIGHT =3m–7.2m								
0.60	schist	4	1	4	1	142	67NE	1
1.05		4	1	5	1	097	76S	1
0.95		4	1	5	1	108	90	1
1.3		4	1	5	1	104	90	1
1.55		4	1	5	1	348	64W	1
1.55		4	1	5	1	126	80NE	1
1.7		4	3	5	1	117	72N	1
2.0		4	1	5	1	106	70S	1
2.35		4	1	4	1	004	78W	1
2.44		4	1	5	1	003	61W	1
2.6		4	1	5	1	090	65S	1
2.8		4	1	5	1	000	60W	1
2.8		4	1	5	1	094	70S	1
2.94		4	3	4	1	015	84W	2
2.94		4	1	5	1	140	76NE	1
3.2		4	1	5	1	098	74N	1
3.39		4	1	5	1	018	76W	1
3.7		4	1	5	1	014	50W	1
3.8		4	1	5	1	093	60S	1
4.25		4	1	5	1	330	78W	1
4.45		4	1	4	1	108	88S	1
4.85		4	1	5	1	108	75S	1
5.97		4	1	4	1	354	60W	1
6.0		4	1	4-5	1	109	74N	1
6.58		4	1	4-5	1	100	58S	1-2
7.2		4	1	5	1	340	62W	2

Distance Along Tape (Metres)	Defect Set No.	Defect Type	Defect Spacing	Defect Persistence	Av. Unit Block Size	Defect Orientation		Ground Water
						Strike	Dip	
7.2		4	1	3	1	106	65S	2
		8.4-10.2M = schist debris failure						
10.56		4	1	4	1	013	53W	2
10.75		4	1	4	1	026	50W	2
10.9		4	1	4-5	1	102	72N	2
11.3		4	1	5	1	002	74E	1
11.3		4	1	5	1	104	80S	2
11.5		4	1	5	1	103	62S	2
11.7		4	1	5	1	014	75W	1-2
11.7		4	1	5	1	117	66S	1-2
11.85		4	7	4-5	1	104	too closed to measure	1
12.4		4	1	4	1	013	82E	1
21.64		4	6	5	1	092	70S	1
12.68		4	1	4	1	017	60W	1
13		4	7	5	1	090	60N	1
		Schist debris to 14.2m						
14.2		4	1	4	1	032	74W	1
14.67		4	7	5	1	102	70N	1
14.85		4	1	5	1	097	60S	1
		Schist debris to 15.56m						
15.56		4	1	5	1	050	69W	1
15.70		4	1	5	1	044	90	1
15.98		4	1	4	1	027	80W	1
16.2		4	1	4	1	030	90	1
16.46		4	1	5	1	098	75S	1
16.62		4	1	5	1	030	70W	1
16.68		4	1	4	1	048	85W	1
16.68		4	1	5	1	090	90	1
16.85		4	2	2	1	112	70S	1
17.12		4	1	5	1	025	65W	1
17.26		4	1	5	1	063	80S	1
17.44		4	7	2	1	103	too closed to measure	1
17.67		4	1	5	1	086	10S	1
18.29		4	1	4	1	097	63S	1
18.38		4	1	5	1	052	90	1
18.5		4	1	5	1	090	45S	1
18.8		4	1	5	1	107	65S	1
19.7		4	1	3	1	008	60W	1
20.0		4	1	5	1	97	56S	1
20.41		4	1	5	1	015	64W	1
20.46		4	1	5	1	095	65S	1
21.16		4	1	2	1	018	90	1
21.48		4	1	4	1	008	60W	1
21.8		4	1	5	1	004	80W	1
22.08		4	1	2	1	340	88W	1
22.22		4	1	5	1	009	90	1
22.43		4	1	5	1	054	90	1
22.65		4	1	4	1	302	64S	1
23.06		4	1	5	1	002	80W	1
23.4		4	1	5	1	356	76W	1

Distance Along Tape (Metres)	Defect Set No.	Defect Type	Defect Spacing	Defect Persistence	Av. Unit Block Size	Defect Orientation		Ground Water
						Strike	Dip	
LOT 100 (D) (continued) & LOT 99 (D) LOT 99 SIGN AT 24m SLOPE HEIGHT = 5m								
23.8		4	1	4	1	043	54W	2
24		4	1 (to 6 up slope)	4	1	038	60W	1
24.32		4	1	4	1	042	66W	1
24.42		4	1	4-5	1	052	80W	1
24.64		4	1	5	1	345	90	1
24.72		4	1	5	1	329	90	1
25.05		4	1	4-5	1	031	60E	1
		water flow between these two joints						
25.3		4	1	4-5	1	031	65W	1
25.77		4	1	4	1	067	60S	1
25.88		4	1	5	1	000	90	1
26.25		4	3	4	1	020	80W	2
26.41		4	1	4	1	356	65W	1
26.58		4	1	4	1	330	85W	2
26.84		4	1	5	1	022	72E	1
26.93		4	1	4	1	022	64E	1
27.04		4	1	5	1	015	75E	1
27.18		4	1	4	1	108	60S	1
		Schist debris from 27.4m–28.1m						
28.7		4	6	3	1	044	60E	1
28.89		4	1	3	1	028	52W	1
28.99		4	1	5	1	029	70W	1
29.14		4	1	5	1	025	90	1
29.32		4	1	4	1	358	75W	1
29.47		4	1	3	1	124	54N	1
29.57		4	1	5	1	118	60S	1
29.76		4	1	5	1	351	72N	1
30.41		4	1	4	1	053	50W	1
30.6		4	1	4	1	116	50N	1
30.85		4	1	4	1	090	88S	1
31.15		4	1	4	1	079	72S	1
31.62		4	6	5	1	069	too closed to measure	1
31.98		4	1	5	1	016	90	1
32.18		4	1	4	1	046	70W	1
32.21		4	1	5	1	018	80E	1
32.5		4	1	5	1	036	40W	1
32.6		4	1	5	1	038	62W	1
33.28		4	1	5	1	032	60W	1
33.49		4	6-7	5	1	044	68W	1
33.69		4	1	5	1	106	70S	1
33.9		4	1	4	1	048	85W	1
33.92		4	1	5	1	049	70W	1
33.97		4	1	4-5	1	014	65W	1
34.95		4	1	3	1	049	72W	1
35.15		4	1	5	1	039	90	1
35.3		3	1	5	1	029	90	1
35.55		4	7	3	1	034	80E	1

Distance Along Tape (Metres)	Defect Set No.	Defect Type	Defect Spacing	Defect Persistence	Av. Unit Block Size	Defect Orientation		Ground Water
						Strike	Dip	
35.55		4	1	5	1	118	62N	1
35.82		4	1	4	1	038	80W	1
35.93		4	1	4	1	046	82W	1
36.21		4	7	4	1	036	70E	1
36.85		4	1	5	1	030	84W	1
37.18		4	1	4	1	129	72S	1
37.45		4	1	5	1	050	52W	1
37.77		4	1	5	1	044	75E	1
37.85		4	1	4	1	093	75N	1
38.3		4	1	5	1	341	72E	1
38.6		4	1	5	1	348	55W	1
38.8		4	1	5	1	125	90 irregular surface	1
		Schist debris for 1m						
39.87		4	1	5	1	022	60W	1
40		4	1	5	1	024	68W	1
40.17		4	1	5	1	029	70W	1
40.36		4	1	4	1	008	74W	1
		Schist debris to 42.6m						
42.6		4	1	3	1	325	69W	1
43.03		4	1	3-4	1	036	82W	1
43.35		4	1	5	1	028	90	1
43.79		4	7	4	1	102	63S	1
44.25		4	7	4	1	107	76S	1
		Schist debris to 45.4m						
45.4		4	7	3	1	356	90	1
45.49		4	7	4-5	1	000	90	1
45.58		4	1	5	1	074	83S	1
45.8		4	1	5	1	315	85S	1
45.92		4	1	5	1	310	82S	1
46.39		4	7	5	1	067	80W	1
46.44		4	1	4	1	119	85S	1
47		4	1	5	1	097	55S	1
47.25		4	1	3	1	336	65E	1
47.33		4	1	5	1	351	65E	1
47.4		4	1	4	1	019	60W	1
47.62		4	7	4	1	072	55N	1
48.5		4	1	4	1	313	90	1
48.76		4	7	4-5	1	312	too closed to measure	1
48.82		4	7	4	1	312	too closed to measure	1
49.1		4	1	4	1	302	80S	1
49.72		4	7	5	1	302	80S	1
50.35		4	6-7	4-5	1	018	76E	1
51.03		4	1	5	1	062	68E	1
51.42		4	1	5	1	051	55E	1
		Schist debris to 52.7m						

```
*DIPS 1.1 DATA INPUT TEMPLATE
*PROJECT TITLES ( 2 lines ) :
        Queenstown Hill Landslide
        Frankton Arm
STRIKE/DIPR
*MAGNETIC DECLINATION (west positive) :
        0
*QUANTITY COLUMN FLAG:
*if the flag is NO QUANTITY do not include a 'quantity' column
        NO QUANTITY
number  ;strike  ;dip     ;
        1       250       30
        2       243       32
        3       060       16
        4       108       16
        5       065       10
        6       060       10
        7       014       05
        8       073       08
        9       078       08
       10       100       32
       11       105       18
       12       227       08
       13       221       14
       14       076       14
       15       084       20
       16       080       17
       17       050       16
       18       090       20
       19       296       27
       20       326       18
       21       322       14
       22       290       28
       23       069       31
       24       074       28
       25       047       38
       26       057       40
       27       029       26
       28       047       25
       29       321       30
       30       110       22
       31       087       29
```

32	064	12
33	062	10
34	060	13
35	057	10
36	050	04
37	162	34
38	151	20
39	052	12
40	182	10
41	147	13
42	106	17
43	103	20
44	101	14
45	099	22
46	086	22
47	267	12
48	065	14
49	040	22
50	075	17
51	069	11
52	059	10
53	058	10
54	077	16
55	087	36
56	102	18
57	049	20
58	105	08
59	099	36
60	080	18
61	072	16
62	078	17
63	080	26
64	067	21
65	059	22
66	056	24
67	050	23
68	054	21
69	093	17
70	064	12
71	075	12
72	080	25
73	088	22

74	071	18
75	077	19
77	089	24
78	072	26
79	090	40
80	098	07
81	089	26
82	070	08
83	070	16
84	085	23
85	097	20
86	080	25
87	106	23
88	109	22
89	094	32
90	090	38
91	091	19
92	059	17
93	059	13
94	057	15
95	059	12
96	085	20
97	079	20
98	080	21
99	101	24
100	102	21
101	100	24
102	083	29
103	069	16
104	058	18
105	077	10
106	070	22
107	065	18
108	065	22
109	006	17
110	118	14
111	114	16
112	103	20
113	100	16
114	065	08

```
*DIPS 1.1 DATA INPUT TEMPLATE
*PROJECT TITLES ( 2 lines ) :
       Queenstown Hill Landslide Joints
       Frankton Arm
*NUMBER OF TRAVERSES :
       0
*TRAVERSE INFORMATION (1 line for each traverse) in the form...
*traverse #;[opt.trav orient;]traverse type;orient. 1;orient. 2;title
*The next line is 'data orientation type flag' , choices are;
*DIP/DIPDIRECTION (of plane)
*TREND/PLUNGE (of pole to plane or of linear structure)
*STRIKE/DIPL  (of plane - left hand rule)
*STRIKE/DIPR  (of plane - right hand rule)
       STRIKE/DIPR
*MAGNETIC DECLINATION (west positive) :
       0
*QUANTITY COLUMN FLAG:
*if the flag is QUANTITY, then the 'quantity' column must be present
*if the flag is NO QUANTITY do not include a 'quantity' column
       NO QUANTITY
*NUMBER OF EXTRA DATA COLUMNS (0-12);
       0
*COLUMN TITLE LINE:
number  ;strike  ;dip     ;
       1       142       63
       2       155       53
       3       044       66
       4       140       79
       5       058       77
       6       038       53
       7       090       90
       8       050       90
       9       300       70
      10       082       60
      11       160       48
      12       087       58
      13       096       58
      14       140       84
      15       020       76
      16       161       73
```

17	158	86
18	167	70
19	160	88
20	148	84
21	148	86
22	050	64
23	042	84
24	346	30
25	175	86
26	163	75
27	129	70
28	179	75
29	120	80
30	038	90
31	039	90
32	120	80
33	008	90
34	218	80
35	330	90
36	345	50
37	030	70
38	190	90
39	290	50
40	220	82
41	098	78
42	054	85
43	125	56
44	142	80

```
*DIPS 1.1 DATA INPUT TEMPLATE
*PROJECT TITLES ( 2 lines ) :
       Marina Heights Failure
       Frankton
*NUMBER OF TRAVERSES :
       0
*TRAVERSE INFORMATION (1 line for each traverse) in the form...
*traverse #;[opt.trav orient;]traverse type;orient. 1;orient. 2;title
*The next line is 'data orientation type flag' , choices are;
*DIP/DIPDIRECTION (of plane)
*TREND/PLUNGE (of pole to plane or of linear structure)
*STRIKE/DIPL  (of plane - left hand rule)
*STRIKE/DIPR  (of plane - right hand rule)
       STRIKE/DIPR
*MAGNETIC DECLINATION (west positive) :
       0
*QUANTITY COLUMN FLAG:
*if the flag is QUANTITY, then the 'quantity' column must be present
*if the flag is NO QUANTITY do not include a 'quantity' column
       NO QUANTITY
*NUMBER OF EXTRA DATA COLUMNS (0-12);
       0
*COLUMN TITLE LINE:
number  ;strike  ;dip     ;
       1       150       32
       2       149       24
       3       153       30
       4       105       40
       5       109       32
       6       105       34
       7       125       22
       8       160       20
       9       170       22
      10       164       24
      11       154       20
      12       156       20
      13       159       28
      14       152       30
      15       165       20
      16       174       18
```

```
      17        180       28
      18        186       24
      19        191       24
      20        193       26
      21        143       15
      22        154       09
      23        161       16
      24        150       18
      25        146       28
      26        172       30
      27        160       20
      28        130       20
      29        145       22
      30        245       22
      31        254       20
      32        245       18
      33        193       24
      34        208       26
      35        131       04
      36        162       23
      37        150       17
      38        164       17
      39        144       20
      40        143       33
      41        244       10
      42        167       16
      43        142       20
      44        323       26
      45        132       20
      46        138       18
      47        216       14

*DIPS 1.1 DATA INPUT TEMPLATE
*PROJECT TITLES ( 2 lines ) :
       Frankton Slide 2
       Frankton
*NUMBER OF TRAVERSES :
       0
*TRAVERSE INFORMATION (1 line for each traverse) in the form...
*traverse #;[opt.trav orient;]traverse type;orient. 1;orient. 2;title
```

```
*The next line is 'data orientation type flag' , choices are;
*DIP/DIPDIRECTION (of plane)
*TREND/PLUNGE (of pole to plane or of linear structure)
*STRIKE/DIPL  (of plane - left hand rule)
*STRIKE/DIPR  (of plane - right hand rule)
      STRIKE/DIPR
*MAGNETIC DECLINATION (west positive) :
      0
*QUANTITY COLUMN FLAG:
*if the flag is QUANTITY, then the 'quantity' column must be present
*if the flag is NO QUANTITY do not include a 'quantity' column
      NO QUANTITY
*NUMBER OF EXTRA DATA COLUMNS (0-12);
      0
*COLUMN TITLE LINE:
number  ;strike ;dip     ;
      1       160       36
      2       170       25
      3       168       22
      4       160       28
      5       151       29
      6       173       20
      7       155       20
      8       162       24
      9       163       23
     10       155       20
     11       156       22
     12       152       22
     13       158       22
     14       148       20
     15       162       20
     16       157       13
     17       160       24
     18       156       20
     19       164       24
     20       169       22
     21       160       22
     22       171       24
     23       172       34
     24       177       26
```

```
      25       166       24
      26       182       24
      27       145       16
      28       060       14
      29       160       15
      30       126       12
      31       226       12
      32       130       26
      33       148       26
      34       151       29
      35       139       24
      36       147       29
      37       099       05
      38       187       30
      39       267       20
      40       154       10
      41       149       08

*DIPS 1.1 DATA INPUT TEMPLATE
*PROJECT TITLES ( 2 lines ) :
       Frankton Slide 3
       Frankton
*NUMBER OF TRAVERSES :
       0
*TRAVERSE INFORMATION (1 line for each traverse) in the form...
*traverse #;[opt.trav orient;]traverse type;orient. 1;orient. 2;title
*The next line is 'data orientation type flag' , choices are;
*DIP/DIPDIRECTION (of plane)
*TREND/PLUNGE (of pole to plane or of linear structure)
*STRIKE/DIPL  (of plane - left hand rule)
*STRIKE/DIPR  (of plane - right hand rule)
       STRIKE/DIPR
*MAGNETIC DECLINATION (west positive) :
       0
*QUANTITY COLUMN FLAG:
*if the flag is QUANTITY, then the 'quantity' column must be present
*if the flag is NO QUANTITY do not include a 'quantity' column
       NO QUANTITY
*NUMBER OF EXTRA DATA COLUMNS (0-12);
       0
```

*COLUMN TITLE LINE:

number	;strike	;dip	;
1	120	24	
2	118	18	
3	123	27	
4	139	28	
5	128	28	
6	142	18	
7	132	17	
8	120	18	
9	179	44	
10	127	21	
11	171	20	
12	150	20	
13	135	20	
14	135	20	
15	138	24	
16	138	22	
17	140	28	
18	144	22	
19	130	23	
20	060	12	
21	140	72	
22	103	08	
23	113	06	
24	228	22	
25	245	25	
26	147	18	
27	163	24	
28	240	20	
29	151	14	
30	133	10	
31	163	06	
32	126	29	
33	118	35	
34	137	38	
35	115	38	
36	116	20	
37	126	22	
38	115	20	

```
      39        115       20
      40        117       23
      41        115       22
      42        128       17
      43        119       22

*DIPS 1.1 DATA INPUT TEMPLATE
*PROJECT TITLES ( 2 lines ) :
       Frankton Slide 4
       Frankton
*NUMBER OF TRAVERSES :
       0
*TRAVERSE INFORMATION (1 line for each traverse) in the form...
*traverse #;[opt.trav orient;]traverse type;orient. 1;orient. 2;title
*The next line is 'data orientation type flag' , choices are;
*DIP/DIPDIRECTION (of plane)
*TREND/PLUNGE (of pole to plane or of linear structure)
*STRIKE/DIPL  (of plane - left hand rule)
*STRIKE/DIPR  (of plane - right hand rule)
       STRIKE/DIPR
*MAGNETIC DECLINATION (west positive) :
       0
*QUANTITY COLUMN FLAG:
*if the flag is QUANTITY, then the 'quantity' column must be present
*if the flag is NO QUANTITY do not include a 'quantity' column
       NO QUANTITY
*NUMBER OF EXTRA DATA COLUMNS (0-12);
       0
*COLUMN TITLE LINE:
number  ;strike  ;dip     ;
       1        124       25
       2        125       24
       3        124       24
       4        118       26
       5        120       24
       6        107       24
       7        112       28
       8        120       20
       9        098       32
      10        102       18
```

```
      11        104       30
      12        108       24
      13        111       26
      14        109       24
      15        127       20
      16        125       22
      17        185       04
      18        125       22
      19        217       55
      20        211       39
      21        214       32
      22        083       23
      23        075       26
      24        091       22
      25        121       22
      26        061       18
      27        147       31
      28        111       38
      29        119       38
      30        112       26
      31        111       26
      32        119       22
      33        127       20
      34        134       22

*DIPS 1.1 DATA INPUT TEMPLATE
*PROJECT TITLES ( 2 lines ) :
       Frankton Slide 5
       Frankton
*NUMBER OF TRAVERSES :
       0
*TRAVERSE INFORMATION (1 line for each traverse) in the form...
*traverse #;[opt.trav orient;]traverse type;orient. 1;orient. 2;title
*The next line is 'data orientation type flag' , choices are;
*DIP/DIPDIRECTION (of plane)
*TREND/PLUNGE (of pole to plane or of linear structure)
*STRIKE/DIPL  (of plane - left hand rule)
*STRIKE/DIPR  (of plane - right hand rule)
      STRIKE/DIPR
*MAGNETIC DECLINATION (west positive) :
```

```
      0
*QUANTITY COLUMN FLAG:
*if the flag is QUANTITY, then the 'quantity' column must be present
*if the flag is NO QUANTITY do not include a 'quantity' column
      NO QUANTITY
*NUMBER OF EXTRA DATA COLUMNS (0-12);
      0
*COLUMN TITLE LINE:
number  ;strike  ;dip     ;
      1       112       24
      2       125       25
      3       125       22
      4       108       22
      5       109       23
      6       117       21
      7       107       23
      8       101       19
      9       116       18
     10       109       20
     11       119       22
     12       088       25
     13       091       21
     14       086       18
     15       086       22
     16       108       24
     17       118       26
     18       097       21
     19       098       19
     20       099       23
     21       123       20
     22       121       20
     23       109       13
     24       109       16
     25       148       21
     26       169       20
     27       157       21
     28       128       24
     29       118       19
     30       120       20
     31       123       32
```

```
      32        110       22
      33        089       24
      34        162       20
      35        182       17
      36        162       18
      37        219       08
      38        208       06
      39        100       18
      40        125       30
      41        260       05
      42        228       12
      43        215       12

*DIPS 1.1 DATA INPUT TEMPLATE
*PROJECT TITLES ( 2 lines ) :
      Frankton Slide 6
      Frankton
*NUMBER OF TRAVERSES :
      0
*TRAVERSE INFORMATION (1 line for each traverse) in the form...
*traverse #;[opt.trav orient;]traverse type;orient. 1;orient. 2;title
*The next line is 'data orientation type flag' , choices are;
*DIP/DIPDIRECTION (of plane)
*TREND/PLUNGE (of pole to plane or of linear structure)
*STRIKE/DIPL  (of plane - left hand rule)
*STRIKE/DIPR  (of plane - right hand rule)
      STRIKE/DIPR
*MAGNETIC DECLINATION (west positive) :
      0
*QUANTITY COLUMN FLAG:
*if the flag is QUANTITY, then the 'quantity' column must be present
*if the flag is NO QUANTITY do not include a 'quantity' column
      NO QUANTITY
*NUMBER OF EXTRA DATA COLUMNS (0-12);
      0
*COLUMN TITLE LINE:
number  ;strike  ;dip     ;
      1       146       28
      2       138       28
      3       127       24
```

4	134	27
5	140	22
6	131	20
7	129	39
8	122	37
9	138	31
10	117	33
11	071	34
12	132	19
13	115	21
14	115	24
15	118	24
16	119	20
17	132	22
18	134	12
19	132	18
20	135	20
21	123	08
22	169	22
23	180	14
24	117	32
25	123	24
26	131	24
27	162	08
28	113	20
29	145	22
30	124	25
31	102	35
32	095	31
33	110	09
34	113	25
35	117	22
36	159	14
37	141	10
38	139	19
39	171	15
40	134	16
41	127	20
42	127	22
43	151	19

44	145	17
45	131	23
46	165	26
47	162	23
48	177	14
49	097	09
50	106	06
51	152	08
52	159	08
53	128	31
54	093	28
55	100	28
56	127	20
57	123	26

APPENDIX E: SAMPLE DESCRIPTIONS AND LOCATIONS.

APPENDIX E

Sample Descriptions and Locations.

Sample Locations.

Ring Shear Testing:

Newman Property: 2171425; 5567600

Goldfields Subdivision: 2170650; 5567250

Hensman Subdivision: 2171700; 5567650

Point Load Testing:

Newman Property: 2171425; 5567600

Goldfields Subdivision: 2170650; 5567250

Hensman Subdivision: 2171700; 5567650

Marina Heights: 2172475; 5568250

Shear Strength Testing:

Newman Property: 2171425; 5567600

Goldfields Subdivision: 2170650; 5567250

Hensman Subdivision: 2171700; 5567650

Marina Heights: 2172475; 5568250

X-ray Diffraction Analysis:

Newman Property: 2171425; 5567600

Goldfields Subdivision: 2170650; 5567250

Hensman Subdivision: 2171700; 5567650

Field Descriptions of Deposits in the Frankton Arm Field Area.

Schist Bedrock:

Fresh to slightly weathered; moderately strong to strong; grey micaceous schist (OTAGO SCHIST Textural Zone IV).

Fresh to slightly weathered; moderately strong to strong; grey quartzofeldspathic schist (OTAGO SCHIST Textural Zone IV).

Fresh to slightly weathered; moderately strong to strong green schist (OTAGO SCHIST Textural Zone IV).

The following surficial deposits are present in places along Frankton Arm (refer figure 2.7 and figure 1.2 – map pocket):

a. Schist colluvium (landslide debris): derived from shallow or exposed bedrock, occasionally up to 1m in thickness. Slightly to highly weathered; dry to wet; loose to compact; greyish-brown; massive; medium to coarse sandy gravel with interlayered medium sand; GP. This is overlain by slightly weathered; wet; soft; greyish-brown; coarsely layered to massive; fine sandy silts with some clay; ML (Bell, 1994 unpubl.).
b. Lake Deposits:
    i) Lake silts: unweathered to slightly weathered; dry to moist; loose to compact; greenish-grey; massive; medium sands with rare fine-medium gravels; angular to sub-angular schist, sub-rounded to rounded Caples Group (Bell, 1985 unpubl.).
    ii) Beach gravels: moist; loose; brown; coarsely layered; sandy fine to medium gravel, Caples Group sub-angular to sub-rounded, angular to sub-angular schist. In places layers of medium to fine sand 50-100mm thick are present (Bell, 1997 unpubl.).
    iii) Lake sands: dry to moist; loose; brown; gravelly medium to coarse sand; gravels are angular to sub-rounded schist; sub-rounded to rounded Caples Group (Bell, 1997 unpubl.).
c. Glacial Till: unweathered to slightly weathered; dry to wet; compact; greenish-grey; massive; medium gravelly sand and sandy medium gravel with minor silt; SP-GP. 1 – 5m in thickness along Frankton Arm (Bell, 1994 unpubl.; Bell, 1997 unpubl.).
d. Alluvial Fan Gravels and Sands: damp to moist; lenses of fine to medium sand present between layers of sandy gravels and more open-textured ("fines free") gravels; gravels are of angular to sub-angular schist (Bell, 1985 unpubl.).
e. Stream Alluvium: schistose gravels, sands and rare silts. Along Frankton Arm there is only a small measure present (does not exceed 1m in thickness). Stream alluvium is reworked till material (Bell, 1989 unpubl.).

f. Topsoil: moist; firm; dark grey sandy, gravelly or clayey silt with some gravel and clay. Sometimes with schist gravels and Caples Group. Small amounts of dry; loose; gravelly sand, silty sand or sandy gravel may be present (Bell, 1997 unpubl.).

g. Filled Ground: coarse angular schists with some fines. Former highway foundations and uncompacted sidecast topsoil. Dry; loose yellow-brown gravelly sand dominated by till and colluvium (Bell, 1997 unpubl.).

APPENDIX F: LABORATORY METHODS AND DATA.

F1: Point Load Testing

F2: Shear Strength Testing

F3: Ring Shear Testing

F4: X-ray Diffraction Analysis

APPENDIX F

1. Point Load Testing

Point load testing was carried out in accordance with the ISRM "Suggested method for determining point load strength: (1995).

Specimens were tested both axially (force applied ⊥ to schistosity) and diametrically (force applied // to schistosity). For diametrical testing specimens with a length/diameter ratio greater than one are suitable for testing. Axial testing requires that the length to diameter ratio lies between 0.3 and 1.0. While for the irregular lump test, lumps of size 50± 35mm are suitable for testing. Through a hydraulic system the load is steadily increased through the platens such that failure occurs within 10-60 seconds.

Calculations

The uncorrected point load strength index (I_s) is calculated as

$$I_s = \frac{P}{D_e^2}$$

Where P = the force at which the sample breaks and D_e is the "equivalent core diameter" and is given by

$D_e^2 = D^2$ for diametrical tests
$= 4A\pi$for axial, block and lump tests:

and

A = WD = minimum cross sectional area of a plane through the platen contact points.

The size-corrected point load strength $I_{s(50)}$ is calculated by applying a "size correction factor F" where

$$I_{s(50)} = F \times I_s$$

The size correction factor can be obtained from the expression

$$F = \left(\frac{D_e}{50} \right)^{0.45}$$

APPENDIX F.

2. Shear Strength Testing.

Shear strength testing was carried out in accordance with the ISRM "Suggested Methods for Determining Shear Strength" (1981).

Specimens were tested parallel to foliation, and in all but one case, the rock tested contained a pre-existing joint plane.

Calculations.

Shear and normal stress are computed as follows:

Normal Stress $\sigma_n = \frac{P_n}{A}$

Shear Stress $\tau = \frac{P_s}{A}$

Where: P_s = total shear force;

P_n = total normal force;

A = area of shear surface overlap (corrected to account for shear displacement).

Graphs of peak shear strength vs. normal stress are presented on the following pages. The peak friction angle and cohesion of the material tested are abstracted from these graphs.

Shear Strength - Sample 1

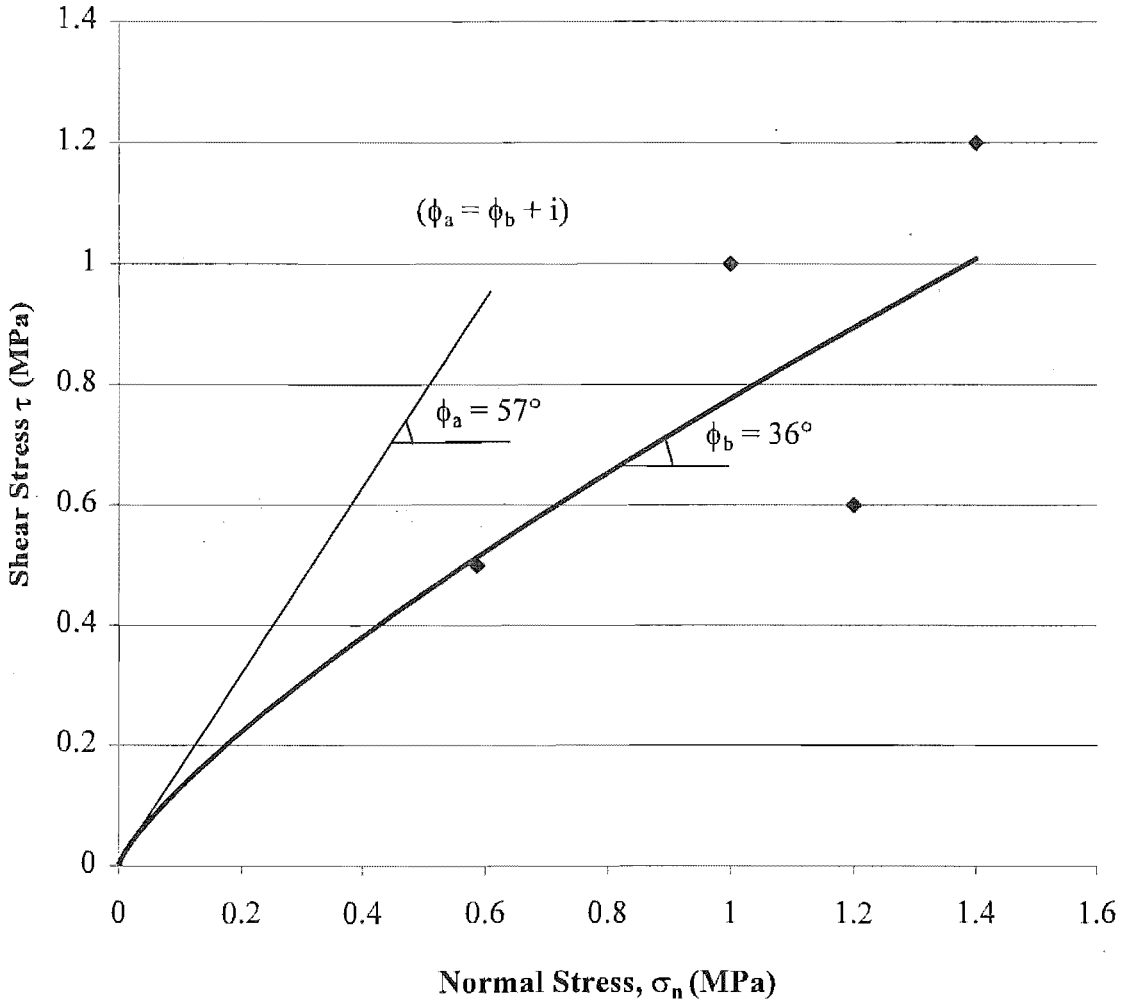

Shear Strength - Sample 3

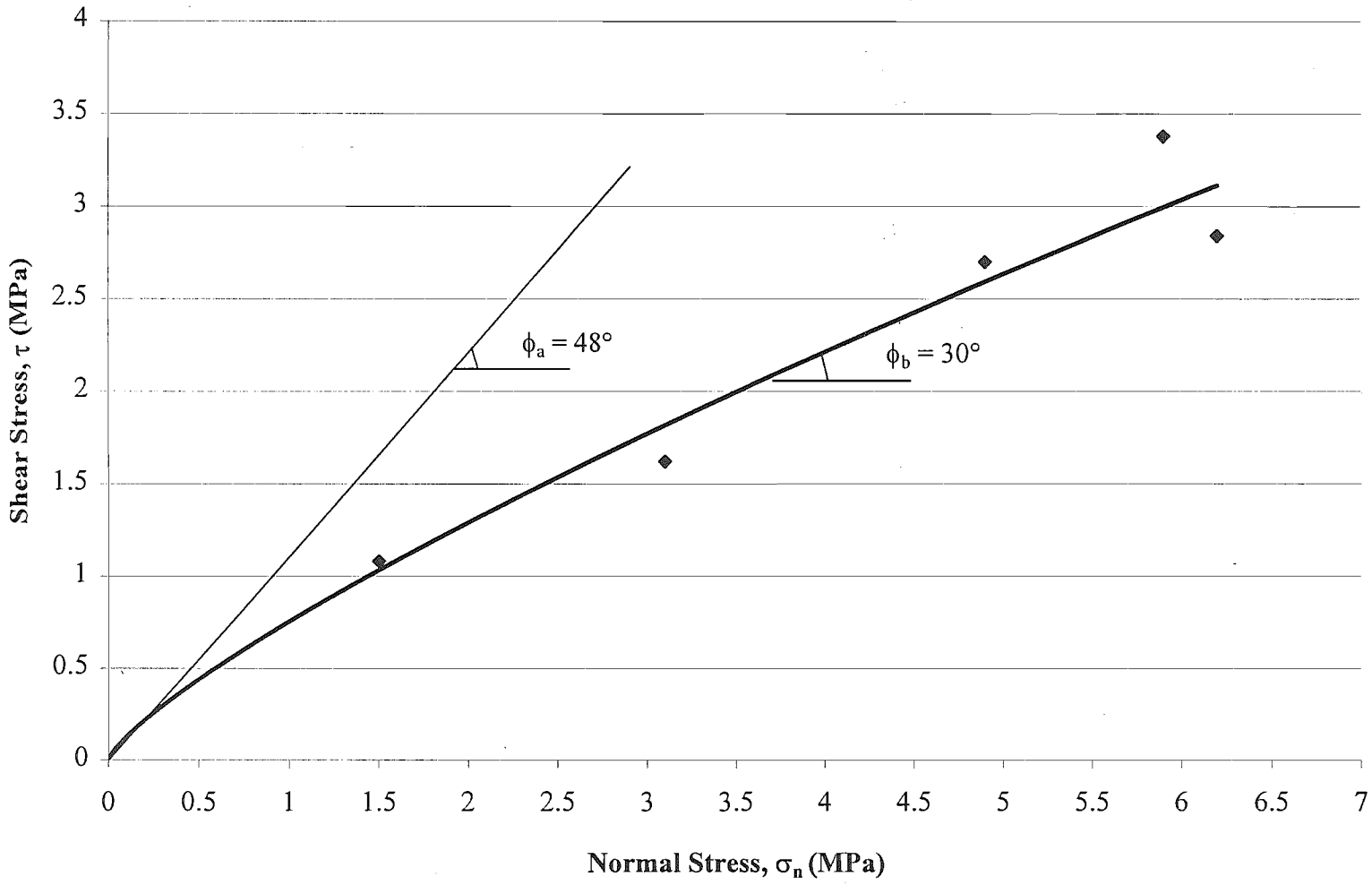

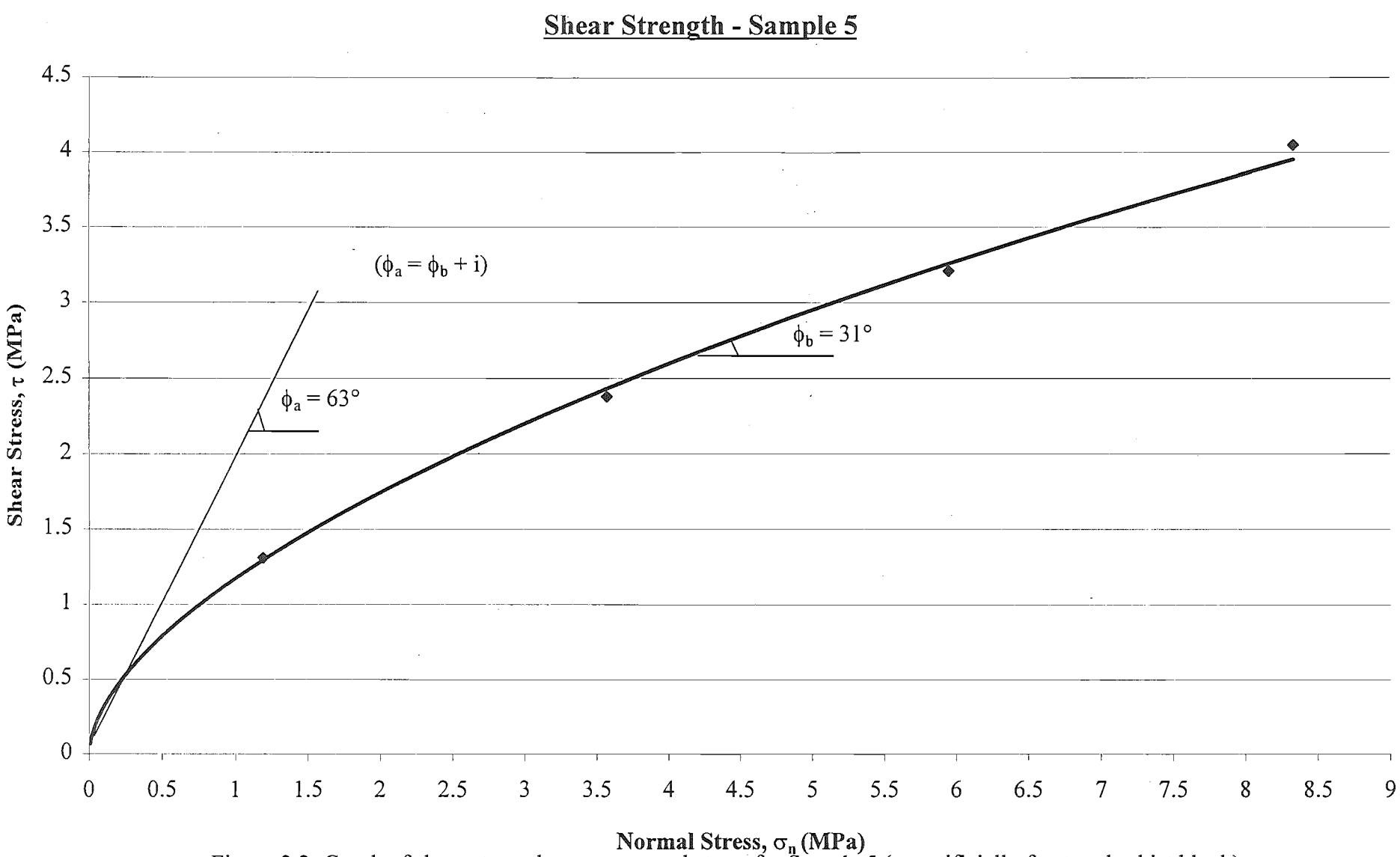

Figure 3.2: Graph of shear strength versus normal stress for Sample 5 (an artificially fractured schist block)

Shear Strength - Sample 6

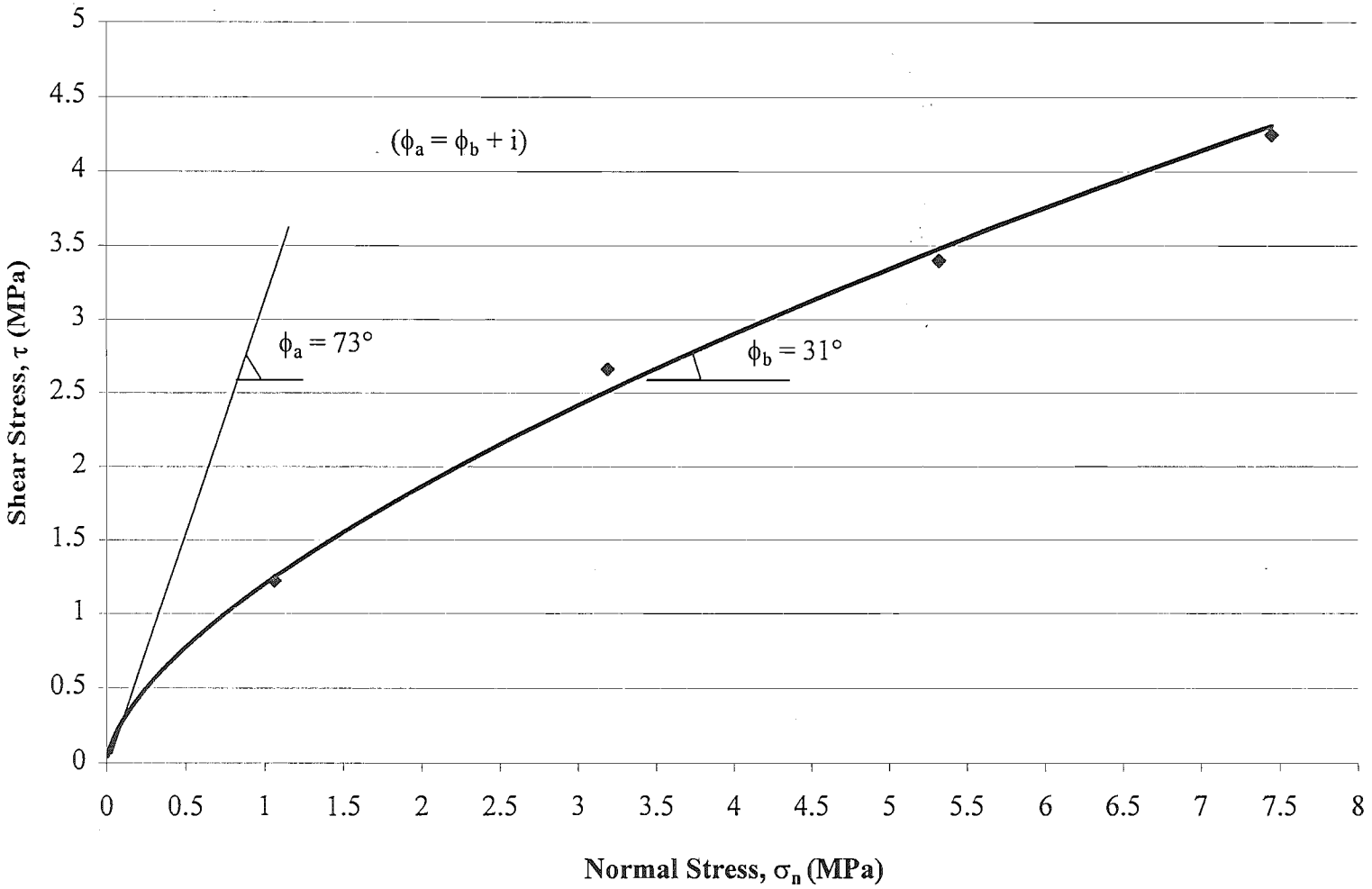

Shear Strength - Sample 7

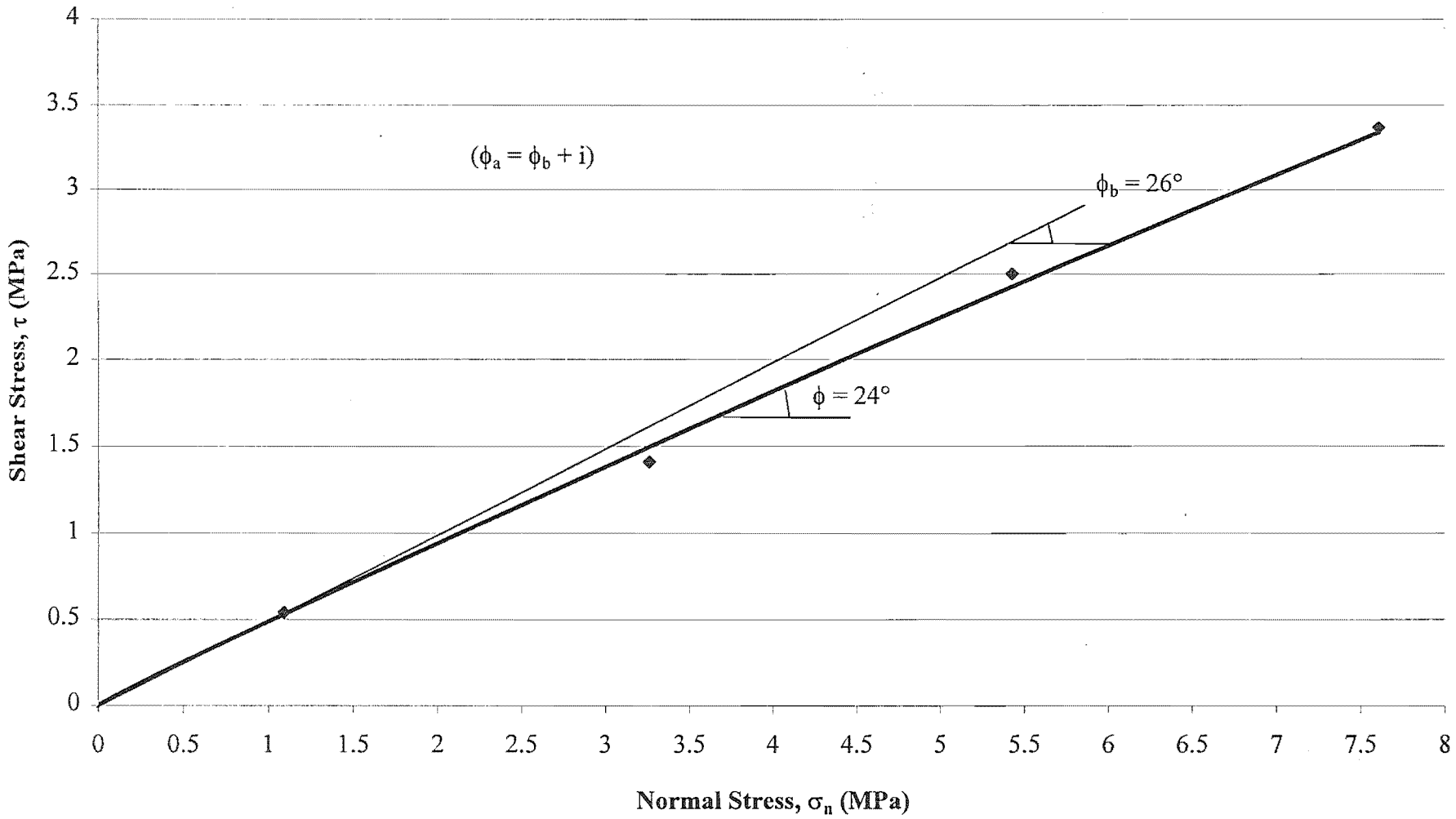

APPENDIX F.

3. Ring Shear Testing

Ring shear testing was performed on the University of Canterbury, Department of Geological Sciences' Bromhead Ring Shear (WF25850). Testing on the material was carried out at moisture contents slightly above their plastic limit. Remoulded samples are then kneaded into a lower annular ring and leveled off to the top of the mould. The upper ring is then replaced with a load hanger and a dial gauge is lowered to take an initial reading. The water bath is then filled around the sample to prevent it from drying out. A weight is placed on the hanger arm, with the specimen in the mould is being allowed to consolidate, and the total time for consolidation recorded. A shear plane is then formed by rotating the lower annular ring, 1-4 rotations within a period of approximately two minutes, whilst the upper ring is held in a fixed position by two load cells. The sample is then allowed to further consolidate so that any excess pore pressures generated during the formation of the shear plane previous step may dissipate.

The normal stress acting on the sample is calculated as follows:

$$\sigma_n = \frac{M_T + (M_w \times 10) \times g}{A \times 1000}$$

where M_T = torque arm mass = 1.143kg

M_W = Mass of hanging weight = 4-20kg in this study.

g = gravitational constant = 9.81 m / s^2

A = sample area = 4.006×10^{-3} m^2

APPENDIX F.

4. X-ray Diffraction (XRD) Analysis.

Samples were wet sieved through a 4ϕ sieve with the material passing then placed in a 1000ml pipette with 20ml of Calgon (sodium hexametaphosphate) added to prevent any flocculation of the clay particles. The pipette was then plunged for 20 seconds with a sample taken from 10cm depth after a period of 8 hours, thus representing the 9ϕ clay fraction of the sample (NZS4402:1986). Samples were then mounted on a glass slide and allowed to dry for XRD testing. Samples were analysed using a Phillips PW1729/PW1710 x-ray diffractometer. Mounts were irradiated with a Cu-anode ($Cu_{k\alpha}$ wavelength 1.5418 A°) at 50kV/40mA.

Clay analysis of the samples involved 3 scans per sample.

1. Air dried (dried at room temperature).
2. Glycolated (12 hours at 60°C in a saturated ethylene-glycol environment).
3. Fired (1 hour at 550°C).

The so called Braggs Law equation ($n\lambda = 2d \sin\theta$) gives the relationship where n=1 for first-order diffraction peaks, 2 for second order peaks etc., between: the x-ray wavelength used, λ; the atomic layer spacing between the diffracting planes, d; and half the angle between the incident x-rays and the diffracted x-rays, θ.

The XRD plots obtained are presented on the following pages with the peaks and the associated mineral identification tabulated.

Geochemistry Laboratory, Department of Geological Sciences, University of Canterbury, New Zealand

XRD Analysis

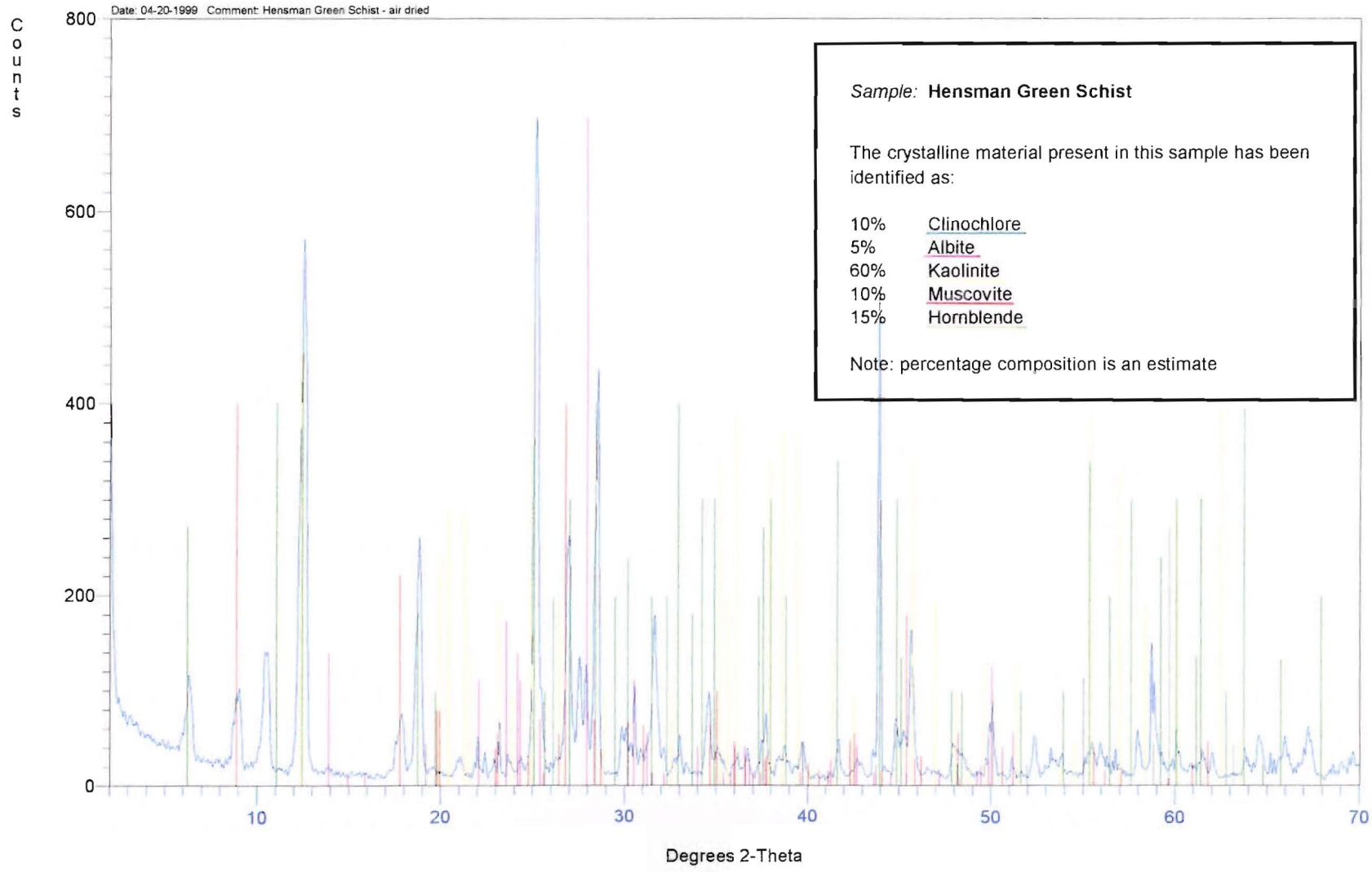

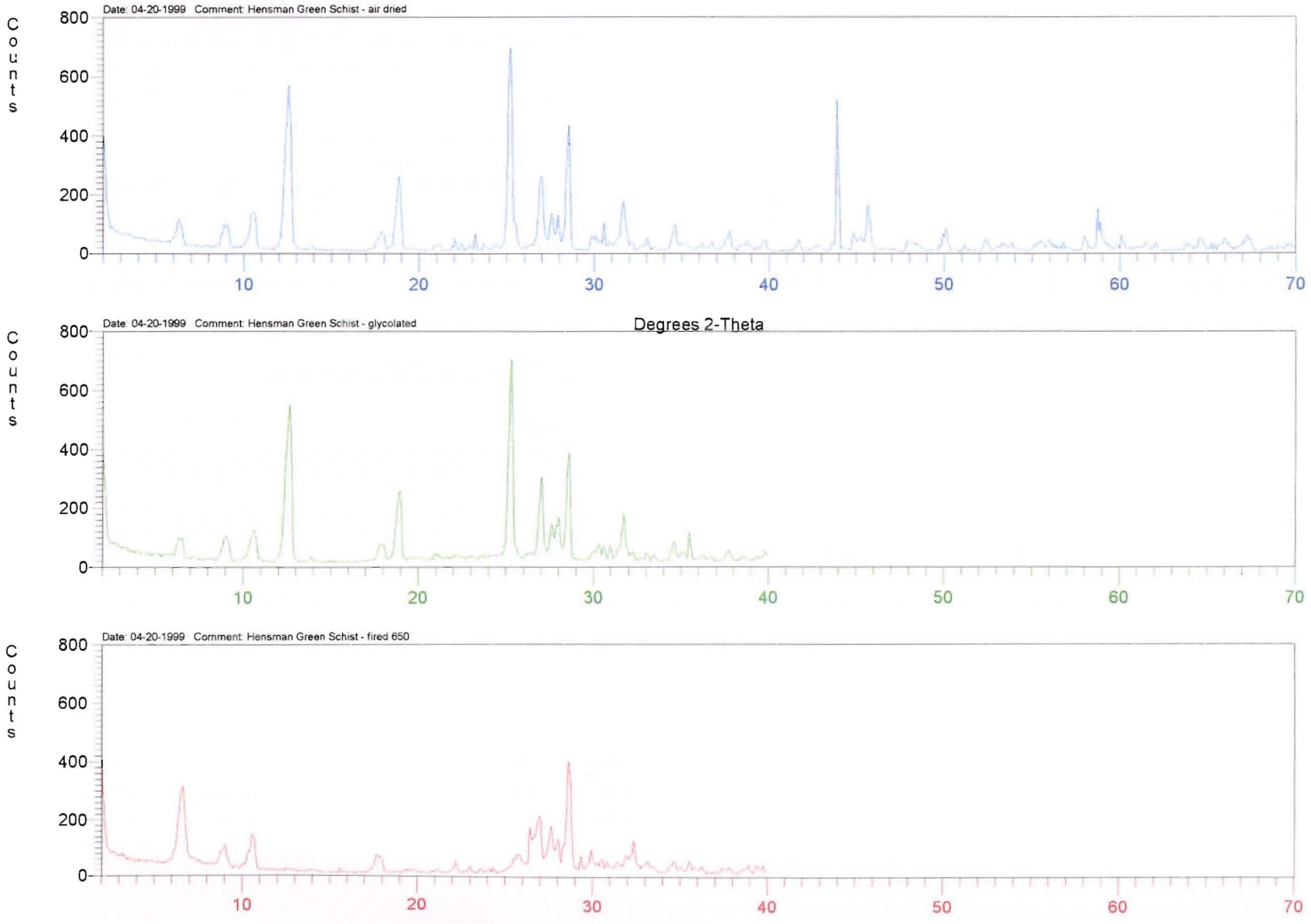
Date: 04-20-1999 Comment: Hensman Green Schist - air dried
Counts
800
600
400
200
0
10
20
30
40
50
60
70
Date: 04-20-1999 Comment: Hensman Green Schist - glycolated
Degrees 2-Theta
Date: 04-20-1999 Comment: Hensman Green Schist - fired 650

Geochemistry Laboratory, Department of Geological Sciences, University of Canterbury, New Zealand

XRD Analysis

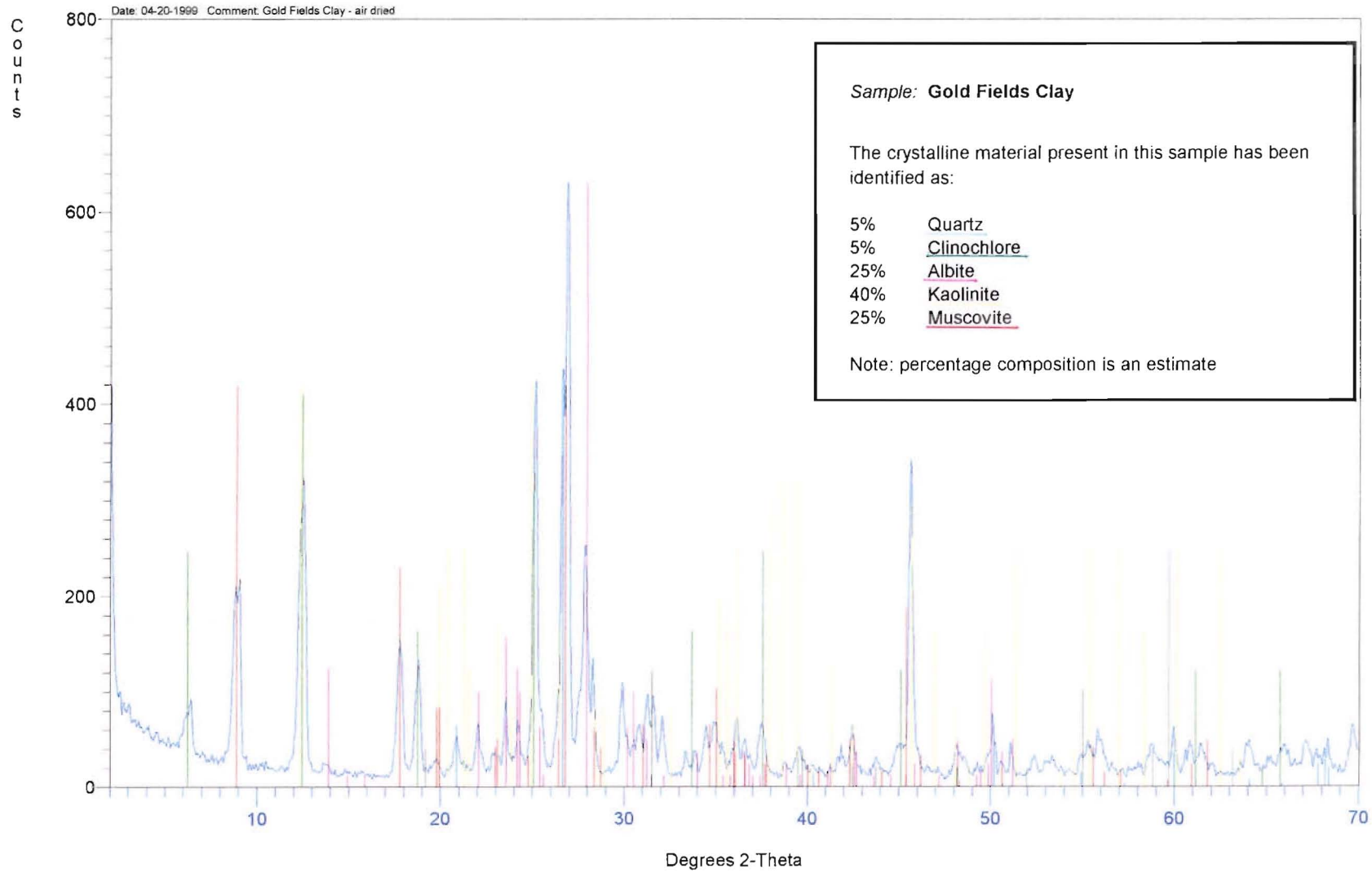

Sample: **Gold Fields Clay**

The crystalline material present in this sample has been identified as:

5%	Quartz
5%	Clinochlore
25%	Albite
40%	Kaolinite
25%	Muscovite

Note: percentage composition is an estimate

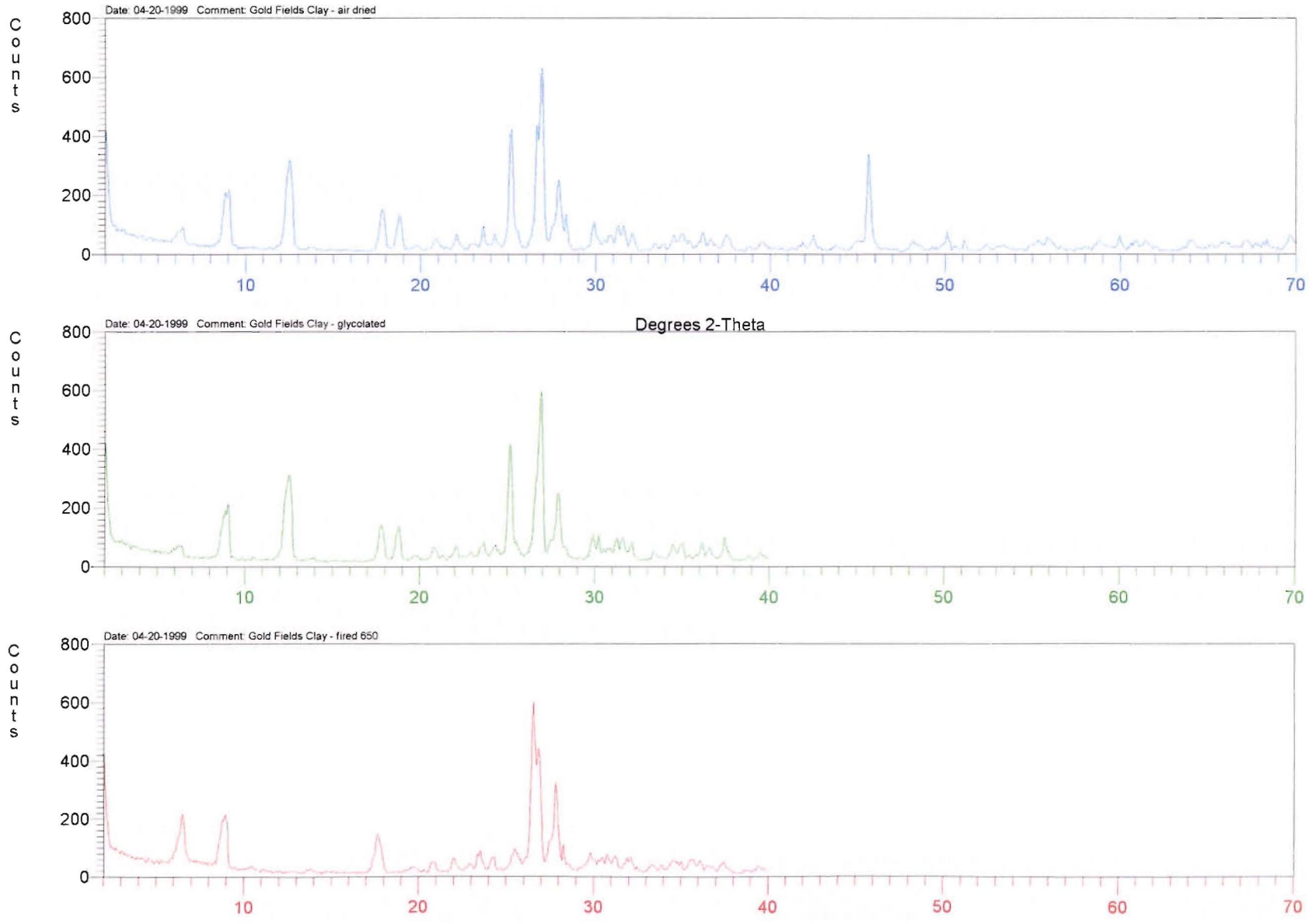
Date: 04-20-1999 Comment: Gold Fields Clay - air dried
Counts
800
600
400
200
0
10
20
30
40
50
60
70
Date: 04-20-1999 Comment: Gold Fields Clay - glycolated
Degrees 2-Theta
Counts
Date: 04-20-1999 Comment: Gold Fields Clay - fired 650
Counts

Geochemistry Laboratory, Department of Geological Sciences, University of Canterbury, New Zealand

XRD Analysis

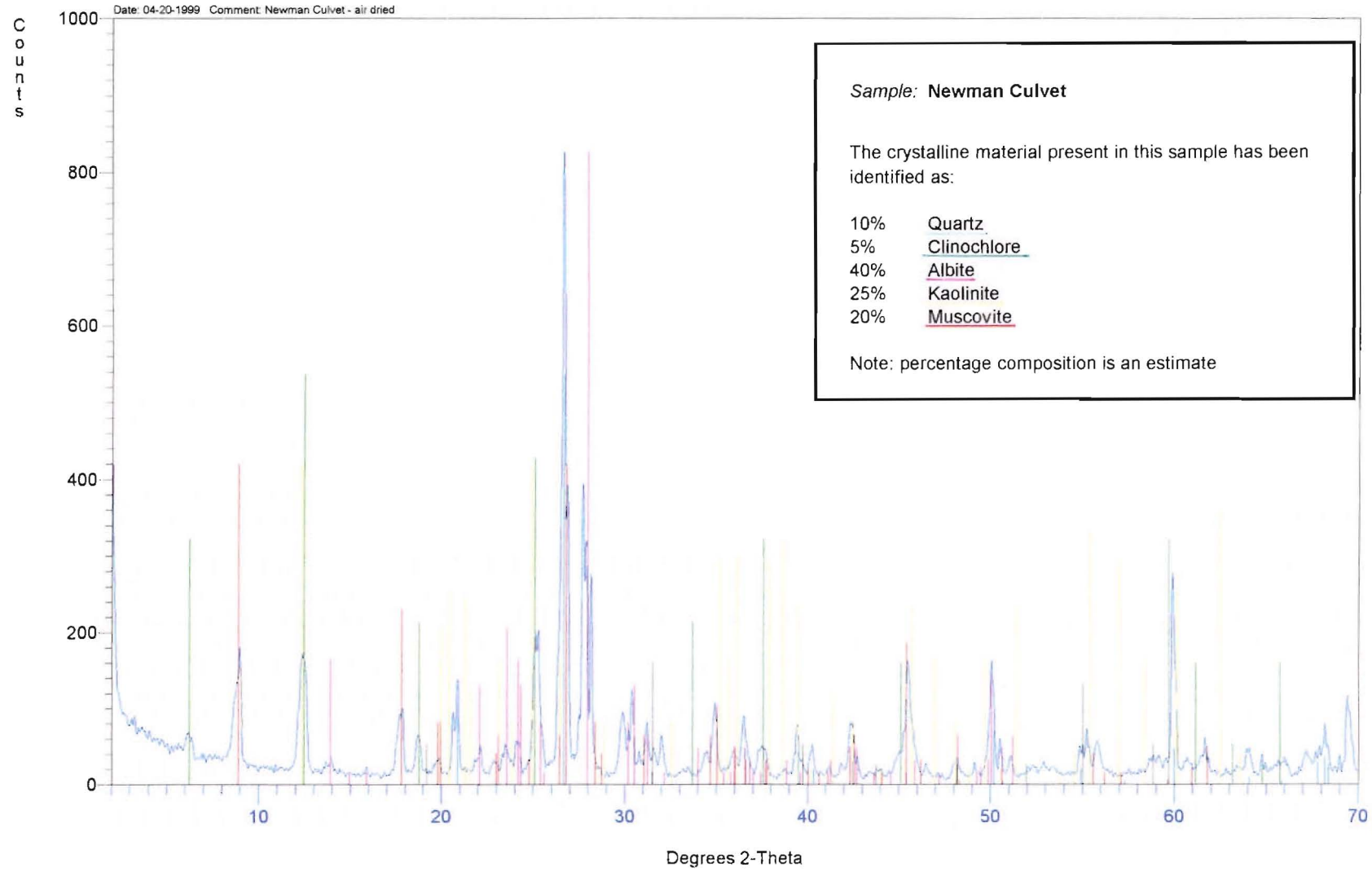

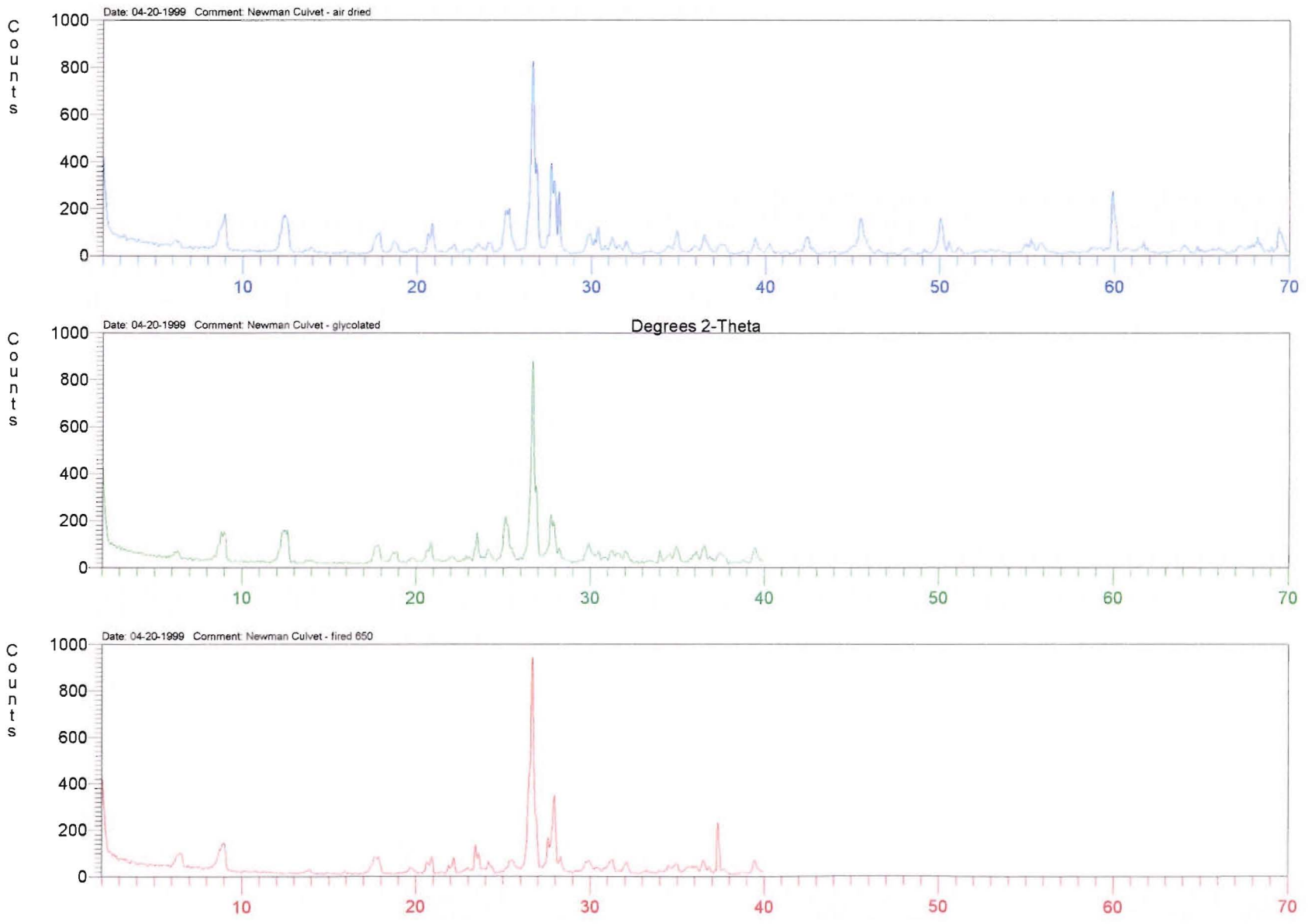
Date: 04-20-1999 Comment: Newman Culvet - air dried
Counts
1000
800
600
400
200
0
10
20
30
40
50
60
70
Date: 04-20-1999 Comment: Newman Culvet - glycolated
Degrees 2-Theta
Date: 04-20-1999 Comment: Newman Culvet - fired 650

Geochemistry Laboratory, Department of Geological Sciences, University of Canterbury, New Zealand

XRD Analysis

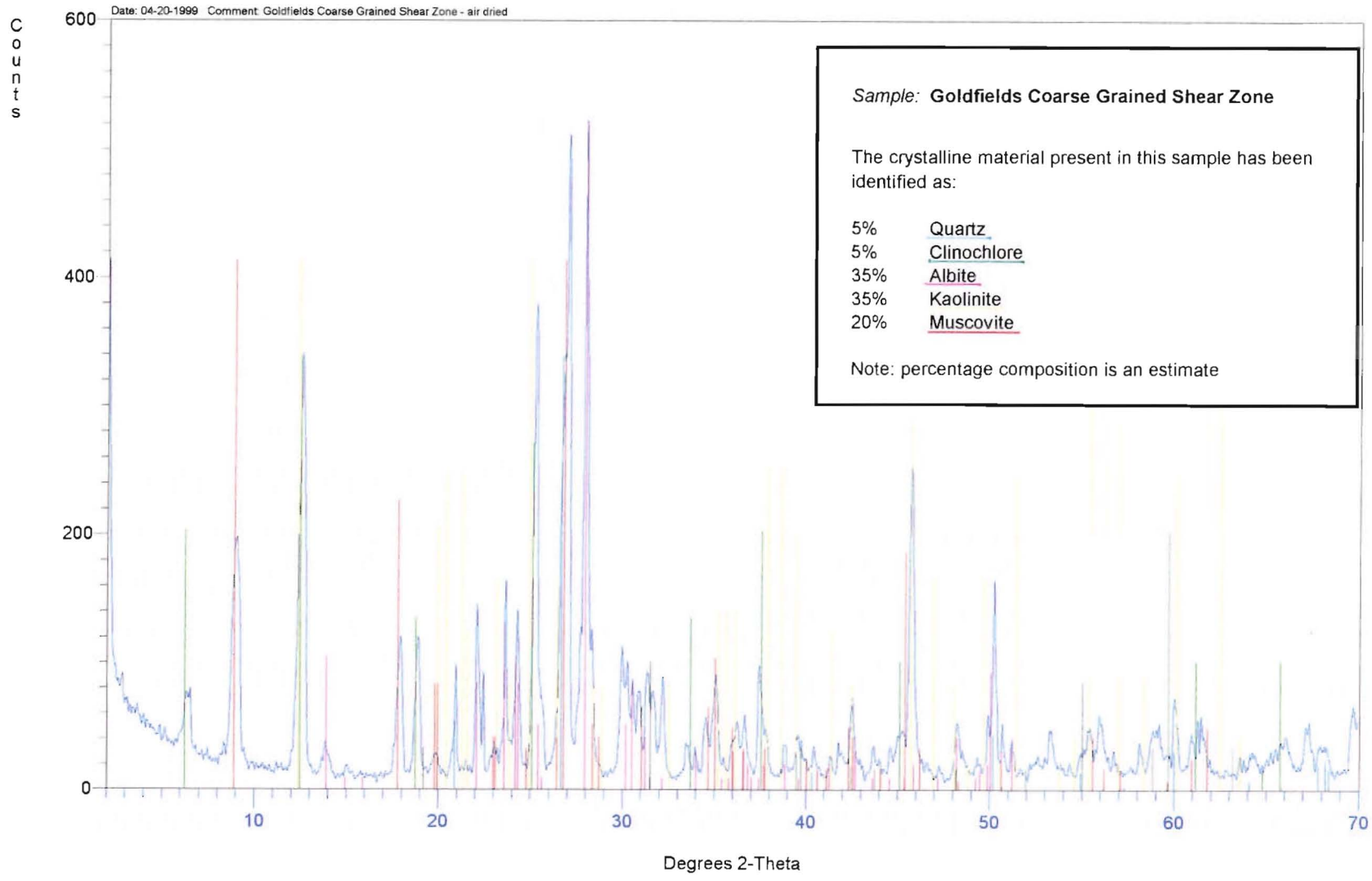

Sample: **Goldfields Coarse Grained Shear Zone**

The crystalline material present in this sample has been identified as:

5%	Quartz
5%	Clinochlore
35%	Albite
35%	Kaolinite
20%	Muscovite

Note: percentage composition is an estimate

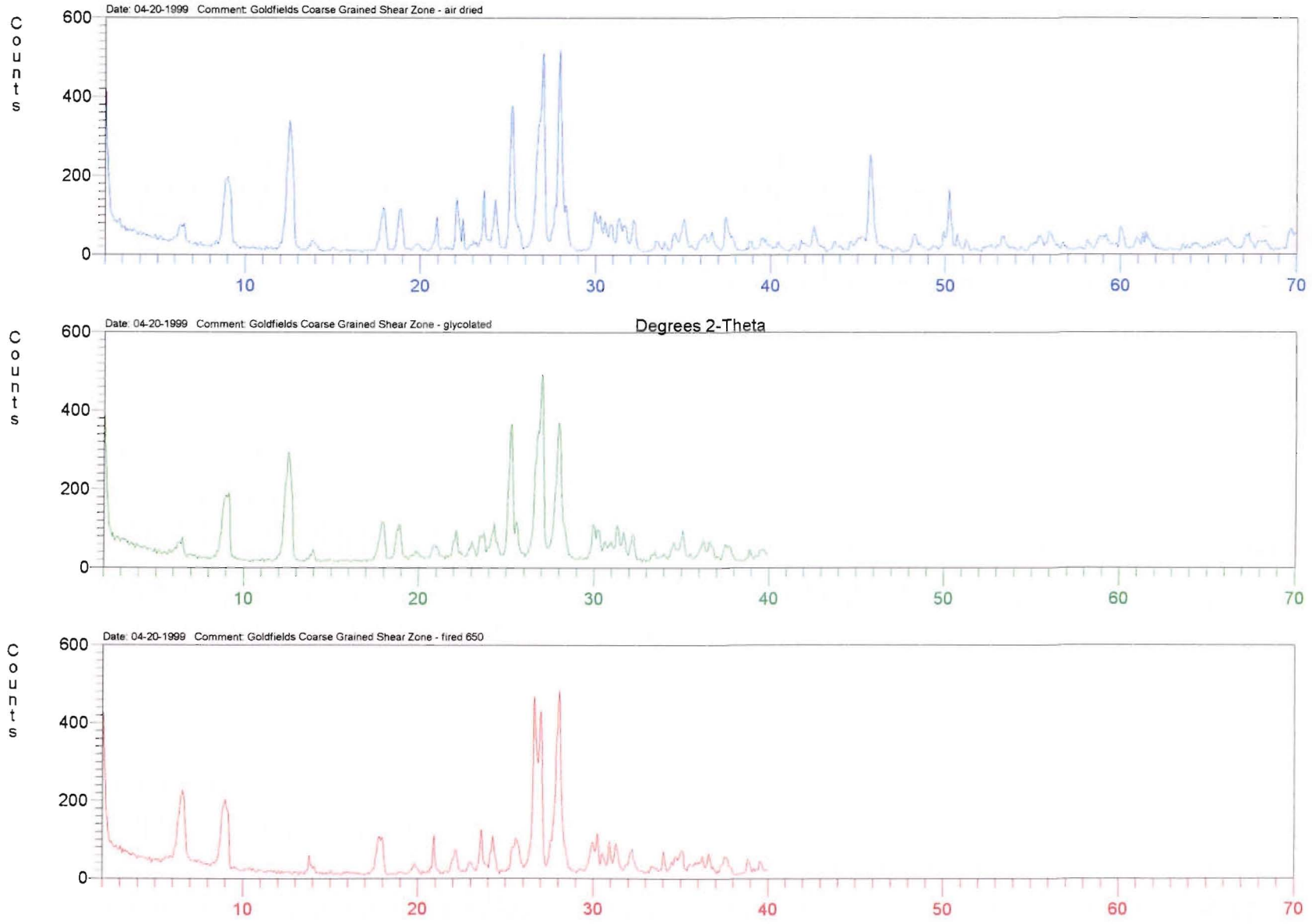
Date: 04-20-1999 Comment: Goldfields Coarse Grained Shear Zone - air dried
Counts
600
400
200
0
10
20
30
40
50
60
70
Date: 04-20-1999 Comment: Goldfields Coarse Grained Shear Zone - glycolated
Degrees 2-Theta
Counts
Date: 04-20-1999 Comment: Goldfields Coarse Grained Shear Zone - fired 650
Counts

Geochemistry Laboratory, Department of Geological Sciences, University of Canterbury, New Zealand

XRD Analysis

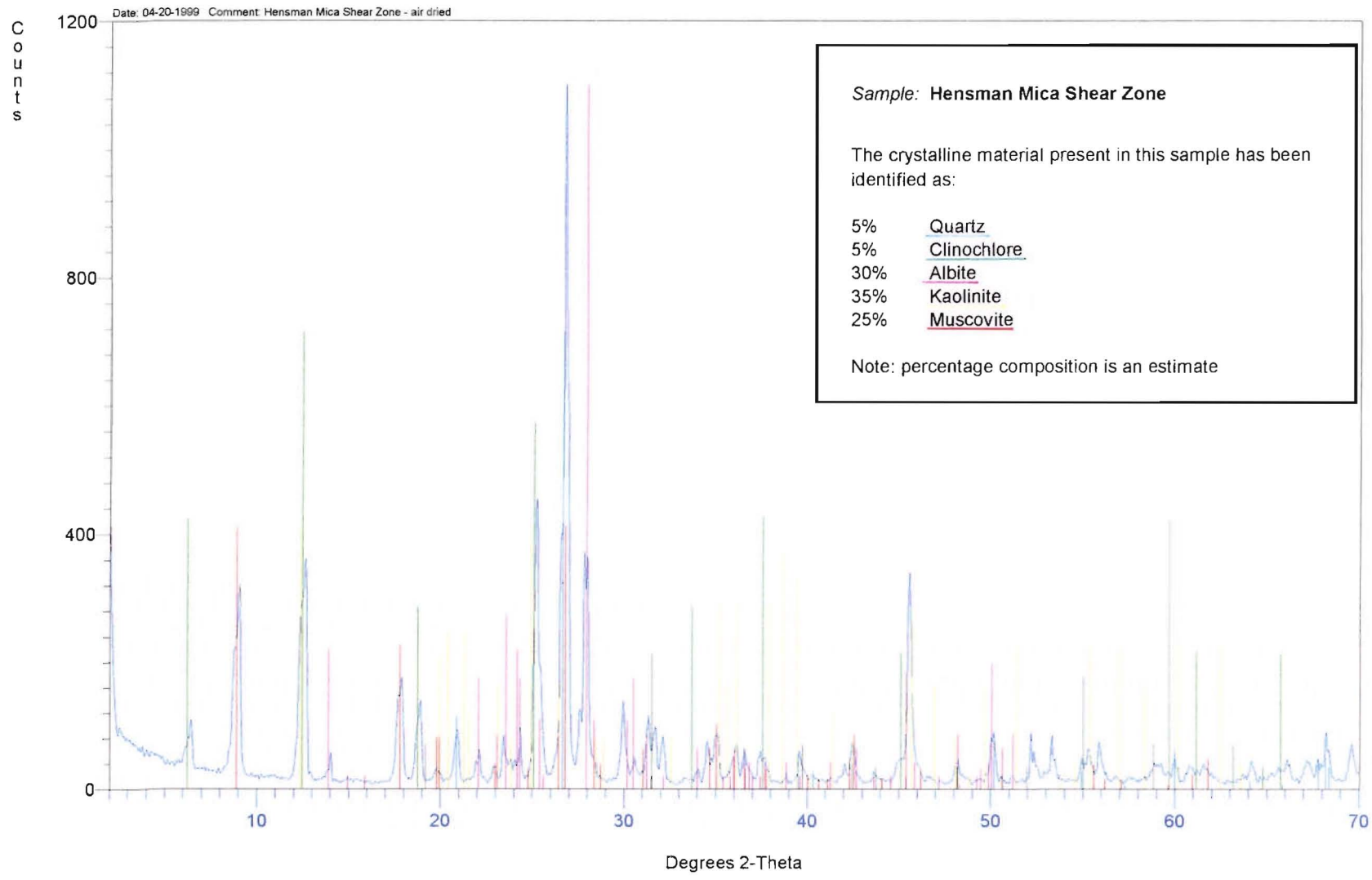

Sample: **Hensman Mica Shear Zone**

The crystalline material present in this sample has been identified as:

5%	Quartz
5%	Clinochlore
30%	Albite
35%	Kaolinite
25%	Muscovite

Note: percentage composition is an estimate

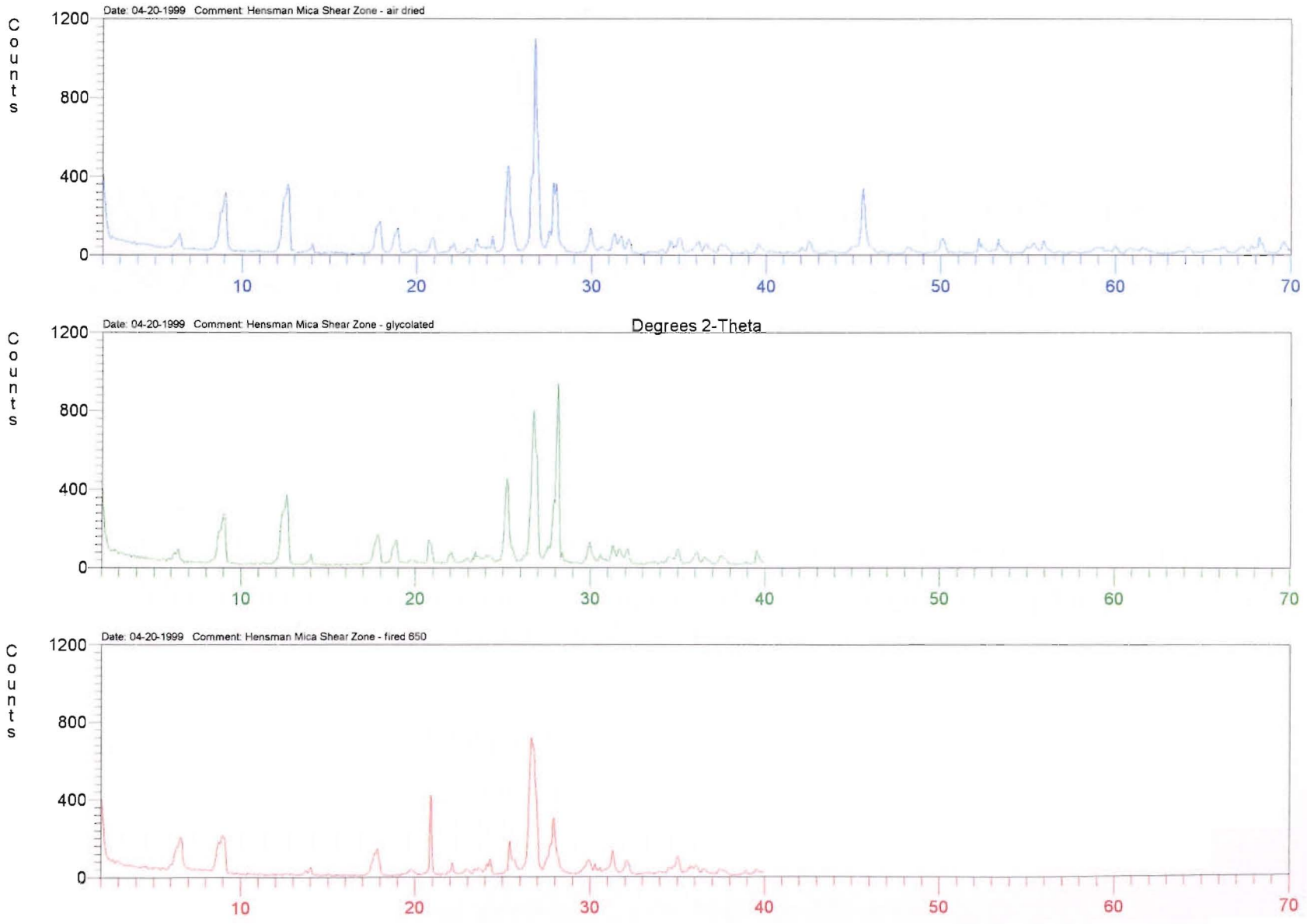
Date: 04-20-1999 Comment: Hensman Mica Shear Zone - air dried
Counts
1200
800
400
0
10
20
30
40
50
60
70
Date: 04-20-1999 Comment: Hensman Mica Shear Zone - glycolated
Degrees 2-Theta
Date: 04-20-1999 Comment: Hensman Mica Shear Zone - fired 650

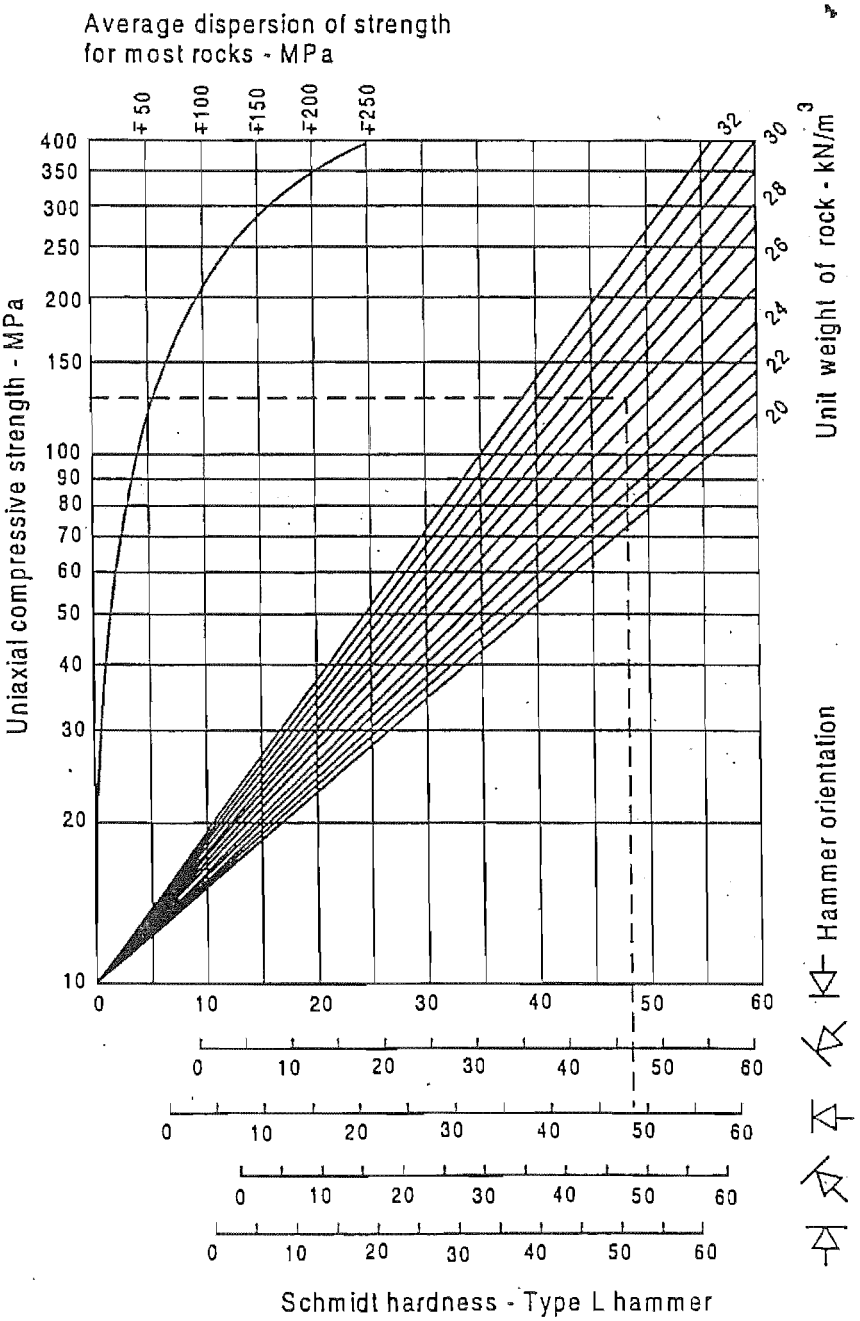
Average dispersion of strength
for most rocks - MPa
∓50
∓100
∓150
∓200
∓250
Uniaxial compressive strength - MPa
400
350
300
250
200
150
100
90
80
70
60
50
40
30
20
10
Unit weight of rock - kN/m3
32
30
28
26
24
22
20
Hammer orientation
0 10 20 30 40 50 60
Schmidt hardness - Type L hammer

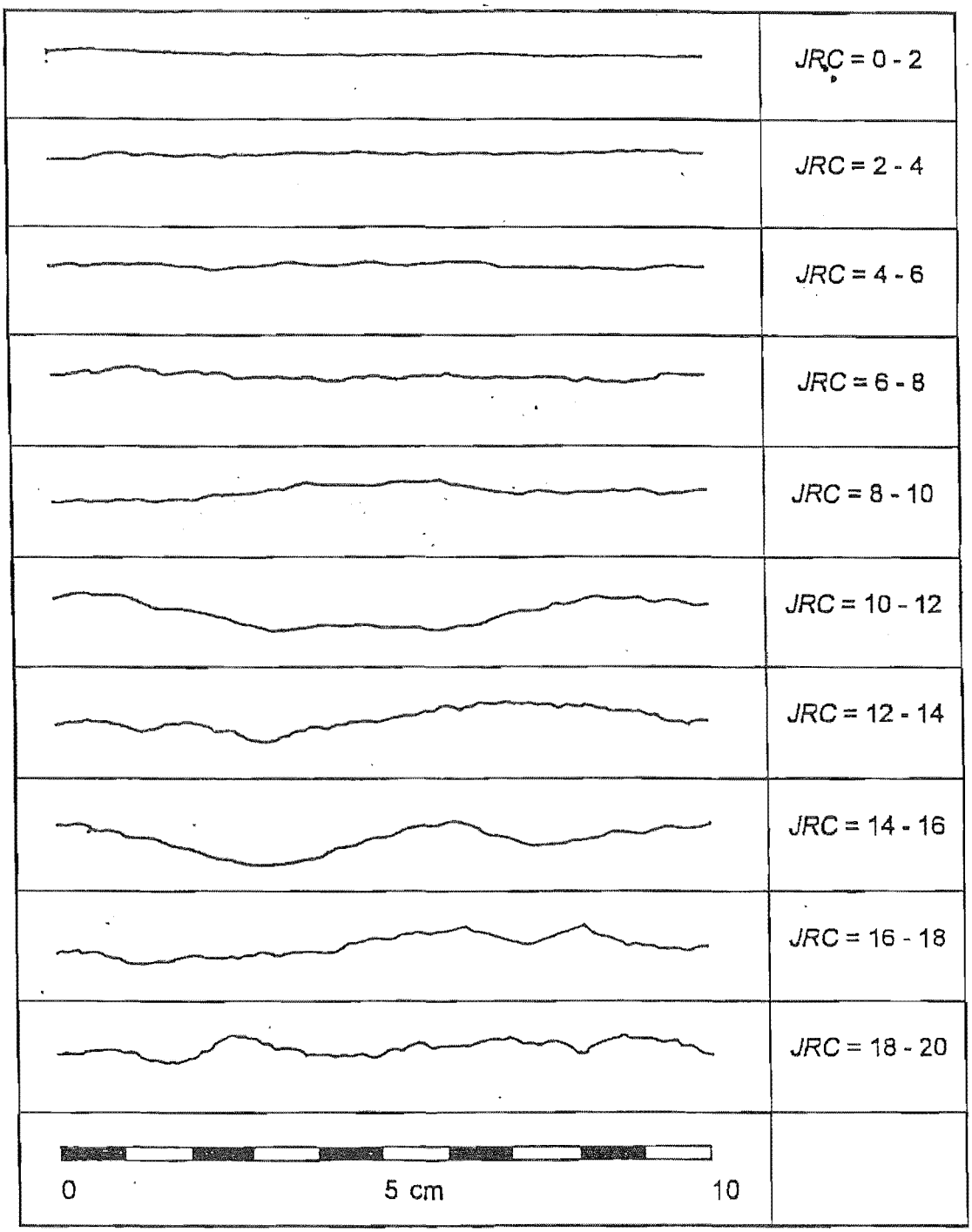
JRC = 0 - 2
JRC = 2 - 4
JRC = 4 - 6
JRC = 6 - 8
JRC = 8 - 10
JRC = 10 - 12
JRC = 12 - 14
JRC = 14 - 16
JRC = 16 - 18
JRC = 18 - 20
0
5 cm
10

APPENDIX G: STEREOGRAPHIC PROJECTION TECHNIQUES.

APPENDIX G.

1. The Fisher Distribution

Under the Fisher method each pole is assigned a normal influence (or Fisher Distribution), rather than a point value as in the Schmidt method. The real advantage of the Fisher method over the Schmidt method is that it smoothes density plots for sparse data sets (Hoek and Diederichs, 1989).

2. The Schmidt Distribution.

In the Schmidt method, each pole is assigned a constant influence value of 1. The integrated zone of influence is a cylinder of constant height with a radius equal to the radius of the counting circle. A counting grid is superimposed on the stereonet plane. The counting circle has an area equivalent to 1% of the lower hemisphere surface. For each pole plotted, any grid point falling within a circle of arbitrary constant radius centred on this pole is incremented by the value of the pole. After the influence of all plotted poles are so distributed, the density plotted at each grid point is calculated by dividing the pole count at that grid point by the total pole influence (Hoek and Diederichs, 1989).

APPENDIX H: LANDSLIDE TERMINOLOGY AND VELOCITY SCALE.

APPENDIX H : DEFINITIONS OF LANDSLIDE FEATURES.

NUMBER	NAME	DEFINITION
1	Crown	Practically undisplaced material adjacent of highest parts of main scarp
2	Main scarp	Steep surface on undisturbed ground at upper edge of landslide caused by movement of displaced material (13, stippled area) away from undisturbed ground; it is visible part of surface of rupture.
3	Top	Highest point of contact between displaced material (13) and main scarp (2)
4	Head	Upper parts of landslide along contact between displaced material and main scarp (2)
5	Minor scarp	Steep surface on displaced material of landslide produced by differential movements within displaced material
6	Main body	Part of displaced material of landslide that overlies surface of rupture between main scarp (2) and toe of surface of rupture (11)
7	Foot	Portion of landslide that has moved beyond toe of surface of rupture (11) and overlies original ground surface (20)
8	Tip	Point on toe (9) farthest from top (3) of landslide
9	Toe	Lower, usually curved margin of displaced material of a landslide, most distant from main scarp (2)
10	Surface of rupture	Surface that forms (or that has formed) lower boundary of displaced material (13) below original ground surface (20); mechanical idealisation of surface of rupture is called *slip surface* in Chapter 13
11	Toe of surface of rupture	Intersection (usually buried) between lower part of surface of rupture (10) of a landslide and original ground surface (20)
12	Surface of separation	Part of original ground surface (20) now overlain by foot (7) of landslide
13	Displaced material	Material displaced from its original position on slope by movement in landslide; forms both depleted mass (17) and accumulation (18); it is stippled in Figure 3-4
14	Zone of depletion	Area of landslide within which displaced material (13) lies below original ground surface (20)
15	Zone of accumulation	Area of landslide within which displaced material lies above original ground surface (20)
16	Depletion	Volume bounded by main scarp (2), depleted mass (17), and original ground surface (20)
17	Depleted mass	Volume of displaced material that overlies surface of rupture (10) but underlies original ground surface (20)
18	Accumulation	Volume of displaced material (13) that lies above original ground surface (20)
19	Flank	Undisplaced material adjacent to sides of surface of rupture; compass directions are preferable in describing flanks, but if left and right are used, they refer to flanks as viewed from crown
20	Original ground surface	Surface of slope that existed before landslide took place

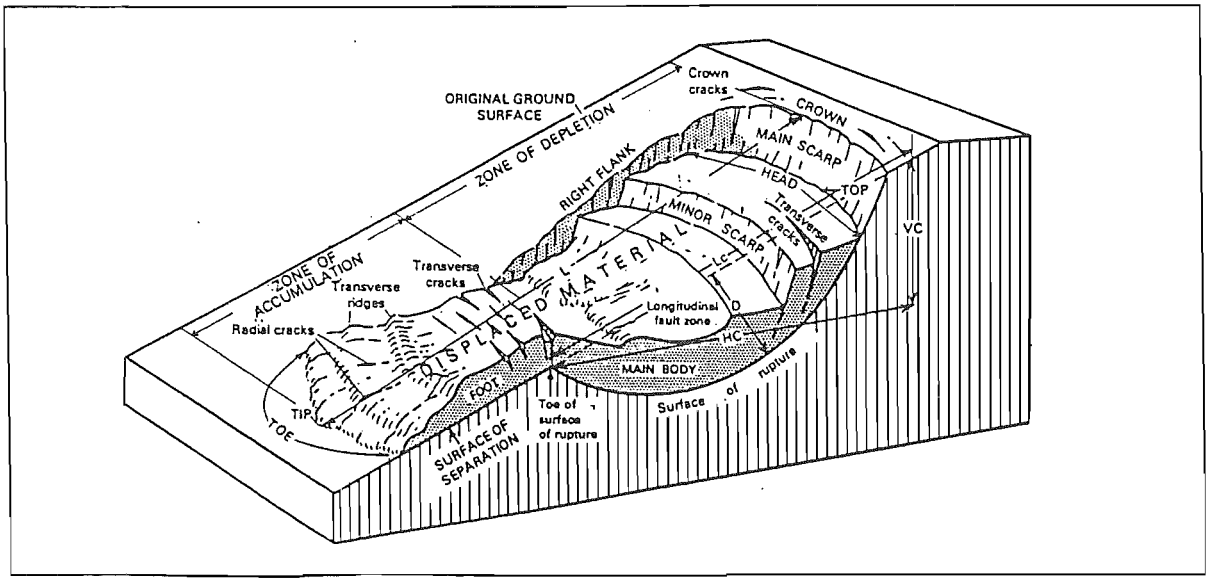

APPENDIX H.

Proposed landslide velocity scale (Cruden and Varnes, 1996).

Velocity Class	Description	Velocity (mm/sec)	Typical Velocity
7	Extremely Rapid	5×10^{3}	5 m/sec
6	Very Rapid	5×10^{1}	3 m/min
5	Rapid	5×10^{-1}	1.8 m/hr
4	Moderate	5×10^{-3}	13 m/month
3	Slow	5×10^{-5}	1.6 m/year
2	Very Slow	5×10^{-7}	16 mm/year
1	Extremely Slow		

APPENDIX I: CONFIDENCE INTERVAL DETERMINATION GRAPH.

APPENDIX I.
CONFIDENCE INTERVAL GRAPH.

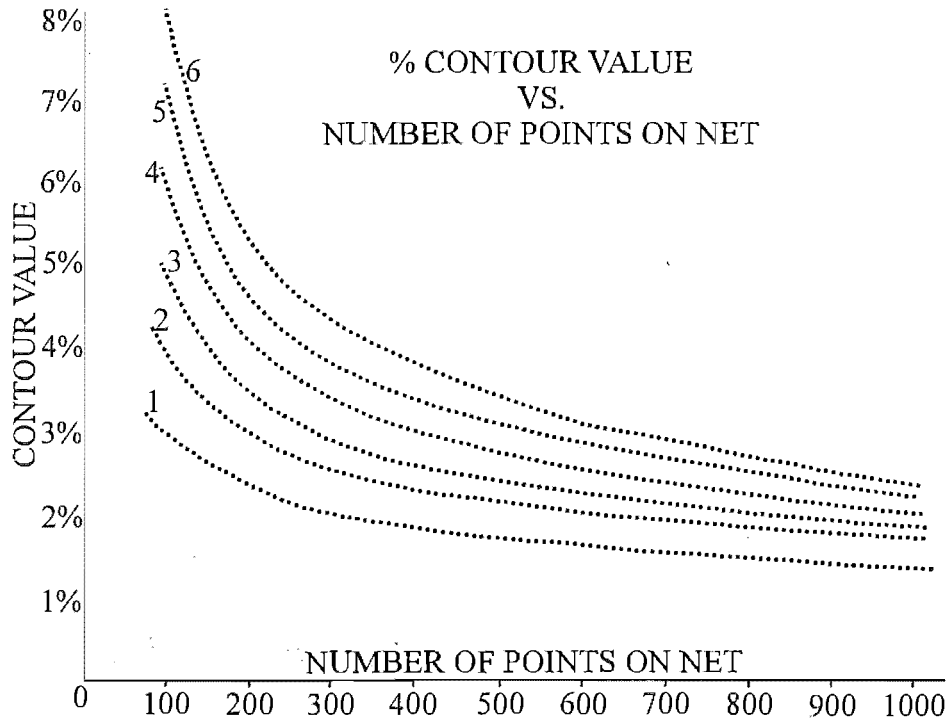

Probability levels for different contour values with respect to sample size. These curves give Poisson expected cell-value frequencies for 100-point to 1000-point sample sizes.

Curve Number	Cell Probability	Net Probability	Cell frequency on random-diagrams for each contour value giving this probability
1	0.05	5.0	5 per diagram
2	0.01	1.0	1 per diagram
3	0.005	0.5	1 for 2 diagrams
4	0.0005	0.05	1 for 20 diagrams
5	0.0001	0.01	1 for 100 diagrams
6	0.00001	0.001	1 for 1000 diagrams

If a diagram contains one or more cells corresponding to a 0.01 per net probability, it may be significant; if it contains one or more corresponding to a 0.001 per net probability, it is probably significant.

APPENDIX J: GEOLOGICAL TIME SCALE.

APPENDIX J.

GEOLOGICAL TIME SCALE

Eras of time	Periods of time	Epochs of time (Cenozoic era only)	Age (millions of years)	Duration (millions of years)
Cenozoic	Quaternary	Recent		2
		Pleistocene	2	
	Tertiary	Pliocene	5	23
		Miocene	25	
		Oligocene	38	40
		Eocene	55	
		Paleocene	65	
Mesozoic	Cretaceous			79
	Jurassic		144	69
	Triassic		213	35
Paleozoic	Permian			38
	Carboniferous		286	88
	Devonian		360	48
	Silurian		408	30
	Ordovician		438	67
	Cambrian		505	85
Precambrian			590	
			590-4000	3520

APPENDIX K: GRAIN SIZE ANALYSIS DATA.

Grain Size Analysis of Sand, Silt and Clay

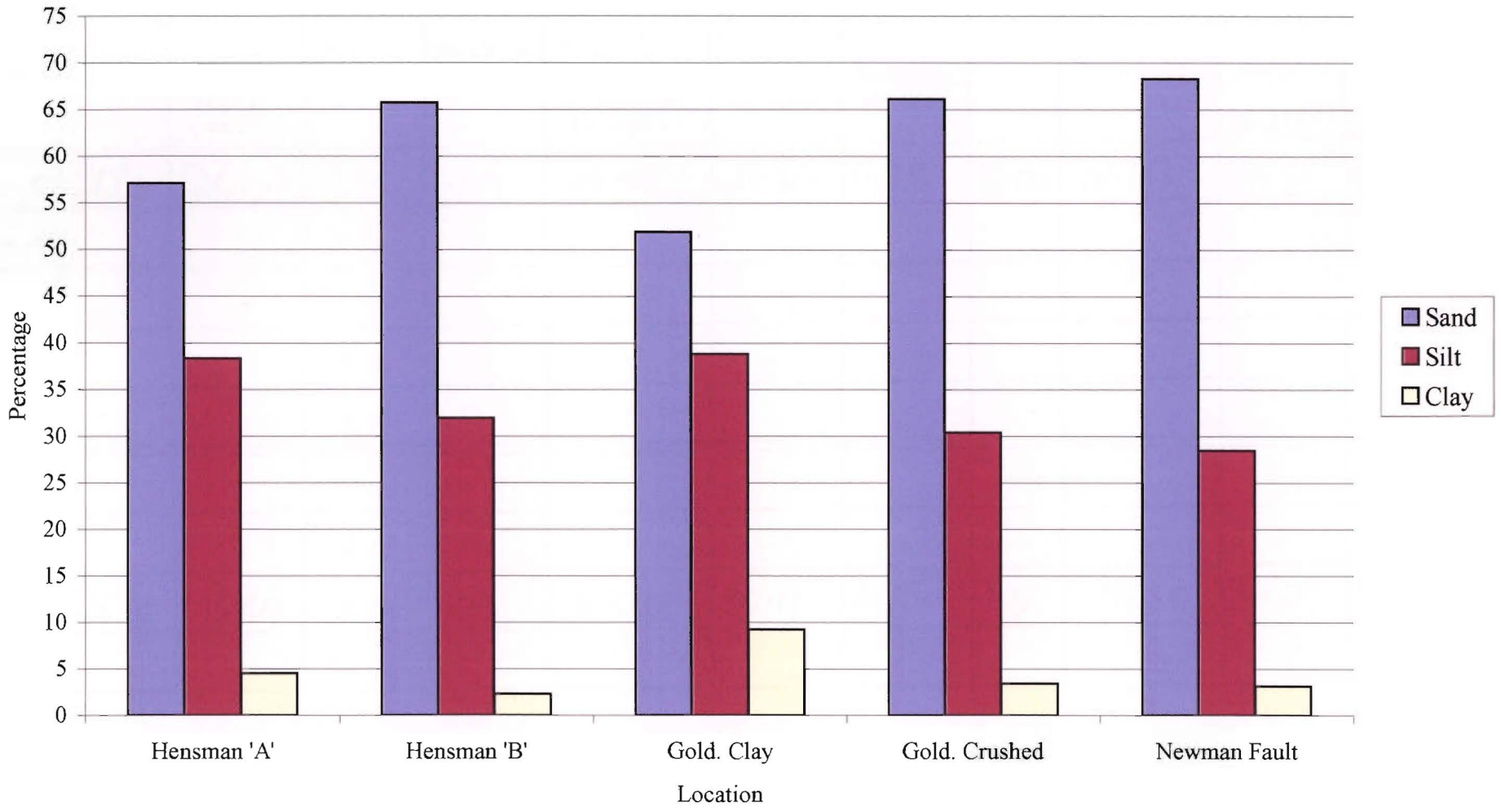

GOLD CLAY

DATA SHEET FOR PIPETTE ANALYSIS

Sample No. 4

Peptizer Calgon Amount peptizer for for 1000 ml. 20 MS ~~gms~~ Mud _____ gms

Diameter ø	Temp.	Withdrawal depth (cm)	Time	Beaker No.	Wt. sample + beaker in gms.	Weight beaker in gms	Weight sample in gms	X50	Weight Fraction	Cumul. weight 42.09	Cumul. percent 51.90%
+ 4.0	20°C	20CM	20 s.	4A	29.98	29.20	0.78	39.00	31.50	73.59	90.75%
+ 4.5			2 m.								
+ 5.0			4 m.								
+ 5.5			8 m.								
+ 6.0			15 m.								
+ 7.0			30 m.								
+ 8.0			2 hr								
+ 9.0	20°C	10CM	8 hr	4B	30.26	30.11	0.15	7.50	7.50	81.09	100%
+10.0			32 hr								

SAND 51.90%
SILT 38.85%
CLAY 9.25%

USHER G.

DATA SHEET FOR PIPETTE ANALYSIS

Sample No. 5.

Peptizer Calgon. Amount peptizer for for 1000 ml. 20 m/s. ~~gms~~ Mud _____ gms

Diameter ø	Temp.	Withdrawal depth (cm)	Time	Beaker No.	Wt. sample + beaker in gms.	Weight beaker in gms	Weight sample in gms	X50	Weight Fraction	Cumul. weight 67.38	Cumul. percent 66.13%
+ 4.0	20°C	20CM	20 s.	SA	28.09	27.40	0.69	34.50	31.00	98.38	96.56%
+ 4.5			2 m.								
+ 5.0			4 m.								
+ 5.5			8 m.								
+ 6.0			15 m.								
+ 7.0			30 m.								
+ 8.0			2 hr								
+ 9.0	20°C	10CM.	8 hr	SB	27.67	27.60	0.07	3.50	3.50	101.88	100%
+10.0			32 hr								

SAND 66.13%
SILT 30.43%
CLAY 3.44%

HENSMAN SHEAR ZONE 'A'

DATA SHEET FOR PIPETTE ANALYSIS

Sample No. 2

Peptizer Calgon Amount peptizer for for 1000 ml. 20 M/S gms Mud _____ gms

Diameter ø	Temp.	Withdrawal depth (cm)	Time	Beaker No.	Wt. sample + beaker in gms.	Weight beaker in gms	Weight sample in gms	X50	Weight Fraction	Cumul. weight 37.92	Cumul. percent 57.09%
+ 4.0	20°C	20CM	20 s.	2A	28.15	27.58	0.57	28.50	25.50	63.42	95.48%
+ 4.5			2 m.								
+ 5.0			4 m.								
+ 5.5			8 m.								
+ 6.0			15 m.								
+ 7.0			30 m.								
+ 8.0			2 hr								
+ 9.0	20°C	10CM	8 hr	2B	32.00	31.94	0.06	3.00	3.00	66.42	100%
+10.0			32 hr								

SAND 57.09%
SILT 38.39%
CLAY 4.52%

HENSMAN SHEAR ZONE 'B'

DATA SHEET FOR PIPETTE ANALYSIS

Sample No. 3.

Peptizer Calgon Amount peptizer for for 1000 ml. 20M/S gms Mud _____ gms

Diameter ø	Temp.	Withdrawal depth (cm)	Time	Beaker No.	Wt. sample + beaker in gms.	Weight beaker in gms	Weight sample in gms	X50	Weight Fraction	Cumul. weight 43.17	Cumul. percent 65.73%
+ 4.0	20°C	20 CM	20 s.	3A	28.87	28.42	0.45	22.50	21.00	64.17	97.71%
+ 4.5			2 m.								
+ 5.0			4 m.								
+ 5.5			8 m.								
+ 6.0			15 m.								
+ 7.0			30 m.								
+ 8.0			2 hr								
+ 9.0	20°C	10 CM.	8 hr	3B	27.32	27.29	0.03	1.50	1.50	65.67	100%
+10.0			32 hr								

SAND 65.73%
SILT 31.98%
CLAY 2.29%

NEWMAN S. CULVERT.

DATA SHEET FOR PIPETTE ANALYSIS

Sample No. 1

Peptizer Calgon Amount peptizer for for 1000 ml. 20 ~~gms~~ Mud _____ gms

Diameter ø	Temp.	Withdrawal depth (cm)	Time	Beaker No.	Wt. sample + beaker in gms.	Weight beaker in gms	Weight sample in gms	X50	Weight Fraction	Cumul. weight 75.39	Cumul. percent 68.29%
+ 4.0	20°C	20cm	20 s.	1A	29.74	29.04	0.70	35.00	31.50	106.89	96.82%
+ 4.5			2 m.								
+ 5.0			4 m.								
+ 5.5			8 m.								
+ 6.0			15 m.								
+ 7.0			30 m.								
+ 8.0			2 hr								
+ 9.0	20°C	10cm	8 hr	1B	31.59	31.52	0.07	3.50	3.50	110.89	100%
+10.0			32 hr								

SAND 68.29%
SILT 28.53%
CLAY 3.18%

APPENDIX L: SENSITIVITY ANALYSIS DATA.

Analysis of Plane Failure with Tension Crack in Slope Face.
Queenstown Hill Landslide.
INPUT DATA

Height of slope - H	530		
Angle of slope face - φ_f	19	radians=	0.3316
Angle of upper slope - φ_s	16	radians=	0.2792
Angle of failure plane - φ_p	16	radians=	0.2792
z_w/z	0.5		
Horizontal acceleration - α	0		
Tension in bolts - T kN	0		
Inclination of T to normal of failure plane - θ	0	radians=	0
Cohesive strength of failure surface - c kN/m²	0		
Angle of friction on failure surface - ϕ	30	radians=	0.5235
Distance of tension crack behind slope crest - b	50		
Unit weight of rock - γ kN/m³	18		
Unit weight of water - γ_w kN/m³	10		

OUTPUT DATA

z	88.63
z_w	44.315
W	1E+06
A	1653.6
U	366391
V	9819.1
F numerator	512617
F denominator	369857
Factor of Safety - FOS	1.386

Tension Crack in Slope Face:

$Z = (H\cot\varphi_f - b)(\tan\varphi_f - \tan\varphi_p)$

$W = 0.5\gamma_r H^2[(1 - Z/H)^2\cot\varphi_p(\cot\varphi_p\tan\varphi_f - 1)]$

$A = (H\cot\varphi_f - b)\sec\varphi_p$

$U = 0.5\gamma_w Z_w A$

$V = 0.5\gamma_w Z_w^2$

$$FS = \frac{[cA + (W\cos\varphi_p - U - V\sin\varphi_p)\tan\phi]}{(W\sin\varphi_p + V\cos\varphi_p)}$$

When U=V=0, a=T=0:

$$FS = \frac{\tan\phi}{\tan\varphi_p} = 2.01$$

Analysis of Plane Failure with Tension Crack in Slope Face.
Queenstown Hill Landslide Seismic Sensitivity Analysis.
INPUT DATA

Height of slope - H	530		
Angle of slope face - φ_f	19	radians=	0.33155
Angle of upper slope - φ_s	16	radians=	0.2792
Angle of failure plane - φ_p	16	radians=	0.2792
z_w/z	0.5		
Horizontal acceleration - α	0.5		
Tension in bolts - T kN	1		
Inclination of T to normal of failure plane - θ	0	radians=	0
Cohesive strength of failure surface - c kN/m^2	5		
Angle of friction on failure surface - ϕ	20	radians=	0.349
Distance of tension crack behind slope crest - b	50		
Unit weight of rock - γ kN/m^3	18		
Unit weight of water - γ_w kN/m^3	10		

OUTPUT DATA

z	85.752
z_w	44.315
W	1244125
A	1431.86
U	317265
V	9819.1
F numerator	263540
F denominator	352303
Factor of Safety - FOS	0.74805

Tension Crack in Slope Face:

$Z = (H\cot\varphi_f - b)(\tan\varphi_f - \tan\varphi_p)$

$W = 0.5\gamma_r H^2[(1 - Z/H)^2\cot\varphi_p(\cot\varphi_p\tan\varphi_f - 1)]$

$A = (H\cot\varphi_f - b)\sec\varphi_p$

$U = 0.5\gamma_w Z_w A$

$V = 0.5\gamma_w Z_w^2$

$$FS = \frac{[cA + (W\cos\varphi_p - U - V\sin\varphi_p)\tan\phi]}{(W\sin\varphi_p + V\cos\varphi_p)}$$

Queenstown Hill Sensitivity to Cohesion

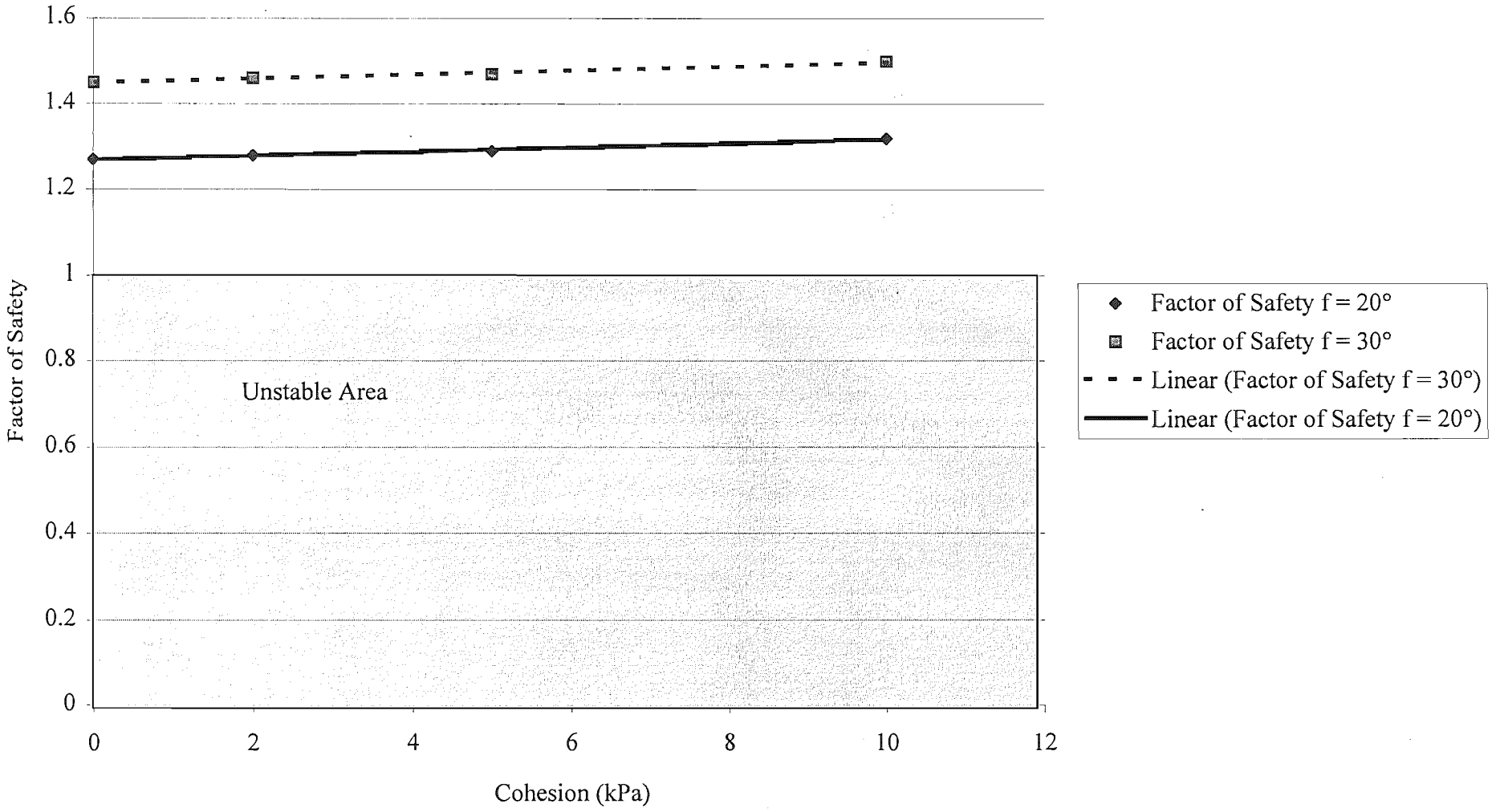

Queenstown Hill Sensitivity to Friction and Angle of Failure Plane

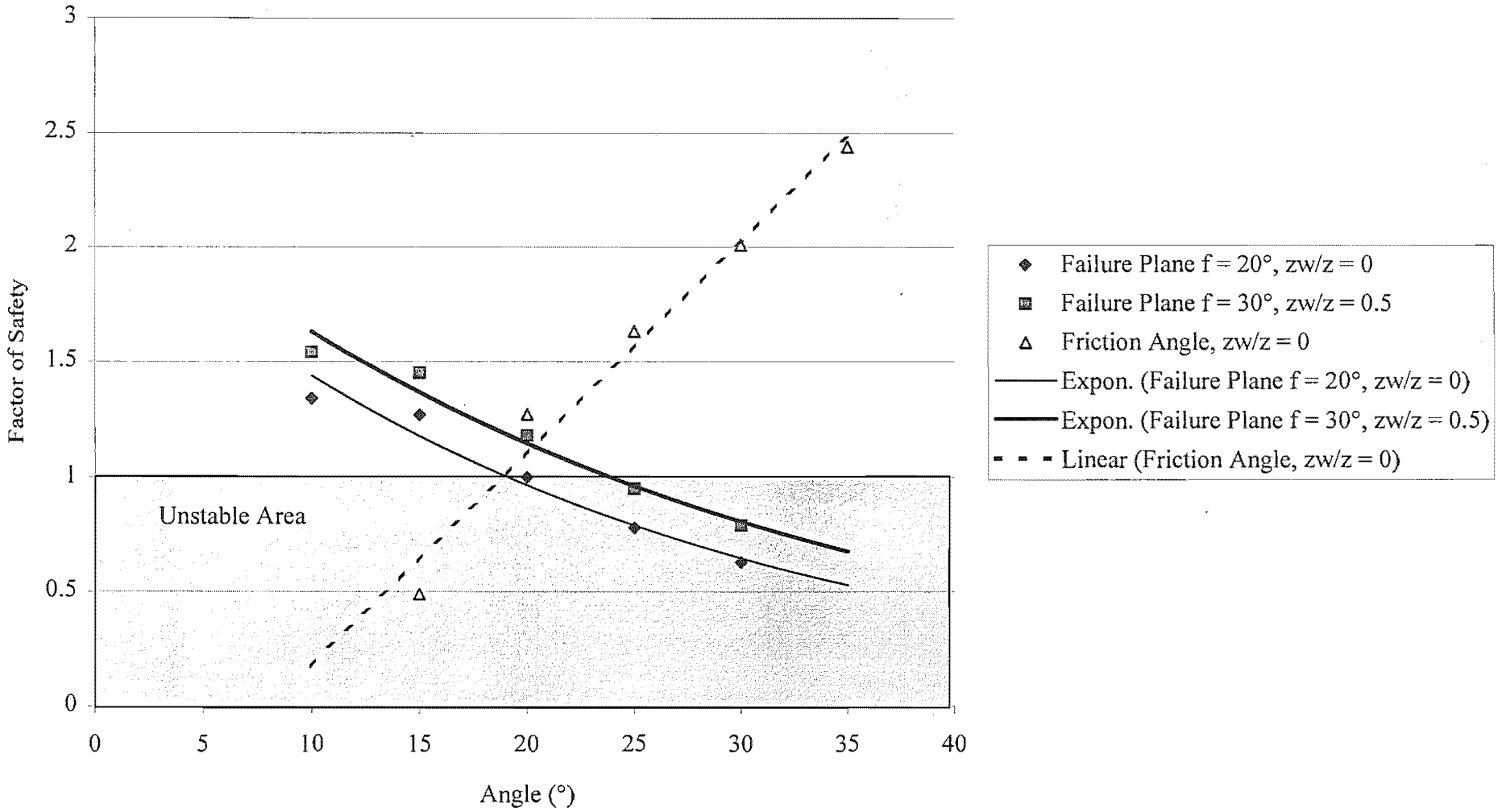

Queenstown Hill Sensitivity to Depth of Perched Water Table

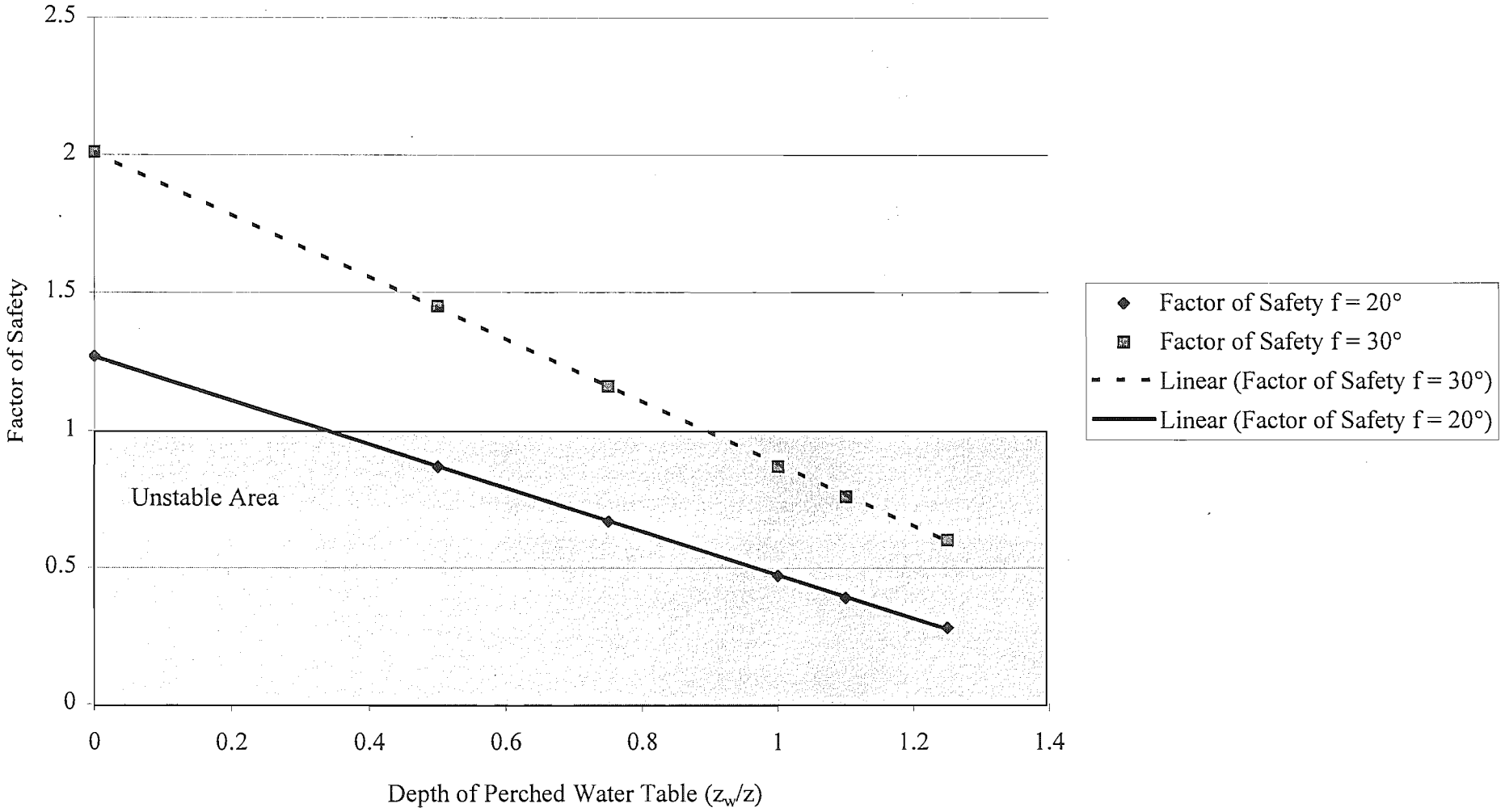

Queenstown Hill Sensitivity to Seismic Acceleration

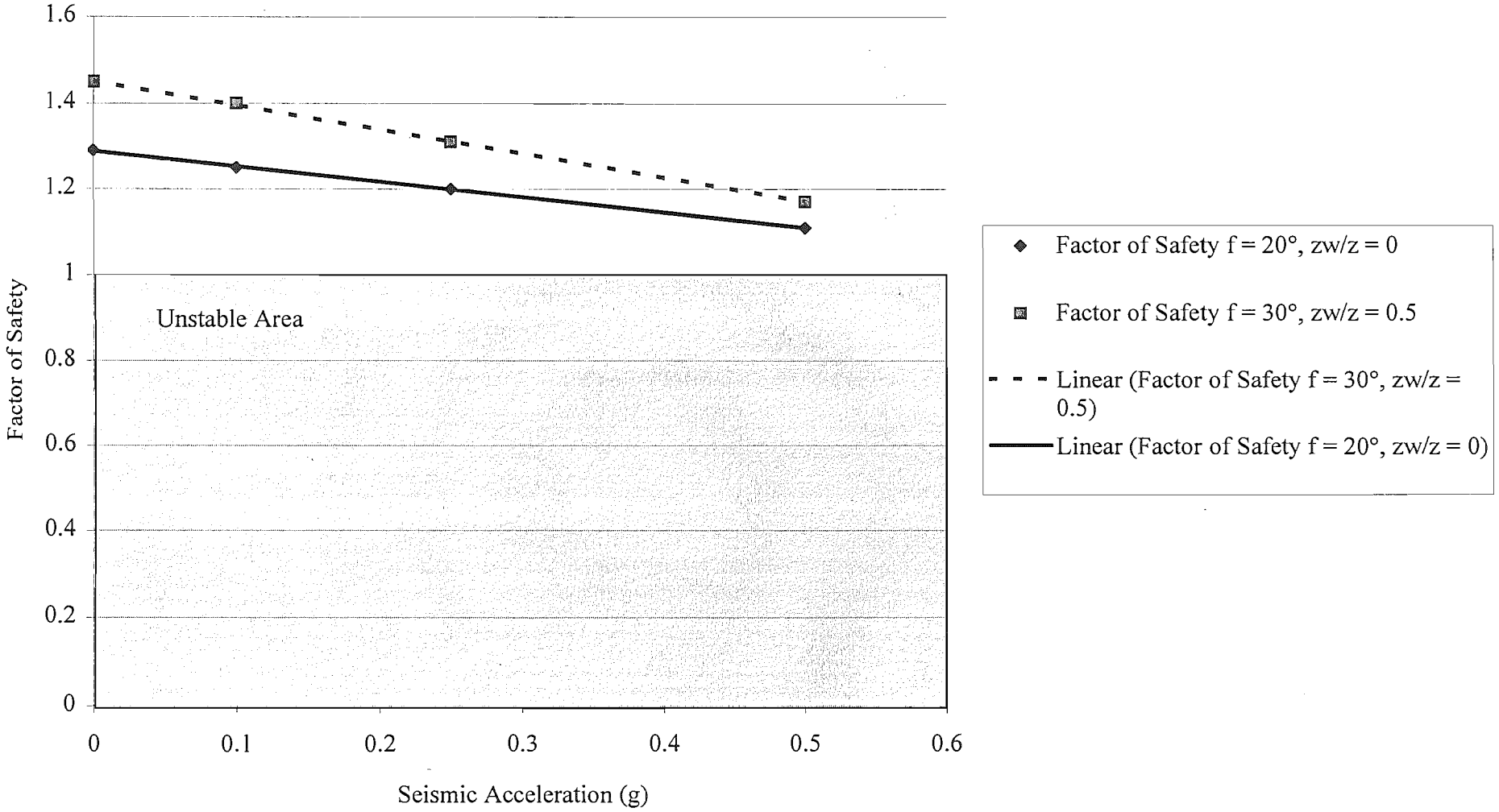

MARINA HEIGHTS FAILURE SENSITIVITY ANALYSIS.
Analysis of Plane Failure with Tension Crack in Slope Face.
INPUT DATA

Height of slope - H	220		
Angle of slope face - φ_f	28	radians=	0.4886
Angle of upper slope - φ_s	28	radians=	0.4886
Angle of failure plane - φ_p	21	radians=	0.36645
z_w/z	0.5		
Horizontal acceleration - α	0		
Tension in bolts - T kN	0		
Inclination of T to normal of failure plane - θ	0	radians=	0
Cohesive strength of failure surface - c kN/m²	0		
Angle of friction on failure surface - ϕ	30	radians=	0.5235
Distance of tension crack behind slope crest - b	106		
Unit weight of rock - γ kN/m³	18		
Unit weight of water - γ_w kN/m³	10		

OUTPUT DATA

z	45.5025
z_w	22.7513
W	275004
A	287.412
U	32694.9
V	2588.1
F numerator	128791
F denominator	100951
Factor of Safety - FOS	1.27577

Tension Crack in Slope Face:

$Z = (H\cot\varphi_f - b)(\tan\varphi_f - \tan\varphi_p)$

$W = 0.5\gamma_r H^2[(1 - Z/H)^2\cot\varphi_p(\cot\varphi_p\tan\varphi_f - 1)]$

$A = (H\cot\varphi_f - b)\sec\varphi_p$

$U = 0.5\gamma_w Z_w A$

$V = 0.5\gamma_w Z_w^2$

When U=V=0, a=T=0:

$$FS = \frac{\tan\phi}{\tan\varphi_p} = 1.5$$

$$FS = \frac{[cA + (W\cos\varphi_p - U - V\sin\varphi_p)\tan\phi]}{(W\sin\varphi_p + V\cos\varphi_p)}$$

MARINA HEIGHTS FAILURE SEISMIC SENSITIVITY ANALYSIS.
Analysis of Plane Failure with Tension Crack in Slope Face.
INPUT DATA

Height of slope - H	220		
Angle of slope face - φ_f	28	radians=	0.4886
Angle of upper slope - φ_s	28	radians=	0.4886
Angle of failure plane - φ_p	21	radians=	0.36645
z_w/z	0.5		
Horizontal acceleration - α	0.5		
Tension in bolts - T kN	0		
Inclination of T to normal of failure plane - θ	0	radians=	0
Cohesive strength of failure surface - c kN/m²	0		
Angle of friction on failure surface - ϕ	30	radians=	0.5235
Distance of tension crack behind slope crest - b	106		
Unit weight of rock - γ kN/m³	18		
Unit weight of water - γ_w kN/m³	10		

OUTPUT DATA

z	45.5025
z_w	22.7513
W	275004
A	287.412
U	32694.9
V	2588.1
F numerator	100353
F denominator	100951
Factor of Safety - FOS	0.99407

Tension Crack in Slope Face:

$Z = (H\cot\varphi_f - b)(\tan\varphi_f - \tan\varphi_p)$

$W = 0.5\gamma_r H^2[(1 - Z/H)^2\cot\varphi_p(\cot\varphi_p\tan\varphi_f - 1)]$

$A = (H\cot\varphi_f - b)\sec\varphi_p$

$U = 0.5\gamma_w Z_w A$

$V = 0.5\gamma_w Z_w^2$

When U=V=0, a=T=0:

$$FS = \frac{\tan\phi}{\tan\varphi_p} = 1.5$$

$$FS = \frac{[cA + (W\cos\varphi_p - U - V\sin\varphi_p)\tan\phi]}{(W\sin\varphi_p + V\cos\varphi_p)}$$

Marina Heights Failure Sensitivity to Cohesion

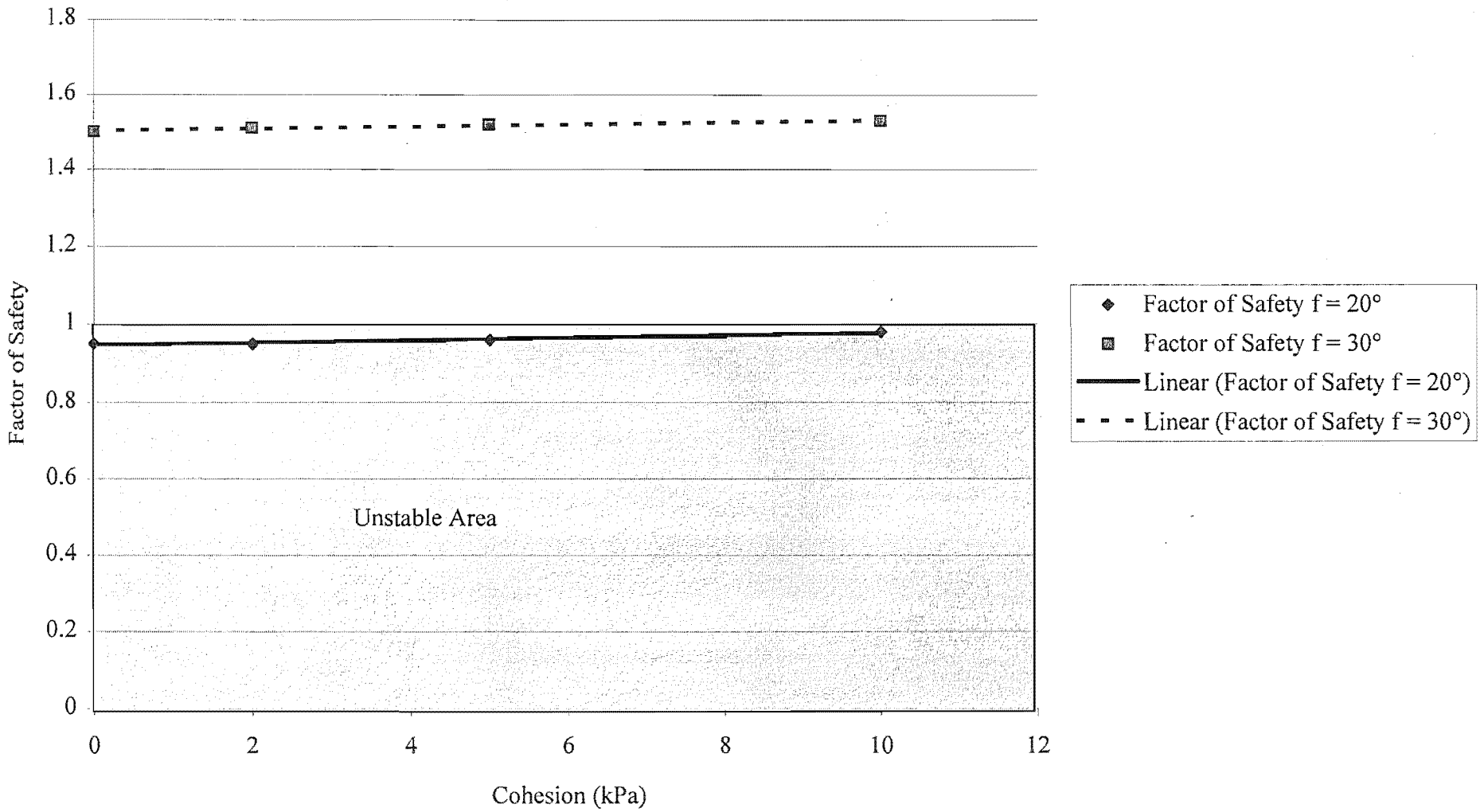

MarinaHeights Failure Sensitivity to Friction and Angle of Failure Plane

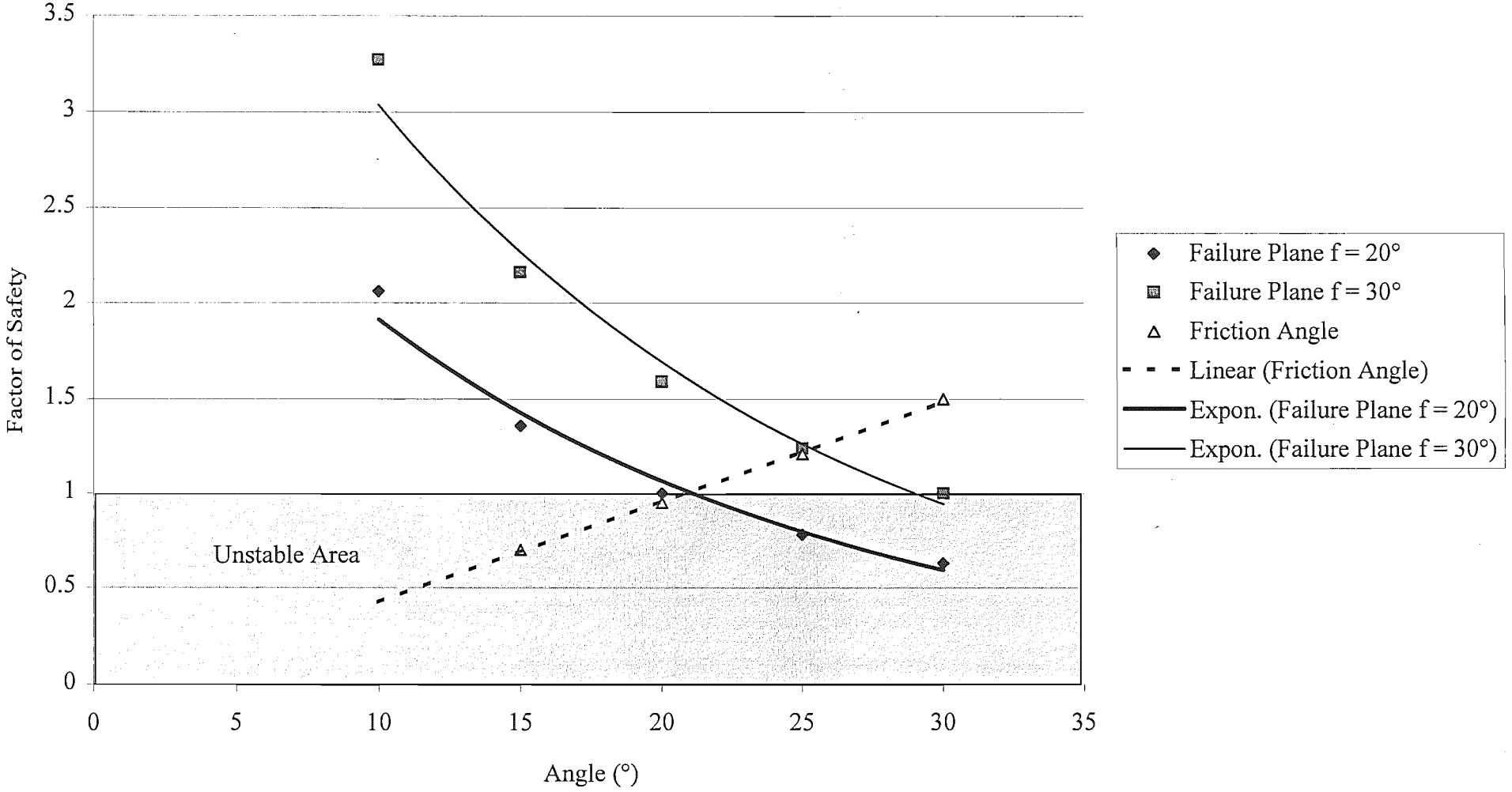

Marina Heights Failure Sensitivity to Depth of Perched Water Table

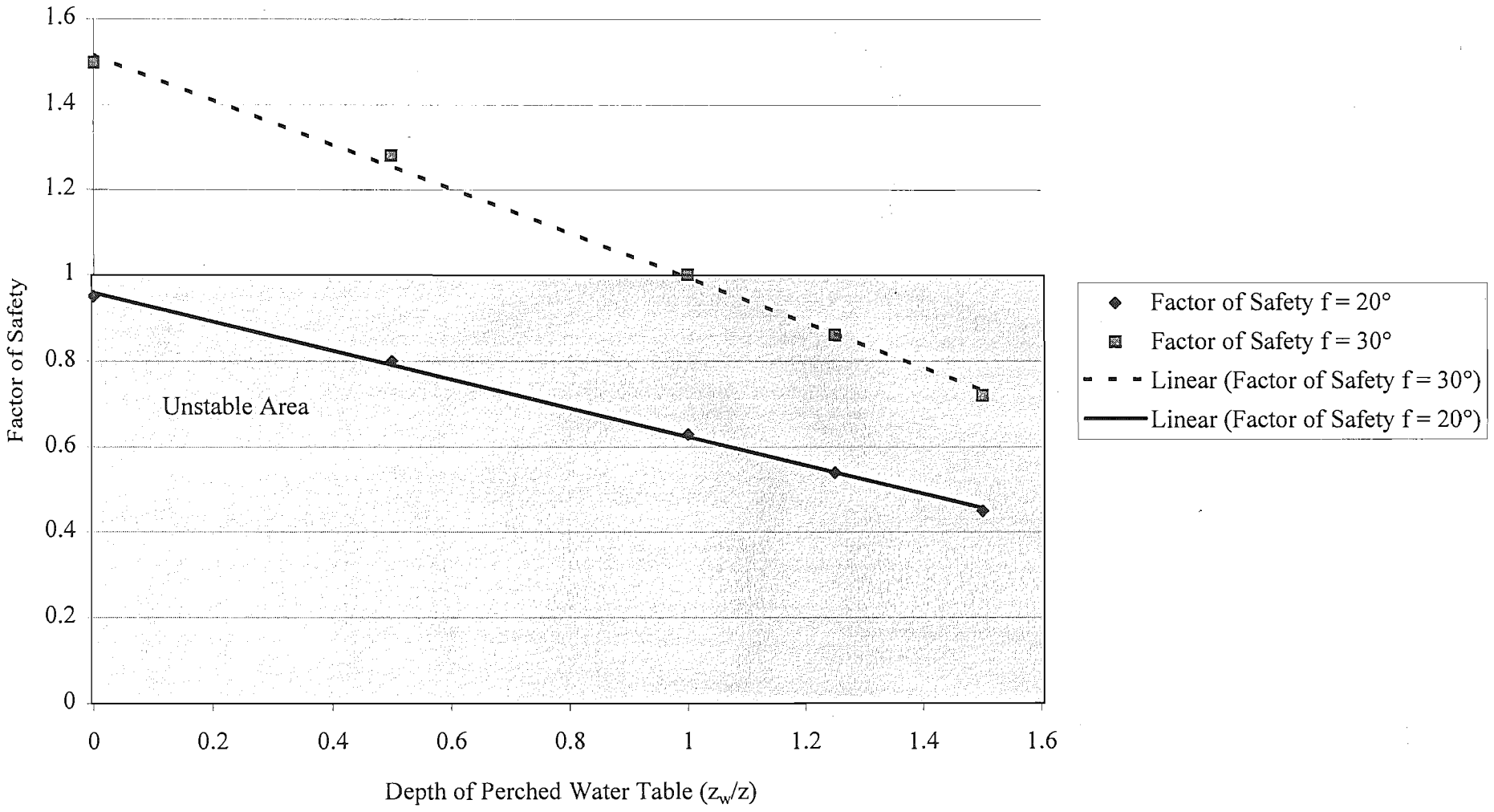

Marina Heights Sensitivity to Seismic Acceleration

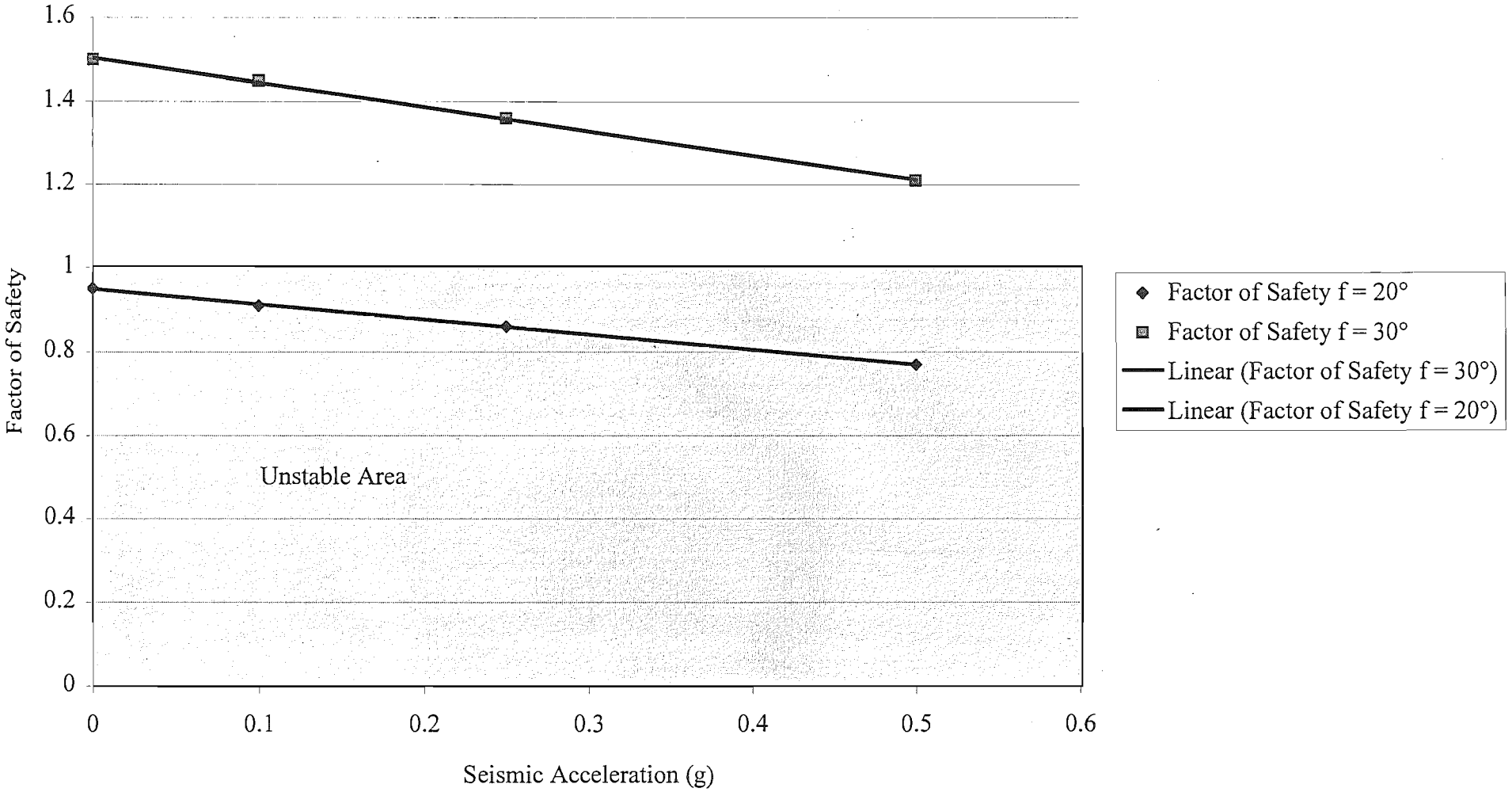

SLIDE NO. 2 SENSITIVITY ANALYSIS.
Analysis of Plane Failure with Tension Crack in Slope Face.
INPUT DATA

Height of slope - H	170		
Angle of slope face - φ_f	25	radians=	0.43625
Angle of upper slope - φ_s	25	radians=	0.43625
Angle of failure plane - φ_p	22	radians=	0.3839
z_w/z	0.5		
Horizontal acceleration - α	0		
Tension in bolts - T kN	0		
Inclination of T to normal of failure plane - θ	0	radians=	0
Cohesive strength of failure surface - c kN/m^2	0		
Angle of friction on failure surface - ϕ	30	radians=	0.5235
Distance of tension crack behind slope crest - b	27		
Unit weight of rock - γ kN/m^3	18		
Unit weight of water - γ_w kN/m^3	10		

OUTPUT DATA

z	21.0236
z_w	10.5118
W	76223.1
A	313.068
U	16454.5
V	552.49
F numerator	31177.6
F denominator	29060.8
Factor of Safety - FOS	1.07284

Tension Crack in Slope Face:

$Z = (H\cot\varphi_f - b)(\tan\varphi_f - \tan\varphi_p)$

$W = 0.5\gamma_r H^2[(1 - Z/H)^2\cot\varphi_p(\cot\varphi_p\tan\varphi_f - 1)]$

$A = (H\cot\varphi_f - b)\sec\varphi_p$

$U = 0.5\gamma_w Z_w A$

$V = 0.5\gamma_w Z_w^2$

When U=V=0, a=T=0:

$$FS = \frac{\tan\phi}{\tan\varphi_p} = 1.43$$

$$FS = \frac{[cA + (W\cos\varphi_p - U - V\sin\varphi_p)\tan\phi]}{(W\sin\varphi_p + V\cos\varphi_p)}$$

SLIDE NO. 2 SEISMIC SENSITIVITY ANALYSIS.
Analysis of Plane Failure with Tension Crack in Slope Face.
INPUT DATA

Height of slope - H	170		
Angle of slope face - φ_f	25	radians=	0.43625
Angle of upper slope - φ_s	25	radians=	0.43625
Angle of failure plane - φ_p	22	radians=	0.3839
z_w/z	0.5		
Horizontal acceleration - α	0.5		
Tension in bolts - T kN	0		
Inclination of T to normal of failure plane - θ	0	radians=	0
Cohesive strength of failure surface - c kN/m²	0		
Angle of friction on failure surface - ϕ	30	radians=	0.5235
Distance of tension crack behind slope crest - b	27		
Unit weight of rock - γ kN/m³	18		
Unit weight of water - γ_w kN/m³	10		

OUTPUT DATA

z	21.0236
z_w	10.5118
W	76223.1
A	313.068
U	16454.5
V	552.49
F numerator	22938.2
F denominator	29060.8
Factor of Safety - FOS	0.78932

Tension Crack in Slope Face:

$Z = (H\cot\varphi_f - b)(\tan\varphi_f - \tan\varphi_p)$

$W = 0.5\gamma_r H^2[(1 - Z/H)^2\cot\varphi_p(\cot\varphi_p\tan\varphi_f - 1)]$

$A = (H\cot\varphi_f - b)\sec\varphi_p$

$U = 0.5\gamma_w Z_w A$

$V = 0.5\gamma_w Z_w^2$

When U=V=0, a=T=0:

$$FS = \frac{\tan\phi}{\tan\varphi_p} = 1.43$$

$$FS = \frac{[cA + (W\cos\varphi_p - U - V\sin\varphi_p)\tan\phi]}{(W\sin\varphi_p + V\cos\varphi_p)}$$

Slide No. 2 Sensitivity to Cohesion

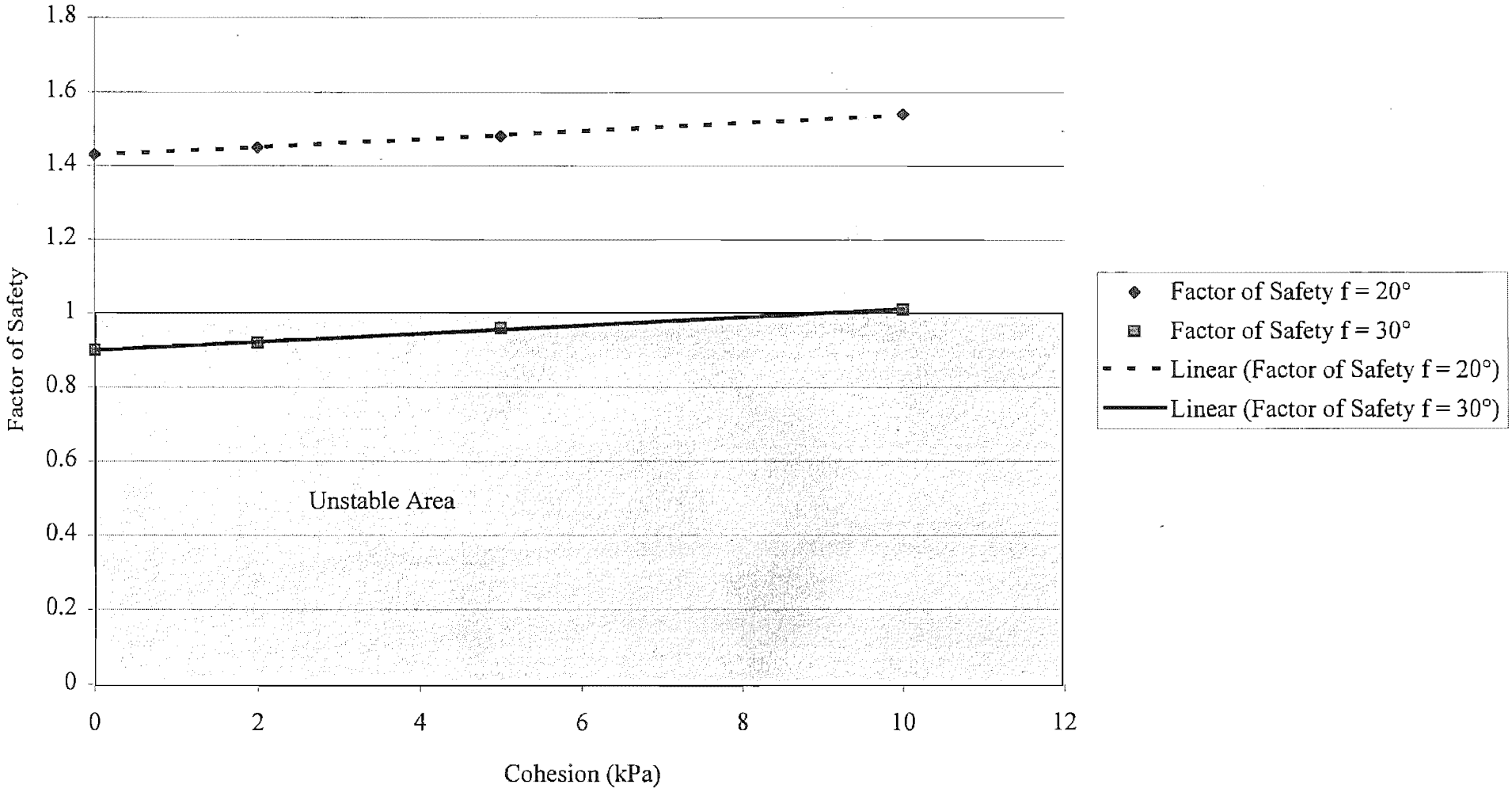

Slide No. 2 Sensitivity to Angle of Failure Plane and Friction

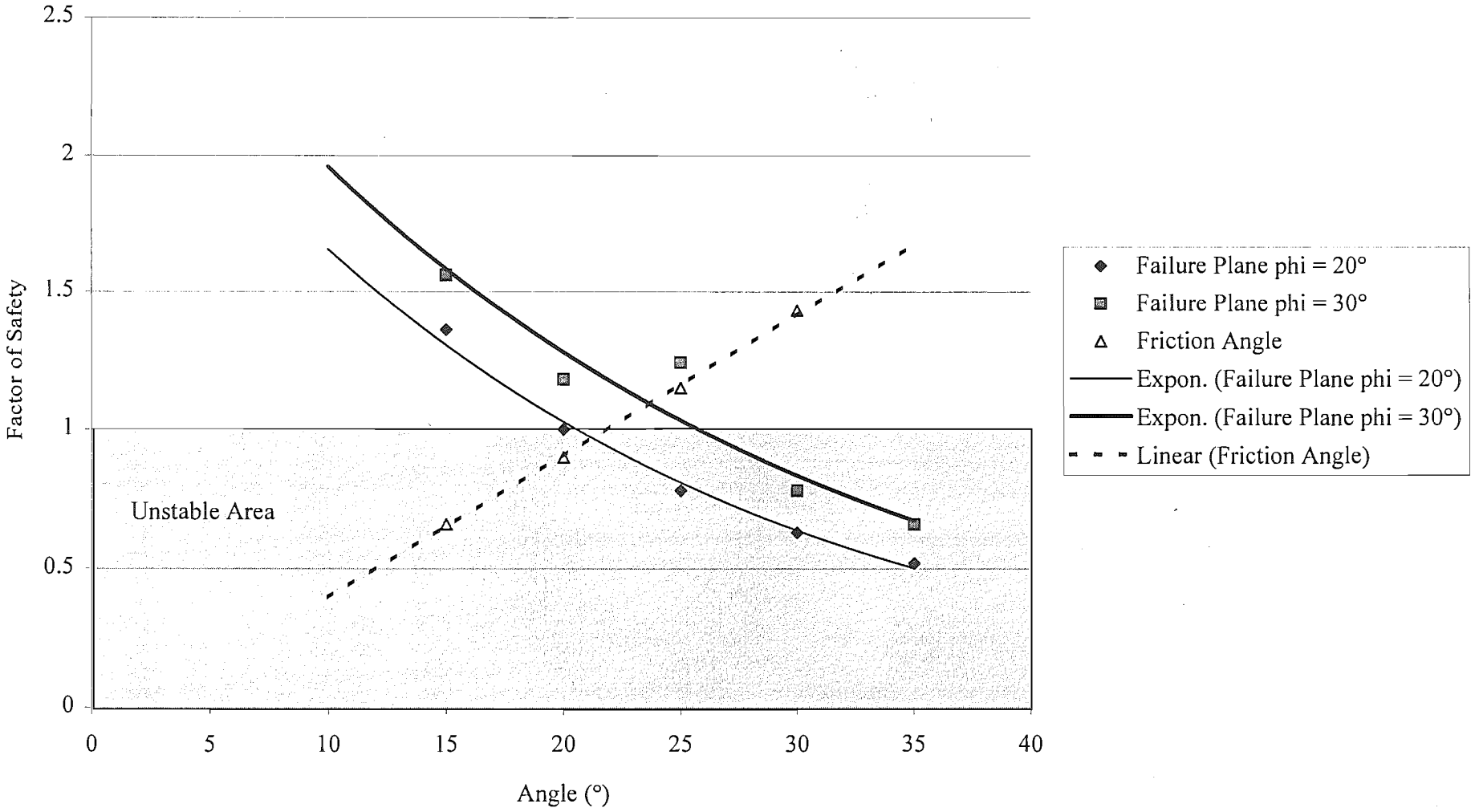

Slide No. 2 Sensitivity to Depth of Perched Water Table

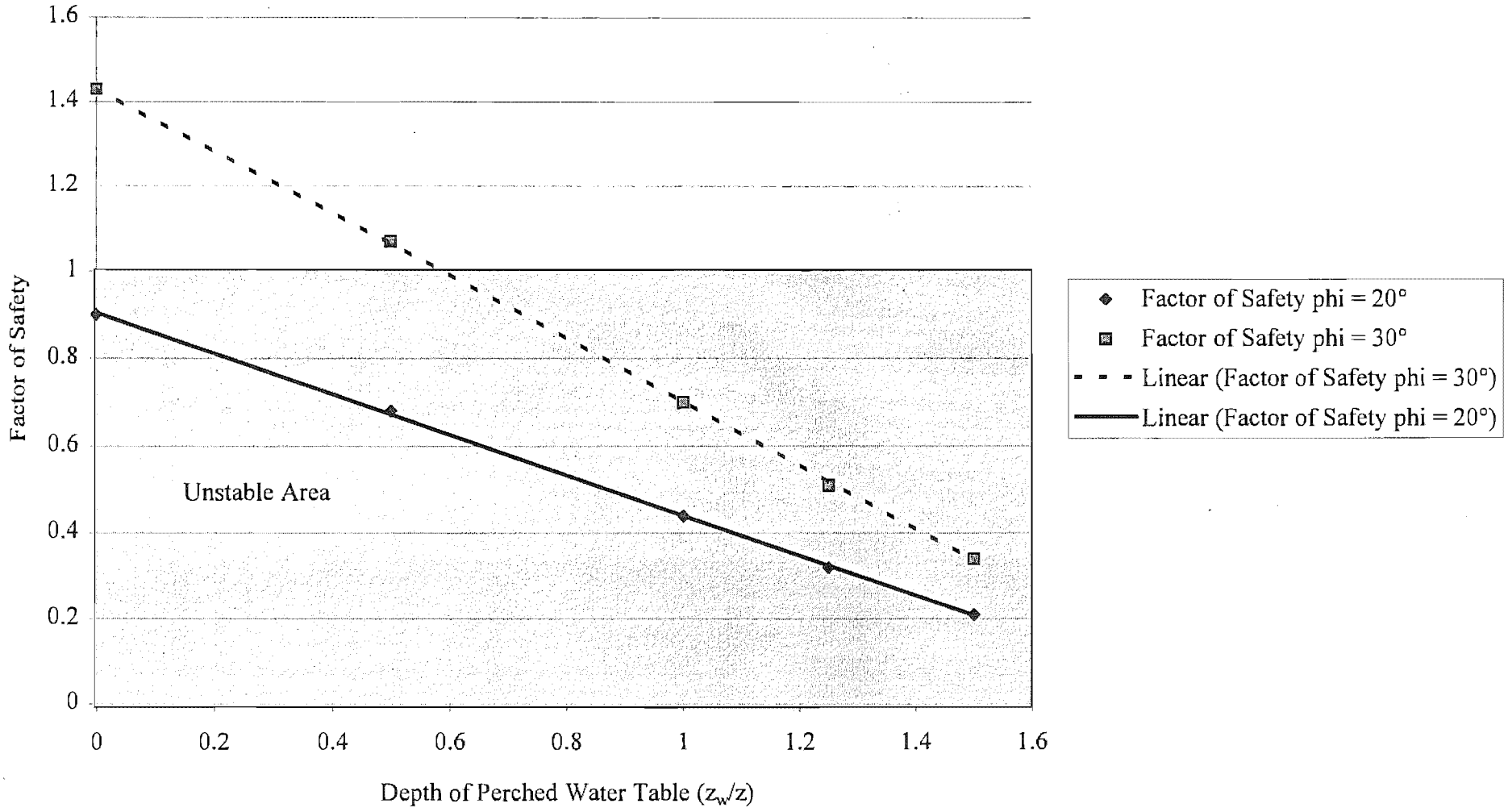

Slide No. 2 Sensitivity to Seismic Acceleration

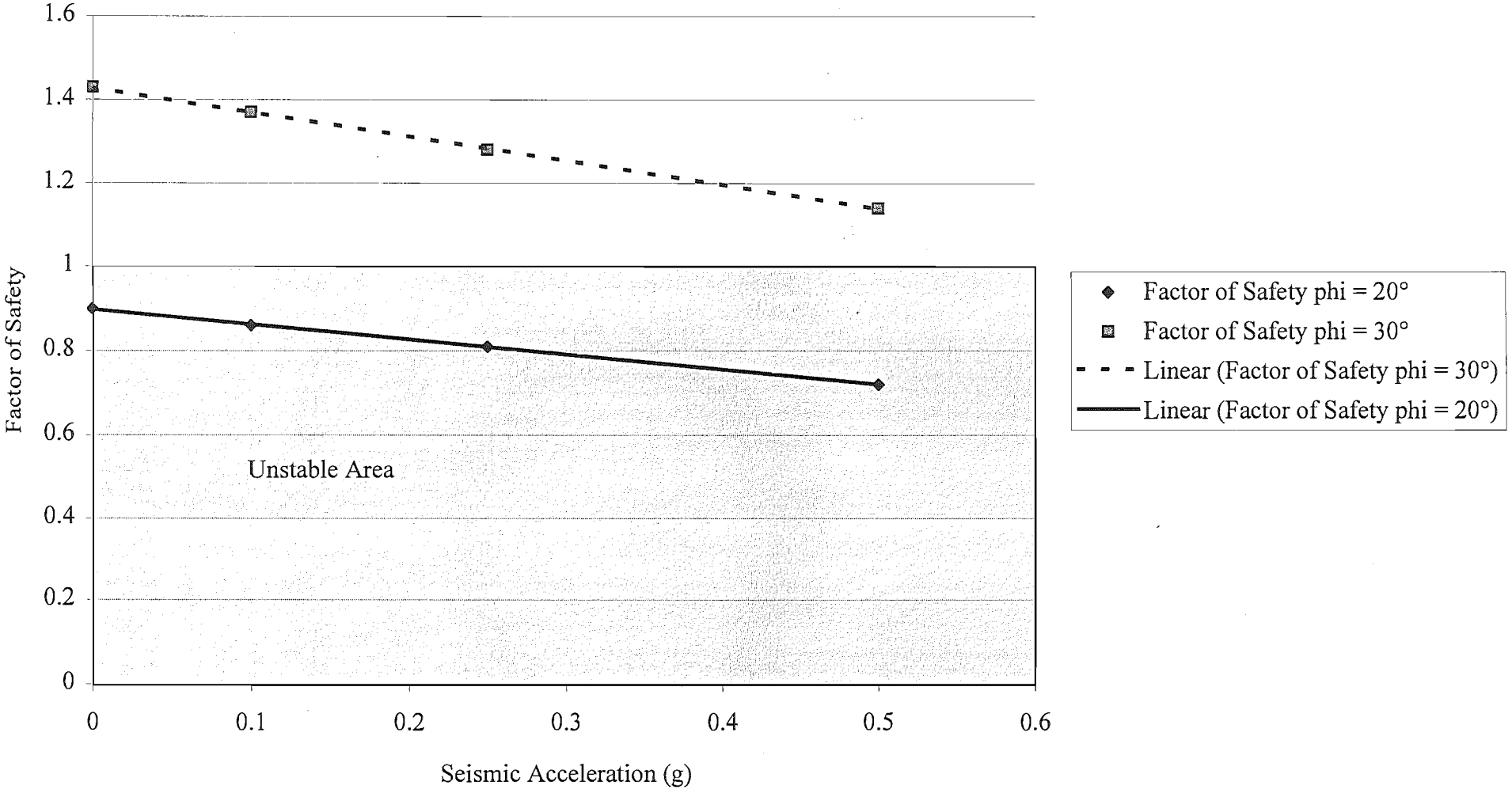

SLIDE NO. 3 SENSITIVITY ANALYSIS.
Analysis of Plane Failure with Tension Crack in Slope Face.
INPUT DATA

Height of slope - H	190		
Angle of slope face - φ_f	28	radians=	0.4886
Angle of upper slope - φ_s	28	radians=	0.4886
Angle of failure plane - φ_p	21	radians=	0.36645
z_w/z	0.5		
Horizontal acceleration - α	0		
Tension in bolts - T kN	0		
Inclination of T to normal of failure plane - θ	0	radians=	0
Cohesive strength of failure surface - c kN/m^2	0		
Angle of friction on failure surface - ϕ	30	radians=	0.5235
Distance of tension crack behind slope crest - b	63		
Unit weight of rock - γ kN/m^3	18		
Unit weight of water - γ_w kN/m^3	10		

OUTPUT DATA

z	43.5168
z_w	21.7584
W	193792
A	274.87
U	29903.6
V	2367.14
F numerator	86683
F denominator	71646.4
Factor of Safety - FOS	1.20987

Tension Crack in Slope Face:

$Z = (H\cot\varphi_f - b)(\tan\varphi_f - \tan\varphi_p)$

$W = 0.5\gamma_r H^2[(1 - Z/H)^2\cot\varphi_p(\cot\varphi_p\tan\varphi_f - 1)]$

$A = (H\cot\varphi_f - b)\sec\varphi_p$

$U = 0.5\gamma_w Z_w A$

$V = 0.5\gamma_w Z_w^2$

When U=V=0, a=T=0:

$$FS = \frac{\tan\phi}{\tan\varphi_p} = 1.5$$

$$FS = \frac{[cA + (W\cos\varphi_p - U - V\sin\varphi_p)\tan\phi]}{(W\sin\varphi_p + V\cos\varphi_p)}$$

SLIDE NO. 3 SEISMIC SENSITIVITY ANALYSIS.
Analysis of Plane Failure with Tension Crack in Slope Face.
INPUT DATA

Height of slope - H	190		
Angle of slope face - φ_f	28	radians=	0.4886
Angle of upper slope - φ_s	28	radians=	0.4886
Angle of failure plane - φ_p	21	radians=	0.36645
z_w/z	0.5		
Horizontal acceleration - α	0.5		
Tension in bolts - T kN	0		
Inclination of T to normal of failure plane - θ	0	radians=	0
Cohesive strength of failure surface - c kN/m²	0		
Angle of friction on failure surface - ϕ	30	radians=	0.5235
Distance of tension crack behind slope crest - b	63		
Unit weight of rock - γ kN/m³	18		
Unit weight of water - γ_w kN/m³	10		

OUTPUT DATA

z	43.5168
z_w	21.7584
W	193792
A	274.87
U	29903.6
V	2367.14
F numerator	66643
F denominator	71646.4
Factor of Safety - FOS	0.93017

Tension Crack in Slope Face:

$Z = (H\cot\varphi_f - b)(\tan\varphi_f - \tan\varphi_p)$

$W = 0.5\gamma_r H^2[(1 - Z/H)^2\cot\varphi_p(\cot\varphi_p\tan\varphi_f - 1)]$

$A = (H\cot\varphi_f - b)\sec\varphi_p$

$U = 0.5\gamma_w Z_w A$

$V = 0.5\gamma_w Z_w^2$

When U=V=0, a=T=0:

$$FS = \frac{\tan\phi}{\tan\varphi_p} = 1.5$$

$$FS = \frac{[cA + (W\cos\varphi_p - U - V\sin\varphi_p)\tan\phi]}{(W\sin\varphi_p + V\cos\varphi_p)}$$

Slide No. 3 Sensitivity to Cohesion

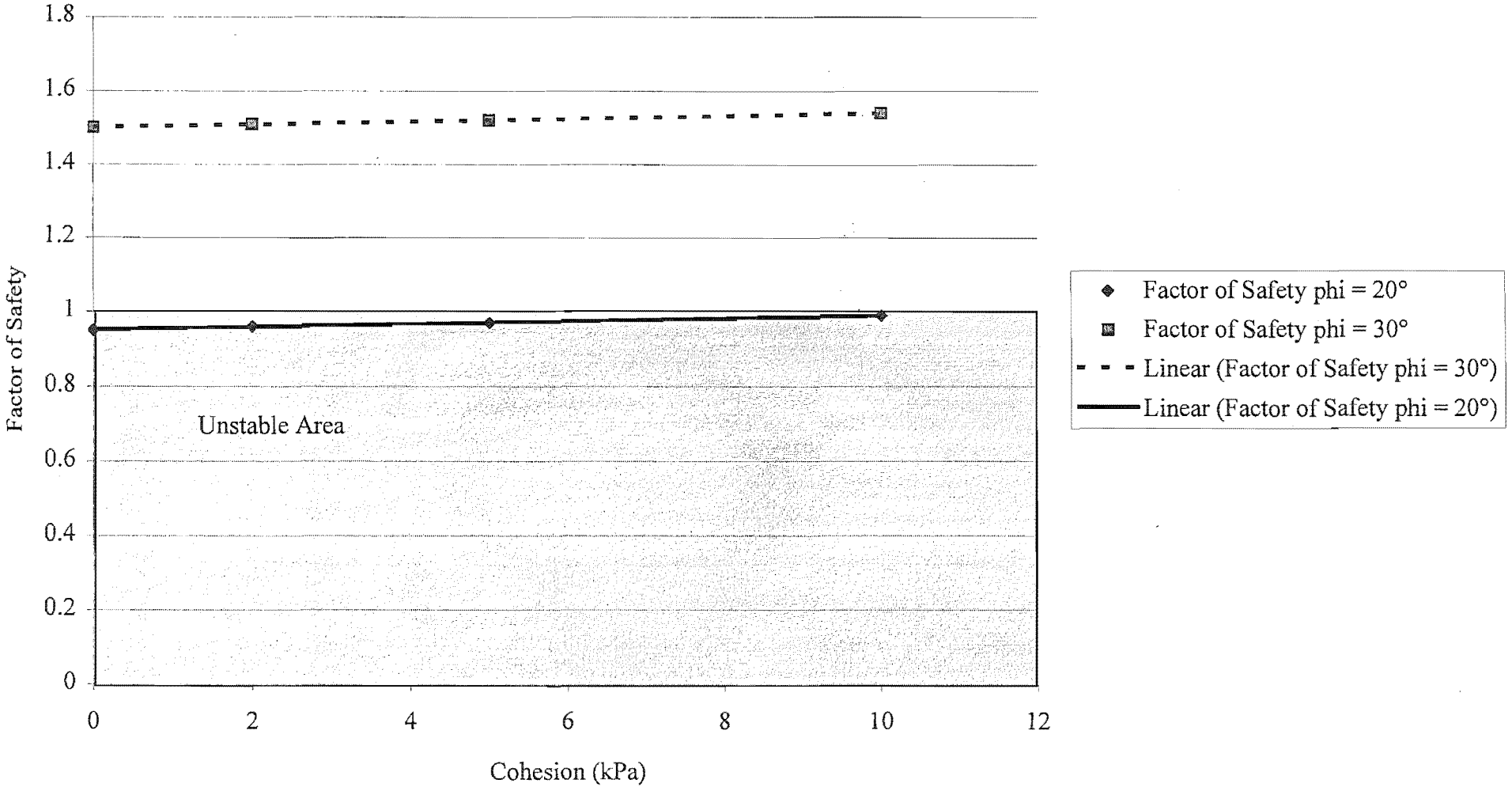

Slide No. 3 Sensitivity to Friction and Angle of Failure Plane

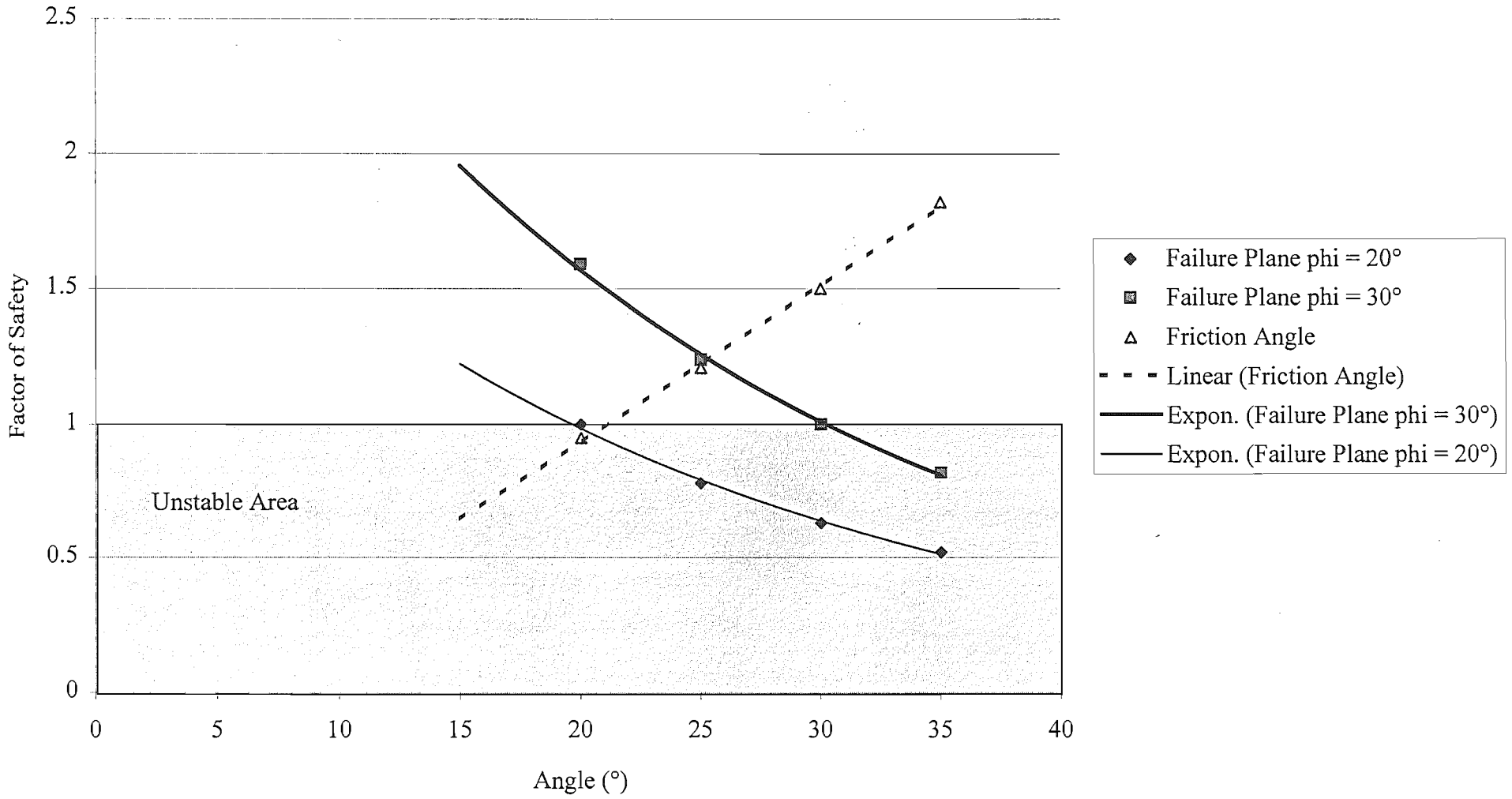

Slide No. 3 Sensitivity to Depth of Perched Water Table

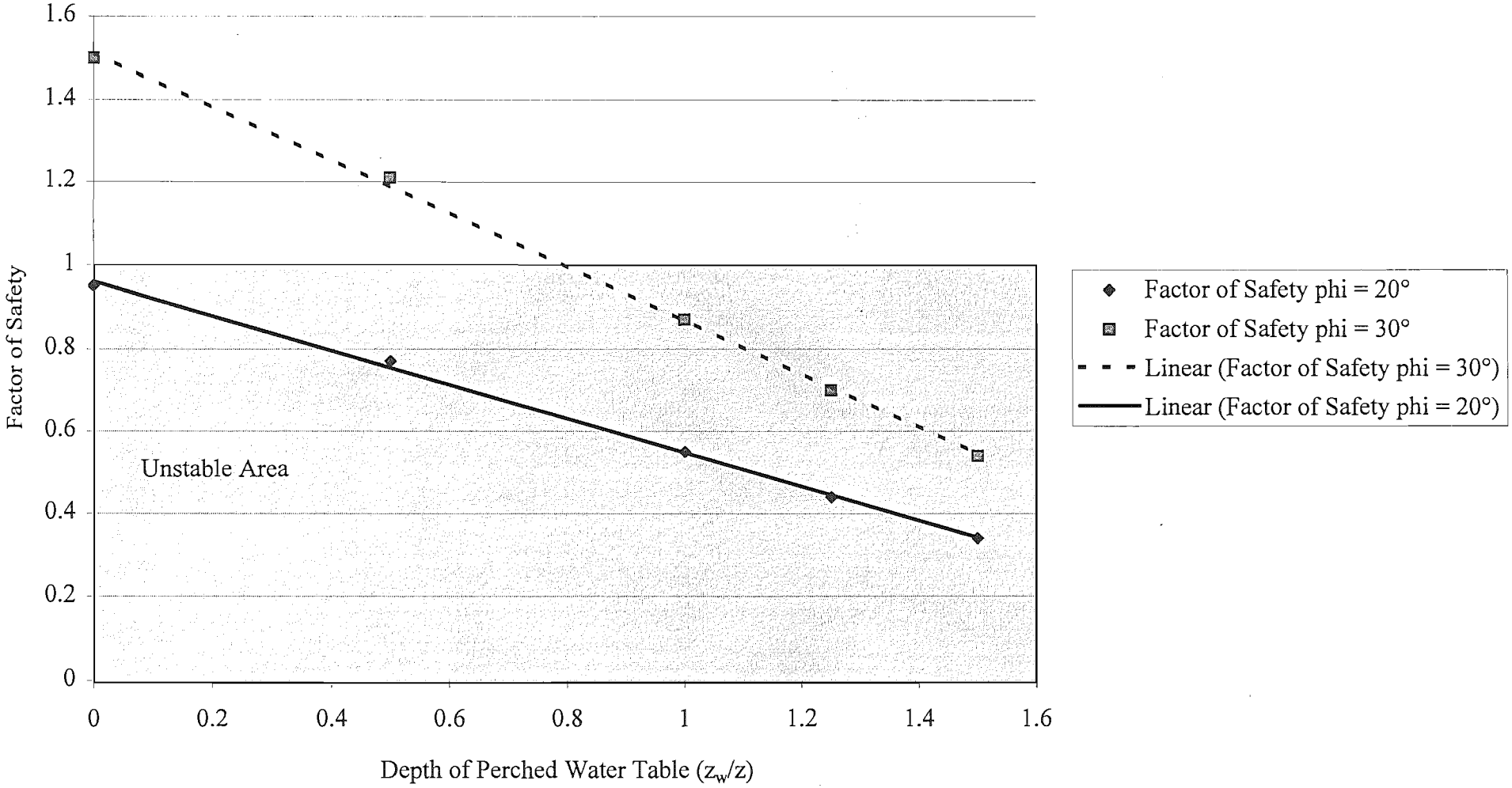

Sldie No. 3 Sensitivity to Seismic Acceleration

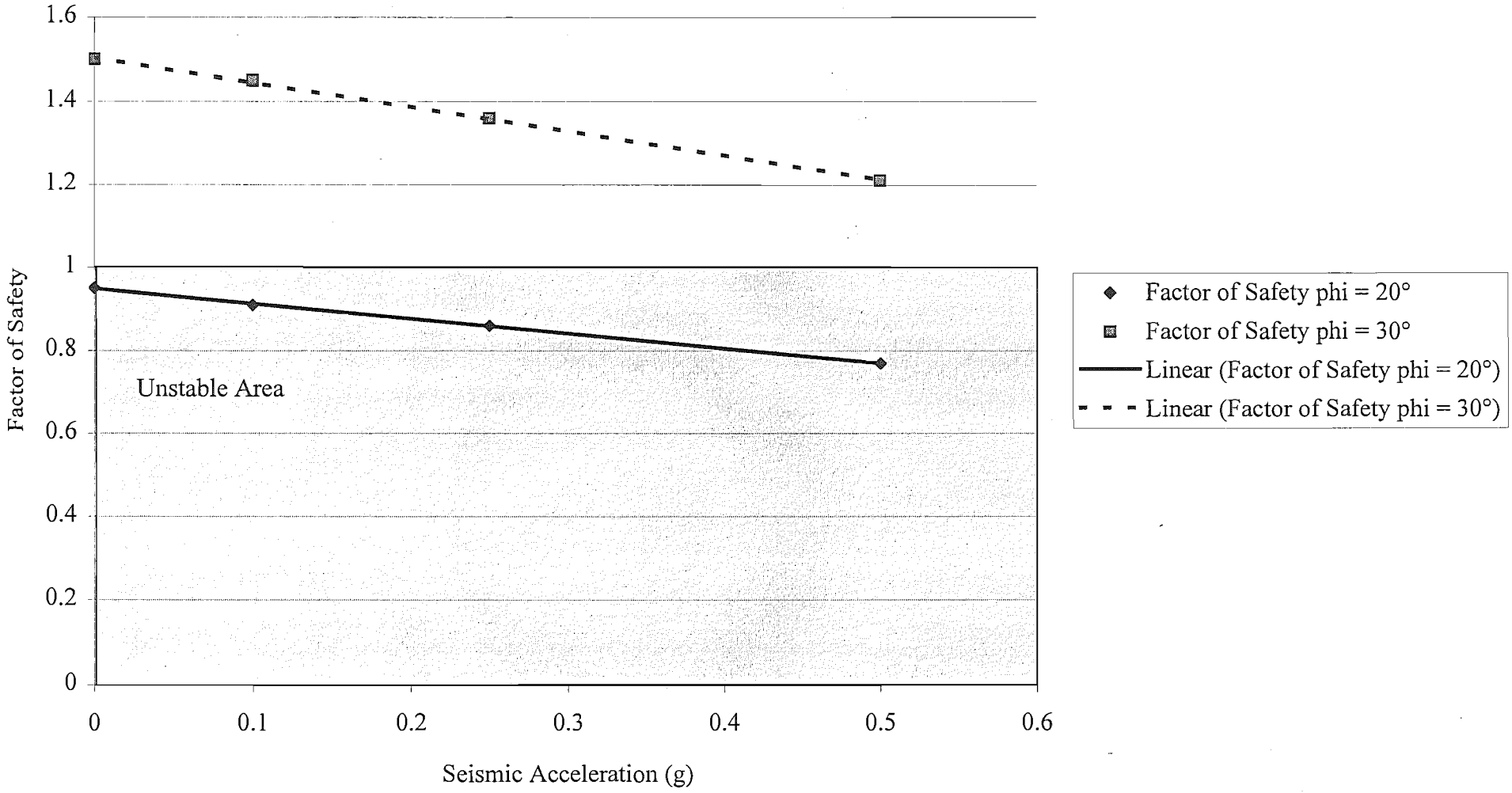

SLIDE NO. 4 SENSITIVITY ANALYSIS.
Analysis of Plane Failure with Tension Crack in Slope Face.

INPUT DATA

Height of slope - H	175		
Angle of slope face - φ_f	26	radians=	0.4537
Angle of upper slope - φ_s	26	radians=	0.4537
Angle of failure plane - φ_p	25	radians=	0.43625
z_w/z	0.5		
Horizontal acceleration - α	0		
Tension in bolts - T kN	0		
Inclination of T to normal of failure plane - θ	0	radians=	0
Cohesive strength of failure surface - c kN/m^2	0		
Angle of friction on failure surface - ϕ	30	radians=	0.5235
Distance of tension crack behind slope crest - b	8		
Unit weight of rock - γ kN/m^3	18		
Unit weight of water - γ_w kN/m^3	10		

OUTPUT DATA

z	7.51558
z_w	3.75779
W	24879.2
A	318.019
U	5975.23
V	70.6049
F numerator	9549.49
F denominator	10576.5
Factor of Safety - FOS	0.90289

Tension Crack in Slope Face:

$Z = (H\cot\varphi_f - b)(\tan\varphi_f - \tan\varphi_p)$

$W = 0.5\gamma_r H^2[(1 - Z/H)^2\cot\varphi_p(\cot\varphi_p\tan\varphi_f - 1)]$

$A = (H\cot\varphi_f - b)\sec\varphi_p$

$U = 0.5\gamma_w Z_w A$

$V = 0.5\gamma_w Z_w^2$

When U=V=0, a=T=0:

$$FS = \frac{\tan\phi}{\tan\varphi_p} = 1.24$$

$$FS = \frac{[cA + (W\cos\varphi_p - U - V\sin\varphi_p)\tan\phi]}{(W\sin\varphi_p + V\cos\varphi_p)}$$

SLIDE NO. 4 SEISMIC SENSITIVITY ANALYSIS.
Analysis of Plane Failure with Tension Crack in Slope Face.
INPUT DATA

Height of slope - H	175		
Angle of slope face - φ_f	26	radians=	0.4537
Angle of upper slope - φ_s	26	radians=	0.4537
Angle of failure plane - φ_p	25	radians=	0.43625
z_w/z	0.5		
Horizontal acceleration - α	0.5		
Tension in bolts - T kN	0		
Inclination of T to normal of failure plane - θ	0	radians=	0
Cohesive strength of failure surface - c kN/m²	0		
Angle of friction on failure surface - ϕ	30	radians=	0.5235
Distance of tension crack behind slope crest - b	8		
Unit weight of rock - γ kN/m³	18		
Unit weight of water - γ_w kN/m³	10		

OUTPUT DATA

z	7.51558
z_w	3.75779
W	24879.2
A	318.019
U	5975.23
V	70.6049
F numerator	6515.47
F denominator	10576.5
Factor of Safety - FOS	0.61603

Tension Crack in Slope Face:

$Z = (H\cot\varphi_f - b)(\tan\varphi_f - \tan\varphi_p)$

$W = 0.5\gamma_r H^2[(1 - Z/H)^2\cot\varphi_p(\cot\varphi_p\tan\varphi_f - 1)]$

$A = (H\cot\varphi_f - b)\sec\varphi_p$

Tension Crack behind Slope Crest:

$Z = H + b\tan\varphi_s - (b + H\cot\varphi_f)\tan\varphi_p$

$W = 0.5\gamma_r(H^2\cot\varphi_f X + bHX + bZ)$

$X = (1 - \tan\varphi_p\cot\varphi_f)$

$A = (H\cot\varphi_f + b)\sec\varphi_p$

$U = 0.5\gamma_w Z_w A$

$V = 0.5\gamma_w Z_w^2$

When U=V=0, a=T=0:

$$FS = \frac{\tan\phi}{\tan\varphi_p} = 1.24$$

$$FS = \frac{[cA + (W\cos\varphi_p - U - V\sin\varphi_p)\tan\phi]}{(W\sin\varphi_p + V\cos\varphi_p)}$$

Slide No. 4 Sensitivity to Cohesion

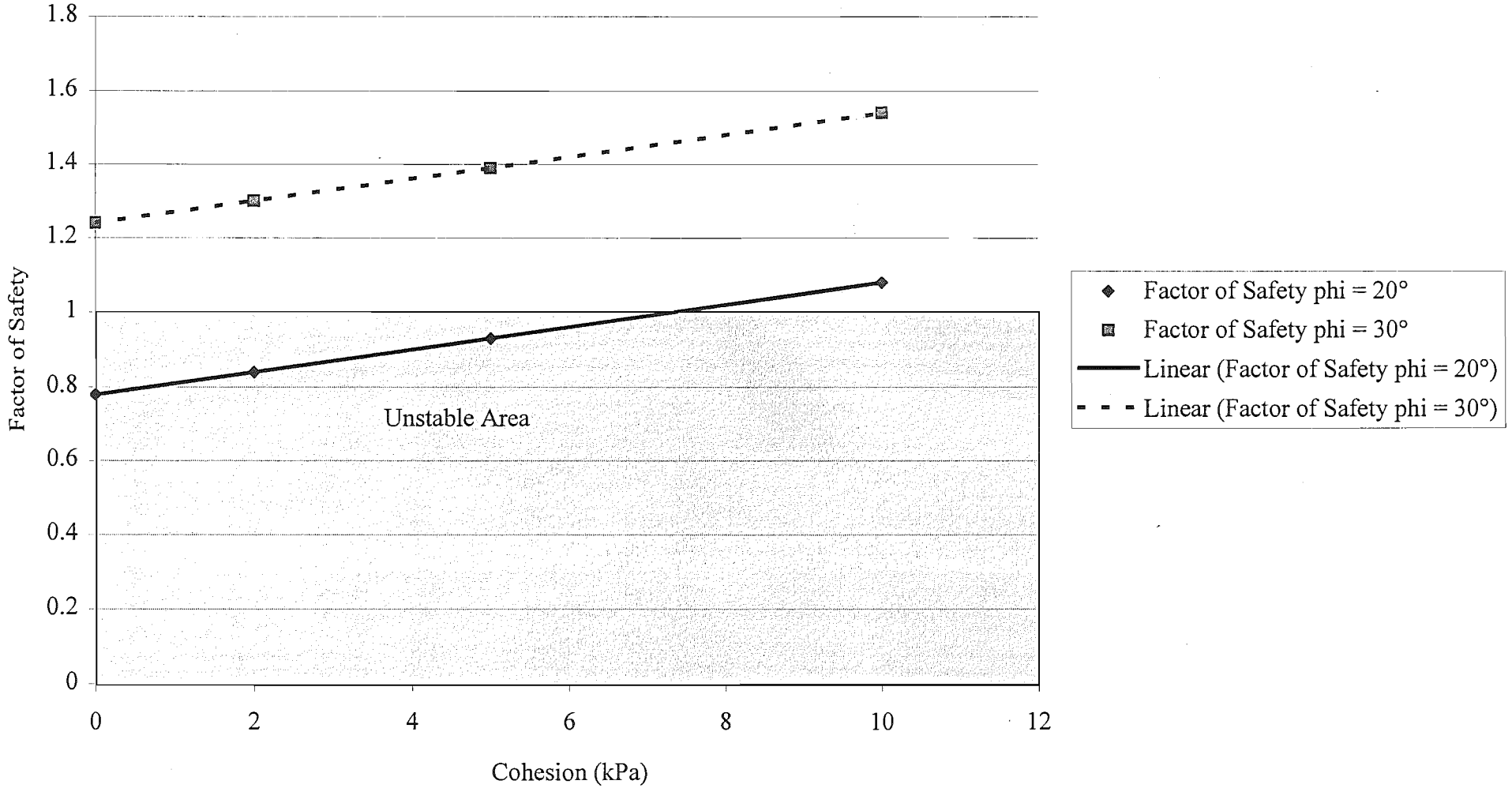

Slide No. 4 Sensitivity to Friction and Angle of Failure Plane

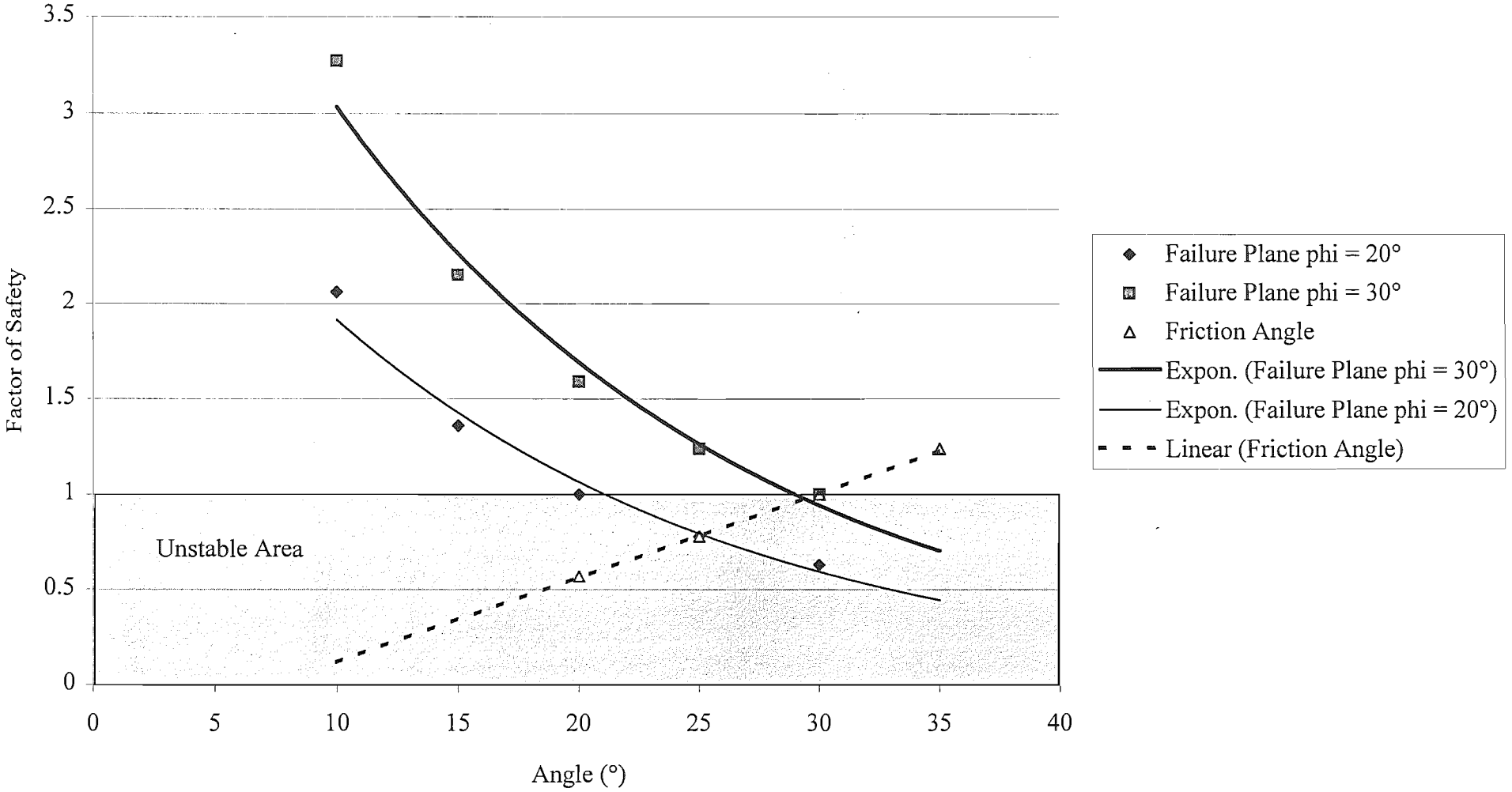

Slide No. 4 Sensitivity to Depth of Perched Water Table

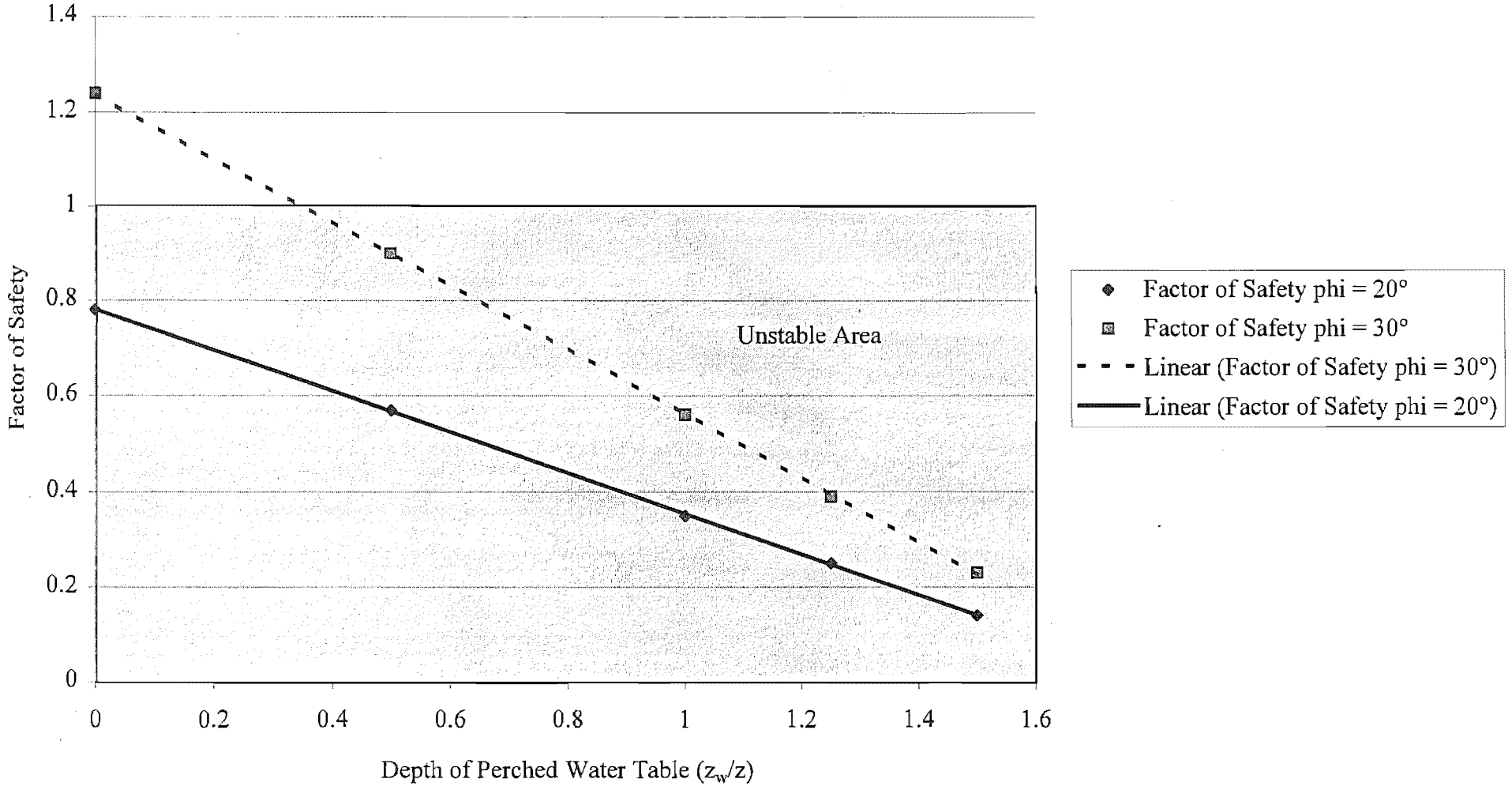

Slide No. 4 Sensitivity to Seismic Acceleration

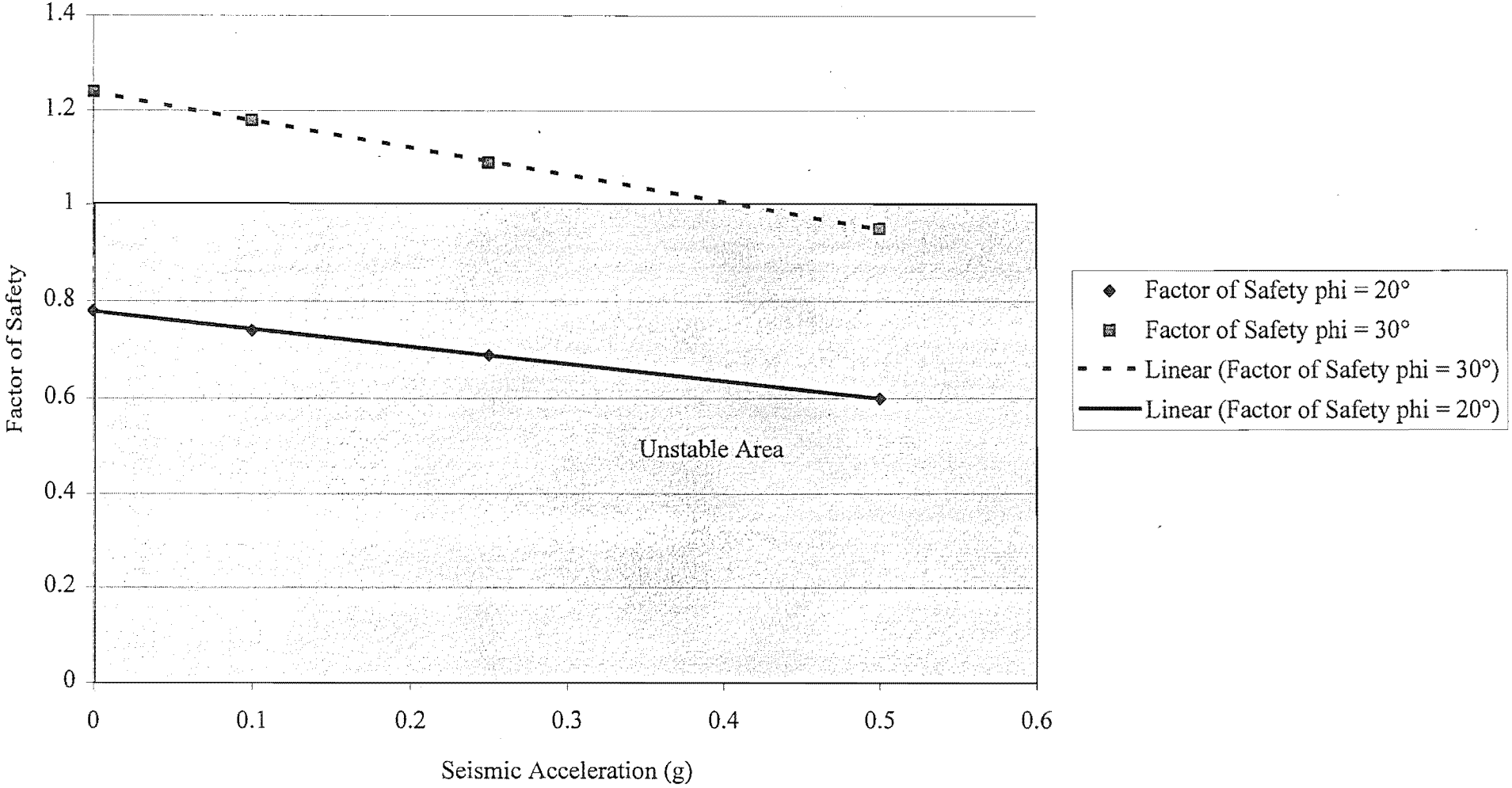

SLIDE NO. 5 SENSITIVITY ANALYSIS.
Analysis of Plane Failure with Tension Crack in Slope Face.

INPUT DATA

Height of slope - H	160		
Angle of slope face - φ_f	20	radians=	0.349
Angle of upper slope - φ_s	20	radians=	0.349
Angle of failure plane - φ_p	18	radians=	0.3141
z_w/z	0.5		
Horizontal acceleration - α	0		
Tension in bolts - T kN	0		
Inclination of T to normal of failure plane - θ	0	radians=	0
Cohesive strength of failure surface - c kN/m²	0		
Angle of friction on failure surface - ϕ	30	radians=	0.5235
Distance of tension crack behind slope crest - b	26		
Unit weight of rock - γ kN/m³	18		
Unit weight of water - γ_w kN/m³	10		

OUTPUT DATA

z	16.1509
z_w	8.07545
W	68897.9
A	393.447
U	15886.3
V	326.064
F numerator	28595.4
F denominator	21596.9
Factor of Safety - FOS	1.32406

Tension Crack in Slope Face:

$Z = (H\cot\varphi_f - b)(\tan\varphi_f - \tan\varphi_p)$

$W = 0.5\gamma_r H^2[(1 - Z/H)^2\cot\varphi_p(\cot\varphi_p\tan\varphi_f - 1)]$

$A = (H\cot\varphi_f - b)\sec\varphi_p$

$U = 0.5\gamma_w Z_w A$

$V = 0.5\gamma_w Z_w^2$

When U=V=0, a=T=0:

$$FS = \frac{\tan\phi}{\tan\varphi_p} = 1.78$$

$$FS = \frac{[cA + (W\cos\varphi_p - U - V\sin\varphi_p)\tan\phi]}{(W\sin\varphi_p + V\cos\varphi_p)}$$

SLIDE NO. 5 SEISMIC SENSITIVITY ANALYSIS.
Analysis of Plane Failure with Tension Crack in Slope Face.
INPUT DATA

Height of slope - H	160		
Angle of slope face - φ_f	20	radians=	0.349
Angle of upper slope - φ_s	20	radians=	0.349
Angle of failure plane - φ_p	18	radians=	0.3141
z_w/z	0.5		
Horizontal acceleration - α	0.5		
Tension in bolts - T kN	0		
Inclination of T to normal of failure plane - θ	0	radians=	0
Cohesive strength of failure surface - c kN/m²	0		
Angle of friction on failure surface - ϕ	30	radians=	0.5235
Distance of tension crack behind slope crest - b	26		
Unit weight of rock - γ kN/m³	18		
Unit weight of water - γ_w kN/m³	10		

OUTPUT DATA

z	16.1509
z_w	8.07545
W	68897.9
A	393.447
U	15886.3
V	326.064
F numerator	22451.9
F denominator	21596.9
Factor of Safety - FOS	1.03959

Tension Crack in Slope Face:

$Z = (H\cot\varphi_f - b)(\tan\varphi_f - \tan\varphi_p)$

$W = 0.5\gamma_r H^2[(1 - Z/H)^2\cot\varphi_p(\cot\varphi_p\tan\varphi_f - 1)]$

$A = (H\cot\varphi_f - b)\sec\varphi_p$

Tension Crack behind Slope Crest:

$Z = H + b\tan\varphi_s - (b + H\cot\varphi_f)\tan\varphi_p$

$W = 0.5\gamma_r(H^2\cot\varphi_f X + bHX + bZ)$

$X = (1 - \tan\varphi_p\cot\varphi_f)$

$A = (H\cot\varphi_f + b)\sec\varphi_p$

$U = 0.5\gamma_w Z_w A$

$V = 0.5\gamma_w Z_w^2$

When U=V=0, a=T=0:

$$FS = \frac{\tan\phi}{\tan\varphi_p} = 1.45$$

$$FS = \frac{[cA + (W\cos\varphi_p - U - V\sin\varphi_p)\tan\phi]}{(W\sin\varphi_p + V\cos\varphi_p)}$$

Slide No. 5 Sensitivity to Cohesion

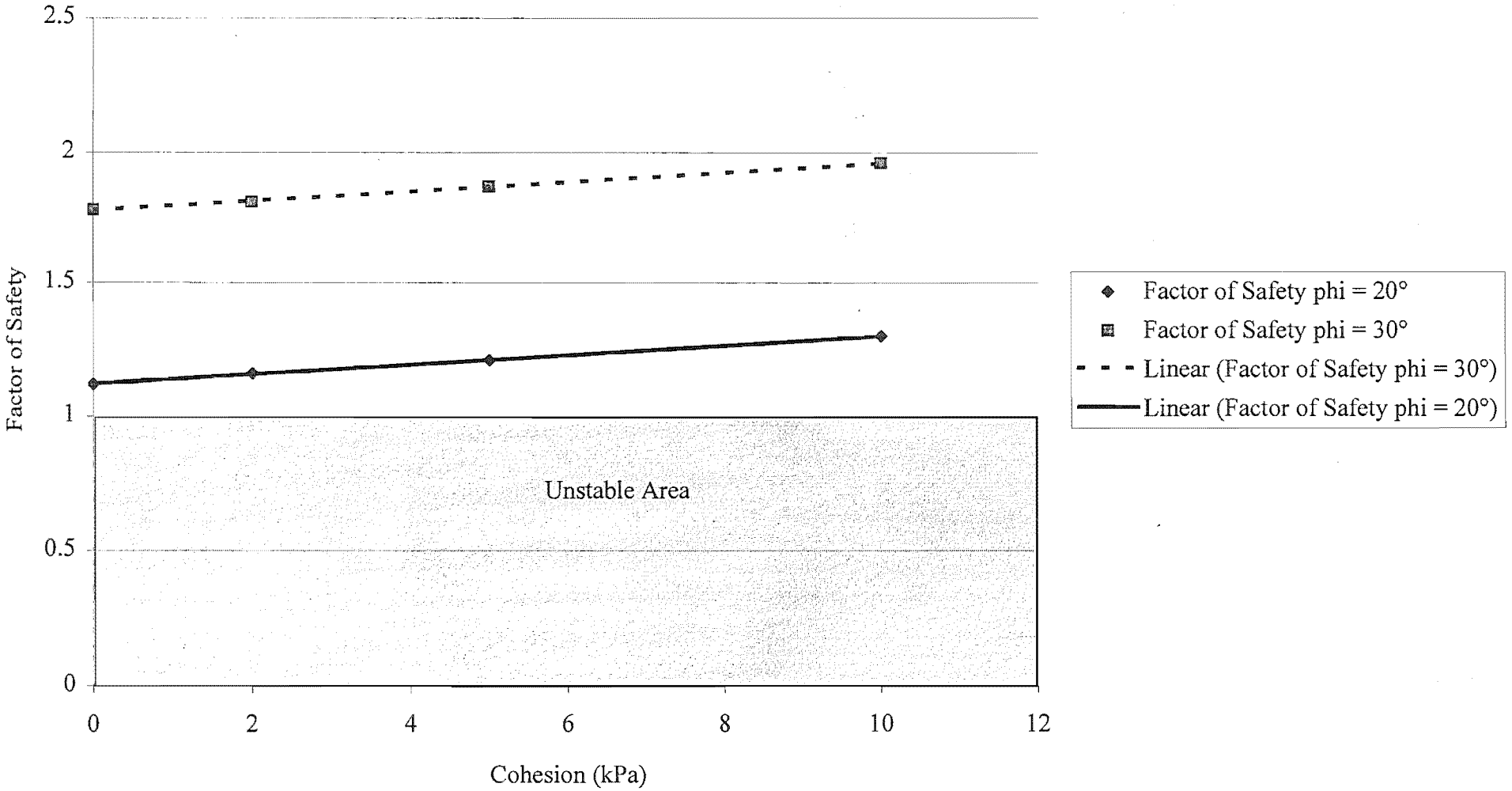

Slide No. 5 Sensitivity to Friction and Angle of Failure Plane

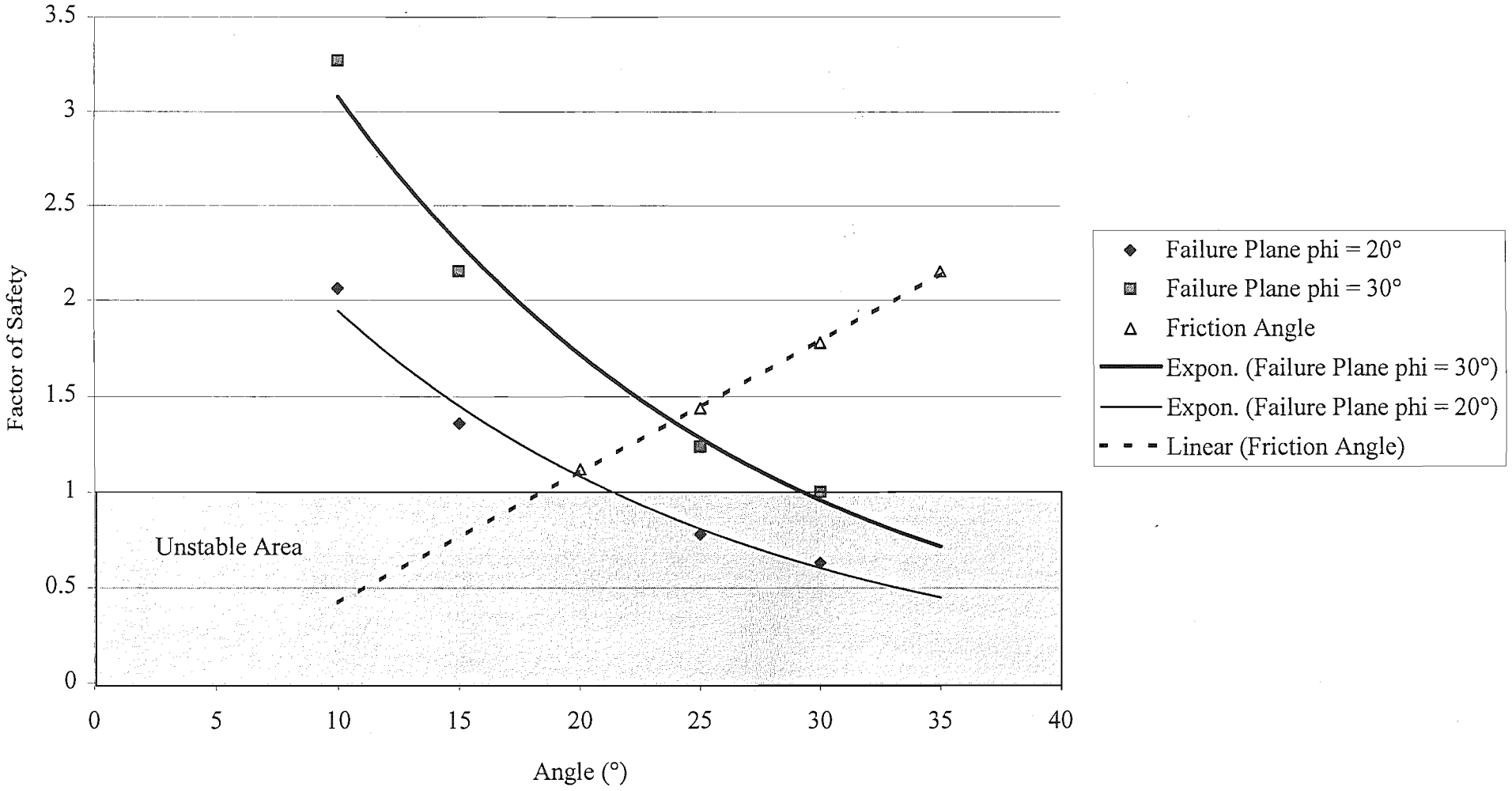

Slide No. 5 Sensitivity to Depth of Perched Water Table

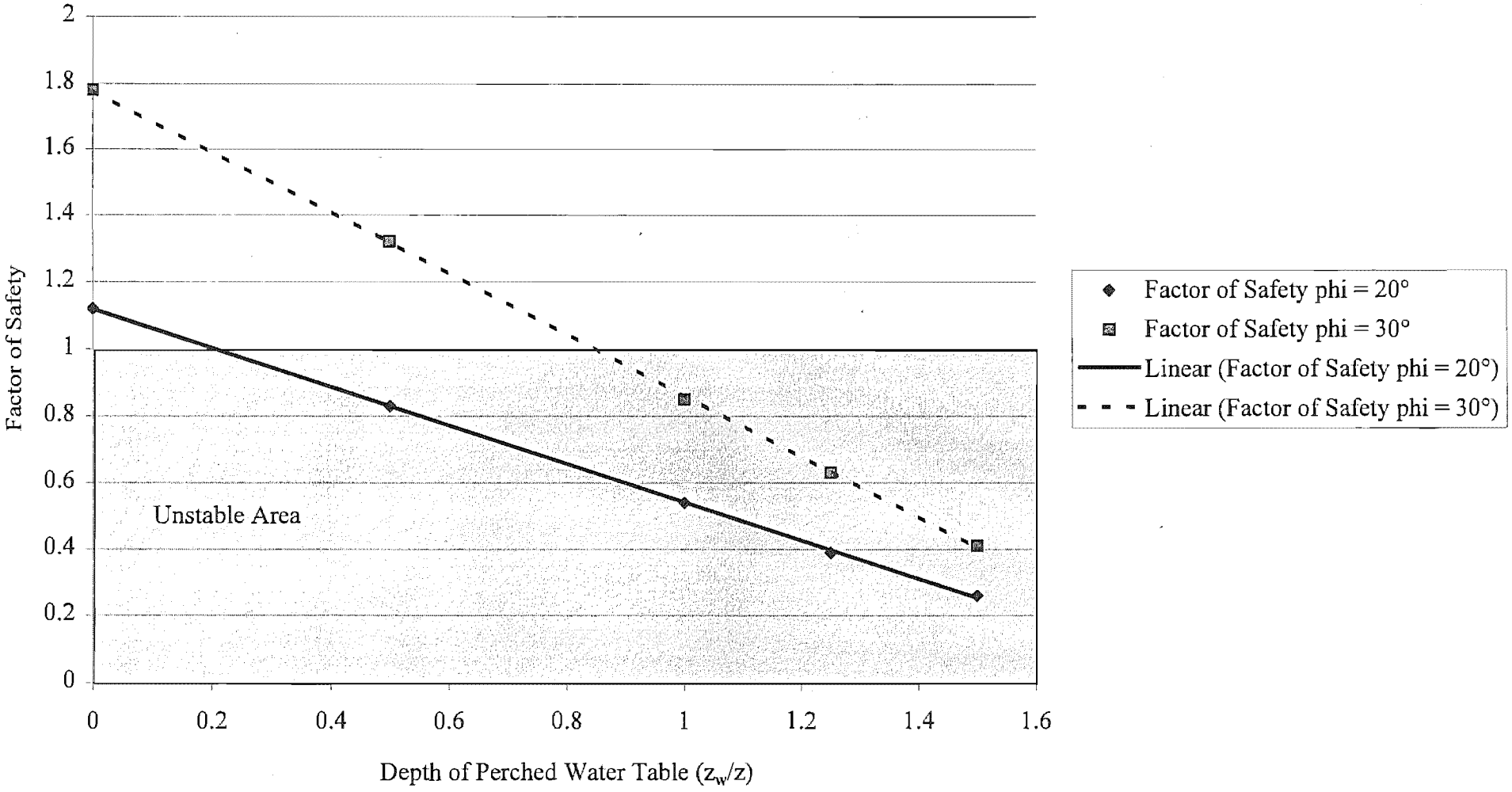

Slide No. 5 Sensitivity to Seismic Acceleration

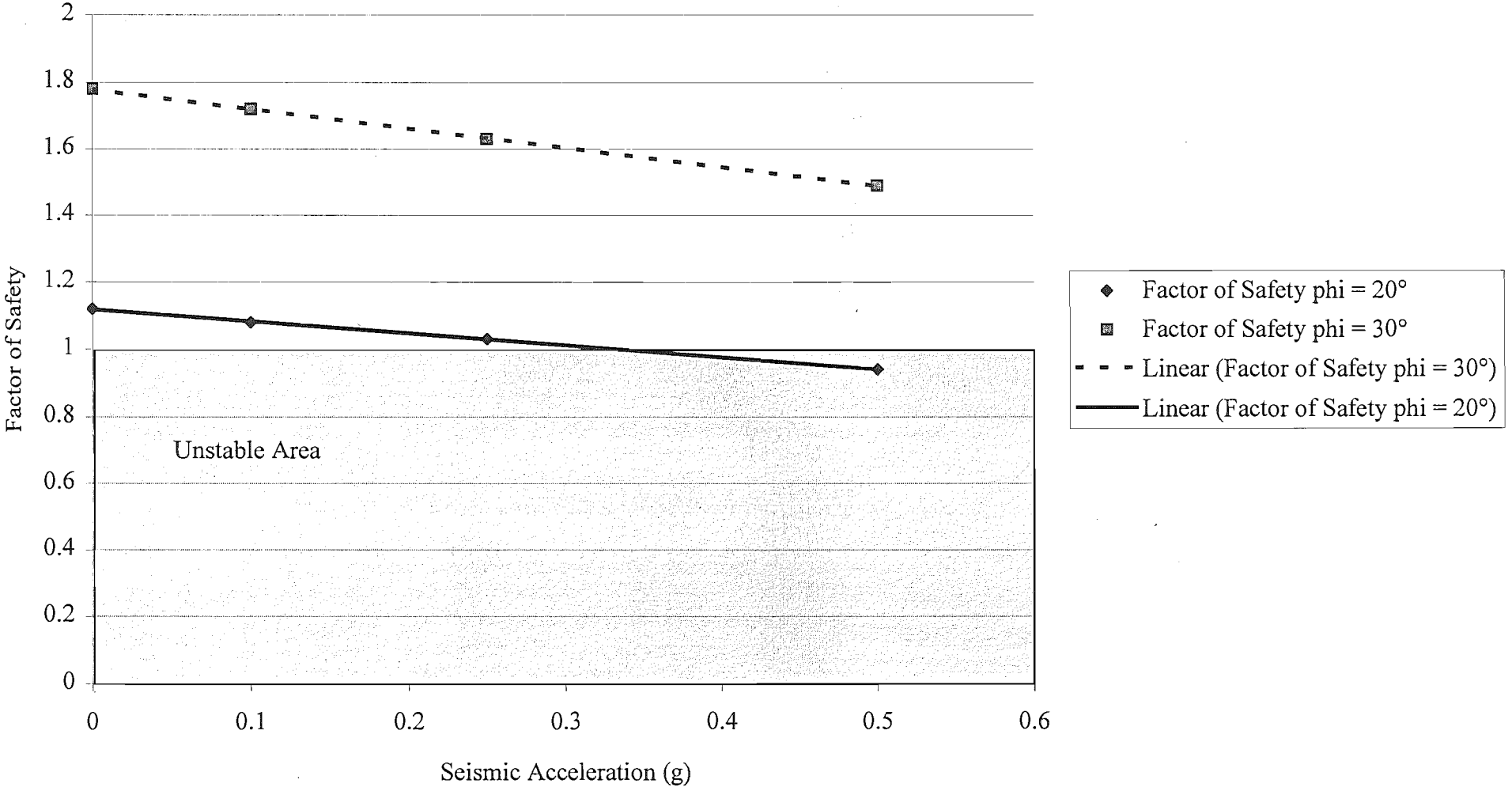

SLIDE NO. 6 SENSITIVITY ANALYSIS.
Analysis of Plane Failure with Tension Crack in Slope Face.

INPUT DATA

Height of slope - H	140		
Angle of slope face - φ_f	25	radians=	0.43625
Angle of upper slope - φ_s	25	radians=	0.43625
Angle of failure plane - φ_p	18	radians=	0.3141
z_w/z	0.5		
Horizontal acceleration - α	0		
Tension in bolts - T kN	0		
Inclination of T to normal of failure plane - θ	0	radians=	0
Cohesive strength of failure surface - c kN/m²	0		
Angle of friction on failure surface - ϕ	30	radians=	0.5235
Distance of tension crack behind slope crest - b	59		
Unit weight of rock - γ kN/m³	18		
Unit weight of water - γ_w kN/m³	10		

OUTPUT DATA

z	34.1079
z_w	17.054
W	135176
A	229.49
U	19568.6
V	1454.19
F numerator	62653.8
F denominator	43147
Factor of Safety - FOS	1.4521

Tension Crack in Slope Face:

$Z = (H\cot\varphi_f - b)(\tan\varphi_f - \tan\varphi_p)$

$W = 0.5\gamma_r H^2[(1 - Z/H)^2\cot\varphi_p(\cot\varphi_p\tan\varphi_f - 1)]$

$A = (H\cot\varphi_f - b)\sec\varphi_p$

$U = 0.5\gamma_w Z_w A$

$V = 0.5\gamma_w Z_w^2$

When U=V=0, a=T=0:

$$FS = \frac{\tan\phi}{\tan\varphi_p} = 1.78$$

$$FS = \frac{[cA + (W\cos\varphi_p - U - V\sin\varphi_p)\tan\phi]}{(W\sin\varphi_p + V\cos\varphi_p)}$$

SLIDE NO. 6 SEISMIC SENSITIVITY ANALYSIS.
Analysis of Plane Failure with Tension Crack in Slope Face.
INPUT DATA

Height of slope - H	140		
Angle of slope face - φ_f	25	radians=	0.43625
Angle of upper slope - φ_s	25	radians=	0.43625
Angle of failure plane - φ_p	18	radians=	0.3141
z_w/z	0.5		
Horizontal acceleration - α	0.5		
Tension in bolts - T kN	0		
Inclination of T to normal of failure plane - θ	0	radians=	0
Cohesive strength of failure surface - c kN/m^2	0		
Angle of friction on failure surface - ϕ	30	radians=	0.5235
Distance of tension crack behind slope crest - b	59		
Unit weight of rock - γ kN/m^3	18		
Unit weight of water - γ_w kN/m^3	10		

OUTPUT DATA

z	34.1079
z_w	17.054
W	135176
A	229.49
U	19568.6
V	1454.19
F numerator	50600.3
F denominator	43147
Factor of Safety - FOS	1.17274

Tension Crack in Slope Face:

$Z = (H\cot\varphi_f - b)(\tan\varphi_f - \tan\varphi_p)$

$W = 0.5\gamma_r H^2[(1 - Z/H)^2\cot\varphi_p(\cot\varphi_p\tan\varphi_f - 1)]$

$A = (H\cot\varphi_f - b)\sec\varphi_p$

$U = 0.5\gamma_w Z_w A$

$V = 0.5\gamma_w Z_w^2$

When U=V=0, a=T=0:

$$FS = \frac{\tan\phi}{\tan\varphi_p} = 1.78$$

$$FS = \frac{[cA + (W\cos\varphi_p - U - V\sin\varphi_p)\tan\phi]}{(W\sin\varphi_p + V\cos\varphi_p)}$$

Slide No. 6 Sensitivity to Cohesion

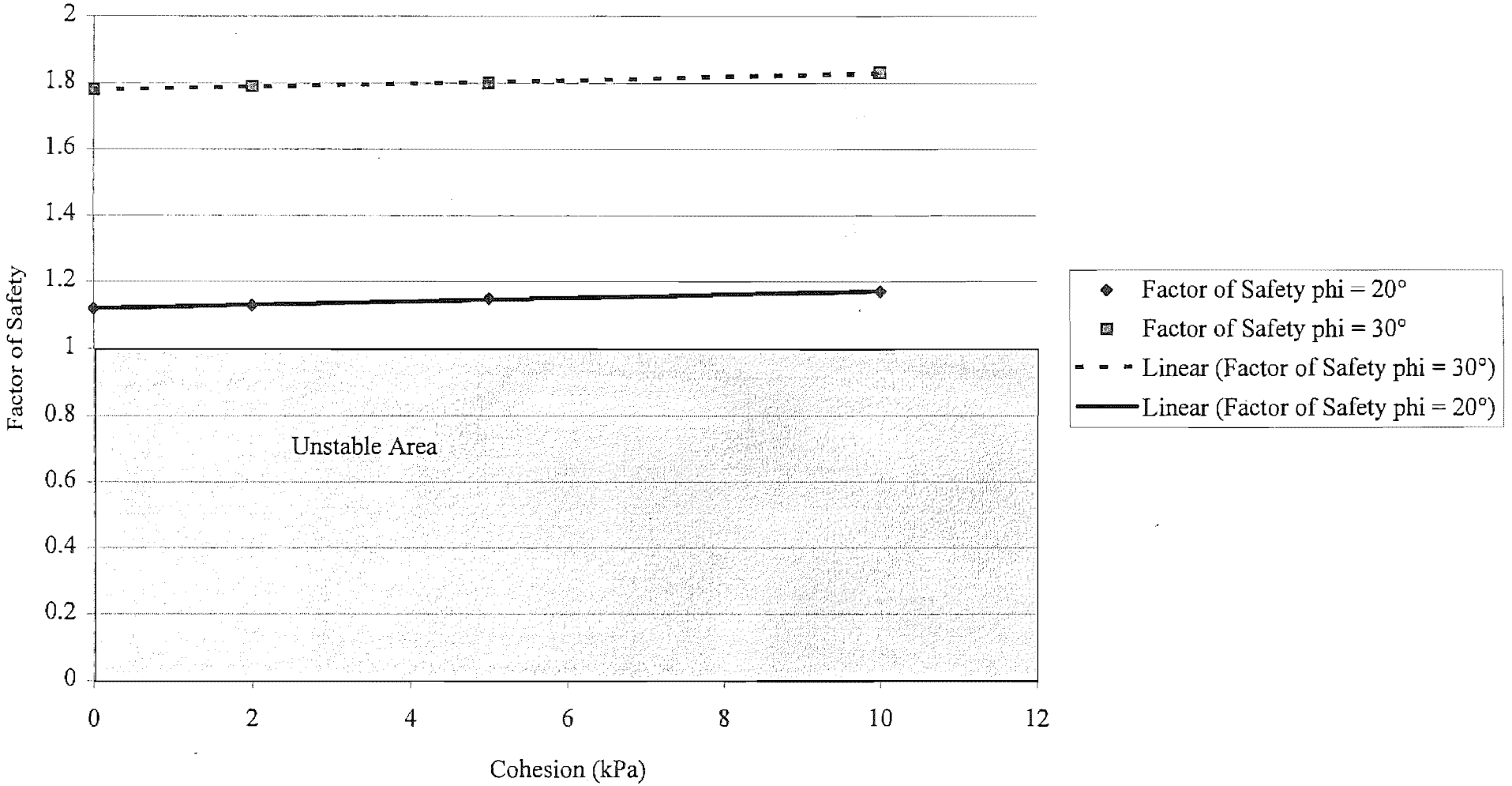

Slide No. 6 Sensitivity to Friction and Angle of the Failure Plane

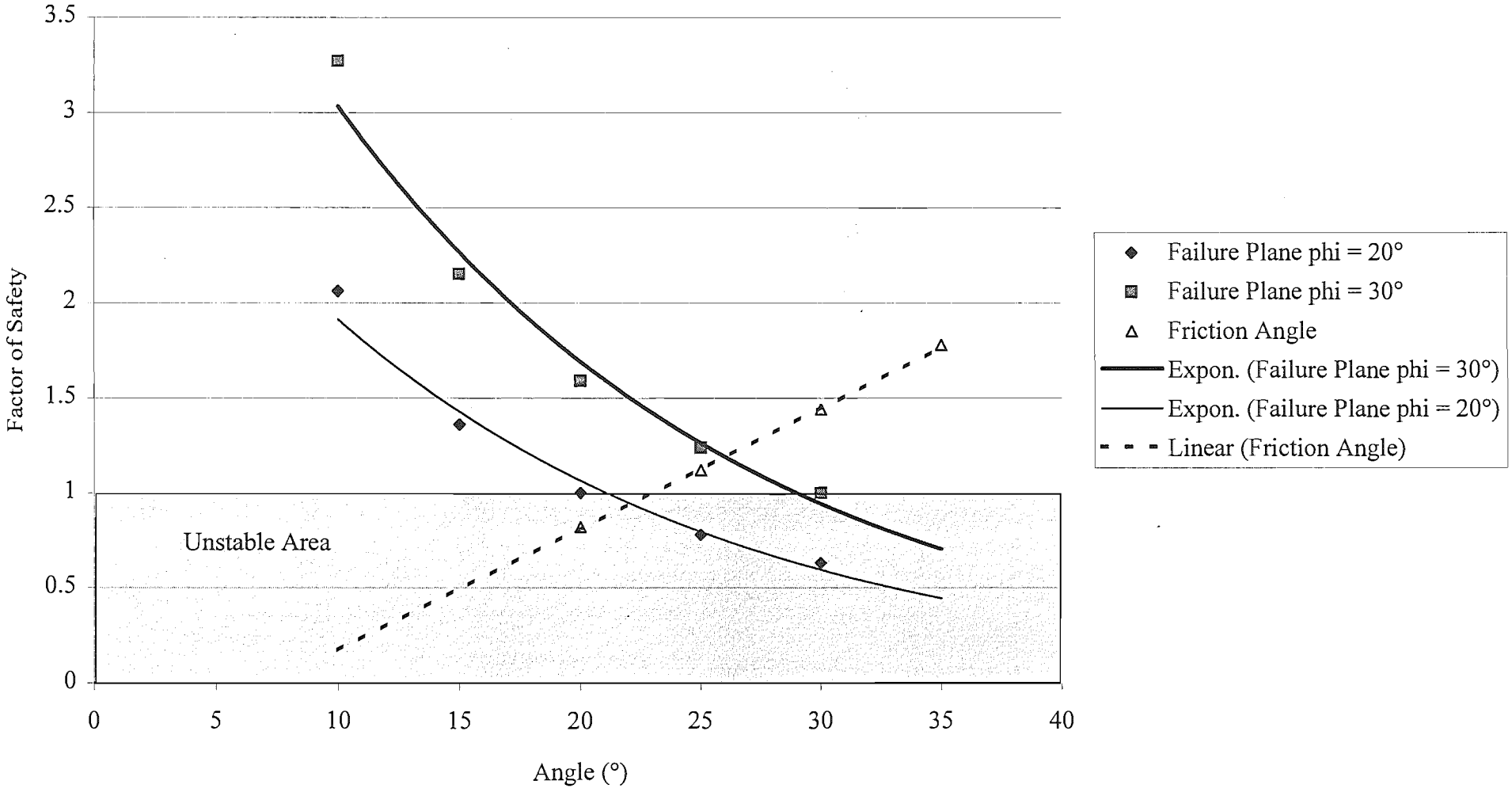

Slide No. 6 Sensitivity to Depth of Perched Water Table

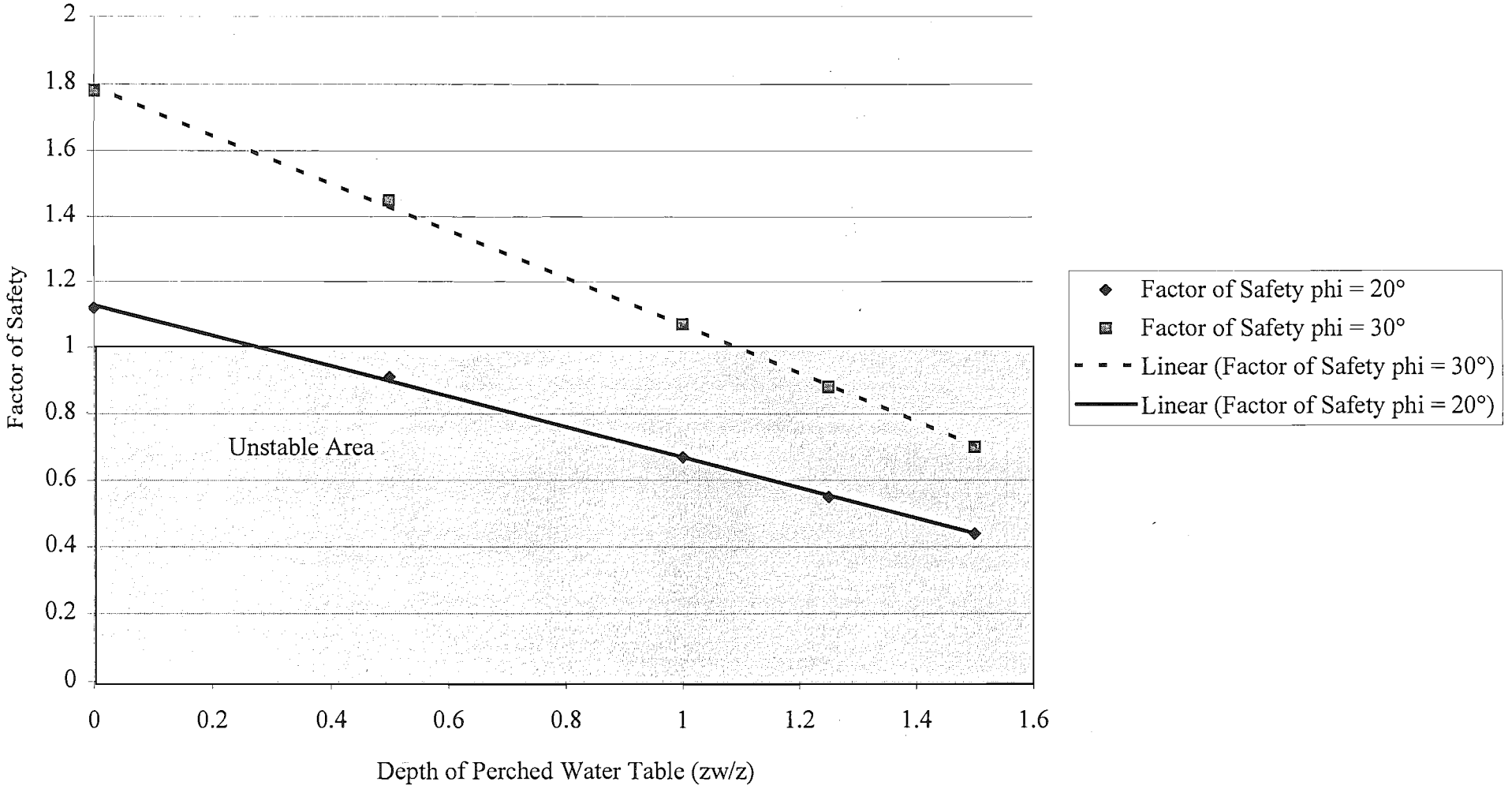

Slide No. 6 Sensitivity to Seismic Acceleration